



**ScuDo**  
Scuola di Dottorato ~ Doctoral School  
WHAT YOU ARE, TAKES YOU FAR



Doctoral Dissertation  
Doctoral Program in *Architectural and Landscape Heritage* (XXXI Cycle)

**Geomatics support to the metric  
documentation of the archaeological heritage.  
Tests and validations on the use of low-cost,  
rapid, image-based sensors and systems.**

**Lorenzo Teppati Losè**

\* \* \* \* \*

**Supervisors**

Prof. Antonia Spanò, Supervisor  
Prof. Filiberto Chiabrando, Co-Supervisor

**Doctoral Examination Committee:**

Prof.ssa Achille Cristiana, Politecnico di Milano, *Referee*  
Prof.ssa Tucci Grazia, Università degli Studi di Firenze, *Referee*  
Prof. Georgopoulos Andreas, National Technical University of Athens  
Prof. Remondino Fabio, Fondazione Bruno Kessler  
Prof. Rodríguez Miranda Álvaro, Universidad del País Vasco

Politecnico di Torino  
May 27, 2019



I hereby declare that, the contents and organisation of this dissertation constitute my own original work and does not compromise in any way the rights of third parties, including those relating to the security of personal data.

Lorenzo Teppati Losè  
Turin, May, 27, 2019

This thesis is licensed under a Creative Commons License, Attribution - Noncommercial - NoDerivative Works 4.0 International: see [www.creativecommons.org](http://www.creativecommons.org). The text may be reproduced for non-commercial purposes, provided that credit is given to the original author.



L'amare il proprio lavoro (che purtroppo  
è privilegio di pochi) costituisce la  
migliore approssimazione concreta alla  
felicità sulla terra: ma questa è una  
verità che non molti conoscono.

Primo Levi, *La chiave a stella*  
(1978)

Loving one's work, unfortunately the  
privilege of a few, represents the best,  
most concrete approximation of  
happiness on earth. But this is a truth not  
many know.

Primo Levi, *The Wrench*  
(1978)





## **Abstract**

The research that will be presented in this thesis work is dedicated to the geomatic support to the metric documentation of Cultural Heritage (CH) and in particular of the archaeological heritage. Several aspects connected with this topic will be addressed during the development of this contribute, especially related with the sustainability of the employed techniques, their main characteristics and the implications connected with their deployment. The concept of sustainability of an approach to the documentation of a CH artefact can present several facets and was thus treated considering different aspects in the course of this dissertation. The first element connected with the concept of sustainability is related with the time component: this element has become a crucial point in the last years and for this reason the concept and the issues related with the definition of rapid mapping and its fields of application have first been defined in this contribute. A second element is the economical sustainability of the instruments and techniques deployed to solve the task of CH documentation: for several reasons, especially in the field of archaeological documentation, the available resources faced a constant decrease in the last years, leading to the attempt of different researchers to stress all the available technological and methodological solutions in order to reach the best optimised balance between costs and performances in the deployment of different techniques. Connected with these issues, is the optimisation of the employed resources: both in terms of the works of people involved in the process of documentation, both in terms of the technological solutions adopted and in the overall process of treatment of the collected data. Finally, the solutions adopted must also be sustainable in terms of response to the need of documentation of the users, i.e. the community of archaeologists, and the products derivable from these processes need to respond to the requirements of the different branches of archaeology and to support the research activities of this community.

Among the different instruments and techniques that the geomatics community can deploy to respond to these needs it was decided to focus on the image-based solutions, i.e.

photogrammetry. These approaches are able to perfectly support these research issues, due their main characteristics: they are flexible, low-cost, adaptable to several situations and most of the times able to respond to differentiated needs of several research areas of archaeology. The methodology behind these approaches was thus reported and revised in this thesis and the main last research addresses were identified. This framework was ulteriorly restrict to two main categories of sensors: Unmanned Aerial Vehicle (UAVs) and spherical camera systems. Concerning UAVs systems, which are by now a consolidated field of research of geomatic with their own methodologies, the focus was set on operative issues connected to the optimisation of their use in context of CH documentation. Different tests were performed on CH site to set up the adopted methodological framework and more extensive analyses were achieved on two selected archaeological sites. Several aspects have been tackled, starting from the enhancement of the flight planning and camera orientation phases, through the different georeferencing strategies and finally till the use of the products generated in a photogrammetric approach. In this sense their use for multi-temporal monitoring of archaeological areas was an approach particularly researched.

On the other hand, the use of spherical system in a photogrammetric approach is a relative new field of research and the methodological validation of this approaches for task of CH documentation from the community of researchers is still ongoing. In this thesis work the aim was thus to test and validate the deployment on the field of such systems (and the use of the derived products), to underline the main issues that will need a further investigation in the following years and to try to define best practices and guidelines for their use in the field of archaeological documentation.

Finally, the possible integrations between the datasets acquired with these two systems were evaluated. In particular, the possibility of co-register aerial and terrestrial data derived from UAVs and spherical systems was stressed, in the direction of the future development of a multi-sensors and multi-scale approach between these two categories of sensors and techniques.

# Preface

The research that will be presented in the following sections is articulated in four main sections that are dedicated to different issues connected with the documentation of CH, and in particular of the archaeological heritage. The first topic that will be addressed is related with the time component: time has become a crucial element in the overall balance of a survey and the optimisation of this component in the different phases of a survey has been an object of great interest in the last years. For this reason, the first chapter of the thesis is devoted to the definition of rapid mapping, how it has evolved during time, the main research addresses on this topic and finally how it can be deployed for the documentation of CH. To deepen the implications connected with the documentation of the archaeological heritage, and to tackle its needs, it was then decided to dedicate chapter 2 to the definition of the scales of archaeological documentation and their connection with the support provided by the geomatics approaches to these kinds of applications. Four main scales have thus been identified and described for the documentation of the archaeological heritage. A section of the chapter was then devoted to the collection and comment to the main standards and guidelines that are dedicated to the definition of best practices for the documentation of CH, with all the issues associated with their application in real case scenarios. The different geomatics instruments and techniques that can contribute to the documentation tasks connected with these four scales of survey and representation (related to the information content, level of detail, accuracy) are then reported and described.

Among these different techniques the image-based approach was the one chosen to be further analysed and researched in this work, especially thanks to the major development that it has undergone in the last decades and to its sustainability in terms of cost, flexibility and rapidity of deployment. In chapter 3 a brief history of the evolution of these approaches is then reported, the geometrical fundamentals of photogrammetry, all the issues connected with the modelling of different types of cameras and the evolution that photogrammetry undergone thanks to the contamination with the field of Computer Vision (CV) and the adoption of Structure from Motion (SfM) algorithms are reported and described. The second part of this chapter is dedicated to the definition of spherical images and to their

processing with photogrammetric approaches. In first instance, a brief history of these systems and their evolution is reported; then, the issues connected with the generation of spherical images from single images and the different approaches that can be adopted are described and analysed; finally, all the issues connected with the use of these 360 data in a photogrammetric approach were described.

The next part of this chapter is dedicated to UAVs: these platforms and their components are described, the deployment of these systems in the field of CH documentation is analysed and some best practices connected to UAVs photogrammetry are reported as well. In the last part of the chapter the different products that can be generated from a photogrammetric approach are indicated and detailed and the different software solutions adopted during the development of the work are stated.

Chapter 4 is the experimental core of the work, where the selected sensors and techniques were deployed on different CH sites: different strategies for both the collection and processing of the data were proposed, tested, analysed and validated. The different test cases were selected to respect some main characteristics and following a specified strategy: tests on different CH sites were performed in order to set up and validate the proposed methodological approaches, while more specific applications were achieved and evaluated on two different archaeological sites. The first section of the chapter is dedicated to aerial sensors and techniques and several issues are tackled: the impact of flight planning and camera orientation on the generation of the 3D model, the different strategies that can be adopted for the georeferencing of the products and finally the use of this products (especially their use for the multitemporal monitoring of the archaeological excavations). The second part is dedicated to terrestrial sensors and techniques, in this case two spherical systems were in depth tested and analysed: the best acquisition strategies that can be adopted with these systems, the different approaches for the processing of the dataset acquired, the georeferencing strategies and finally the use of the derived photogrammetric products are described. A specific focus in this chapter was devoted to the proposal of enhanced strategies for the georeferencing of the datasets and of co-registration approaches between different dataset (these approaches were proposed, tested, analysed and validated). The two final chapters are dedicated to summarizing the different issues emerged during the development of this research and to identify the further perspective in the researches connected with the main topics treated in this work

# Contents

|   |    |
|---|----|
| 1. Abstract.....  |    |
| 2. Preface .....  |    |
| 3. List of Tables.....  |    |
| 4. List of Figures.....   |    |
| 5. Abbreviations .....  |    |
| 6. Low cost image-based solution for Rapid Mapping of CH.....                     | 1  |
| 1.1 Rapid Mapping aims and definition.....  | 1  |
| 1.2 Image-based approach (aerial and terrestrial) .....                           | 4  |
| 1.3 Georeferencing problems and strategies .....                                  | 6  |
| 1.4 Rapid Mapping application in archaeological/architectural heritage.....       | 8  |
| 7. The needs of documentation in Archaeology and the Geomatics response .....     | 10 |
| 2.1 The four scales in archaeological documentation .....                         | 14 |
| 2.1.1 Landscape Archaeology .....   | 14 |
| 2.1.2 Building Archaeology .....  | 15 |
| 2.1.3 Field Archaeology.....  | 16 |
| 2.1.4 Detailed Archaeology.....   | 16 |
| 2.2 Norms and standards for the documentation of Cultural Heritage.....           | 17 |
| 2.2.1 International charters.....   | 18 |
| 2.2.2 Examples of principles, guidelines and specifications for CH.....           | 23 |
| 2.3 Geomatics contribute in the documentation of the Archaeological Heritage..... | 29 |

|       |   |    |
|-------|---|----|
| 2.3.1 | Instruments and techniques in relation with the new needs of archaeology .....  | 32 |
| 2.3.2 | Landscape Archaeology .....   | 37 |
| 2.3.3 | Building Archaeology .....  | 39 |
| 2.3.4 | Field Archaeology .....   | 41 |
| 2.3.5 | Detailed Archaeology .....  | 42 |
| 8.    | Image-based approaches for 3D modelling from reality. Theory and practice ..... | 44 |
| 3.1   | Brief notes on the history and evolution of the discipline .....                | 46 |
| 3.2   | Geometrical fundamentals and digital photogrammetry .....                       | 48 |
| 3.2.1 | Camera models and calibration of digital cameras .....                          | 54 |
| 3.2.2 | Interior Orientation .....  | 64 |
| 3.1.1 | Focal Length (or principal distance) .....                                      | 65 |
| 3.1.2 | Principal Point .....   | 65 |
| 3.1.3 | Radial Distortion .....   | 65 |
| 3.1.4 | Decentring Distortion .....   | 66 |
| 3.1.5 | Other Parameters .....  | 67 |
| 3.2.3 | Exterior Orientation (E.O.) .....   | 68 |
| 3.3   | The SfM based photogrammetric workflow adopted in this research .....           | 69 |
| 3.3.1 | Acquisition strategies .....  | 71 |
| 3.3.2 | The correspondence problem (Tie Points extraction and matching) .....           | 72 |
| 3.3.3 | 3D reconstruction .....   | 75 |
| 3.3.4 | The traditional approach: stereo digital plotting .....                         | 76 |
| 3.3.5 | The innovative approach: SfM .....  | 77 |
| 3.5   | Spherical images .....  | 79 |
| 3.5.1 | Historical notes on panoramic images .....                                      | 79 |
| 3.5.2 | First analogic revolution .....   | 80 |
| 3.5.3 | Second digital revolution .....   | 82 |
| 3.5.4 | Stitching of images (approaches derived from the CV domain) .....               | 83 |

|       |   |     |
|-------|---|-----|
| 3.5.5 | Software solution for the stitching .....   | 86  |
| 3.6   | Spherical Photogrammetry .....  | 88  |
| 3.6.1 | Modelling and Calibration of Spherical Cameras .....  | 91  |
| 3.6.2 | Spherical camera systems: Single camera, Dual camera, Multicamera   | 96  |
| 3.7   | Unmanned Aerial Vehicle: UAV's .....  | 100 |
| 3.7.1 | Definition of UAVs and their components .....   | 101 |
| 3.7.2 | UAVs deployment in the field of heritage documentation.....   | 105 |
| 3.7.3 | UAVs photogrammetry: best practices .....   | 107 |
| 3.8   | Products derived from the CV photogrammetric approach.....  | 110 |
| 3.9   | Employed software solutions for the photogrammetric approach.....   | 113 |
| 3.9.1 | Opensource.....   | 113 |
| 3.9.2 | Commercial .....  | 114 |
| 9.    | Aerial and terrestrial sensors and techniques deployment on selected CH test sites                        | 116 |
| 4.1   | Aerial Sensors and techniques.....  | 118 |
| 4.1.1 | Flight Plan and Camera Orientation.....   | 118 |
| 4.1.2 | Georeferencing strategies and GCPs.....   | 155 |
| 4.1.3 | Use of the photogrammetric derived products. The multitemporal<br>approach in the site of Hierapolis..... | 166 |
| 4.2   | Terrestrial Sensors and techniques. Calibration and analyses on two<br>spherical systems.....             | 187 |
| 4.2.1 | Camera Calibration .....  | 187 |
| 4.2.2 | Camera Calibration approaches .....   | 189 |
| 4.2.3 | Camera calibration approaches adopted in this research.....   | 192 |
| 4.2.4 | Calibration with a known 2D test field .....  | 192 |
| 4.2.5 | Self-Calibration.....   | 194 |

|       |   |     |
|-------|---|-----|
| 4.2.6 | Multicamera systems: Freedom 360 .....  | 196 |
| 4.2.7 | Dual camera systems: GoPro Fusion .....   | 210 |
| 4.3   | Tests performed in the framework of CH documentation with 360 cameras<br>.....  | 225 |
| 4.3.1 | Best practices and acquisition strategies .....   | 225 |
| 4.3.2 | Processing of data derived from 360 systems. To stitch or not to stitch?<br>That's the question. ....   | 231 |
| 4.3.3 | Analyses and comparisons between acquisitions performed in time lapse<br>and video mode. Validation of these approaches on four different datasets<br>..... | 233 |
| 4.3.4 | Georeferencing Strategies .....   | 250 |
| 4.3.5 | Use of some of the photogrammetric products derived from the<br>acquisitions performed with spherical systems. ....   | 254 |
| 10.   | Discussion.....   | 266 |
| 11.   | Conclusion.....   | 275 |
| 12.   | References .....  | 280 |



## List of Tables

|  |     |
|--|-----|
| Table 1 Example of dedicated stitching software for commercial cameras.....  | 86  |
| Table 2 Examples of commercial software packages for stitching of images .....   | 87  |
| Table 3 Examples of freeware and opensource software for the stitching of images   | 87  |
| Table 4 360 cameras. Examples of Single camera system.....   | 97  |
| Table 5 360 cameras. Examples of Dual camera systems .....   | 98  |
| Table 6 360 cameras. Examples of Multiple camera systems .....   | 99  |
| Table 7 Rocca San Silvestro. Density analysis on the two selected sample A and B .....   | 127 |
| Table 8 Main specifications of the DJI platforms used in this research .....   | 133 |
| Table 9 Giuseppe Galliano Barrack. Inspire 2 dataset parameteres.....  | 137 |
| Table 10 Giuseppe Galliano Barrack. Main specifications of the flight performed with the Spark .....   | 138 |
| Table 11 Giuseppe Galliano Barrack, comparison of focal length a PP coordinates estimated from the two considered software for flight ID 3 .....   | 140 |
| Table 12 Northern Necropolis of Hierapolis. Main characteristics of the flights completed in 2017 with the Phantom 4 (platform 2) .....  | 146 |
| Table 13 Hierapolis, Northern Necropolis. Phantom 4 flights processing main characteristics.....   | 146 |
| Table 14 Hierapolis, Northern Necropolis. Flight planning and camera orientation of the missions completed in 2018 with the Mavic Pro and Spark .....  | 148 |
| Table 15 Hierapolis, Northern Necropolis. Mavic Pro and Spark flights processing main characteristics.....   | 148 |
| Table 16 Hierapolis, area of the Apollo Sanctuary. Flight planning, camera orientation and processing parameters of the missions completed in 2017 with the Phantom 4 (platform 2).....            | 150 |
| Table 17 Hierapolis, area of the Apollo Sanctuary. Flight planning and camera orientation parameters of the missions completed in 2018 with the Mavic Pro (platform 1) and Spark (platform 4)..... | 152 |

|  |     |
|--|-----|
| Table 18 Savigliano, processing configurations. On the left the combination of the five flights described at page 135 together, on the right the different GCPs configurations ..... | 159 |
| Table 19 Savigliano, mean RMSe value on GCPs and CPs for the 4 projects in the three GCPs configuration with the Phantom 4.....  | 160 |
| Table 20 Savigliano, mean RMSe value on GCPs and CPs for the 4 projects in the three GCPs configuration with the Phantom 4 Pro .....   | 160 |
| Table 21 Savigliano, mean RMSe value on GCPs and CPs for the 4 projects in the three GCPs configuration with the Mavic Pro .....   | 161 |
| Table 22 Nymphaeum of Apollo, main parameters for the processing of the UAVs dataset collected in 2017.....  | 163 |
| Table 23 Nymphaeum of Apollo, accuracy of the TLS dataset processing.....  | 164 |
| Table 24 Nymphaeum of Apollo, comparison between TLS extracted coordinates and photogrammetric computed coordinates.....   | 165 |
| Table 25 Main specifications of the classic mount by Freedom 360.....  | 197 |
| Table 26 Main specifications of GoPro Hero 4 silver .....  | 197 |
| Table 27 Estimated I.O. parameters of the six action cameras separately considered and processed.....  | 201 |
| Table 28 Estimated I.O. parameters of the six cameras mounted on the rig and automatically processed with the native Exif .....  | 203 |
| Table 29 Estimated I.O. parameters of the six cameras mounted on the rig and processed after the Exif modification .....   | 204 |
| Table 30 GoPro Fusion main specifications .....  | 211 |
| Table 31 GoPro Fusion. Estimated I.O. parameters through Agisoft Lens .....  | 214 |
| Table 32 RMSe in mm of GCPs and CPs on the two cameras projects for self-calibration. Seven measured points were used as GCPs and seven as CPs .....                                 | 215 |
| Table 33 GoPro Fusion. Estimated I.O. parameters through the self-calibration approach.....  | 216 |
| Table 34 Reprojection error of TPs extracted to the enhanced self-calibration approach   | 216 |
| Table 35 Corner wall. C2C analyses of the sample area; number of points included in the preselected range of values .....  | 218 |

|   |     |
|---|-----|
| Table 36 Stairs. C2C analyses of the sample area; number of points included in the preselected range of values .....  | 219 |
| Table 37 RMSe on GCPs and CPs for the processing of spherical images acquired in the calibration field .....  | 223 |
| Table 38 Reprojection error of TPs extracted from the processing of spherical images .  | 223 |
| Table 39 Photogrammetric 360 model. C2C analyses of the sample areas; number of points included in the preselected range of values.....                       | 224 |
| Table 40 Valentino Castle, test on the impact of the sensor to object distance on GCPs and CPs RMSe value on the datasets acquired with the GoPro Fusion..... | 227 |
| Table 41 Rocca San Silvestro, dataset 1. Processing parameters after the exif modification.....   | 234 |
| Table 42 Rocca San Silvestro, processing parameters of the CRP set acquired with the Canon EOS 5D Mark II .....   | 235 |
| Table 43 Rocca San Silvestro – church, accuracy of the TLS processing.....  | 235 |
| Table 44 Rocca San Silvestro, mean values of the C2C distance analysis on the two photogrammetric datasets of the church compared with the TLS dataset.....   | 237 |
| Table 45 Rocca San Silvestro, dataset 2. Processing parameters on the modified exif dataset .....   | 240 |
| Table 46 Rocca San Silvestro – south area, accuracy of the TLS processing.....  | 241 |
| Table 47 Northern Necropolis, Hierapolis. Dataset 3. Processing parameters of the time lapse dataset .....  | 242 |
| Table 48 Hierapolis, Northern Necropolis. Accuracy of the TLS processing .....  | 243 |
| Table 49 Hierapolis, Northern Necropolis. Mean values of the C2C distance analysis on the dataset 3 and the TLS dataset.....                                  | 244 |
| Table 50 Hierapolis, Northern Necropolis. Mean values of the C2C distance analysis on the dataset 3 and the UAVs 2018 dataset.....                            | 245 |
| Table 51 Northern Necropolis, Hierapolis. Dataset 4. Processing parameters of the video dataset .....   | 246 |
| Table 52 Hierapolis, Northern Necropolis. Mean values of the C2C distance analysis on the dataset 4 and the TLS dataset.....                                  | 247 |

|   |     |
|---|-----|
| Table 53 Hierapolis, Northern Necropolis. Co-registration approach, comparison on the coordinates of camera stations estimated with the co-registration approach and with the traditional approach..... | 252 |
| Table 54 Hierapolis, Northern Necropolis. Co-registration approach, comparison on the coordinates of control points estimated with the co-registration approach and measured on the field.....          | 253 |



## List of Figures

|  |    |
|--|----|
| Figure 1 Some examples of different typologies of codified targets .....   | 7  |
| Figure 2 Ruins of the Forum, Rome, (c. 1743). Bernardo Bellotto. Source: Melbourne, National Gallery of Victoria ( <a href="https://www.ngv.vic.gov.au/">https://www.ngv.vic.gov.au/</a> ) .....   | 11 |
| Figure 3 On the left Mortimer Wheeler during Maiden Castle excavation (Source: UCL - University College London). On the right example of a modern excavation conducted with Wheeler grid method (Monticello Department of Archaeology - Virginia) .....            | 12 |
| Figure 4 Different recording levels of CH as described in RecorDIM. The choice of the level to adopt is related with the purpose of the projects, the expected results and the resources available .....   | 26 |
| Figure 5 Major recording tools and instruments for CH documentation and their relations with the three level of recording .....  | 27 |
| Figure 6 Pyramidal representation of the documentation process. On the left the different survey techniques, on the right their relation with the different representation scales (Source: Author's elaboration based on Tucci & Bonora, 2014) .....               | 34 |
| Figure 7 Panorama of sensors and techniques according to scene dimension and complexity (Remondino & Campana, 2014) .....  | 35 |
| Figure 8 Schematic representation of the different steps for the documentation of CH artefacts (Ioannides et al., 2005) .....  | 37 |
| Figure 9 Example of the use airborne LiDAR, and trees filtering algorithms from the detection of hidden archaeological features. Source: (Doneus et al., 2008) .....   | 38 |
| Figure 10 Evolution of the process of documentation in the field of building archaeology over the years, safety level of the operators has not always been improved .....  | 40 |
| Figure 11 Evolution in the systems for aerial documentation of archaeological evidences. On the left an air balloon on the archaeological site of Hierapolis (1997). On the right a small and portable multicopter platform on the site of Hierapolis (2018) ..... | 41 |
| Figure 12 Representation of the cycles of evolution of photogrammetry based on the long waves' theory of Krondatiev. (Source: Author elaboration) .....  | 47 |

|  |    |
|--|----|
| Figure 13 Scheme of the ideal 3D perspective projection based on the pinhole camera model. (Source: Author elaboration) .....  | 49 |
| Figure 14 Pinhole camera model and geometry of image formation in these types of cameras. (Source: G. Verhoeven, 2016) .....   | 50 |
| Figure 15 Left: Central perspective projection. (Source: Fabio Remondino & Stylianidis, 2016). Right: Exterior orientation and projective imaging (Source: T Luhmann, Robson, Kyle, & Harley, 2006) .....  | 51 |
| Figure 16 Schematic representation of camera systems. On the left traditional film cameras, on the right computational cameras (Förstner & Wrobel, 2016) .....   | 54 |
| Figure 17 Thin lens system representation. $F, F'$ define the focal point while $f, f'$ define the focal distance. $h$ and $h'$ are the object and image size, $s$ and $s'$ are object and image distance. $O$ is the optical centre. (Source: Author elaboration based on G. Verhoeven, 2016) .....   | 55 |
| Figure 18 Thick lens system representation. $F, F'$ define the focal point while $f, f'$ define the focal distance. $h$ and $h'$ are the object and image size, $s$ and $s'$ are object and image distance. $P$ and $P'$ are the principal points, while $N$ and $N'$ are the nodal points (Source: Author elaboration based on G. Verhoeven, 2016) .....  | 56 |
| Figure 19 Thin lens system. Ray tracing. $a$ is the ray parallel with the optical axis that will refract and be redirected from the focal point $F'$ . Ray $b$ will pass through the centre of the thin lens and will not be deviated from its path. Ray $c$ will pass through the object focus $F$ , it will be parallel to optical axis after the refraction. (Source: Author elaboration based on G. Verhoeven, 2016) ..... | 57 |
| Figure 20 Ray tracing techniques used to explain how object distance influences image distance. Image distance $s'$ is equal to photogrammetric focal length and $PP$ is the principal point. (Source: Author elaboration based on G. Verhoeven, 2016) .....   | 58 |
| Figure 21 Schematic representation of the relation between Focal length and FoV. (Source: Author elaboration) .....  | 59 |
| Figure 22 Examples of symmetrical lens design (Zeiss Planar on the top left) and asymmetrical lens design (Tessar's design on the down left). On the right part of the images a section of a Canon lens. ....  | 60 |
| Figure 23 Example of different type of radial distortion effects. Ideal lens (A), Pincushion distortion (B), Barrel distortion (C), Fisheye distortion (D). (Source: Author elaboration) .....   | 60 |

|  |    |
|--|----|
| Figure 24 Fisheye lenses classification. Circular fisheye (left) and full format or diagonal fisheye (right). (Source: Schneider, Schwalbe, & Maas, 2009).....   | 61 |
| Figure 25 Schematic representation of central perspective geometry (left) and fisheye projection geometry (right). (Source: Schneider et al., 2009).....   | 62 |
| Figure 26 Schematic representation of the geometrical modelling of fisheye cameras. (Source: Schneider et al., 2009).....  | 64 |
| Figure 27 Schematic representation of the shift between theoretical PP and real PP65   |    |
| Figure 28 Example of the variation of radial distortion profile at different focal lengths from: (Guidi & Remondino, 2012).....  | 66 |
| Figure 29 Example of the variation of decentring distortion profile at different focal lengths from: (Guidi & Remondino, 2012).....  | 67 |
| Figure 30 Non-ideal image sensor .....   | 68 |
| Figure 31 Epipolar geometry. Epipolar plane for convergent images. (Source: Luhmann et al., 2006).....   | 73 |
| Figure 32 Example of a stereo-configuration. $X'$ and $X''$ are the two corresponding point of the object point $X$ . $Lx'$ and $Lx''$ are the image rays from the projection centres $O'$ and $O''$ (that forms the baseline $B$ ). Source:(Förstner & Wrobel, 2016).....             | 76 |
| Figure 33 SfM triangulation pipeline. Source: <a href="http://theia-sfm.org/sfm.html#chapter-sfm">http://theia-sfm.org/sfm.html#chapter-sfm</a> .  | 78 |
| Figure 34 Robert Barker, view of Edinburgh from Calton Hill (source: City of Edinburgh Council – Libraries) .....  | 79 |
| Figure 35 AI-vista panoramic camera. Source: <a href="http://historiccamera.com/">http://historiccamera.com/</a> .....   | 81 |
| Figure 36 Camera equipped with a swing lens. The Horizont 202 (Source: <a href="http://www.sovietcams.com/">http://www.sovietcams.com/</a> ) .....   | 81 |
| Figure 37 Example of a rotating camera manufactured by Seitz (Source: <a href="https://www.roundshot.com">https://www.roundshot.com</a> ).....   | 82 |
| Figure 38 The 8mm F3.5 Circular fisheye manufactured by Sigma (on the left. Source: <a href="https://www.sigmaphoto.com/">https://www.sigmaphoto.com/</a> ). An example of images acquired from a circular fisheye lens – GoPro Fusion (on the right. Source: Author elaboration)..... | 82 |
| Figure 39 Example of the quality of a spherical image (here represented in an equirectangular projection) achievable using the Google Street View application and a commercial smartphone. Basilica di San Nicola, Tolentino (MC), Italy. Source: Author's photo .....                 | 83 |

|   |     |
|---|-----|
| Figure 40 Example of multiple images stitched into a single panorama, Rainbow bridge, Tokyo. Source: Author’s photo .....                                     | 84  |
| Figure 41 Examples of ghosting (left) and parallax (right) errors in the stitching process. ....  | 86  |
| Figure 42 Schematic representation of PSP processing phase (Source: Fangi, 2015)  | 89  |
| Figure 43 Schematic representation of the PSP workflow. Source: author’s elaboration .  | 90  |
| Figure 44 Schematic representation of the equirectangular projection (Source: Fangi & Nardinocchi, 2013) .....  | 92  |
| Figure 45 Schematic representation of the relation between spherical and terrestrial coordinate systems (Source: Fangi & Nardinocchi, 2013) .....             | 93  |
| Figure 46 Epipolar geometry of two spherical images (Source: Fangi & Nardinocchi, 2013) .....   | 94  |
| Figure 47 Epipolar plane on a spherical image and extraction of a set of point for the construction of epipolar line (Source: Fangi & Nardinocchi, 2013)..... | 95  |
| Figure 48 Example of plotting of the epipolar line for SP (Source: Luhmann et al., 2006) .....  | 96  |
| Figure 49 Timeline of military and civilian evolution of UAVs use (Source: Giones & Brem, 2017) .....   | 101 |
| Figure 50 Schematic representation of the UAVs pipeline (Source: adapted from Nex & Remondino, 2014) .....  | 108 |
| Figure 51 Schematic representation of DSM and DTM features. (Source: <a href="https://3dmetrca.it/dtm-dsm-dem/">https://3dmetrca.it/dtm-dsm-dem/</a> ) .....  | 111 |
| Figure 52 Aerial views of the archaeological site of Rocca San Silvestro (left) and some structures of the archaeological site of Hierapolis (right) .....    | 116 |
| Figure 53 San Giuliano chapel in Savigliano (top-right), the Giuseppe Galliano barrack in Mondovì (top-left) and the Valentino Castel (bottom).....           | 117 |
| Figure 54 Examples of different flight grids typologies that can be projected with the dedicated software solutions .....                                     | 119 |
| Figure 55 The UBIK DIATI MK01 platform and an image of the fieldwork at Rocca San Silvestro .....   | 122 |
| Figure 56 Rocca San Silvestro. Flight plans and camera configuration .....  | 124 |

|   |     |
|---|-----|
| Figure 57 Rocca San Silvestro, graphical representation of the mean RMSe of the CPs in the seven projects.....  | 125 |
| Figure 58 Rocca San Silvestro. The two sample areas that were chosen to perform further analyses and their location indicated on an orthoimage of the site (left). ....                       | 126 |
| Figure 59 Rocca San Silvestro. Graphical representation of the density analysis on the two selected samples A and B for project 1 and 4.....  | 129 |
| Figure 60 Rocca San Silvestro, Sample A (left) and Sample B (right). Position of the vertical sections extracted for the two sample areas. ....   | 130 |
| Figure 61 Rocca San Silvestro, Sample A. Semiautomatic sections extracted from the seven photogrammetric point clouds and from the TLS reference point cloud.....                             | 131 |
| Figure 62 Rocca San Silvestro, Sample B. Semiautomatic sections extracted from the seven photogrammetric point clouds and from the TLS reference point cloud.....                             | 132 |
| Figure 63 Flight planning for platforms 1,2 and 3 for the test performed at Savigliano..  | 135 |
| Figure 64 Giuseppe Galliano Barrack. Flight plans of the three flights completed with the Inspire 2 .....   | 137 |
| Figure 65 Giuseppe Galliano Barrack, Acquisition with the Spark (flight ID 3). Camera station positions (left) and control point position (right) .....                                       | 139 |
| Figure 66 Giuseppe Galliano Barracks, flight ID 3. RMSe comparison for GCPs and CPs computed in the two software solutions tested.....  | 139 |
| Figure 67 Giuseppe Galliano Barrack, C2C analysis between TLS and photogrammetric model.....  | 141 |
| Figure 68 Giuseppe Galliano Barrack, Key Plan of the extracted section (left), camera stations of the UAVs flight (centre) and position of the acquired scan with the two lasers (right)..... | 142 |
| Figure 69 Giuseppe Galliano Barrack. Comparison of the Semiautomatic sections extracted with the 3D Reshaper software .....   | 143 |
| Figure 70 Giuseppe Galliano Barrack, Example of integration of datasets: the final model (left), the Inspire 2 model (centre - blue) and the Spark model (right - blue)                       | 144 |
| Figure 71 Overall map of Hierapolis, in blue the area of the Northern Necropolis acquired in the 2017 and in red the area acquired in 2018 (source: D’Andria, Scardozzi, & Spanò, 2008).....  | 145 |

|   |     |
|---|-----|
| Figure 72 Northern Necropolis of Hierapolis. Flight planning and camera orientation of the missions completed in 2017 with the Phantom 4 (platform 2) .....                           | 146 |
| Figure 73 Overall map of Hierapolis, in blue the area of the Apollo Sanctuary (source: D'Andria, Scardozzi, & Spanò, 2008) .....  | 149 |
| Figure 74 Hierapolis, area of the Apollo Sanctuary. Flight planning and camera orientation of the missions completed in 2017 with the Phantom 4 (platform 2)....                      | 151 |
| Figure 75 Hierapolis, area of the Apollo Sanctuary. Flight planning and camera orientation of the missions completed in 2018 with Mavic Pro (platform 1) and Spark (platform 4) ..... | 154 |
| Figure 76 Hierapolis, Nymphaeum of Apollo. Gross error on direct georeferencing derived from two different platforms .....  | 156 |
| Figure 77 Rocca San Silvestro, 4 GCPs configuration. Position and type of GCPs  | 157 |
| Figure 78 Rocca San Silvestro, Graphical representation of the mean RMSe of the CPs in the seven projects, using only 4 GCPs .....  | 158 |
| Figure 79 Savigliano, the three GCPs configurations adopted in the processing of the four datasets. In yellow the points used as GCPs .....   | 159 |
| Figure 80 Co-registration approach. Proposed strategy for two datasets of the same objects .....  | 162 |
| Figure 81 Nymphaeum of Apollo, position of the scans acquired in the 2017 campaign  | 164 |
| Figure 82 Natural features selected to be used to validate the co-registration approach..   | 164 |
| Figure 83 Nymphaeum of Apollo, General overview of the C2C analyses. The areas where major changes occurred are underlined in red and green .....                                     | 167 |
| Figure 84 Nymphaeum of Apollo, the two areas selected to deepen the analysis between 2017 and 2018 dataset.....   | 168 |
| Figure 85 Nymphaeum of Apollo, Area 1, C2C analysis between the models derived from 2017 and 2018 UAVs dataset.....   | 170 |
| Figure 86 Nymphaeum of Apollo, Area 2, C2C analysis between the models derived from 2017 and 2018 UAVs dataset.....   | 173 |
| Figure 87 Nymphaeum of Apollo, mesh derived from the photogrammetric approach. In yellow 2017 dataset and in blue 2018 dataset .....  | 175 |
| Figure 88 Nymphaeum of Apollo, volume computation on two samples of 2017 dataset  | 176 |
| Figure 89 Nymphaeum of Apollo, volume computation on two samples of 2018 dataset...   | 177 |

|  |     |
|--|-----|
| Figure 90 Nymphaeum of Apollo, volume computation on a niche of 2018 dataset.....  | 178 |
| Figure 91 Nymphaeum of Apollo, results of the analysis performed on the two DSM.....   | 179 |
| Figure 92 Hierapolis, Northern Necropolis. DEM derived from UAVs 2018 dataset (left) and overlay of the automatically extracted contour lines on the shaded model (right).....   | 180 |
| Figure 93 Hierapolis, Northern Necropolis. Slope analysis of the area acquired in with the UAVs flights of the 2018.....   | 181 |
| Figure 94 Hierapolis, Northern Necropolis. Terrain profiles extracted in Qgis with the qProf plugin. Comparison between 2017 (top) and 2018 (down) datasets.....   | 182 |
| Figure 95 Nymphaeum of Apollo, general orthophoto of the area in 2017 and 2018.....  | 183 |
| Figure 96 Nymphaeum of Apollo, details of the produced orthophotos on two specific areas.....  | 184 |
| Figure 97 Nymphaeum of Apollo, integration of data derived from the archaeological documentation of the past years and the ortophoto produced with the 2018 UAVs data....  | 185 |
| Figure 98 Hierapolis, Northern Necropolis. Comparison between the ortophotos derived from the 2017 (high flight altitude) and 2018 (low flight altitude) datasets  | 186 |
| Figure 99 Geometry of image acquisition of the test field on the left (Luhmann et al., 2006). On the right example of some images of the checkboard panel.....   | 190 |
| Figure 100 The wooden checkboard panel used for the calibration procedure. On the left the CNC machine during the cutting phase.....   | 193 |
| Figure 101 Examples of non-suitable environments for the creation of a calibration field. In the left and central images, it's not possible to complete a correct photogrammetric process due to the lack of features in the scene. In the right image the coating of the walls is too reflective. In all the three cases the overall illumination of the scene was not good enough..... | 194 |
| Figure 102 The calibration field and a detail of some of the target distributed on its surface.....  | 195 |
| Figure 103 The classic mount by Freedom 360. The complete kit (left), the 3D printed rig (centre) and the complete system with the six GoPro.....  | 196 |
| Figure 104 The basic Hero 4 kit (left) and the front/back of the action cam (right)  | 197 |
| Figure 105 The 3D printed support design to hold the Hero 4 (left) and the network of the acquired images of the 3D calibration field (right).....   | 199 |

|   |     |
|---|-----|
| Figure 106 The 6 cameras on the Freedom 360 rig (left) and the network of the acquired images of the 3D calibration field (right).....  | 199 |
| Figure 107 RMSe on GCPs and CPs in the eight different photogrammetric projects .....   | 200 |
| Figure 108 Graphical representation of Estimated principal point coordinates of the six cameras separately considered and processed .....   | 201 |
| Figure 109 Graphical representation of the estimated principal point coordinates of the six cameras mounted on the rig and automatically processed with the native Exif information.....                                    | 202 |
| Figure 110 Image residuals for the 360 configuration automatically processed with the native Exif.....  | 203 |
| Figure 111 Graphical representation of the estimated principal point coordinates of the six cameras mounted on the rig and processed after the Exif modification.....   | 204 |
| Figure 112 Sparse cloud. Tie point quality based on reprojection error. 360 configuration: automatic process with native Exif (A), process with modified Exif (B).....  | 206 |
| Figure 113 Visual inspection of the Dense Cloud generated in Photoscan. 360 configuration: automatic process with native Exif (A), process with modified Exif (B).....  | 206 |
| Figure 114 C2C distances analysis performed in CloudCompare with LiDAR data set as ground truth. Max distance set at 0.01 m. 360 configuration: automatic process with native Exif (A), process with modified Exif (B)..... | 207 |
| Figure 115 Freedom 360. Stitching of the six cameras and overlapping areas between images .....   | 208 |
| Figure 116 Camera parameters used in three different approach in AutoPano Giga.....   | 209 |
| Figure 117 Stitching aberration related with the use of different approach for camera interior parameters estimation.....   | 209 |
| Figure 118 GoPro Fusion, 360 camera .....   | 210 |
| Figure 119 Example of two images acquired by back (left) and front (right) cameras of the GoPro Fusion in the same moment.....  | 211 |
| Figure 120 Some phases of acquisition of the 3D calibration field with the GoPro Fusion.....  | 212 |
| Figure 121 Acquisition scheme of the 3D calibration field achieved with the GoPro Fusion and example of acquired images.....  | 212 |

|  |     |
|--|-----|
| Figure 122 Bowl effect on the back camera of the GoPro Fusion. Red lines should be straight walls. Top view of sparse cloud (left) and dense cloud (right).....  | 213 |
| Figure 123 Examples of the images acquired of the printed checkboard for the calibration with Agisoft Lens.....  | 214 |
| Figure 124 Classification of the reprojection errors on TPs of the two cameras separately considered. Threshold set at 5 pixels .....  | 217 |
| Figure 125 The two sample areas analysed: a corner between two walls and a portion of the fire stairs .....  | 218 |
| Figure 126 C2C analysis on the corner wall. TLS set as reference and point cloud from front (left) and back (right) cameras as compared elements.....  | 218 |
| Figure 127 C2C analysis on the stairs. TLS set as reference and point cloud from front (left) and back (right) cameras as compared elements.....   | 219 |
| Figure 128 Semi-automatic sections extracted from the different dataset of the stairs sample .....   | 220 |
| Figure 129 GoPro Fusion. Stitching of the two cameras and overlapping areas between images .....   | 221 |
| Figure 130 Example of spherical image of the calibration field derived from the stitching of front and back camera of GoPro Fusion .....   | 222 |
| Figure 131 View of the acquisition scheme achieved with the GoPro Fusion .....   | 223 |
| Figure 132 C2C analysis on the two sample areas. TLS set as reference and point cloud from 360 images as compared elements. Corner wall on the left and stairs on the right.....   | 224 |
| Figure 133 Valentino, Castle. Example of images acquired with different sensor to object distance.....   | 226 |
| Figure 134 Valentino Castle, 3D models derived from the two 360 datasets acquired at different distances from the object.....  | 227 |
| Figure 135 Examples of “circular” acquisition performed with 360 systems.....  | 231 |
| Figure 136 Rocca San Silvestro, the medieval church. Position of the church on a general plan of the site (left – source: Francovich & Dallai, 2010) and an aerial image of the church in 2016 .....   | 233 |
| Figure 137 Rocca San Silvestro, dataset 1. Acquisition scheme of the data collected in time lapse mode with the Freedom 360. Camera stations showed on an extract of the UAVs orthophoto (left) and on the 3D model in the photogrammetric software (right)..... | 234 |

|   |     |
|---|-----|
| Figure 138 Rocca San Silvestro, graphical representation of the C2C distance analysis on the two photogrammetric datasets of the church compared with the TLS dataset.....  | 236 |
| Figure 139 Rocca San Silvestro, view of a portion of the 3D polygonal model derived from the two photogrammetric datasets.....  | 237 |
| Figure 140 Rocca San Silvestro, view of a portion of the orthophoto derived from the two photogrammetric datasets .....   | 238 |
| Figure 141 Rocca San Silvestro, entrance of the site. Position on a general plan of the site (left – source: Francovich & Dallai, 2010) and an image of the area in 2016..  | 239 |
| Figure 142 Rocca San Silvestro, dataset 2. Acquisition scheme of the data collected in video mode with the Freedom 360. Camera stations showed on an extract of the UAVs orthophoto (left) and on the 3D model in the photogrammetric software (right) ....                   | 240 |
| Figure 143 C2C analysis between the TLS and photogrammetric dataset .....   | 241 |
| Figure 144 Hierapolis, Northern Necropolis dataset 3. Acquisition scheme of the data collected in time lapse mode with the GoPro Fusion. Camera stations showed on an extract of the UAVs orthophoto (left) and on the 3D model in the photogrammetric software (right) ..... | 242 |
| Figure 145 Hierapolis, Northern Necropolis. C2C analysis (left) between dataset 3 and TLS dataset (right) .....   | 243 |
| Figure 146 Hierapolis, Northern Necropolis. C2C analysis (left) between dataset 3 and UAVs 2018 dataset (right) .....   | 245 |
| Figure 147 Hierapolis, Northern Necropolis dataset 4. Acquisition scheme of the data collected in time lapse mode with the GoPro Fusion. Camera stations showed on an extract of the UAVs orthophoto (left) and on the 3D model in the photogrammetric software (right) ..... | 246 |
| Figure 148 Hierapolis, Northern Necropolis. C2C analysis (left) between dataset 4 and TLS dataset (right) .....   | 247 |
| Figure 149 Hierapolis, Northern Necropolis. Scheme of the acquisition performed around a single tomb with the GoPro Fusion.....   | 248 |
| Figure 150 Hierapolis, Northern Necropolis. Examples of aberration that can be present on the orthoimage generated from the 360 dataset.....  | 249 |
| Figure 151 Hierapolis, Northern Necropolis. Co-registration of dataset 3 with the UAVs acquisition.....   | 251 |

|   |     |
|---|-----|
| Figure 152 Graphical representation of the normal distribution of the deviation in the three coordinates components between the camera positions estimated with the co-registration and the traditional approach.....                                   | 252 |
| Figure 153 Rocca San Silvestro, a portion of the church’s floor in 2016 (left) and 2017 (right) .....   | 254 |
| Figure 154 Rocca San Silvestro. C2C analysis between CRP (2016) and 360 dataset (2017).....   | 254 |
| Figure 155 Rocca San Silvestro, dataset 2. Automatic extraction of contour lines, overlaid on the orthophoto (up) and on the shaded representation of the DSM (down).....   | 256 |
| Figure 156 Rocca San Silvestro, dataset 2. Slope analysis performed on the DSM.   | 257 |
| Figure 157 D8 method coding to identify flow direction (left), codification used in this research (centre), schematic representation of the method process of flow direction assignment (right). Source: (elaborated from: Siqueira, et al., 2016)..... | 258 |
| Figure 158 Rocca San Silvestro, dataset 2. Flow direction analysis computed with the D8 method.....   | 258 |
| Figure 159 Flow accumulation computation method. Source: ( <a href="http://pro.arcgis.com">http://pro.arcgis.com</a> )..  | 259 |
| Figure 160 Rocca San Silvestro, dataset 2. Watersheds (top) and the related stream network (down).....  | 259 |
| Figure 161 Hierapolis, Northern Necropolis. Slope analysis on the DSM derived from the processing of the spherical dataset 3 .....  | 260 |
| Figure 162 Hierapolis, Northern Necropolis. Slope analysis performed on different datasets with different resolutions .....   | 261 |
| Figure 163 Hierapolis, Northern Necropolis. Terrain profiles extracted in Qgis with the qProf plugin on the 360 acquisition (dataset 3) .....   | 262 |
| Figure 164 Rocca San Silvestro, dataset 1. Stratigraphic analyses of the west wall of the church (source: Arrighetti, 2017) reported on the orthophoto generated from the Freedom 360 system .....  | 263 |
| Figure 165 Hierapolis, Northern Necropolis. Overlay of the data derived from “Atlante di Heirapolis di Frigia, Vol. II” and the orthophoto generated from the spherical dataset (dataset 3).....  | 265 |
| Figure 166 Research trend (not complete) of the works related with spherical photogrammetry .....   | 279 |





## Abbreviations

**ASPRS:** American Society for Photogrammetry and Remote Sensing

**BBA:** Bundle Block Adjustment

**BIM:** Building Information Modeling

**CAD:** Computer-Aided Drafting

**CCD:** Charge-Coupled Devices

**CH:** Cultural Heritage

**CIPA:** Comité International de la Photogrammétrie Architecturale

**CMOS:** Complementary Metal Oxide Semiconductor

**CNC:** Computer Numerical Control

**COTS:** Commercial Off The Shelf

**CPs:** Check Points

**CRP:** Close Range Photogrammetry

**CV:** Computer Vision

**DIY:** Do It Yourself

**DEM:** Digital Elevation Model

**DLT:** Direct linear transformation

**DMI:** Distance Measuring Instrument

**DTM:** Digital Terrain Model

**DSM:** Digital Surface Model

**DSLR:** Digital single-lens reflex

**EASA:** European Union Aviation Safety Agency

**EMS:** Emergency Management System

**ENAC:** Ente nazionale per l'aviazione civile. Italian Civil Aviation Authority

**ENSG:** Information National School of Geographic Sciences

**E.O.:** Exterior Orientation  
**Exif:** Exchangeable image file format  
**FoV:** Field of View  
**Fps:** Frames per second  
**GCI:** Getty Conservation Institute  
**GCPs:** Ground Control Points  
**GIS:** Geographic information system  
**GPS:** Global Positioning System  
**GNSS:** Global Navigation Satellite System  
**GSD:** Ground Sample Distance  
**GUI:** Graphical User Interface  
**HBIM:** Heritage Building Information Modeling  
**HDR:** High Dynamic Range  
**ICAHM:** International Scientific Committee on Archaeological Heritage  
**ICOMOS:** International Council on Monuments and Sites  
**IGN:** National Institute of Geographic and Forestry  
**IMU:** Inertial Measurement Unit  
**ICAO:** International Civil Aviation Authority  
**I.O.:** Interior Orientation  
**IR:** Infrared  
**ISPRS:** International Society for Photogrammetry and Remote Sensing  
**JCGM:** Joint Committee for Guides in Metrology  
**LiDAR:** Light Detection and Ranging  
**MISP:** Multi-Image Spherical Photogrammetry  
**MMS:** Mobile Mapping System  
**MP:** Mega Pixels  
**MTOW:** Maximum Take Off Weight  
**NIR:** Near Infrared  
**PPK:** Post Processed Kinematic  
**PSP:** Panoramic Spherical Photogrammetry  
**RANSAC:** RANdom SAmples Consensus  
**RC:** Remote Controlled

**RGB:** Red Green Blue

**RMSe:** Root Mean Square error

**ROA:** Remotely Operated Aircraft

**RPAS:** Remotely Piloted Aerial System

**RPV:** Remotely Piloted Vehicle

**RTK:** Real Time Kinematic

**SAR:** Synthetic-aperture radar

**SfM:** Structure from Motion

**SHGM:** Directorate of Civil Aviation

**SIFT:** Scale-invariant feature transform

**SLAM:** Simultaneous Localisation and Mapping

**SURF:** Speeded Up Robust Feature

**SP:** Spherical Photogrammetry

**TIN:** Triangulated Irregular Network

**TLS:** Terrestrial Laser Scanning

**TPs:** Tie Points

**TS:** Total Station

**UAS:** Unmanned Aerial Systems

**UAVs:** Unmanned Aerial Vehicles

**UNESCO:** United Nations Educational, Scientific and Cultural Organization





# **Chapter 1**

## **Low cost image-based solution for Rapid Mapping of CH**

As it will be described in the following sections, Rapid Mapping has been traditionally intended as a tool for the generation of cartographic products in a rapid way through the use of data collected from remote sensing approaches, e.g. satellites or airborne images. In the last years it has undertaken several innovations and developments, connected both with the development of image-based and range-based techniques, Unmanned Aerial Vehicles (UAVs) photogrammetry and with the contaminations with other fields of research. In the following sections the term will be defined, its transformations will be briefly analysed and some consolidated experiences will be reported, the image-based approach will be described, the use of low cost and Commercial Off The Shelf (COTS) systems will be explored with the connected issues, and finally some experiences of rapid mapping in the field of CH documentation will be reported as well.

### **1.1 Rapid Mapping aims and definition**

The definition of the term Rapid Mapping is not widely recognized, generally it is used to indicate the provision of geospatial data in a limited amount of time and with the aim of mapping a determined event or phenomena. This approach is generally adopted in case of emergency scenarios; it ensures the safety of the involved operators, a quick response to the need of rapidly available products and an easy management of data. Several examples can be found in the literature connected to this approach and incapsulated in all the phases of the disaster management cycle (Ajmar, Boccoardo, Disabato, & Giulio Tonolo, 2015; Bitelli, Camassi, Gusella, & Mognol, 2004; Voigt et al., 2011).

As reported in a previous work (Calantropio, Chiabrando, Sammartano, Spanò, & Teppati Losè, 2018), lot of efforts have been devoted inside the geomatics community in this field of research, especially to provide a rapid response in case of emergency scenarios. The main aims of the researchers were connected especially with the attempt to find the best possible balance between resources available and employed, rapidity of the whole process from acquisition to delivery of the products, accuracy of the data and products provided and finally, use of the products for aims of emergency managements, analysis and assessments.

One of the most known and established projects in this sense is represented by the Copernicus Emergency Management Service (EMS), defined as: “*Copernicus is an EU programme aimed at developing European information services based on satellite Earth Observation and in situ (non space) data*”<sup>1</sup>. The most established procedures for services and projects like Copernicus are generally related with remote sensing approaches, as is well documented in the scientific literature techniques that use Light Detection And Ranging (LiDAR) data (Dong & Guo, 2012; He et al., 2016; Kwan & Ransberger, 2010; Li et al., 2008), satellite images (Ajmar et al., 2015; Bitelli et al., 2004; Tralli, Blom, Zlotnicki, Donnellan, & Evans, 2005; Voigt et al., 2007) and airborne aerial images (Ambrosia et al., 2010; Rupnik, Nex, & Remondino, 2014; Vetrivel, Gerke, Kerle, & Vosselman, 2015) are the most diffused.

In the last year the European Commission responsible for the Copernicus programme started to evaluate the possible interaction of Copernicus in support of CH documentation, preservation and management. On April 2017, a workshop titled “Copernicus for Cultural Heritage” was organised in Brussels to tackle the issues connected with this interaction. Moreover, several European founded Horizon 2020 projects are deepening these topics, two examples can be traced in the HERACLES (HERitage Resilience Against CLimate Events on-Site)<sup>2</sup> and PROTHEGO (PROTection of European Cultural HERitage from GeO-hazards)<sup>3</sup> projects.

Several approaches have been proposed and tested over the years to process and interpret the data collected from different sensors, however the most diffused one is still connected with the visual interpretation of the spatial data with the manual works of several operators, like for the maps provided by Copernicus EMS. This is for sure a time-consuming operation and it requires the involvement of several operators. As will be reported in the following sections, the aims of the researchers are moving now in the direction of providing geospatial data at higher scale, reducing the operational time in the field and optimizing the

---

<sup>1</sup> <https://emergency.copernicus.eu>

<sup>2</sup> <http://www.heracles-project.eu/>

<sup>3</sup> <http://www.prothego.eu/home.html>

general workflow through the establishment of standards and guidelines. These aims can be reached also thanks to the developments of both image-based and range-based solutions (aerial and terrestrial) and the availability of new COTS and low-cost sensors.

However, the definition of rapid mapping has gained also other meanings in the past decades and new sensors, techniques, methodologies and applications have been developed as well.

One of the main developments of rapid mapping was connected with the so-called Mobile Mapping Systems (MMSs), an overview of their early developments can be found in (Tao & Li, 2017). MMSs are generally composed from different elements: digital imaging devices and/or ranging devices, positioning and/or georeferencing devices and computational systems. Considering that image-based and range-based systems used for airborne applications were not suitable for the field of application of these systems, other sensors were tested and implemented for MMSs. Imaging sensors that were firstly tested were generally composed of digital frames cameras or action cameras. The configuration of these devices in multiple cameras arrays led also to the development of *ad hoc* sensor solutions; the research field around 360 panoramic cameras widely benefits from these innovations. It was in 2007, with the introduction of Google *Street View* service, that the exponential growth of these systems started for real, and that MMSs became a standard for the documentation of urban area. It is possible to notice that the market of 360 cameras and the development of MMSs gain mutual benefits from their parallel development in the last years.

Likewise, range-based techniques follow a similar path of development in connection with these systems. In a first moment traditional terrestrial laser scanners were adapted to the needs derived from their use on a moving vehicle, thereafter dedicated solutions were projected and developed (Petrie, 2010).

Despite the sensor or sensors employed in an MMS, two are the main challenges for the researchers working in this field: the georeferencing of the data acquired (e.g. Ellum & El-Sheimy, 2002) and their synchronisation (e.g. Blázquez, Colomina, & Castelldefels, 2012). The first sensors employed for the georeferencing of the data acquired from other devices were Global Positioning System (GPS) and Global Navigation Satellite System (GNSS) receivers. On the other hand, for the relative positioning, several solutions can be adopted: generally Inertial Measurement Unit (IMU) or Distance Measuring Instrument (DMI) approaches are used.

As already reported, one of the most challenging aspect of these systems is connected with the synchronisation and processing of all the data collected by these platforms equipped with multiple devices acquiring in the same moment.

Indeed, the miniaturisation of sensors and electronic components and the development of the researches connected with this sector created new scenarios in the last years in the field of rapid mapping.

On the one hand the exponential growth and development of UAVs connected to the new available sensors led to the successful deployment of these platforms for rapid mapping applications. On the other hand, the portability that MMS reached allows to expand their deployment also for other applications (such as operation of indoor mapping).

Moreover, contaminations with other fields of research are producing new progress in the field of rapid mapping and MMS. One of this contamination with the field of robotic research on mapping and navigation has for example produced Simultaneous Localisation and Mapping (SLAM)-based MMS that use the homonymous algorithm (Riisgaard & Blas, 2004).

The research presented in this thesis will focus only on image-based approach, more specifically the potentialities derived from the use of 360 cameras and UAVs for rapid mapping applications on the field of CH documentation will be further tested and analysed, for further information connected to other MMS approaches is possible to refer to the dedicated literature (e.g. Chiabrandò, Sammartano, & Spanò, 2017; Jaakkola et al., 2010; Pellenz, Lang, Neuhaus, & Paulus, 2010; Sammartano, 2018) .

## **1.2 Image-based approach (aerial and terrestrial)**

The advantages of image-based techniques will be further described in Chapter 3, in relation to CH documentation, however it is possible to report almost the same advantages for other fields of applications.

As reported by Patias about CH in (Fryer, Mitchell, & Chandler, 2007): “[...] *photogrammetry is called upon to offer its services at a variety of levels and in all possible combinations of object complexities, scientific procedures, quality requirements, usage of final products, time restrictions and budget limitations*”; this statement fit perfectly the contribute that photogrammetry can provide not only in the field of CH documentation but also in other fields of application.

Concerning the aerial point of view, even in the sector of rapid mapping, the exponential development and diffusion of UAVs and their deployment in the photogrammetric procedures represented a ground-breaking element. They became a complementary, or even a substitute, of previously consolidated approaches such as remote sensing techniques or airborne images. Several experiences have been conducted by the community of the researchers in the last years (Boccardo, Chiabrandò, Dutto, Tonolo, & Lingua, 2015; Duarte, Nex, Kerle, & Vosselman, 2017; Ezequiel et al., 2014; Rester, Spruyt, De Groeve,

Damme, & Ali, 2013) in order to evaluate their use in real case scenarios. Generally, they have proven to be a valuable solution for the provision of higher resolution data if compared to more consolidated approaches and secondly, they are easier and safer to deploy. Moreover, UAVs allow to acquire data below the cloud line, thus being less affected from weather conditions compared to airborne or satellite techniques. The integration of nadir and oblique images is another key element for the success of this technique and for the provision of high detailed 3D models, this topic has been stressed by several authors (Aicardi, Chiabrandò, et al., 2016; Duarte et al., 2017; Rupnik et al., 2014; Vetrivel et al., 2015) and it became almost a consolidated approach. In an emergency scenario, UAVs contributed in the last years to several phases of disaster cycle management: supporting activities of first aid support and intervention, to assist the phases of Building Damage Assessment, to grant a continuous monitoring of buildings and infrastructures and to support all the post disaster and reconstruction phases.

An analysis of the contribute that UAVs can supply in all this phases and their integration with more consolidated procedure can be found in the previously cited work (Calantropio, Chiabrandò, Sammartano, Spanò, et al., 2018). In the scenario presented in that research the contribute of the data collected through UAVs platform was crucial to integrate the products provided by the traditional techniques; the 3D component was especially useful to aid the interpretation of the damages. In the same scenario, they also allow to work on more detailed scales, as reported in another work presented in 2017 (Chiabrandò, Di Lolli, et al., 2017) that exploited the possibility to deploy UAVs systems also on singular buildings and analysed how these systems can be combined with other approaches to provide rapid mapping solutions. Moreover, approaches of rapid mapping using UAVs have become widespread also in other fields of application and are a consolidated practice, as will be further describe in section 3.7.

On the other hand, the use of terrestrial systems for rapid mapping approaches have been developed simultaneously with the deployment of UAVs in this sector. This development can be explained thanks to the availability of low cost and COTS solutions and to the enhancement of image-based algorithms and approaches also for these kinds of sensors. Moreover, the development of the so-called geo-information crowdsourcing granted new possibilities for the collection of data derived from different sources that can contribute to the rapid mapping of a determined area. New platforms were developed in order to organize, manage and share these data: OpenStreetCam<sup>4</sup> and Mapillary<sup>5</sup> are two of the examples of these kinds of platforms. Services like these are similar to the ones developed by Google and allows to share georeferenced images connected to 2D maps.

---

<sup>4</sup> <https://www.openstreetcam.org>

<sup>5</sup> <https://www.mapillary.com/>

The technological solutions that led the revolution in this sector are related with the diffusion of action cameras with on-board GPS/GNSS sensors, 360 cameras with the same characteristics and to the upgrading of the sensors embedded in personal devices such as smartphone and tablet. Furthermore, photogrammetric software solutions were developed and adapted to enhance the processing of the data derived from these types of sensors.

In the case of smartphone, the growing quality of the cameras embedded in the device is coupled with the growing number of sensors, allowing different tests in emergency scenarios with a device that almost everyone possess and is available at a quite low cost (Dabove, Di Pietra, & Lingua, 2018; Fritsch & Syll, 2015). Action cameras and other sensors, such as steadicam, can be successfully used for rapid mapping purposes as well (Balletti, Guerra, Tsioukas, & Vernier, 2014; Calantropio, Colucci, & Teppati Losè, 2017; Calantropio, Patrucco, Sammartano, & Teppati Losè, 2018; Gonçalves, Pérez, & Duarte, 2018). In the same way, also omnidirectional cameras, or in general spherical images, can be used in this and other scenarios where the time component is crucial (Cingolani & Fangi, 2011; D'Annibale, Piermattei, & Fangi, 2011; Fangi, 2015a; Kwiatek & Tokarczyk, 2014). For the aim of this thesis, it is now important to define and clarify how are intended in this work the concepts of low cost and COTS before advancing further in the dissertation.

In this research low cost is intended as: “*cheap, or not costing as much as other things of the same type*”<sup>6</sup>, e.g. a 360 camera worth \$1000 can be considered cheap if the top level products of the same type can cost up to \$40000.

Commercial Off The Shelf (COTS) is defined as: “*COTS (Commercial off-the-shelf) satisfy the needs of the purchasing organization, without the need to commission custom-made*”<sup>7</sup>. This definition can be often associated with the definition of Mass Market: “*A product that is designed for the mass market is intended to be bought by as many people as possible, not just by people with a lot of money or a special interest*”<sup>8</sup>.

These two definitions have influenced the choice of the sensors to test and deploy on the field, the adopted approaches and, partially, also the overall outline of the work.

### 1.3 Georeferencing problems and strategies

One of the main issues related with the use of these rapid mapping approaches is related with the georeferentiation of the products, and for the image-based approach also on their scaling. The phase of the planning, distribution and measurement of Ground Control Points

---

<sup>6</sup> <https://dictionary.cambridge.org/dictionary/english/low-cost>

<sup>7</sup> [https://en.wikipedia.org/wiki/Commercial\\_off-the-shelf](https://en.wikipedia.org/wiki/Commercial_off-the-shelf)

<sup>8</sup> <https://dictionary.cambridge.org/it/dizionario/inglese/mass-market>

(GCPs) is for sure one of the most time consuming on the field and in case of post disaster scenarios, even one of the most dangerous for the operators involved. Several strategies can be adopted to solve this issue:

- *Traditional/standard strategy.* In this approach a large number of pre-signalized targets (some examples of different typologies of targets are shown in Figure 1), or natural features, where it is not possible to position the targets, is placed on the scene that need to be surveyed and then measured with traditional topographic techniques (TS or GPS/GNSS). A bigger number of targets allows also a higher redundancy of the measurements that can be used to ensure the quality of the overall photogrammetric process. The targets need to be homogenously distributed all over the scene and clearly recognizable on the acquired images. This is the most consolidated and reliable approach, but also the one that requires the major efforts and time on the field.



*Figure 1 Some examples of different typologies of codified targets*

- *Enhanced strategy.* This strategy is derived from the traditional one, but it aims in reducing the number of targets adopting some shrewdness, e.g. with a combination of different acquisition schemes together, using oblique images, etc. Further information can be found for example in (Aicardi, Chiabrandò, et al., 2016; Calantropio, Calantropio et al., 2018; Chiabrandò, Lingua, Maschio, & Teppati Losè, 2017; Chiabrandò & Teppati Losè, 2017).
- *Direct georeferencing.* This strategy is traditionally adopted in the field of remote sensing. In airborne photogrammetry, for example, the combination of GPS/GNSS sensor and IMU platforms mounted on the aircraft with a known geometry of the camera employed allows to retrieve both Interior Orientation (I.O.) and Exterior Orientation (E.O.) parameters and achieve accurate products. With the development of UAVs and the implementation of the on-board sensors, this strategies can be transposed also to low-altitude dataset acquired with unmanned

platforms (Calantropio et al., 2018; Fazeli, Samadzadegan, & Dadrasjavan, 2016; Stöcker, Nex, Koeva, & Gerke, 2017). MMS are also adopting similar strategies, synchronizing data derived from positioning systems with the data of the other sensors mounted on the platform.

- *Co-registration with other data.* Another strategy, that has been particularly researched in the last years, is related with the co-registration of data with other datasets already acquired, adopting a multitemporal or multi-sensor approach. This approach can be performed following different strategies, and despite being not-always easy achievable, it can return really promising outcomes.

The choice of the best strategy to adopt is related with several factors. If the system employed (e.g. if the UAVs platform employed is equipped with and Real Time Kinematic -RTK- or Post Processed Kinematic -PPK-, or with inertial sensors) it is possible to rely on quite accurate positioning data and perform a direct georeferencing of the camera stations, solving E.O. directly and in a quick way. The number and position of the GCPs on the ground is highly influenced by the flight plan that will be adopted (as will reported in section 4.1.2), the dimension of the area to cover within the survey and the conformation of the area (morphological conformation, dangerous areas, etc.). The co-registration strategy is highly influenced by the source of available data, it can be performed processing the data together or extracting information from older dataset to be used in the most recent, e.g. coordinates of natural features that can be used as GCPs.

Moreover, the accuracy of the requested products from the survey need to be carefully evaluated in order to adopt the right strategy.

These strategies, except for the direct georeferencing, were adopted and tested in this research, both for aerial datasets (as will be reported in section 4.1.2) and both for terrestrial datasets (as will be reported in section 4.3.4).

## **1.4 Rapid Mapping application in archaeological/architectural heritage**

It has been reported in the previous sections that the rapid mapping approaches are generally related with emergency scenarios and disaster management conditions. However, especially in the last years, this approach has been adopted also for the documentation of CH, due to several reasons. In general terms it is possible to say that the resources for the documentation of heritage artefacts have been constantly decreasing and consequently a general optimisation of the documentation process needed to be achieved. This

optimisation involved the type of instruments to use on the field, their cost, and also the time to spend for the fieldwork, leading to the necessity to perform the acquisition in a more rapid way. Secondly, CH was subjected to several dangers and destructions all over the world, both manmade and natural; this fact shed a light on the necessity to develop instruments that can safeguard at least the memory of these places through a rapid and as much exhaustive documentation as possible.

For these purposes, the first approaches were again derived from the remote sensing field testing airborne images, LiDAR and satellite images (Fernandez-Diaz et al., 2014; Keay, Parcak, & Strutt, 2014; Morrison, 2013). Other experience reported on the use of image-based and range-based techniques on the same contexts but on a different scale (Campana & Remondino, 2008; Hayakawa et al., 2007; Mara, Breuckmann, & Lang-Auinger, 2009; Richter, Kuester, Levy, & Najjar, 2012).

In this work two main approaches were tested for the rapid documentation of archaeological heritage: the use of UAVs (section 4.1) and the use of 360 immersive cameras (section 4.2).

## Chapter 2

### The needs of documentation in Archaeology and the Geomatics response

The study of the past and the definition of *Archaeology* have an history that can be traced almost through all the human evolution. Every civilisation, in a certain moment of its development, have felt the need to face itself with the people that have lived before, especially if they left behind prominent material evidences. The word archaeology is derived from the Greek *ἀρχαιολογία*, composed by the words *ἀρχαῖος* (ancient) and *λόγος* (intended in this case as study). The Greek historian Thucydides (V century B.C.) is one of the first authors that used the term archaeology related with the concept of understanding and studying ancient civilizations. Starting from this embryonic stage, the discipline undergone several evolution steps, till its modern formulation, and is still evolving. It is possible to state that there is a gap between Thucydides first formulation of the term and its next step of evolution in meaning and function. Only during the Humanism (XV century) a new interest was raised in this field: the will of rediscover the classical culture of the past, in order to create a cultural revolution after the so called “dark centuries”, gave new life to all the disciplines related to the historical research and study. This phase can be considered as the first moment in which the structure of archaeology as a discipline started to be defined. The interest that reside in this period is not only related with the rehabilitation of the texts of the authors of the past, but especially with the rediscovery of the material evidences left behind by the past civilisations. The first collections of artefacts from the past started already in the first half of the XV century and were promoted by the most influencing and powerful families of Italy; the first core of the Vatican Museums, for example, was established in this period. In the XVII and XVIII centuries Italy maintained a central role, but countries all over Europe started also to give their massive contribution to the study of the past. In these two centuries it is possible to trace massive travels of scholars, especially towards Greece and in general the East part of Europe. What is important to underline about this phase of evolution of the historical/archaeological studies is the will of documenting the traces of the past: the study of the drawings and descriptions of the archaeological sites between XVII and XVIII centuries, with all its related issues concerning the reliability of this products, is still nowadays an independent sector of research. Examples like the one from Canaletto (Figure 2) represents a precious source of

information of the condition of a determined artefacts in a precise moment; obviously all the issues related with the personal perception of the artist need to be carefully considered.



*Figure 2 Ruins of the Forum, Rome, (c. 1743). Bernardo Bellotto. Source: Melbourne, National Gallery of Victoria (<https://www.ngv.vic.gov.au/>)*

Moreover, it is possible to glimpse in this will of documenting the evidences from the past a sort of awareness of the vulnerability of these old artefacts and a consciousness of the importance of transfer their knowledge to the future generations. This will can as well be traced in the foundation of museums all over Europe in this period.

In the XVIII century field archaeology was born and big campaigns of excavations were started, the adopted methodology and the purposes of this excavations were still far from the modern conception of archaeology, but all the different elements that will lead to its conformation were already there.

In the half of the XVIII century, an event that can be considered as the first systematic archaeological excavations of history started: The Bourbons dynasty began excavating the ancient cities of Pompei and Ercolano. For the following fifty years the works (which were still very far from the modern archaeological structure of excavation) unearthed several buildings of the two cities; in the meantime, a lot of ancient materials were dispersed all over Europe. The two cities were also involved in the political, military and economical facts of the next century. In the half of the XIX century Giuseppe Fiorelli became the head of the excavations and something started changing in the documentation and dissemination of the data collected in the field. Within the progress of these big campaigns it became clear the need to collect, organize, document and publish the huge amount of data coming from the field in order to better understand them.

In the same period, thanks to the development of the Neoclassical movement and through the writings of personalities like Johann Joachim Winckelmann (1717-1768), the artworks of the past gained a central role in the culture of the time, especially the one of Greek and Roman periods. The writings of these years are more related with the history of arts, however, they had a strong influence also on the archaeological studies.

Heinrich Schliemann (1822-1890) is one of the most controversial figures in the history of evolution of archaeology, he was one of the first scholars that tried, with a good degree of success, to combine the study of the written sources with the research on the field. Moreover, he was really meticulous in documenting through his diaries the progresses of his researches. The drawbacks of his work derive as well from his qualities: he became too confident and uncritical towards the ancient literature and too subjective in the writing of his memories.

What can be really considered a turning point in the history of archaeology is the adoption of the stratigraphic method: the concept itself is derived from geology, in this field it was developed in the XIX century, however it took another century to be introduced and refined in the archaeological discipline. It was Sir Robert Eric Mortimer Wheeler (1890-1976) the first to adopt the stratigraphic methodology in his excavation of Maiden Castle during the '30s of the XX century. The awareness that every layer is important, and consequently also the relations between the different layers, led to an evolution both in the role and in the process of documentation in archaeology (Figure 3). The concept that not only the structures but also single layers and all the artefacts position needed to be documented was slowly developing in the community of archaeologists.



***Figure 3 On the left Mortimer Wheeler during Maiden Castle excavation (Source: UCL - University College London<sup>9</sup>). On the right example of a modern excavation conducted with Wheeler grid method (Monticello Department of Archaeology - Virginia<sup>10</sup>)***

<sup>9</sup> <https://www.flickr.com/photos/uclnews/6891372331>

<sup>10</sup> <https://www.daacs.org/sites/east-kitchen-yard/#home>

It was only in the 80's that Edward Harris set up and wrote down the rules of archaeological stratigraphy and their representation principles (Harris, 1989). The Harris methodology led to a real revolution in the world of archaeology and is still today one of the main pillars of the discipline, widely accepted all over the world.

Finally, an overview on a crucial point in the evolution of the discipline must be briefly cited: the long debate between *processual* and *post-processual* archaeology. To summarize, and simplify, the main point of *processual* archaeology resides in a rigorous "faith" in the scientific method with the aim of overcome the limits of the historical approach of archaeology and collect as many data as possible from every single evidence. Processual archaeologists are focused on the study of cultural processes that led to the evolution of past civilization. On the other hand, *post-processual* archaeologists emphasize the subjectivity of archaeological research and researchers in the process of interpretation. This debate was also alimeted by the evolution of computers and digital technologies in general, occupied a span of time of around thirty years in the archaeology communities and, even today, is still open. However, it is possible to say that archaeologists came to a compromise between these two schools of thoughts: considering the human subjectivity in the interpretation process and trying to obtain the higher objectivity from the application of the scientific method. All these factors led to a final reflection about the nature of archaeology, that need to be considered as a discipline and not as a science: it uses the methodology derived from the scientific approach, but it doesn't possess all the characteristics of a traditional science.

One of the most evident characteristics that is missing in this comparison is the impossibility of iterate the experiments: this is particularly true in case of excavations. Once a layer is perturbed or removed, it is destroyed or modified forever. Therefore, a rigorous, complete, standardize and accurate documentation is mandatory. The same concept is valid also in the other fields of application: even small artefact or buildings are subject to (hopefully) slow, but constant decay and their documentation is therefore a crucial point. The other issue that need to be considered is that archaeology is constantly evolving due to its intrinsic nature (every new discover can create new theories and set a term of comparison) thus, what seem insignificant today, can became important tomorrow and vice versa. This is another significant point that need to be considered while setting up the standard for the documentation of archaeological artefacts (as it will be reported in section 2.2.2).

All these factor considered, it is possible to underline that archaeology and geomatics are influencing each other: the methodologies of geomatics are somehow modifying archaeological approaches (Roosevelt, Cobb, Moss, Olson, & Ünlüsoy, 2015; Sapirstein & Murray, 2017) to documentation (archaeologists are starting thinking more in three

dimensions and transpose reality in 2D only in a second phase) and in parallel, geomatics is trying to adapt and enhance its techniques and methodologies to respond to archaeological needs (Balletti, Guerra, Scocca, & Gottardi, 2015; Dell'Unto, Landeschi, Apel, & Poggi, 2017; Remondino & Campana, 2014).

## **2.1 The four scales in archaeological documentation**

To clarify more in depth the documentation problem in archaeology it is possible to analyse the main different scales in which archaeologists operates: Landscape, Building, Field and Detailed. These four scales are adopted in all the different chronological declinations of archaeology (Prehistorical, Classic, Medieval, Industrial, etc.) and are directly related with the general methodological framework adopted by the discipline. The four scales will be presented in a decreasing order, starting from the smaller scale to the largest. Each scale responds to the peculiar needs of the different field of research and application. Thus, a direct correspondence between the four scales and the different sectors of the discipline is not fixed, the division defined here is intended as a set of complementary methodologies and applications that contributes to the general study and understanding of a context and/or a general wider research question. The four scales, that operate with a common background but with peculiar methodologies, need to be integrated together with a common aim of research; these considerations need to be taken in account also for the documentation at these different scales ( as will be described in section 2.3).

### **2.1.1 Landscape Archaeology**

The definition of landscape archaeology can be traced back in the late '70 when the term began to be used and this area of the discipline start to shape its aims, instruments and methodologies. Landscape archaeology aims to analysing how the human action and interactions have modified the surrounding environment during time and tries to reconstruct the appearance of the historical landscape in a specific period. The growth of this field of research was particularly stimulated from the development of new geographical tools and resources, such as Geographic Information System (GIS) and remote sensing, as will be reported in section 2.3.2. The main development of landscape archaeology is again related with the debate between *processual* and *post-processual* archaeologists: the first ones are responsible for the introduction of the latest technological advancements in this field, while the second helped in differentiate the points of view in the researches conducted in this sector of the discipline. Between the main technological advancements that contributed to landscape archaeology it is possible to indicate for example GPS/GNSS,

GIS, Remote Sensing and Aerial Photogrammetry. On the other hand, in the study of historical landscape the introduction of a more human-centred view changed the approaches of different schools of researchers. It became important not only the reconstruction of the landscape itself in a determinate period, but also how the people living in that landscape influenced the shaping of environment and, vice versa, how the environment influenced humans and their activities.

Like almost every “subdiscipline” in archaeology, the landscape archaeology is highly multi- and inter- disciplinary. It involves expertise from different scientific sectors, among the other: geomatics, geophysics, economy, ecology, geography, historical studies, sociology, anthropology, etc.

### **2.1.2 Building Archaeology**

The field of building archaeology was methodologically defined thanks to a joint effort of researchers working in different Italian groups at the end of the '70 (Brogiolo, 2002). The first area of research that strongly contributed in this sector was the one of medieval archaeology; the main evolution step in this sector of the discipline can be identified in the transposition of the stratigraphic methodologies to the study of the built heritage and to the foundation of a new sector of archaeology that is methodologically partially independent from the history of architecture. In the same years some considerations about the documentation and representation of the different phases of the building history of sites and buildings were achieved as well. As reported by one of the main founder of the building archaeology in Italy (Parenti, 2002), what really characterize this field of archaeology is the possibility to study any building artefact (despite the existence of other historical sources) and without any prejudice. At the same time, the contributes of other disciplines are fundamental in order to gather and extract all the possible existing information from the historical structures. As is reported before, building archaeology is a quite young sector of the discipline and it uses both the instruments refined by the older sectors of field archaeology and the new technological advancements. One of the differences between building archaeology and field archaeology is that the first is configured as a non-destructive operation, except for small collection of samples for chemical analyses that are usually non-invasive. More specifically, it is possible to describe building archaeology as the process of historical reconstruction of a building through direct observations of specific markers on the fabric: materials, connection between elements, gaps and continuity, building techniques, etc. These material sources are thereafter integrated with other sources such as written and iconographic. Usually all the different sources contribute together to

date the different building phases: both to a relative and absolute chronology (Brogiolo & Cagnana, 2012).

Even in this sector of archaeology the documentation phase is really important and, again, geomatics techniques (in a first-time laser scanner and then photogrammetry) represented a big change in the process of research.

It is interesting to notice that in this field the contribute of geomatics developed earlier if compared with other sectors of archaeology thanks to the affinity between building archaeology and architecture.

### **2.1.3 Field Archaeology**

It is possible to trace in the literature different definitions of field archaeology (Drewett, 1999), but generally it encompasses all the activities that archaeologists can achieve on the field. However, in this research the definition will be further circumscribe: field archaeology will coincide with the process of excavation and all the activities related with it. As Drewett reported: *“Excavation remains, however, both the most detailed and the most destructive, and yet potentially the most informative, technique available to the field archaeologist”*. The destructive nature of field archaeology is clearly underlined in this sentence and again the importance of documentation in this process is evident. Moreover, in Drewett’s definition is also important to notice that excavation is referred as the most potentially detailed and informative action than archaeologists can undertake. Archaeologists have always been aware of the destructive nature of their discipline and thus recording not only the findings but also the process of excavation has always been a priority. In addition, documentation phases have been, and are still today, considered as part of the interpretative process. Photography was largely used for the documentation of excavations, thanks to its capability to record all the main characteristics of a scene in a precise moment. This massive use of photography opened the way for the further deployment and diffusion of photogrammetry in this field of archaeology.

### **2.1.4 Detailed Archaeology**

The more detailed section of archaeology, and maybe also the more complex in terms of documentation activities, is the one that can be defined as detailed archaeology or micro-stratigraphy. This sector of archaeology works on the recognition and interpretation of the relations between small elements. The origin of this branch of the discipline was highly stimulated from the prehistorical archaeology. Material evidences of the period investigated from this kind of archaeology are in fact fewer and fainter compared with the

historical ones. Generally, also the stratigraphies identifiable on the field are thinner and their relations more complex to understand. All these factors led to a greater attention in the recognition of small interfaces and interactions between the different layers. Detailed archaeology can vary in scale between centimetres and millimetres, from small artefacts, layers connections to chemical and physical analyses. During the evolution of the discipline these techniques have been applied also to other contexts and chronological periods. Micro-stratigraphy was successfully applied to the study of frescos and wall paintings to identify the different periods of work of the artists or the subsequent modifications to the artwork. Likewise, these techniques can be adopted for the study of the coating of the buildings. Thus, detailed archaeology can contribute also in the definition of the different building phases of a structure. Moreover, is possible to comprehend in the scale of micro also the study of small findings and artefacts. In this case the object of interest can vary for different characteristics such as materials, shape, dimensions, etc. and the documentation techniques adopted need to be chosen according to all these factors.

## **2.2 Norms and standards for the documentation of Cultural Heritage**

The International Organisation for Standardisation (ISO), one of the major international organisation responsible of the issuance of standards, defines a standard as: “*A document established by consensus and approved by a recognized body that provides for common and repeated use, rules, guidelines or characteristics for activities or their results, aimed at the achievement of the optimum degree of order in a given context*” (ISO/IEC Guide 2:2004).

Starting from the first half of the XX century it appears clear the need of setting up standards for CH documentation, in order to better study, preserve and restore them; the first achievements in this sense are the International Charters (a brief history of their origin and evolution will be reported in the following section 2.2.1).

The definition of standards in the field of documentation have always been a central and crucial point and still today it is an issue non-totally solved. One of the main problems can be traced in the word *consensus*, embedded in the ISO definition of standard. The biggest challenge is in fact to find a common point of view between all the parties involved in the process of documentation. The geomatics community was also focused on researching and reflecting on this topic, in order to define the best strategies and practice to employ its own instruments and methodologies.

Several initiatives were undertaken during the last decades to set up standard among the geomatics community, an overview of the principal actions that were performed in this

sense will be reported in the section 2.2.2. A main issue reside in the process of communication between the producers of the documentation and the users. The main international societies involved in the documentation processes (CIPA<sup>11</sup>, ISPRS<sup>12</sup> and ICOMOS<sup>13</sup>) tried in the past decades to bridge the gap between these two categories; the RecorDIM project, the Metric Survey Specifications for Cultural Heritage, the 3x3 rules represents some of the efforts in this direction and will be described in section 2.2.2. Unfortunately, up to date, despite these efforts, there are no widely recognize standards for the documentation of CH, and ad hoc specifications are usually created for every single survey episode. Another problem is that specifications are usually not able to catch up with the technological development, and their aging is quite fast.

### **2.2.1 International charters<sup>14</sup>**

The first document that placed the focus also on the documentation of CH was the Athens Charter in the 1931, during the First International Congress of Architects and Technicians of Historic Monuments. Among the seven points contained in this document it is suggested that *“Each country, or the institutions created or recognised competent for this purpose, publish an inventory of ancient monuments, with photographs and explanatory notes”* and *“Each country constitute official records which shall contain all documents relating to its historic monuments”*.

It is only after thirty-three years, with the Venice Charter, that the attention was again focused on the issues related with the documentation of CH. The Venice Charter for the Conservation and Restoration of Monuments and Sites was developed in 1964 by the Second International Congress of Architects and Specialists of Historic Buildings, adopted by ICOMOS (International Council on Monuments and Sites) in 1965. In fact, ICOMOS was created as a result of the Venice Charters. In this chart two articles are of particular interest for our reflection:

---

<sup>11</sup> <http://cipa.icomos.org/>

<sup>12</sup> <http://www.isprs.org/>

<sup>13</sup> <https://www.icomos.org/en/>

<sup>14</sup> The integral texts of the Charters cited in this paragraph are available on <https://www.icomos.org/en/resources/charters-and-texts>

- Article 2. “*The conservation and restoration of monuments must have recourse to all the sciences and techniques which can contribute to the study and safeguarding of the architectural heritage.*”
- Article 16. “*In all works of preservation, restoration or excavation, there should always be precise documentation in the form of analytical and critical reports, illustrated with drawings and photographs. Every stage of the work of clearing, consolidation, rearrangement and integration, as well as technical and formal features identified during the course of the work, should be included. This record should be placed in the archives of a public institution and made available to research workers. It is recommended that the report should be published.*”

It is interesting to notice that for the first time in an international document the crucial role of *precise* documentation is underlined and that this kind of documentation needs to be repeated during the different stages of research and restoration that will interested the cultural artefact.

The *Convention for the protection of the architectural heritage of Europe* written in Granada in 1985 was ratified by 42 members of European Union and aims at establishing a common framework for conservation policies in Europe. Even in this case documentation is indicated as an important practice that need to be realised as soon as possible for the CH of each state.

The Washington Charter, titled *Charter for the Conservation of Historic Towns and Urban Areas*, was written and adopted in the 1987 by the ICOMOS General Assembly and recognised a series of guidelines for the intervention of conservation in historic urban areas. The chart aims to integrate the principles of Venice Charter, widening the horizon from the single monuments to the general historic urban areas. As for the Venice Charter it is reaffirm the principle that “*before any intervention, existing conditions in the area should be thoroughly documented*”.

In 1990 the work of the International Scientific Committee on Archaeological Heritage Management (ICAHM) led to the adoption of the *Charter for the Protection and Management of the Archaeological Heritage* by the General Assembly of ICOMOS. This chart is totally focused on Archaeological Heritage and is highly influenced by the methodological maturity that the archaeological discipline was reaching in that period. Concerning our topic, two articles are particularly of interest:

- Article 4. *“The protection of the archaeological heritage must be based upon the fullest possible knowledge of its extent and nature. General survey of archaeological resources is therefore an essential working tool in developing strategies for the protection of the archaeological heritage. Consequently archaeological survey should be a basic obligation in the protection and management of the archaeological heritage. At the same time, inventories constitute primary resource databases for scientific study and research. The compilation of inventories should therefore be regarded as a continuous, dynamic process. It follows that inventories should comprise information at various levels of significance and reliability, since even superficial knowledge can form the starting point for protectional measures.”*
- Article 5. *“Archaeological knowledge is based principally on the scientific investigation of the archaeological heritage. Such investigation embraces the whole range of methods from non-destructive techniques through sampling to total excavation. It must be an overriding principle that the gathering of information about the archaeological heritage should not destroy any more archaeological evidence than is necessary for the protectional or scientific objectives of the investigation. Non-destructive techniques, aerial and ground survey, and sampling should therefore be encouraged wherever possible, in preference to total excavation. As excavation always implies the necessity of making a selection of evidence to be documented and preserved at the cost of losing other information and possibly even the total destruction of the monument, a decision to excavate should only be taken after thorough consideration. [...]”*

The principles contained in these two articles recall what was partially described in chapter one. One of the main issues in archaeology is the need of carefully document all the possible evidences connected to an artefact or a site, at different scales. The discipline is often compelled to be partially destructive and thus the role of documentation became crucial. After fixing these points, it became quickly clear for the scientific community that a multi- and inter-disciplinary approach was mandatory, in order to collect the best quality and quantity of information as possible from an archaeological artefact.

The *Charter on the Protection and Management of Underwater Cultural Heritage* adopted by ICOMOS six years later in 1996 reiterate that the same principles of documentation need to be adopted also for underwater Cultural Heritage. Article 8 state: *“All investigation*

*must be thoroughly documented in accordance with current professional standards of archaeological documentation. Documentation must provide a comprehensive record of the site, which includes the provenance of underwater cultural heritage moved or removed in the course of investigation, field notes, plans and drawings, photographs and records in other media”.*

In the same year, 1996, the *Principles for the recording of monuments, groups of buildings and sites* were conceived and adopted. The chart state that “[...] *recording is one of the principal ways available to give meaning, understanding, definition and recognition of the values of the cultural heritage[...]*” and it is organised in five main subsections:

- *The reasons for recording.* Several reasons can be reported in this case. First of all, recording CH is important to increase our knowledge of heritage and its evolution. The recorded data can then be used to involve people and let them acknowledge the value of CH and its preservation. Moreover, it is a fundamental medium to aid management and maintenance of CH.
- *Responsibility for recording.* National level of commitment should be present. People involved in the documentation process should possess adequate skills and sensibility and inter-disciplinary cooperation should be pursued. There should be people in charge of controlling the process of documentation and assure the quality of the derived products.
- *Planning for recording.* The importance of the preliminary phase of planning of the survey is here underlined. First, all the existing sources of information of the CH artefact must be retrieved. After this preliminary research, the effective survey must be planned and prepared: the appropriate techniques to employ must be selected in relation with the artefact characteristics, attended results and expected level of detail.
- *Content of records.* This section describes all the fundamental information that should be reported in the final survey products. Different aspects concerning the preparation of the survey reports are reported as well.
- *Management, dissemination and sharing of records.* The last section is dedicated to the archiving of the data collected and processed, the standard to use and the accessibility of the documents.

All the five sections aim to define some general principles related to the whole process of documentation of a heritage artefact.

The *Principles for the preservation and conservation/restoration of wall paintings*, discussed and adopted in 2003 are centred on wall paintings and the importance of documentation is again underlined in this document.

Some important indication can be found also in the documents produced by the United Nations Educational, Scientific and Cultural Organization (UNESCO). In the General Conference of the 1956, held in New Delhi, UNESCO adopted the *Recommendation on International Principles Applicable to Archaeological Excavations*. Among the other recommendation present in the document it is interesting to report the attention the UNESCO dedicated to documentation of the archaeological heritage that suggest the creation of national bodies that need to set up central documentation offices for this kind of heritage. Another important document is the *Manual for Activities directed at the Underwater Cultural Heritage*, published in 2011 and derived from the *UNESCO Convention on the Protection of the Underwater Cultural Heritage, adopted in 2001*. Among the different rules established from the convention it is important to underline the contents of rule 26 and 27:

- Rule 26. *“The documentation programme shall set out thorough documentation including a progress report of activities directed at underwater cultural heritage, in accordance with current professional standards of archaeological documentation.”*
- Rule 27. *“Documentation shall include, at a minimum, a comprehensive record of the site, including the provenance of underwater cultural heritage moved or removed in the course of the activities directed at underwater cultural heritage, field notes, plans, drawings, sections, and photographs or recording in other media.”*

The principles reported in these two rules are similar to what is reported also in other international documents already cited in the text, despite being focused on the underwater heritage. However, it is probably missing a similar document focused on the “ground” archaeological heritage.

Starting with Athens Charter in 1931 till today, all these documents aimed to define general principles that need to be considered and followed when approaching the study, restoration, conservation and dissemination issues related with a CH artefact. From the inspiring principles of these charters several technical documents were derived and a brief description of part of them will be reported in the following section.

## 2.2.2 Examples of principles, guidelines and specifications for CH

One of the most known and detailed system of specification for CH is for sure the one of the **Metric Survey Specifications for Cultural Heritage**, published by the English Heritage (Andrews, Bedford, & Bryan, 2009). The text is divided in eight sections, the first three sections describe the “*general terms, performance and presentation requirements common to all services* (Andrews et al., 2009)”, while the other five sections contain specific standards related with the techniques employed during the survey:

- **Section 1:** General conditions and project information. This section refers to all different aspects that need to be taken into account to write an agreement between the customer and the operator. All the aspects of the contract are explained and good practices are reported starting from a brief project of the survey and of the techniques that will be deployed till the legal and safety aspects related to the operations on the field.
- **Section 2:** General performance and control of metric survey. The general performances and requirements of the metric survey are stated (they will be further detailed in the sections dedicated to each different techniques) and the standards for the metric control of the survey are stated as well.
- **Section 3:** Format, presentation and provision of survey data. This section defines the characteristics of all the different products derivable from the data collected in the field, e.g. file format, characteristics of survey report and Computer-Aided Drafting (CAD) drawings layout.
- **Section 4:** Standard specifications for image-based survey. This section is dedicated to the image-based survey, standards to be followed during the photogrammetric process and characteristics to be respected in the products derived are reported.
- **Section 5:** Standard specifications for measured building survey. Measured building is defined as “*the supply of metric survey data pertaining to buildings and presented as plans, sections, sectional elevations and elevations*”. The description of all the derivable products, such as plans, sections, etc., are then presented.
- **Section 6:** Standard specifications for topographic survey. This section is related with the measurements (2D or 3D) of natural and artificial landscape features.
- **Section 7:** Standard specifications for the collection, registration and archiving of terrestrial laser scan data. This section is dedicated to laser scanning survey, starting from the collection of data, through the processing, till the delivering and archiving.

- **Section 8:** Standard specifications for the supply of Building Information Modelling (BIM). This section is focused on the definition BIM characteristics and the supply of BIM products.

One of the main values of the Metric Survey Specifications for CH is the fact that they describe both the different characteristics of the various techniques and the expected specifications of the products to deliver after a survey. On the other hand, one of the main limits of this document is the fact that, despite its name, only tangible heritage is considered and particularly only built and topographic heritage (Blake, 2010).

During its period of activity, the English Heritage promoted also the **Heritage3D project**, with the intention to set up clear standards specifically for the use of laser scanner in the field of CH documentation. One of the results of this project is the publication of a text exploring the use of laser scanner in CH applications and setting up clear standards (Barber & Mills, 2007). The achievements of this project were also included in the final publication of the Metric Survey Specifications for Cultural Heritage in 2009.

Another interesting initiative is the **RecorDIM** project, described as a “Partnership for Heritage Recording, Documentation and Information Management” (Letellier, 2007) developed from the collaboration between ICOMOS and GCI (Getty Conservation Institute) and CIPA Heritage Documentation. The main aim of this publication is to provide principles and guidelines for the documentation of CH and to create awareness among the people in charge for the heritage conservation and management. The book derived from the project is centred on the conservation process, how is clearly declared in the introduction of the text, and all the issues related with the documentation process are addressed in this framework. After a brief history of the RecorDIM initiative the authors identify twelve questions, corresponding to the twelve chapters of the text, which answers represents different guidelines and principles. The twelve questions and answers are the following:

1. *Why?* The documentation of CH is fundamental to enhance the knowledge about the artefact and better understand it, promote the involvement of local and global communities and ensure maintenance and management of the heritage. Also, to hand down CH to future generations.
2. *When?* It is possible to say that CH documentation need to be achieved whenever it is possible but especially when database or information system for CH are created; when some new information are discovered, during any type of conservation works (before, during and after) and finally in case of CH exposure to any kind of risk.

3. *Who should carry out heritage information activities?* The third answer states that documentation of CH should be carry out by experts, but that it is useful to involve also voluntary people that want to participate in the process.
4. *Who is responsible?* The first level of responsibility to ensure an adequate and updated recording of CH places is delegated to the people in charge of heritage managements. Secondly, everyone involved in the conservation chain is responsible in the process of recording, managing and sharing information.
5. *Where do heritage information activities fit into the conservation process?* CH documentation is a crucial and central part of the conservation process and should be fully integrated with it.
6. *What is the first planning step?* The first step in the process of CH documentation is a preliminary research and examination of already existing sources.
7. *What should the records contain?* CH artefacts must be accurately identified and located. Records should contain the major number of information possible: metric, qualitative, quantitative, conservation and management information, risk assessment, etc.
8. *What level of commitment is needed from decision makers?* A commitment to the acquisition of information about the artefacts is needed as well as the commitment to conservation. Guidelines and standards need to be defined for acquisition phases, processing, archiving and exchange of the records.
9. *Who should have access to heritage information?* The wider number of people possible to reach.
10. *What level of detail is required?* The level of detail should be appropriate for an efficient planning and development of the site, research, conservation, management of the site and creation of permanent records.
11. *What scope, level, and methods should apply?* All these features need to be appropriate to the nature and importance of the site, the need of the project, the purpose of record and the resources available. The adopted methodologies and techniques should be clearly stated and described. Non-intrusive techniques should be preferred.
12. *How should records be kept and identified?* Records should use standardized formats, be preserved in a safe and accessible place, possess a backup and constantly migrated to the most current supports.

The RecorDIM project establish also an interesting conceptual and pragmatic division of the different level of CH recordings, as shown in Figure 4.

| Levels of Heritage Recording  |  |  |   |
|---|--|--|---|
|   | <b>A</b><br>Reconnaissance Record<br>Low Accuracy                                  | <b>B</b><br>Preliminary Record<br>Midrange Accuracy  | <b>C</b><br>Detailed Record<br>High Accuracy  |
| <b>Purpose of Recording</b>   | Reconnaissance<br>Initial inventory<br>Initial planning<br>Reference data          | Planning<br>Initial condition<br>Investigation<br>Stabilization<br>Pre-design<br>Reference data                | As-found condition<br>Design<br>Construction<br>As-built record<br>Maintenance/monitoring<br>Posterity                                    |
| <b>Accuracy of Drawings</b>   | Not to scale   | Plans and elevations<br>± 5.0 in. (± 10 cm)<br>Details<br>± 1.0 in. (± 2 cm)                                   | Plans and elevations<br>± 0.5 in. (± 1 cm)<br>Details<br>± 0.1 in. (± 2 mm)   |
| <b>Results</b>  | Photographic report<br>Photo-key plan<br>Initial condition<br>Descriptive sketches | Measured drawings<br>Asset description/condition<br>Observations<br>Photographic report                        | Measured drawings<br>Asset description/condition<br>Observations<br>Photographic report   |
| <b>Cost</b><br><small>(will vary in absolute terms with scale and complexity of site)</small> | Low<br>(a few days on site by recording team)                                      | Moderate<br>(several weeks or more on site by heritage recording team and input by conservation professionals) | Moderate to high<br>(extensive and possibly ongoing activity on site by recording team and increased input by conservation professionals) |

*Figure 4 Different recording levels of CH as described in RecordIM. The choice of the level to adopt is related with the purpose of the projects, the expected results and the resources available*

The three levels are described as:

- **Reconnaissance Record** (Low Accuracy). This level aims to the identification of the CH artefact main characteristics and problem areas, can be performed in a limited amount of time and with the involvement of few operators. The derived products are not scaled and usually comprehend sketches, photos and written reports.
- **Preliminary Record** (Midrange Accuracy). More accurate than the reconnaissance recording and complementary to it, includes measurable graphic records. Identification and description of the main features needed for preliminary analyses in the conservation process. Accuracy of the products  $\pm 10$  cm for plans, elevation and cross sections and  $\pm 2$  cm for structural and other elements.
- **Detailed Record** (High Accuracy). Generally, the most accurate level for CH recording. It can be pursued only when high resources are available and can be achieved also in several years through different survey campaigns. Accuracy of the products vary between  $\pm 10$  mm and  $\pm 25$  mm for plans, elevation and cross sections and  $\pm 2$  mm and  $\pm 5$  mm for structural and building elements.

The three levels can be used together over time and can be integrated between each other's depending on the peculiar needs of the projects and on the resources available from time to time. Obviously, the higher is the accuracy of the level of recording, the higher are the resources needed to achieve it and the time to be dedicated to acquisition and processing

phases. Furthermore, the RecorDIM projects highlight also the relations between the different employed techniques and instruments and the levels of detail of the recording process, bearing in mind that the choice of the techniques to be used is highly influenced by the different factors previously reported: expected results, desired accuracy, resources and time available. The following Figure 5 illustrates the relations between the three level of recording and the major recording instruments and tools now available. As will be reported in the following sections, one of the aims of this thesis work is to demonstrate that low cost image-based system can be successfully deployed to produce results that are comprehend between the level B (Midrange Accuracy) and C (High Accuracy) of recording for CH, and that can be obviously useful for level A (Low Accuracy).

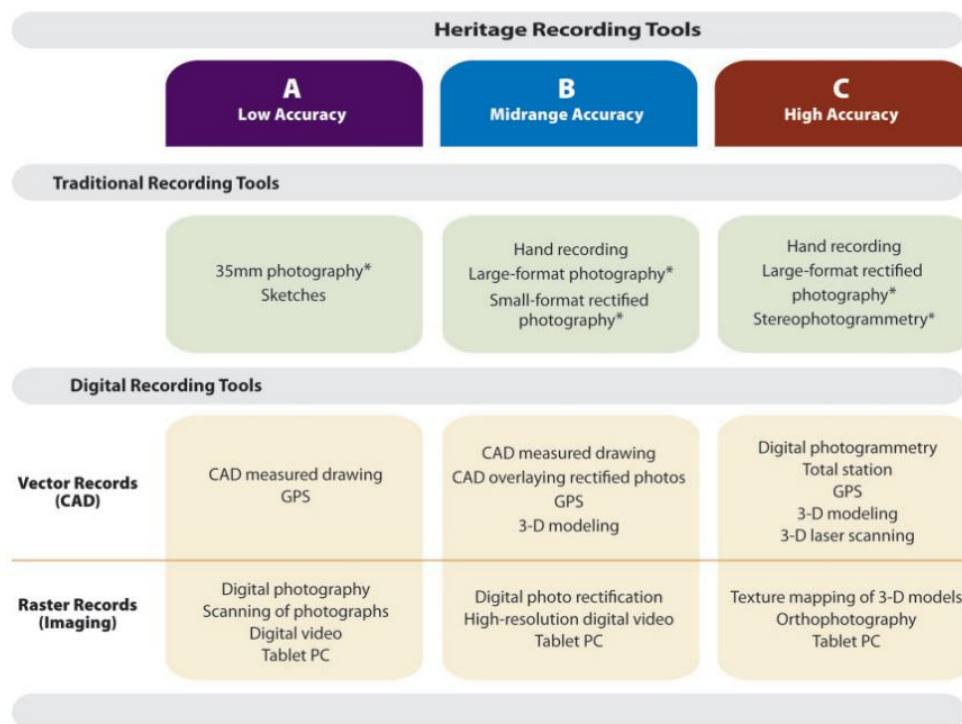


*Figure 5 Major recording tools and instruments for CH documentation and their relations with the three level of recording*

Another interesting work providing guidelines for CH documentation is the so called “**3x3 rules**” of CIPA (Waldhäusl, Ogleby, Lerma, & Georgopoulos, 2013), this contribute is an update of the work already presented in the 1994 at the ISPRS Commission V Symposium in Melbourne (Waldhäusl, P., Ogleby, 1994). The update of the first work presented in the 1994 became necessary due to the evolution that photogrammetry undergone in the last decades. As recalled by its name, this text reports 3 rules for 3 different steps of the photogrammetric acquisition phase: 3 geometric rules, 3 camera rules and 3 procedural rules. These rules are intended also for non-expert users and aims to establish and recall some basic principles to be followed to perform a correct photogrammetric acquisition. Specifically, the 3x3 rules suggest advices for the metric control of the survey, the setting

up of the camera (focus, exposures, camera format, etc.) and the archiving of the data collected.

Moreover, important guidelines and principle for CH documentation can be also extracted from texts that seems far from CH recording. An interesting case can be traced in one of the Good Practice Guide of the National Physical Laboratory, the national measurements standards laboratory of United Kingdom. The **Good Practice Guide number 80** (Flack & Hannaford, 2005) reports six general guidelines principles that are perfectly applicable in the field of CH documentation, and that are:

- *“**The Right Measurements:** Measurements should only be made to satisfy agreed and well specified requirements.*
- ***The Right Tools:** Measurements should be made using equipment and methods that have been demonstrated to be fit for purpose.*
- ***The Right People:** Measurement staff should be competent, properly qualified and well informed.*
- ***Regular Review:** There should be both internal and independent assessment of the technical performance of all measurement facilities and procedures.*
- ***Demonstrable Consistency:** Measurements made in one location should be consistent with those made elsewhere.*
- ***The Right Procedures:** Well-defined procedures consistent with national or international standards should be in place for all measurements.”*

The six rules, despite the fact that they have been conceived for field close to metrology, perfectly recall some of the main topic that have been stressed by texts centred on CH documentation.

Another similar example is the American Society for Testing and Materials, **Committee E57**, ASTM E57, established in 2006 to discuss about issues related with 3D imaging systems. The work of this committee is focused mainly on laser scanner and optical range camera (Cheok, Lytle, & Saidi, 2008), but again, some of the principles reported are common with the field of CH.

Summarizing the contents of the different charters, guidelines, principles and the reflexions of various authors is possible to write down some general consideration about the documentation of CH, and in particular of archaeological/architectural heritage:

- Always consider the needs and expectations of all the different operators involved in CH management (architects, archaeologist, restorers, engineers, people in charge of the management of CH, visitors, communities, etc.).

- Chose the best tools and techniques in relation with the accuracy needed and the level of detail requested.
- Adopt declared and shared standards and formats.
- Record multi-source, multi-scale, multi-contents data and work for their integration.
- Take care of the archiving and management of data, also in a long-term perspective.
- Set up user-friendly platforms and system for the management of the collected data in order to let different kind of user to access them.
- Disseminate the products of the survey to the wider number of people possible.

Finally, a consideration on the evolution that technologies and methodologies undergone in the last 10 years is necessary; the lack of new researches focused on the definition of general standards and guidelines for the documentation of CH is probably related with the rapidity of this evolution. To reach a good level of maturity in the reflection on these topics it is necessary that the new methodologies have been stressed to their limits and that their deployment have been investigated in all the possible scenarios. Considering that this process is still developing, more time will be probably necessary to set up a reflection for the general definition of updated standards and guidelines. Some organisations are moving toward this direction, an example is represented by the Historic England, a commission founded in the 2015 from the previous English Heritage. This commission is thus moving in the direction of setting up new standards and guidelines that are developing in parallel with the methodological and technological evolution of the disciplines connected with the survey of CH, following the line that was already traced from the Metric Survey Specifications for Cultural Heritage.

## **2.3 Geomatics contribute in the documentation of the Archaeological Heritage**

The central issue to bear in mind when dealing with the documentation of an archaeological artefact, or CH object in general, is related with its intrinsic nature: they are complex and presenting a great variety of features at different scales. Moreover, as is reported in (D'Ayala & Smars, 2003) and widely accepted: *“The geometry of the object is not the only parameter to be recorded. All specificities making the object unique are meaningful; all potential values - architectural, artistic, historical, scientific and social - are parameters to consider”* and, as reported by Clark in (Letellier et al., 2011): *“Understanding the*

*physical fabric of a site is an important first step in finding the right conservation strategy, and documentation is the first step in understanding” .*

Thus, the documentation of CH should possess some basic requirements (Patias, 2006):

- Should be multi-dimensional, multi-source, multi-content, multi format and with declared levels of detail and accuracy.
- Digital 3D databases, also including historical images and sources should be created.
- Multi-dimensional information should be managed in a rational way and shared with other users.
- The information collected should be shared on multiple level through the web, to be used from different people.

In this framework some guidelines to bear in mind (as partially reported also in section 2.2.2) when operating in the field of the documentation of CH have been detailed again by (D’Ayala & Smars, 2003):

- **Objectivity:** considering that a fully objective record of CH is not achievable and a partial subjectivity will always be present, it is fundamental to try to establish and guarantee an objective basis for the documentation process. It is clear that “[...] *the use of any specific set of data necessarily influences any decision-making process. The manner in which a survey is executed significantly influences further actions*”. Thus, it is crucial to find a balance between the operator subjectivity and the objectivity of the employed techniques. It is also important to consider the fact that, as often recalled in the community of archaeologists, also documentation is a first phase of interpretation of the surveyed object, a joint effort between producers and users of the data is then definitely necessary.
- **Values:** documenting the whole entirety of the surveyed CH artefact is utopian, for different reasons (technical, economical, for the nature of the artefacts, etc.). It is thus important to define a set of criteria to outline the elements worth recording, or, at least, a list of priorities. “*The recorder’s choices are critical [...] What is seen today as uninteresting may appear tomorrow as extremely valuable. The importance of thorough recording is emphasised by the common loss of minor details which may disappear at the moment of new conservation work, leading to loss of integrity or of historical evidence.*”

- **Learning process:** “[...] *surveying is a learning process and a certain period of contact time between the operator and the object is necessary to assimilate the features recorded, whatever the purpose of the recording. A deeper knowledge of the building will inform sensible decisions*”.
- **Continuity:** “*Documentation should not be seen as an activity confined within a set time [...] Therefore, a basic requirement is that the results of documentation should be available for future use*”. The time-dimension or the so-called multi-temporal, 4D data is important as the other three dimensions.
- **Fabric:** “*Documentation should not stop at the surface*”. The three-dimensional component is fundamental in almost all CH objects and need to be taken in account and recorded. Integration of different documentation techniques and instruments can be a key factor to reach the most complete documentation of all the features of an artefact.
- **Documentation sets:** “*Information gathered during documentation may be large and manifold*” and “*Classifying and organising data facilitates understanding and represent a first step toward interpretation.*” Also, the production of traditional 2D drawings can help in this process, especially thematic drawings of different professionals that can help understanding the history of the building. Other 2D/3D products can be useful as well. Sets of thematic drawings (geometry, materials, pathologies etc.) can be prepared. A specific set prepared by one specialist can bring insight to other specialists who are working on other sets.
- **Redundancy:** “*Every piece of information is associated with uncertainty. Documentation data should be supplemented by information about the quality of the data. Control procedures offer a way to assess quality.*”

As different authors reported (e.g. Letellier, 2007; Patias, 2007) and as is well known among the operators in the field, a crucial point before, during and after a survey campaign is the definition of a detailed survey project for the knowledge of the artefacts. It is mandatory to select the right technology to use, the right methodologies, to adopt good practices, standards and guidelines and finally to have clearly defined the final expected outputs of the survey with the relative levels of detail and quality assessment. Moreover, the time and the resources available (both human and economic) for the work are other key factors to be considered and that can highly impact on the documentation phases.

### 2.3.1 Instruments and techniques in relation with the new needs of archaeology

In a nutshell, the 3D modelling of an object or a scene can be described as the whole process of transformation of real data into digital data: it starts with the acquisition phase and ends with an interactive 3D model available on a computer. The need and use of 3D models are nowadays widespread in almost every field of research and industry and models are part of everyday activities in the life of people. Several techniques allow to generate complete 3D models of an object or a scene and the best solution need to be chosen in accordance with the final use that the model will be devoted to. Methods and techniques for the reconstruction of a 3D model can be divided into two main categories (Remondino & El-Hakim, 2006):

- *Contact methods* (e.g. rulers, callipers, coordinate measuring machine, etc.)
- *Non-contact methods* (photogrammetry, X-ray, laser scanning, etc.)

Nowadays, the most used techniques for the generation of 3D models belong to the area of non-contact methods, except for part of the industry that is still using contact methods (mainly coordinate measuring machines).

*Non-contact* methods can be ulteriorly divided in two main categories:

- *Range-based* techniques: these techniques are able to directly retrieve 3D coordinates. These systems provide measurement of sensor-target distances and angles, thanks to an a-priori knowledge of different parameters of the employed device.
- *Image-based* techniques: can refer both to photogrammetry and Computer Vision (CV), adopting similar techniques but with different aims. These systems are based on the recording of multiple images of a scene, later processed to extract metric information.

As reported by (Tucci & Bonora, 2014), even if they are generated from different techniques, the data collect from the survey of a real world object present some common features:

- First of all, they are collected and stored in a digital form (real world information are converted in digital format). This is an advantage as well as a limit: the data are

more flexible and easier to manage and share, but the risk of losing data due to the technological advancements and the changing of technology is a point of fragility.

- The data are always 3D. Even if 2D drawings are needed the data collected in the field will record 3D data for every part of the object that will be surveyed. Also the acquisition of 2D images is finalised to their conversion in 3D measurements.
- The time to spend on the site for the survey operations is shorter than in the past and data can be collected in a really limited amount of time, both with range-based and image-based sensors. However, the time needed to plan and prepare the operation on the field should not be underestimated. Moreover, the time that need to be devoted to the post-processing phases is quite long.
- The survey is performed without a direct contact with the object, except only for the placement of pre-signalized target when they are needed. In case of particular fragile objects or particular situation is possible to record the data without any contact with the artefact.
- A sampling of the object at high resolution is performed. Resolution is intended as “*smallest change in a quantity being measured that causes a perceptible change in the corresponding indication*” (Bipm, 2006). In general terms, it is possible to say that the resolution in the acquisition phase is directly related with the level of detail in the restitution phase: the higher is the resolution, the bigger is the reachable scale of representation. However, this relation is influenced by several other factors that need to be carefully considered. The definition of standards for the quality of geospatial data products have been a topic stressed by several researchers and international organisation: e.g. the American Society for Photogrammetry and Remote Sensing (ASPRS), the Joint Committee for Guides in Metrology (JCGM), the already cited ISPRS and CIPA, etc. The definition of the different indicators that will be adopted to evaluate and validate data, products and approaches in this research will be described in section 3.3.
- Texture and Red Green Blue (RGB) information are usually associated with the geometric information, providing other valuable data of the object characteristics.

The research of this thesis will focus on *non-contact methods* for the generation of 3D models (in particular on *image-based* solution, see Chapter 2) and, starting from the definition derived both from CV and geomatics, on *modelling from reality* (Ikeuchi & Sato, 2001). Nevertheless, a brief outlook of the different techniques that can contribute to the documentation of archaeological/architectural heritage will be reported in the following sections, in relation with the different scales of representation.

Generally, an interesting way to represent the relation between the possible survey techniques that can be adopted and the different representation scales in the process of documentation of CH is through a pyramidal scheme (Figure 6) as already reported in (Tucci & Bonora, 2014) and similarly to the concept reported in (Letellier, 2007) and showed in Figure 4.

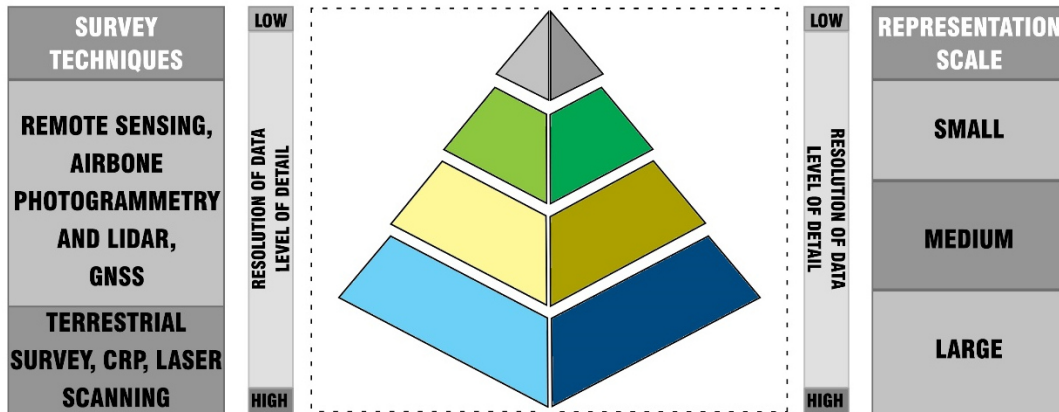


*Figure 6 Pyramidal representation of the documentation process. On the left the different survey techniques, on the right their relation with the different representation scales (Source: Author's elaboration based on Tucci & Bonora, 2014)*

This pyramidal scheme shows once again the importance of the coexistence of different levels of detail in the documentation process that are directly correlated with the techniques employed and the attended scale of representation. These considerations lead to another central issue in the documentation process: the problem of integration of data derived from different sensors and with different scales. The higher is the number of sensors and techniques employed, the higher can be the differences in the data collected: the integration of these data in a single multi-scale model occupied and is still occupying a large number of researchers (Adami, Fassi, Fregonese, & Piana, 2018; Balletti et al., 2015; Bianchi et al., 2016; Cardenal Escarcena et al., 2011; Chiabrande, Sammartano, et al., 2017; Chiabrande, Spanò, Sammartano, & Teppati Losè, 2017; Luigi Fregonese et al., 2016; Remondino, Girardi, Rizzi, Benedetti, & Gonzo, 2009).

Another key-factor that needs to be considered is the ratio between the cost of the adopted solution and the resources available, both in term of economic and human resources. All these elements are part of the preliminary documentation project and need to be carefully evaluated and discussed in order to perform the survey in the most efficient way and to reach the attended results without wasting time and resources. The phase of planning of the survey is particularly import and need to be conducted with a joint effort of the producers and users of the survey data. Several techniques are today available and the level of detail and complexity of the model carried out from a survey is quite impressive. However, this

complexity and density of information came with a high cost to pay in term of resources to employ in order to reach it, and also complexity in the process of archiving and managing them. One of the most important things to consider and analyse in the preliminary phase of the project is the final objective of the survey, moreover, a discussion with the people that will use these data is crucial. It would be pointless to produce enormous quantities of data if they are not needed, and the process will also result in a waste of energies and resources. The three levels suggested from the RecorDIM project (Figure 4) are a good example of a correct approach to these issues and consequently, as already reported, the techniques to employ need to be chosen in accordance with these levels of recording.

As described at the beginning of the section, several techniques are nowadays available to the operators and researchers involved in the process of documentation and they can cover a wide range of scales. It needs to be stressed that till few years ago the major part of the efforts of researchers were devoted to the development and implementation of new sensors, while today the focus have been shifted to the integration of these sensors together and to the management and interpretation of different data together. A general overview of the different techniques and their correlation with the ranges of application is reported in Figure 7.

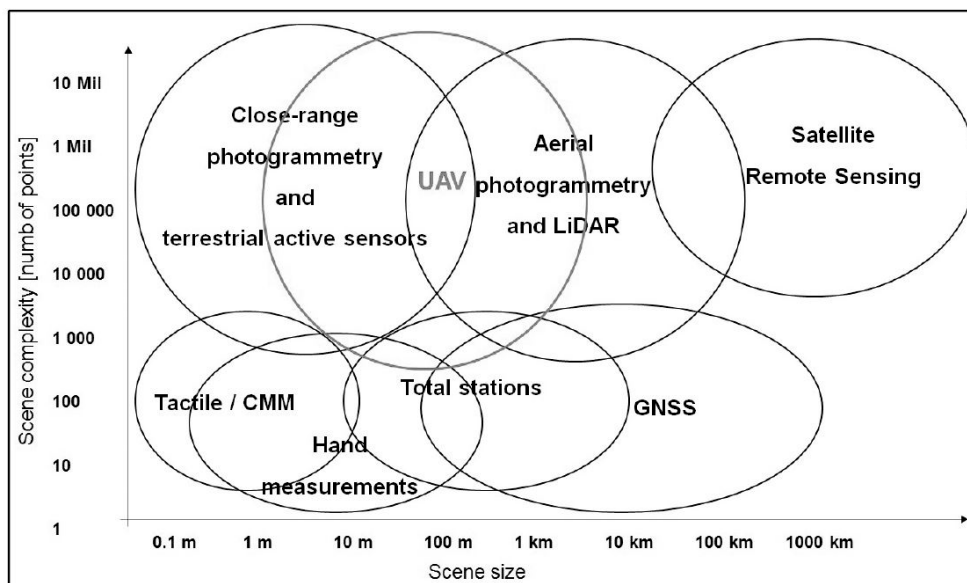


*Figure 7 Panorama of sensors and techniques according to scene dimension and complexity (Remondino & Campana, 2014)*

Needless to say, a perfect all-in-one solution doesn't exist and generally, a good documentation project should include the integrated use of different techniques, selected and applied considering the nature of the object to survey, the aims of the survey, the desired scale, the available resources and the expected accuracy.

Finally, a general schematic overview of the whole process of documentation is reported in (Ioannides, Georgopoulos, & Scherer, 2005) and showed in Figure 8, despite not being a recent publication this text still present several valid arguments. Especially the general

preliminary preparation of the fieldwork and the creation of the survey project are still valid, while small updates need to be considered in relation with the last technological developments. As is possible to see in the image, a lot of efforts and time are dedicated to the preliminary phases: the collection of the existing data, the setting up of the methodology, the choice of the techniques and the characteristics of the final products are all key elements that need to be carefully considered and investigated before the phases of data collection on the field. This phase of preparation is conducted in close cooperation with the committers of the documentation process and the final users of the products. It is interesting to notice again that nowadays the time for data collection on the field is becoming shorter and shorter (especially thanks to the latest methodological and technological developments), while the time for the data processing is exponentially growing. This element presents both pros and cons: from one side, especially in case of dangerous areas or limited time/resources available it is possible to complete a work on the field in a short time and in an efficient way; from the other side the risk is to lose contact with the artefact spending more time observing it on a monitor than from reality. As often happens, the best choice is to try to mediate between these two factors.

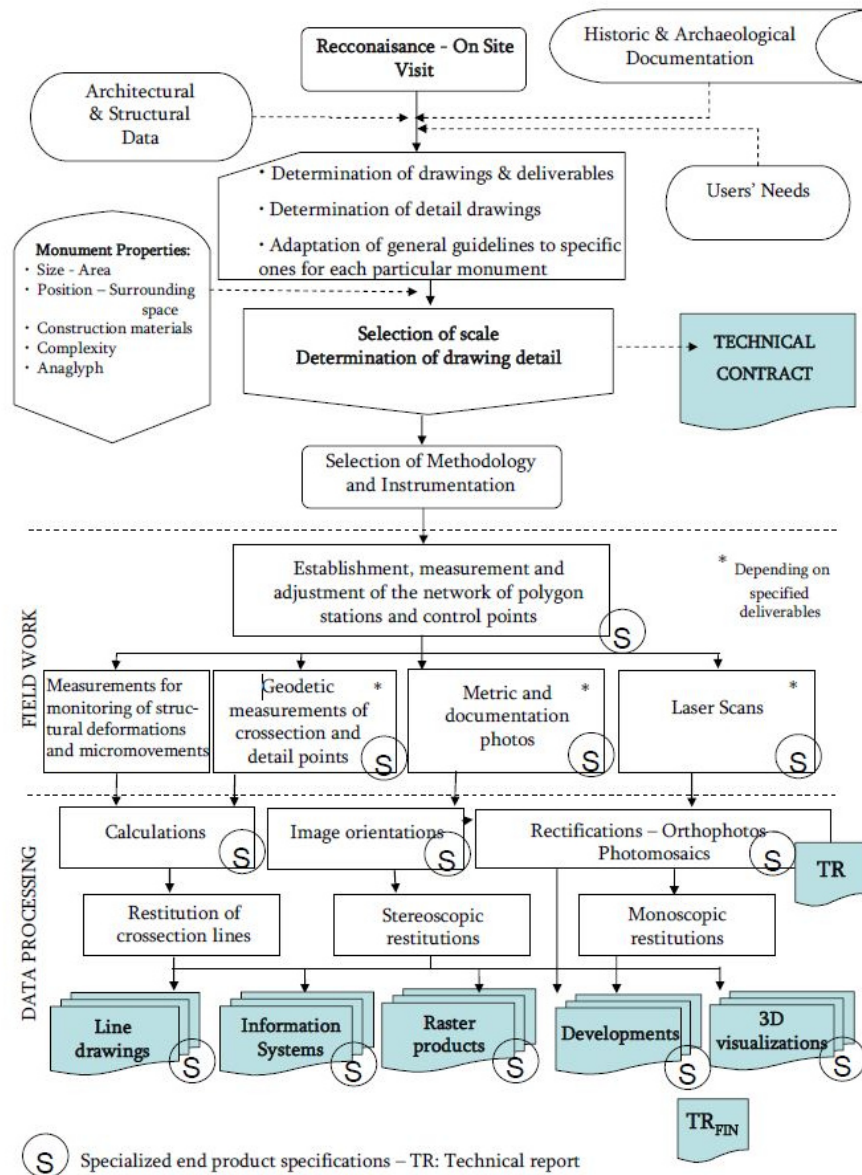
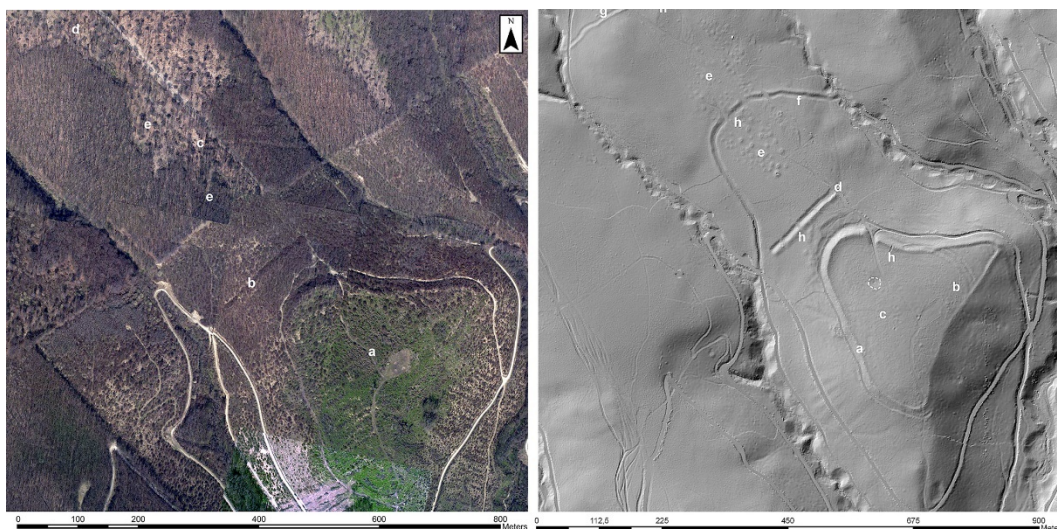


Figure 8 Schematic representation of the different steps for the documentation of CH artefacts (Ioannides et al., 2005)

### 2.3.2 Landscape Archaeology

As already reported in section 2.1.1 a great contribution to the development of landscape archaeology came from the research in the geomatics field (Lasaponara & Masini, 2012). The use of approaches derived from remote sensing, such as satellite images allowed archaeologists to connect field evidences in a wider scenario (Chase, Chase, Fisher, Leisz, & Weishampel, 2012; Powlesland et al., 2006), thanks to the availability of territorial images. Moreover, the different sensors equipped on the satellite opened the discipline to new possible analyses: *Synthetic Aperture Radar* (SAR) derived images are just one of the possible examples. The combined use of photogrammetry and airplane gave then the possibility to reach more detailed reconstructions of the landscape, maintaining a wide area

of interest, thanks also to a general lowering of the costs connected to this kind of data acquisitions (Bewley, 2003). Furthermore, the combined use of airborne LiDAR and photogrammetry allowed the creation of high detailed Digital Surface Model (DSM) and Digital Terrain Model (DTM) (Devereux, Amable, Crow, & Cliff, 2005; Doneus, Briese, Fera, & Janner, 2008), with the possibility to reveal micro and macro evidences not distinguishable from the ground; an example is shown in Figure 9.



*Figure 9 Example of the use airborne LiDAR, and trees filtering algorithms from the detection of hidden archaeological features. Source: (Doneus et al., 2008)*

The algorithms for trees removal are a clear example of this possibility, in areas where a field survey is difficult due to the presence of vegetation. Finally, the development of new sensors, like Near Infra-Red/ Infra-Red (NIR/IR)/ multispectral cameras) gave the possibility to collect new kind of data useful to aid the process of study and interpretation of the historical landscape (Verhoeven, 2012). In general terms, the use of satellite and airborne images created a new approach to this field of archaeology, allowing the possibility to change the point of view on a determined environment and underling features and relations that were not visible from the ground.

Even the operations of field survey have been enhanced by the use of geomatics instruments and techniques: the use of topographic techniques (such as Total Station and GNSS) to retrieve the position of the evidences recognized on the ground is one of the principal examples. The development and diffusion of GPS/GNSS methodologies and instruments represented a ground-breaking element if compared with the traditional topographic approach with TS. It allowed to collect georeferenced data of multiple types of evidences in a more rapid and flexible way.

All these set of different data can converge and contribute to the study and reconstruction of historical landscape; being integrated with the field observations. The instrument that became fundamental to collect, organize and analyse all these different types of data is the

GIS. Since the '90s the community of archaeologists understand the potentialities to use GIS for their researches (Conolly & Lake, 2006; McCoy & Ladefoged, 2009), especially thanks to the possibility to interconnect different elements with the spatial dimension (Lock & Pouncett, 2017). Then, GIS offered also to archaeologists the possibility to manage and connect, through a spatial database, all the complex and stratified data derived from the research on the field. Several research topics are connected with the use of GIS in archaeological contexts, in this research however, all these issues will not be tackled, and this instrument will only be used to perform some circumscribed analyses on the products derived from the tested sensors. Usually the scale of the products of landscape archaeology reaches a maximum of 1:1000.

The contribute of geomatics for the landscape archaeology is then related to a territorial scale and, as has been reported, different techniques can contribute to these kinds of researches; both in the phases of data collection, processing, analyses and management.

### **2.3.3 Building Archaeology**

In the field of building archaeology the scale of interest is different in respect to the landscape archaeology and its similar to the traditional architectural scale of representation (1:200 to 1:50). As reported in section 2.1.2 the main aim of building archaeology is to achieve an architectural and archaeological analyses of the considered artefact and to reconstruct the history of the building and its transformations during time. The analyses vary from general elements of the complex, peculiar technical features, structural and decorative elements and the scale range from 1:200 to 1:20/10, expanding further the traditional architectural scale. Depending on different factors, e.g. the resources available or the degree of complexity of the artefact considered, a whole or partial survey of the complex can be achieved. Usually, general plans and sections of the whole monuments are provided, while detailed analyses and representations are planned and realised only for peculiar elements of interest. The documentation in this field developed in parallel with architecture and again the research in the geomatics community constituted a turning point in this sense. From the first forms of traditional hand recording at the beginning of the discipline, till the more recent techniques introduced by geomatics. The use of laser scanner first allowed to collect huge amount of data in a limited time (Balzani, Santopuoli, Grieco, & Zaltron, 2004; Doneus Neubauer, W., 2005; Forte, Dell'Unto, Issavi, Onsurez, & Lercari, 2012), however the main issue in this sense was related with the intrinsic nature of the data. It was difficult for the community of archaeologists to accept that the beginning of the interpretation phase was moving away from the field to be achieved later in the laboratories. The non-discretized nature of the data collected on the field was a critical issue

for archaeologists, that were used to consider the survey of the artefact as the first step of the process of knowledge. This change required for sure a great effort of abstraction and the risk of losing the contact with the real nature of the object actually exists. It is for sure responsibility of the operators, both from geomatics and archaeology, to mind the gap between these two aspects and maintain the link between them.

Another important moment of revolution in the documentation in this field started with the introduction of photogrammetry (Anderson, 1982; Carbonnell, 1989; Fussell, 1982; Howland, Kuester, & Levy, 2014): first with analogue photogrammetry and then with analytical photogrammetry. Creating rectified images of the building main facades was the first step to reduce the permanence on the field and increase the quantity and quality of information available to complete the interpretation process. Secondly, the revolution of digital photogrammetry and the advent of new algorithms for 3D metric reconstruction from images (more details in section 3.3) led to the possibility to collect and process image data of the whole considered complex.



*Figure 10 Evolution of the process of documentation in the field of building archaeology over the years, safety level of the operators has not always been improved*

Even for building archaeology GIS became an important tool to collect, organize, manage and interpret all the information related with the history of the artefact, in the same manner of what happened with landscape archaeology but on a different scale. The information derived from archive analyses, on-field interpretation, historical sources, etc. can converge in a single georeferenced database and can be connected together to enhance the general historical interpretation. Adopting this instrument in the field of building archaeology entail obviously some methodological reflection, especially due to the fact that the 3D component of the structures analysed need to be carefully represent and considered. This process can be achieved in 2D, e.g. representing the stratigraphic units of a façade in a GIS environment as for example in (Donadio & Spanò, 2015), or in 3D with all the challenges that this approach involves, e.g. in (Dell'Unto et al., 2016). In recent times the two communities are moving their attention also to BIM, more specifically on what is defined as Historical BIM (HBIM). The research is still at its first steps, but the results are promising (L Fregonese et

al., 2017; Garagnani, 2017; Logothetis & Stylianidis, 2016; Scianna, Gristina, & Paliaga, 2014) and in the next years this will probably be one of the central research topic in these field, together with its connection with GIS.

### 2.3.4 Field Archaeology

The documentation connected with field archaeology, i.e. excavations, is maybe the most delicate to achieve with good results. As have been already reported, excavation is a destructive practice, and in this case the recording process should be as detailed and objective as possible. Since the early developments of modern archaeology, the community of researchers have been aware of these issues and a lot of effort have been dedicated to this activity. The first techniques employed were again connected to hand recording, until a first step of evolution started with the introduction of topographic techniques such as TS and GNSS. Photogrammetry was a striking element also in this branch of the discipline (Georgiadis & Tsioukas, 2000; Koistinen, 2000; López et al., 2016), the soil was already fertile thanks to the massive employment of photography to document the different progresses of the excavation, e.g. air balloon were largely adopted to document the end of the excavation campaigns from an aerial point of view (Ceraudo, 2013). Also laser scanning started to be employed with good degree of success. Furthermore, another key element in recent time is related with the diffusion and development of UAVs (Figure 11) and their deployment also for the recording of archaeological excavations (Campana, 2017; Fernández-Hernandez, González-Aguilera, Rodríguez-Gonzálvez, & Mancera-Taboada, 2015; Verhoeven, 2009).



*Figure 11 Evolution in the systems for aerial documentation of archaeological evidences. On the left an air balloon on the archaeological site of Hierapolis (1997). On the right a small and portable multirotor platform on the site of Hierapolis (2018)*

Usually, the time available during an on-going excavation for the documentation is quite limited, especially in case of non-academic works and the requested scales can vary from

1:100 to 1:20. Today the different techniques for the documentation of the archaeological excavation are coexisting, but there is still a strong attachment of the major part of archaeologists to the traditional hand drawing techniques. However, GIS gained the upper hand, together with CAD, for the archiving, management and interpretation also of archaeological excavations (Barceló & Pallarés, 1996; Djindjian, 1998; Katsianis, Tsipidis, Kotsakis, & Kousoulakou, 2008; Katsianis, Tsipidis, Kotsakis, Koussoulakou, & Manolopoulos, 2006). It is necessary to report that the community of researchers is sensible to new technological developments and interested in their application, however they are not totally accepted and employed yet, and a lot of time and efforts are still exploited on the field for this process. In this sense, it is still needed an effort from both the two communities (archaeologists and geomatics) to work together through a common outlook of the documentation process.

### **2.3.5 Detailed Archaeology**

As reported before, the common feature of this sector of research and documentation can be traced in the scale adopted: that is a detailed one. Documentation in this sector can interest both small features on the field, both small findings or artefacts. Instruments and techniques are stressed to their smallest range of working and to their best accuracy to document such elements and the overall process of documentation can be quite challenging in these cases. These applications can be considered as the range limit of geomatics for the documentation of small elements, before entering in the field of metrology. Different techniques can be adopted, and their choice is again related with different elements: the level of detail needed (generally very high in these cases, till scale 1:1), the dimension of the elements that need to be recorded and other key-features of the elements (shape, material, material properties, colour, etc.). In most of these cases, laser techniques and instruments are used, but lately also photogrammetry (if carefully employed and controlled) is playing an important role. Among the different range-based sensors, two main categories of techniques and sensors are used: triangulation-based scanners and structured light scanners. Laser triangulation is a technique able to acquire 3D measurements pairing a laser source with a camera (Boehler, Heinz, & Marbs, 2002), while structured light scanners are composed by one or more cameras and an active light source, projecting on the object a known pattern (Georgopoulos, Ioannidis, & Valanis, 2010). As reported in the literature, also photogrammetric approaches can be stressed to their limits to be used at this scale (Galantucci, Pesce, & Lavecchia, 2016; Nicolae, Nocerino, Menna, & Remondino, 2014; Yanagi & Chikatsu, 2010).

The features to be documented vary from small medium elements (such as decorative elements, statues, etc.), till small elements (pottery sherds, lithic tools, micro-stratigraphies between layers, etc.) and the scales of representation can vary between 1:10 and 1:1. The documentation of the firsts can aid also to achieve a better understand of the object but has important developments also in the field of communication, due to the possibility to collect similar and multiple elements into a single digital repository, easily accessible. The second category is really important both for the understanding of the relations between small layers on the field, barely visible for the human eyes, both for the classification of typological elements in specific classes (Bujakiewicz, Kowalczyk, Podlasiak, & Zawieska, 2006; Gallo, Muzzupappa, & Bruno, 2014; Niven, Steele, Finke, Gernat, & Hublin, 2009; Samaan, Héno, & Pierrot-Deseilligny, 2013).

# Chapter 3

## Image-based approaches for 3D modelling from reality. Theory and practice

Image based approaches (mainly photogrammetry) consists in the process of extracting 3D measurements from 2D images using mathematical models. Generally, photogrammetry can be defined as: “[...] *methods of image measurement and interpretation in order to derive the shape and location of an object, using one or more photograph of the object itself*” (Luhmann, Robson, Kyle, & Harley, 2006). Some key factors can be identified to explain the success of this technique: it is low cost, fast, versatile and easy to deploy on the field if compared with other geomatics techniques. These factors have been stressed and investigated by several authors: (Böhler, 2005; Grussenmeyer, Landes, Voegtle, & Ringle, 2008; Habib & Morgan, 2013; Koutsoudis et al., 2014; Pomaska, 2001; Remondino, Guarnieri, & Vettore, 2005; Wenzel, Rothermel, Fritsch, & Haala, 2013), in particular concerning the application of this technique in the field of CH documentation (El-Hakim, Beraldin, Picard, & Godin, 2004; Kadobayashi, Kochi, & Furukawa, 2004; Patias, 2007). Generally, image-based approaches use principles derived from projective geometry or perspective camera models (a brief overview of the geometrical fundamentals of photogrammetry will be reported in section 3.2).

Since its early development (some historical notes about the discipline are reported in the following section 2) photogrammetry has been considered a ground-breaking technique for several reasons. Obviously, it is not possible to consider photogrammetry as a sort of *one button solution*, but today it can be employed to reach a detailed and accurate documentation with a good ratio between cost and efficiency and can be effectively integrated with other techniques. A list of advantages and disadvantages of photogrammetry is reported by Petros Patias in (John Fryer et al., 2007) and is described below:

### Advantages:

- **Collection of large amounts of data:** this can be achieved at various scales and resolutions, referring to whole areas or to single objects. It can be based on

photogrammetric measurements or on combinations with other types of measurements.

- **Very accurate data:** under the current technology, this is routinely on the order of 1/3 to 1/10 of the image pixel size. More importantly, the whole procedure is regularly monitored and checked to ensure that the quality of the results (accuracy and precision). The mapping is objective, and the results are repeatable, verifiable, with a consistent overall accuracy.
- **3D data:** photogrammetry, by its nature, reconstructs the 3D surface of objects in a detailed and accurate way. The geometric reconstruction is based either on 3D points or continuous surfaces determination.
- **Texture data:** this is a natural consequence since the technique is based upon images of the objects to be reconstructed. Spectral or texture data are very important since they give a natural look to the reconstructed 3D objects, thus enhancing the user's cognition. More importantly, these textures also carries the 3D object's geometry, and therefore allows metric characteristics to be matched with those of the vector data.
- **High resolution and detailed data:** based on the current high rates of advances in technology, photogrammetric sensors are capturing more and more detailed data, which in turn are processed by increasingly effective automatic procedures. Centimetre-level pixel sizes are routinely realised on the object in medium scale mappings and may decrease to millimetre-level or less for close range applications.
- **Geo-referenced data:** data defined above are referred to common reference systems, whether they are global or local coordinate systems. By reference to common ground coordinate systems, the metric characteristics of the data gain one more important advantage: they all refer to real-world geometry and facilitate the ability to extract indirect measurements any time after leaving the monument.
- **Metadata:** this refers to information about the data. Metadata is valuable, since it can be used for tracing down original sources, acquisition times, qualities, metrics, and even ownership.
- **Low-cost and rapid:** the cost of the equipment is becoming less and less expensive and photogrammetry allows to respond also to strict timing requests for the delivery of the products.

#### **Disadvantages:**

Two main disadvantages can be indicated for photogrammetry:

- **Hardware/software:** medium to high-end software and hardware are needed to complete the photogrammetric workflow. However, it is possible to say that these issues have almost been overcome in the last years for two main reasons: the digital approach to photogrammetry allows to use in the best way possible the computational power of the new computers and secondly the development of *off the shelf* cameras in the same period of photogrammetric algorithms and software opened new enhanced solutions for the overall process.
- **Field measurement:** traditional field survey measurements are usually needed to complete a correct photogrammetric process and are part of it. These factors can extend the time needed on the field to complete the work. However, several researches were focused on the last years on the aim of reducing the time needed to complete this phase of the process, optimizing this task with different strategies.
- **Environmental conditions:** if compared with other techniques, photogrammetry is more influenced by the environmental conditions on the field, due to the intrinsic sensor characteristics. Illumination of the scene and general light conditions during the acquisition can highly impact the quality of the images acquired and consequently of the subsequent photogrammetric process.

### 3.1 Brief notes on the history and evolution of the discipline

It is possible to affirm that photogrammetry is old almost as photography itself, however, several years and different evolution steps were necessary to let the discipline reach its own maturity. This has been a constant and long process that is still not finished and it is slowly, but constantly, evolving. Starting from the mid of XIX century the main steps in the evolution of photogrammetry can be traced in four phases:

- Plane table photogrammetry (around 1850-1900)
- Analog photogrammetry (around 1900-1960)
- Analytical photogrammetry (around 1960-present day)
- Digital photogrammetry (around 1980-present day)

The definition of these cycle of evolution of the discipline dates back to the mid of the 80's, is based on the theory of K-waves (or long waves), first defined by the Russian economist Nikolai Kondratiev (Kondratiev, 1925), and can still be considered valid today. Kondratiev

cycles are characterized by alternating phases of growth and decline related to the invention, adoption, development and downturn of a new technology. Although derived from the economic sector, the definitions of this kind of cycles can be extrapolated and applied to other disciplines. In the case of photogrammetry, the phase of growth can be traced in the invention and adoption of the new technology, while its decline is parallel to the coexistence with the following technological evolution, that will result in a new growing phase. A graphical representation of this kind of cycle applied to the evolution of photogrammetry is reported in the following Figure 12.

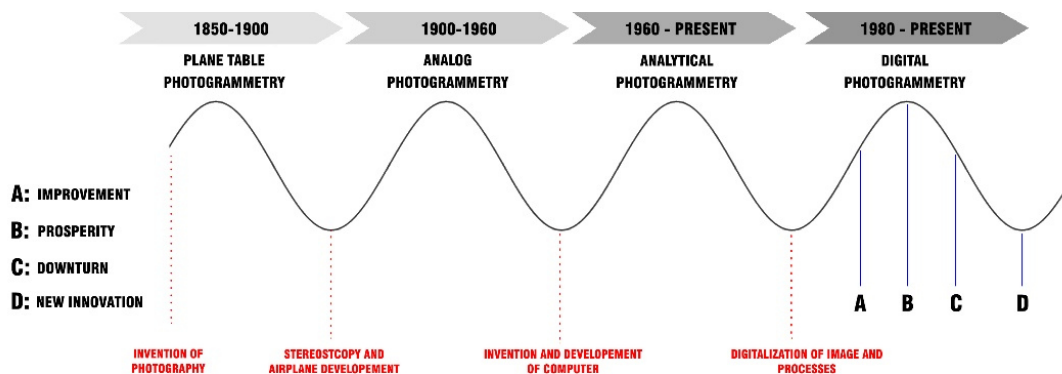


*Figure 12 Representation of the cycles of evolution of photogrammetry based on the long waves' theory of Krondatiev. (Source: Author elaboration)*

The first phase of the discipline referred to the *plane table* photogrammetry. In this phase photogrammetry was adopted to extend the traditional plane table survey and was mainly used for the creation of topographic maps. In the meantime, first experimentations in the acquisition of photographs from the air started through the employment of balloons, though both the technology related to photography and flight were yet not developed enough to reach appreciable results.

The second phase of the discipline can be outlined in the *analog photogrammetry* and is strongly related with two technological advancements: the spread of stereoscopy and the development of the airplane. Stereocomparators and subsequently stereoplottting instruments were developed to realize an accurate plotting of the topography recorded by a couple of images. During the period between the two world wars, stereometric cameras began to be developed and the applications of photogrammetry embraced again both aerial and terrestrial applications.

The third phase of evolution is the *analytical photogrammetry*, the progress of photogrammetry in this cycle is derived from the invention and developing of the computer in the mid of XX century. A purely analytical/numerical approach became the central point

of photogrammetry. Numerical methods allowed to increase the accuracy of the technique and, depending on the mathematical model used, also to improve the flexibility of the methods. As reported in (Luhmann et al., 2006), analytical photogrammetry “[...] *permits over-determination which may improve precision, lead to the detection of gross errors and provide valuable statistical information about the measurements and the results*”. Starting from the 60’s computers were integrated with stereoplotters, giving birth to analytical stereoplotters, allowing a complete numerical reconstruction of the photogrammetric models. Moreover, analytical photogrammetric triangulation (generally defined as bundle adjustment) was developed and thus simultaneous orientation of all the photographs became possible. It is in this period that different authors defined several concepts and constrains that will lead to the following cycle of the discipline (e.g. calibration and self-calibration of cameras).

Finally, the phase in which the discipline is today is the *digital photogrammetry*: this cycle has been activated from the digitalization that interested both the image acquisition and the photogrammetric process. In this phase a lot of efforts were, and are still today, devoted to the automatization of the workflow and to the refinement of the algorithms involved in the process. A more detailed overview of this phase will be reported in the following sections. It is interesting to notice that the last two phases of evolution of the discipline are still coexisting today, however, digital photogrammetry is gaining the upper hand.

## **3.2 Geometrical fundamentals and digital photogrammetry**

The fundamental mathematical model on which photogrammetry is based is the 3D perspective projection: the object point  $X$  is projected on the image plane, the centre of the camera, together with the image point  $X_c$  defines the spatial direction of the ray intersecting the object point  $X$ . This projection is modelled on the concept that during the image formation process, the 3D object is back-projected on the 2D image; the ideal 3D perspective projection based on the pinhole camera model is illustrated in Figure 13 while the ideal modelling of a pinhole camera is showed in Figure 14.

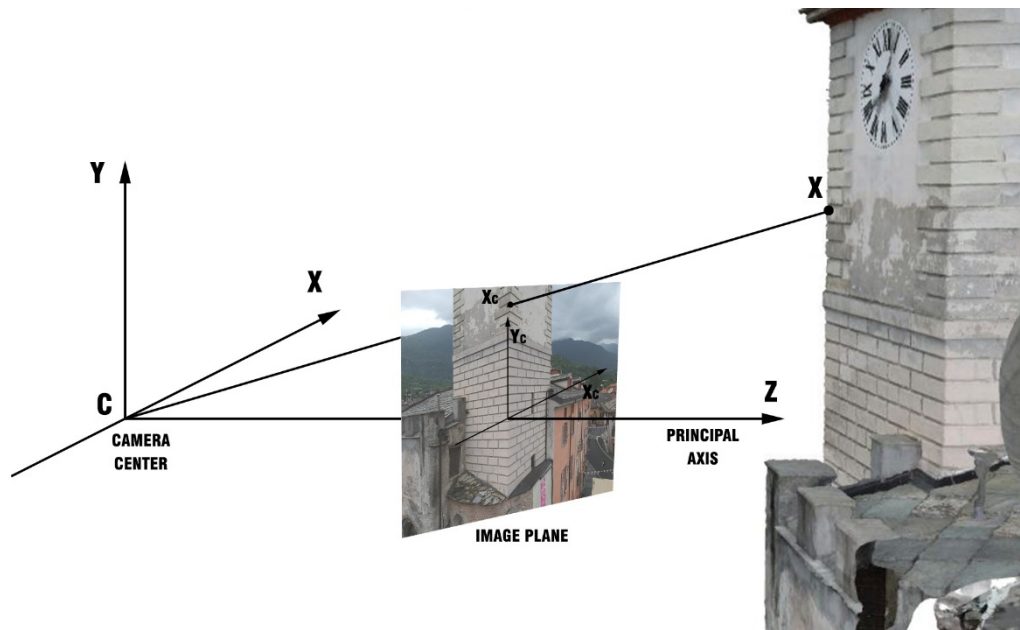


*Figure 13 Scheme of the ideal 3D perspective projection based on the pinhole camera model. (Source: Author elaboration)*

The concept of camera model can be described as: “an abstraction of the real camera sufficiently simplified for solving a task” and the aim is “modelling the geometry of the relation between positions of a set of image points in the sensor area and the corresponding bundle of viewing rays” (Förstner & Wrobel, 2016).

The physical configuration of modern cameras is rather similar to the one of first cameras ever manufactured: a box with a lens and a medium able to be impressed by the electromagnetic radiation. However, each of these three components has undergone several innovation steps during the past decades, becoming more and more complex. The structure of the camera system is based on the pinhole camera model (Figure 14): a simple box with a small hole. Electromagnetic radiations pass through the pinhole and the image is formed inverted on the box surfaces opposite to the hole. The focal length  $f'$  is defined as the distance between the pinhole and the image plane. In the case of ideal pinhole camera, no lens is used. The introduction of lenses in the camera system creates another element that needs to be modelled, because it alters the electromagnetic radiation captured by the camera, the principles for the correction of the distortions introduced by the lens system will be described in section 3.2.1.

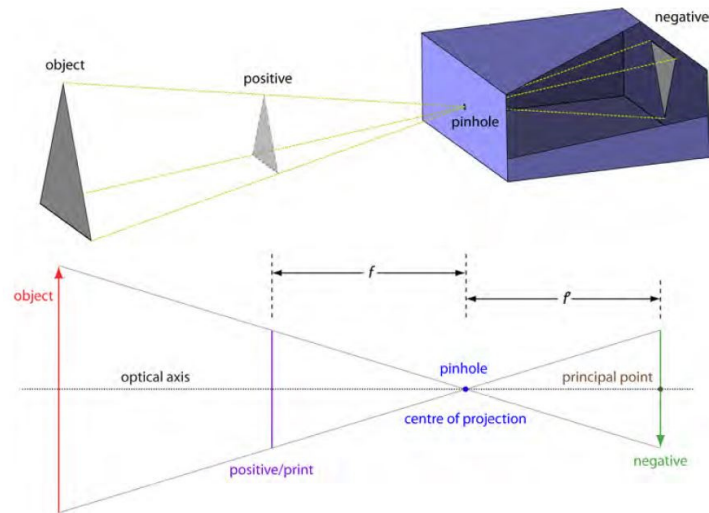


**Figure 14 Pinhole camera model and geometry of image formation in these types of cameras. (Source: G. Verhoeven, 2016)**

The central perspective projection can be ulteriorly defined as shown in Figure 15 - left, where an object point  $A$  is projected on the camera sensor (projection plan) and create an image point  $a$ . A line passing trough the perspective centre  $o$  connects the two points. The principal axis of the camera is defined as the line orthogonal to the projection plane and passing to the perspective centre  $o$ . The point intercepted from this line on the projection plane is defined as principal point (section 3.2.2).

Focal length, or principal distance, is defined as the distance between principal point and perspective centre and is variously indicated in the literature as  $c$  or  $f$ .

Another factor that need to be considered is the presence in this model of two coordinate systems:

- The object coordinate system, defined by the triplet  $(X, Y, Z)$ , and referring to the real-world coordinate system. Perspective centre in this coordinate system is indicated with  $(X_o, Y_o, Z_o)$ ; object point  $A$  with  $(X_A, Y_A, Z_A)$ .
- The image coordinate system, defined by the triplet  $(x, y, z)$ , which origin is located in the perspective centre  $o$  and the  $z$ -axis that concurs with the principal axis. In this system  $x$ -axis and  $y$ -axis are parallel to projection plane. Coordinates of point  $A$  in this system are  $(x_a, y_a)$  or  $(x_a, y_a, -c)$  if principal distance is considered.

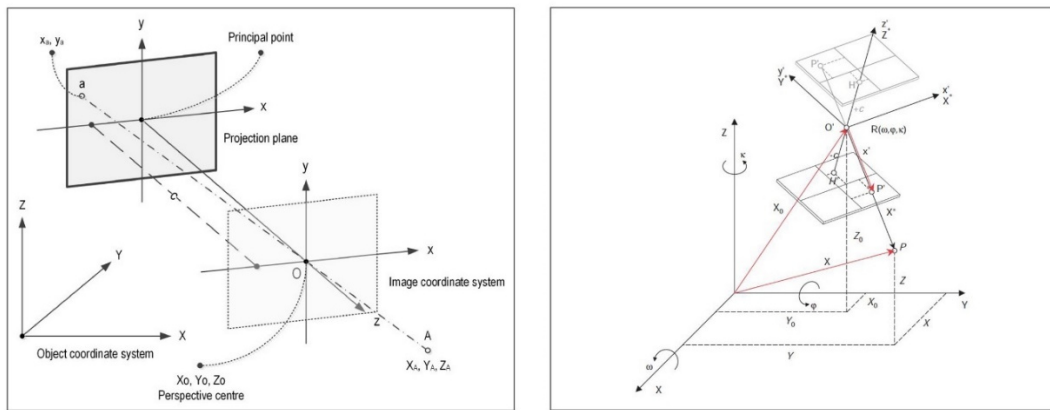


**Figure 15 Left: Central perspective projection. (Source: Fabio Remondino & Stylianidis, 2016). Right: Exterior orientation and projective imaging (Source: T Luhmann, Robson, Kyle, & Harley, 2006)**

After having established these relations it is possible to state that from the intersection of two homologous image rays an object point in three dimensions can be located. If, to achieve the computation of 3D coordinates of one or more points, two images are used it is possible to describe stereo photogrammetry, otherwise, if more than two images are used it is possible to define it as multi-image photogrammetry (Luhmann et al., 2006). Actually, it is possible also to work with one single image, adopting some particular shrewdness and with slightly different methodological approaches, this case is not part of the presented research work, but further information can be found for example in (Aguilera, Gómez Lahoz, & Finat Codes, 2012; Wang, Tsui, Hu, & Wu, 2005; Winkelbach & Wahl, 2001; Zhang, Tsai, Cryer, & Shah, 1999). However, these methods are usually slowest and more complex compared with multiple-views approaches and thus less diffused in the community of researchers.

Base of the traditional analytical photogrammetry is the so-called collinearity principle: as already seen, in an ideal camera system, the perspective centre, the image point and the corresponding object point lies on the same line. Applying the collinearity equations in a multi-view system (Kraus, 2007; Linder, 2009; Luhmann et al., 2006) it is possible to retrieve the object point coordinates as the result of the intersection of back-projected rays from camera centres to image plane.

Finally, another element needs to be introduced to model the central perspective projection (Figure 15 - right): six parameters to describe the relation between the camera coordinate system and the global object coordinate system. The vector  $X_0$  define the spatial location of the image coordinate system, from the origin to the perspective centre  $O'$ , while the rotation matrix  $R$  defines the angular orientation in the space.  $R$  is the results of three independent rotation ( $\omega$ ,  $\varphi$ ,  $\kappa$ ) about the coordinate axes  $X$ ,  $Y$ ,  $Z$ . If the parameters of E.O. are given the vector  $x'$  (the direction from the perspective centre  $O'$  and the image point

$P'$ ) can be transformed into an absolutely oriented spatial ray from the perspective centre and the object point  $P$ .

Based on these factors is possible to derive the collinearity equations:

$$x' = x'_0 + z' \frac{r_{11}(x - x_0) + r_{21}(y - y_0) + r_{31}(z - z_0)}{r_{13}(x - x_0) + r_{23}(y - y_0) + r_{33}(z - z_0)} + \Delta x'$$

$$y' = y'_0 + z' \frac{r_{12}(x - x_0) + r_{22}(y - y_0) + r_{32}(z - z_0)}{r_{13}(x - x_0) + r_{23}(y - y_0) + r_{33}(z - z_0)} + \Delta y'$$

*“These two equations describe the transformation of object coordinates  $(X, Y, Z)$  into corresponding image coordinates  $(x', y')$  as function of the interior orientation parameters  $(x'_0, y'_0, c, \Delta x', \Delta y')$  and exterior orientation parameters  $(X_0, Y_0, Z_0, \omega, \varphi, \kappa)$  of one image”* (Luhmann et al., 2006).

Following these two equations is possible to notice that some constrains must be applied:

- Interior Orientation (I.O. - see section 3.2.2): at least the camera principal distance ( $f$ ) and the principal point coordinates  $(x_0, y_0)$  need to be known or estimated.
- Exterior Orientation (E.O. - see section 3.2.3): this operation involves the computation of six parameters (three orientation angles and three coordinates of the camera station, for each image)

Collinearity equations underline the fact that each object point is projected into a single image point, if not covered by other object points. These equations constitute the base for further computations, such as spatial intersection, spatial resection and bundle block adjustment.

### **Photogrammetry and Computer Vision – The photogrammetric Computer Vision approach**

In the following sections the issues cited in the previous sections will be tackled more in deep, however, due to the fact that notions both from the photogrammetric and CV communities will be reported, a short introduction on the relation of these two research fields is necessary.

It is interesting to notice that, until recent year (around 2000), the photogrammetric community and the CV one followed separated paths, despite working on similar or identical research issues (e.g. the retrieval of the geometry of an object starting from a set of images). A clear analysis of the parallel evolution of these two disciplines is reported in

several authors (Förstner, 2009; Förstner & Wrobel, 2016; Mundy, 1993), starting from their separate research, through the finding of a meeting point, and till a joint effort of shared aims and methodologies that lead to a partial contamination of the two sectors. The difference in the treatment of images information between the two communities is mainly in the final aims of research: CV specialists work for the implementation of solutions able to replicate human capability in the processing of image data, while photogrammetric community is more focused on metric and geometric accuracy. Moreover, CV is more focused on the use of fast techniques, also if this mean to lose some precision, while on the other hand photogrammetry is more focused on precision, at the cost of speed. The need for speed of CV is mainly related with the necessity of autonomous navigation of machines, i.e. the position of the machine needs to be continuously computed from its relations with the surrounding scene.

More specifically, as reported by Mundy in (Mundy, 1993), CV has three main research topics:

- Object recognition: *“The desired outcome is for a recognition algorithm to arrive at the same class for an object as that defined by the human conceptual framework”*
- Navigation: *“[...] the main function is to provide guidance to an autonomous vehicle. [...] A secondary goal of navigation is obstacle avoidance. [...] The objective is to produce an accurate description of the 3D environment around the vehicle”*
- 3D modelling: *“Here the central issue is to recover a complete and reasonably accurate 3D model of an object. The model is then used for a number of applications [...]”*

Instead, the photogrammetric community of researchers have been focused on slightly different themes:

- Mapping: one of the first and most important application of photogrammetry was and is still related with the production of topographic maps.
- Close-range: with the evolution of the discipline and of the different sensors a wider range of scales was achievable adopting a photogrammetric approach, the shorter acquisition distance led to a series of different applications (from architectural scale, till industrial metrology).

Thanks to efforts of the two different communities the bridging of the gap between the two disciplines started in the year 2000, people from each one of the two areas began understanding that cooperation and inter-disciplinarily may led to a better development of the research and to mutual benefits. In the following sections the contributes of the two disciplines will be considered together and the separation of the two approaches will be left behind.

One of the main contribute of CV to the field of photogrammetry was related with the introduction of the algorithms connected with Structure from Motion (SfM); this approach will be described in section 3.3.

### 3.2.1 Camera models and calibration of digital cameras

Traditional cameras with photographic film can be defined as a sort of refined pinhole system, perspective approximate mapping is used to map the scene on the image plane defined by the film. The digital revolution involved also the sector of photography, leading to the creation of the so-called *computational cameras*, where a computer is embedded in the camera to transform and process the raw data acquired. A schematic representation of the two camera systems is showed in Figure 16.

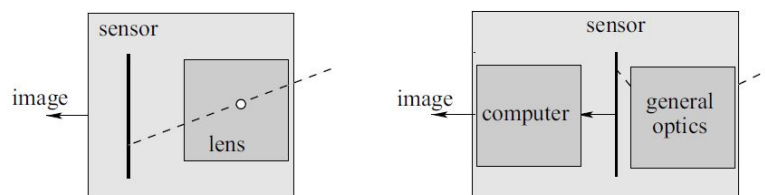


*Figure 16 Schematic representation of camera systems. On the left traditional film cameras, on the right computational cameras (Förstner & Wrobel, 2016)*

In modern digital cameras the optical radiation is detected through a conversion of electromagnetic radiation in an electric signal that is than digitised. Modern camera sensors are composed by one or more detectors able to detect the radiation, usually gathered in focal plane arrays; the most diffused technologies for focal plane array are CCD (Charge-Coupled Devices) and CMOS (Complementary Metal Oxide Semiconductor).

The ideal modelling of a camera has been discussed in the previous section 3.2, thus real camera systems have a slightly different behaviour and additional parameters are needed to model the perturbation that occurs during the process of image formation. Usually these errors are called nonlinear, due to the fact that they do not preserve straight lines. Several causes can be traced to explain these deviations: lens distortions, non-planarity of the sensor, refraction, etc.

Furthermore, the introduction of the lens in the camera system create another element that need to be modelled, because it altered the electromagnetic radiation: again an ideal approximation, called *thin* lens – a lens with no physical thickness, can be used to model and understand the principles of lens behaviour (Figure 17).

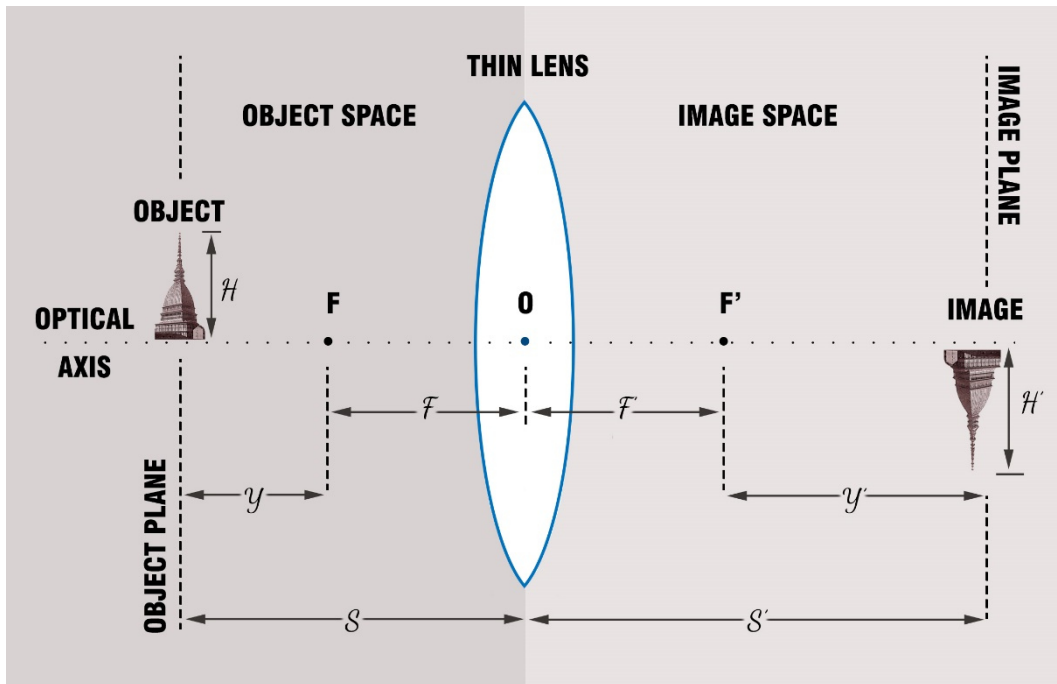


*Figure 17 Thin lens system representation.  $F, F'$  define the focal point while  $f, f'$  define the focal distance.  $h$  and  $h'$  are the object and image size,  $s$  and  $s'$  are object and image distance.  $O$  is the optical centre.  
(Source: Author elaboration based on G. Verhoeven, 2016)*

The thin lens is the centre of this ideal system, the object space is defined in front of the lens and the distance between the object and lens is defined as the object distance  $s$ . The region behind the lens is called image space, where the image will be formed, the distance between image and lens is called image distance and is defined as  $s'$ . The optical axis passes through the centre of the lens and defines two focal points:  $F$  (object-space focal point) and  $F'$  (image-space focal point); focal length is defined as the distance in mm from these two points.

However, as already reported, a real camera system is slightly different from the ideal one and the lens system is not an exception. Lenses aren't composed by a single thin lens but can be considered a composite system of converging and diverging lenses, with a determined physical thickness, mounted concentrically with the optical axis of the camera. A thick lens configuration is reported in the following Figure 18.

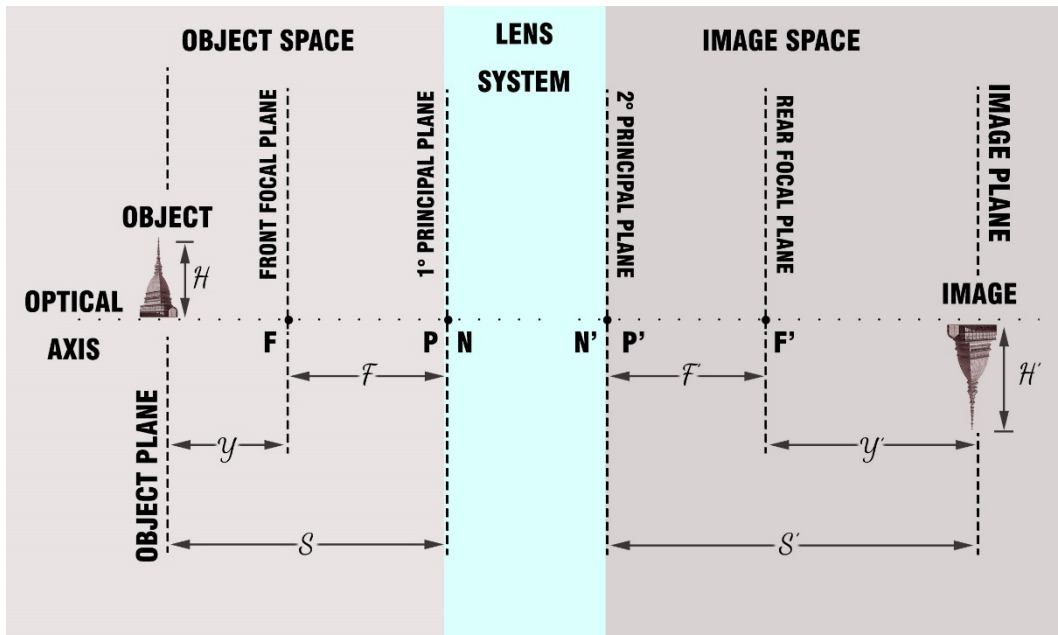


*Figure 18 Thick lens system representation.  $F, F'$  define the focal point while  $f, f'$  define the focal distance.  $h$  and  $h'$  are the object and image size,  $s$  and  $s'$  are object and image distance.  $P$  and  $P'$  are the principal points, while  $N$  and  $N'$  are the nodal points (Source: Author elaboration based on G. Verhoeven, 2016)*

To describe the whole lens system two refracting planes (principal planes) perpendicular with the optical axis need to be identify, they are conjugates and coincide with the nodal planes. Principal points  $P$  and  $P'$  are defined by the intersection of the optical axis with the principal planes, as well as the nodal points  $N$  and  $N'$ .

In order to illustrate the direct relation between focal length and object distance is possible to adopt the principles of ray tracing (Glassner, 1989; Katz, 2002). Ray tracing is a technique for the computation of the path of the light, following its rays and their interactions with the surfaces. This technique is used in geometrical optics and its peculiarity is that the electromagnetic radiation is not considered as a set of waves or photons, but as a set of rays. In a lens system ray tracing is used to determine where the rays will intersect in the creation of the final images, as shown in Figure 19 the location of the generated image in the thin lens system is determined by the intersection of three rays. Ray  $a$  is parallel with the optical axis and will refract and be redirected from the focal point  $F'$ . Ray  $b$  will pass through the centre of the thin lens and will not be deviated from its path. Finally, ray  $c$  will pass through the object focus  $F$ , it will be parallel to optical axis after the refraction.

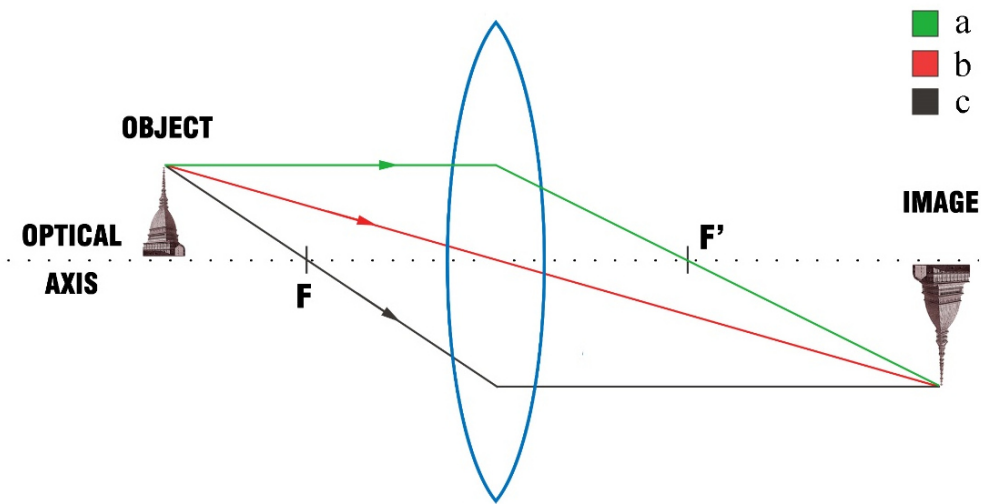


*Figure 19 Thin lens system. Ray tracing. a is the ray parallel with the optical axis that will refract and be redirected from the focal point  $F'$ . Ray b will pass through the centre of the thin lens and will not be deviated from its path. Ray c will pass through the object focus  $F$ , it will be parallel to optical axis after the refraction. (Source: Author elaboration based on G. Verhoeven, 2016)*

Adopting ray tracing technique allows also to demonstrate that, for a far subject, focal length is equal to image distance. As shown in Figure 20, if the distance of the object from the lens increase, the image will be created closer to the focal point  $F'$ .

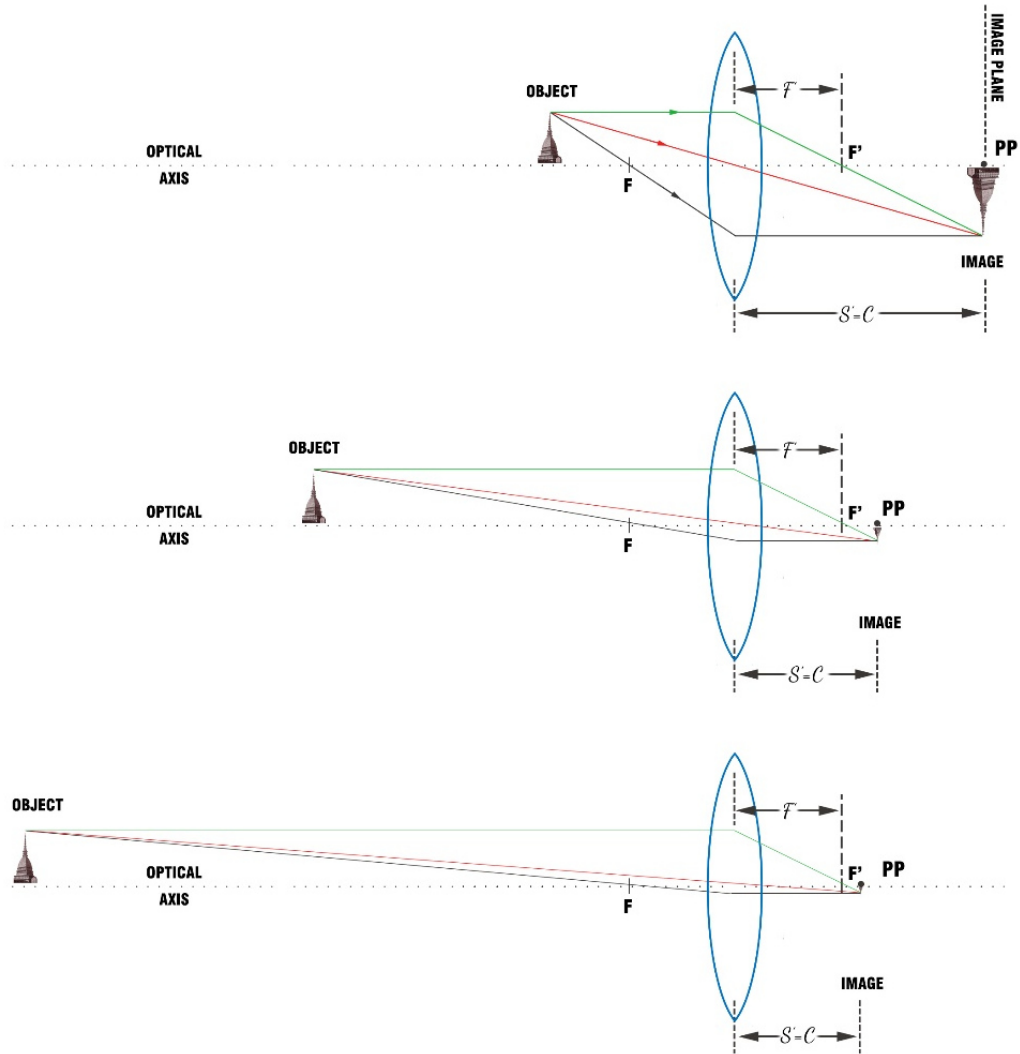


*Figure 20 Ray tracing techniques used to explain how object distance influences image distance. Image distance  $s'$  is equal to photogrammetric focal length and  $PP$  is the principal point. (Source: Author elaboration based on G. Verhoeven, 2016)*

According to the relation between focal length and Field of View (FoV), camera-lens systems are generally classified into six (as shown in Figure 21) main classes, a seventh class can be added to include omnidirectional cameras.

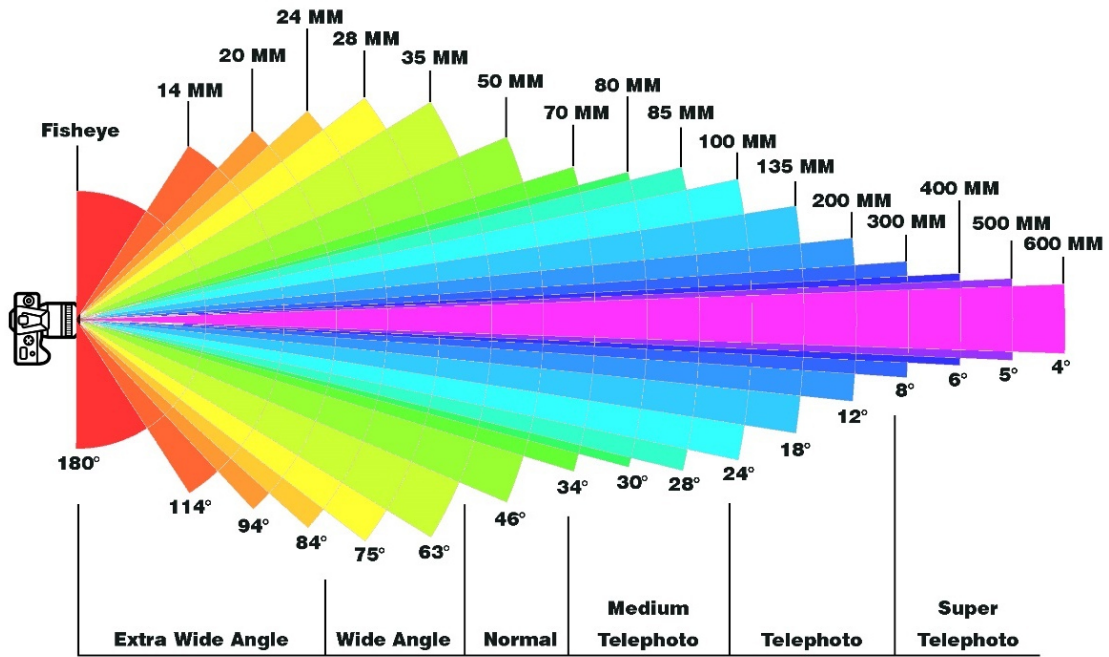


Figure 21 Schematic representation of the relation between Focal length and FoV. (Source: Author elaboration)

Speaking of modern cameras lenses, they can be divided in two main categories based on the way they are manufactured: asymmetrical and symmetrical lenses. Symmetrical lenses usually can reduce the impact of radial distortion, however they are more expensive to produce and then less diffused. On the other hand, asymmetrical lens produces more significant distortion, especially in the corners of the image; they are less expensive to produce. In Figure 22 is possible to see two examples of lens designs (left part of the images) and the complexity reachable from a complex lens system.



**Figure 22** Examples of symmetrical lens design (Zeiss Planar on the top left) and asymmetrical lens design (Tessar's design on the down left). On the right part of the images a section of a Canon lens.<sup>15</sup>

From the brief overview presented above it is clear that lens systems introduce different types of distortion, for example the main effects of distortion on the radial direction in the images are reported in the following Figure 23.

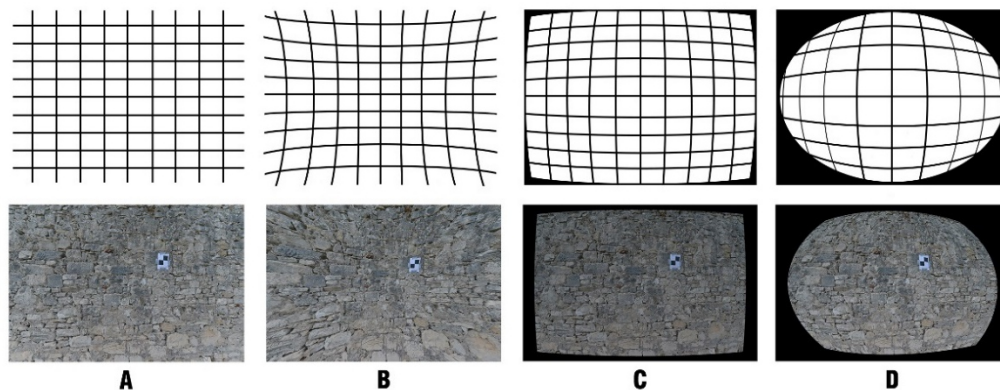


**Figure 23** Example of different type of radial distortion effects. Ideal lens (A), Pincushion distortion (B), Barrel distortion (C), Fisheye distortion (D). (Source: Author elaboration)

Many researchers over the years have studied and modelled the different lens distortions that can affect the process of image generation and a wide bibliography is available on the subject (D. Brown, 1966, 1971, Fraser, 2001, 2013; Fraser & Remondino, 2006; J. G. Fryer & Brown, 1986). What is clear from a survey on the literature available on this topic, is that, especially for low cost consumer grade cameras, the calibration step is a nodal point in the whole photogrammetric process. The process of calibration (i.e. the estimation of the

<sup>15</sup> Lens design from: <http://ilovehatephoto.com/2014/12/30/a-guide-to-optical-lens-design-and-zeiss-nomenclature/>  
Image of the Canon lens from: [https://commons.wikimedia.org/wiki/File:Canon\\_EF\\_200-400mm\\_cut.jpg](https://commons.wikimedia.org/wiki/File:Canon_EF_200-400mm_cut.jpg)

I.O. parameters), which different approaches will be described in section 4.2.2, consist in the estimation of the metric characteristics of the camera. During this phase the following parameters are estimated:

- The position of the perspective centre (Principal Point - PP)
- The focal length ( $f$ )
- The coefficients of the radial distortion of the lens system
- The coefficients of the decentring distortion of the lens system
- The skew coefficient (define the angle between the x and y pixel axes)

On this topic, a brief excursus on fisheye lenses need to be reported, due to the fact that as will be further investigated, they represent the most common solution for the creation of omnidirectional cameras, due to the fact that they can image a large part of the environment. In this kind of lenses, distortions increase non-linearly from the centre to the sides of images and usually the resolution is higher in the centre in respect to the sides; lines that do not pass from the centre of the image are strongly bent. These lenses were designed imitating fishes vision system, they have an extremely short focal length and a wide FoV that reach  $180^\circ$  or beyond and presents obviously some deviations from the traditional pinhole camera model; they do not follow perspective projection. Generally, fisheye lenses are categorized into two main classes: circular fisheye and full format fisheye. These two classes are defined by the size of the image circle diameter related with the image or format sensors as shown in Figure 24.

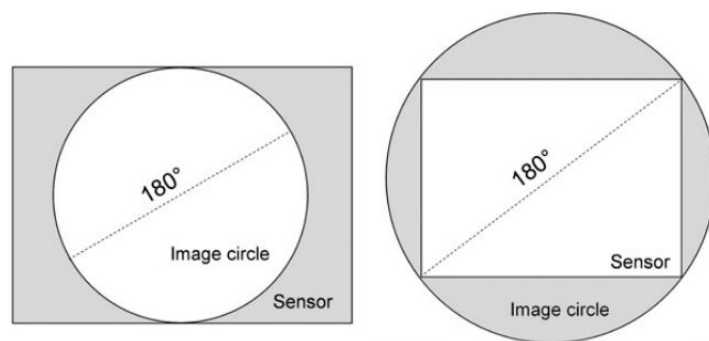


*Figure 24 Fisheye lenses classification. Circular fisheye (left) and full format or diagonal fisheye (right). (Source: Schneider, Schwalbe, & Maas, 2009)*

A further classification can be made according to projection geometry of the lenses that can follow equidistant, equisolid-angle or orthographic projection. The most diffused type of projection in COTS lenses are equidistant and equisolid-angle and will be further described and their modelling analysed.

It has already been reported that fisheye lenses do not follow central perspective geometry and the differences between this model and the typical fisheye projection are showed also in Figure 25.

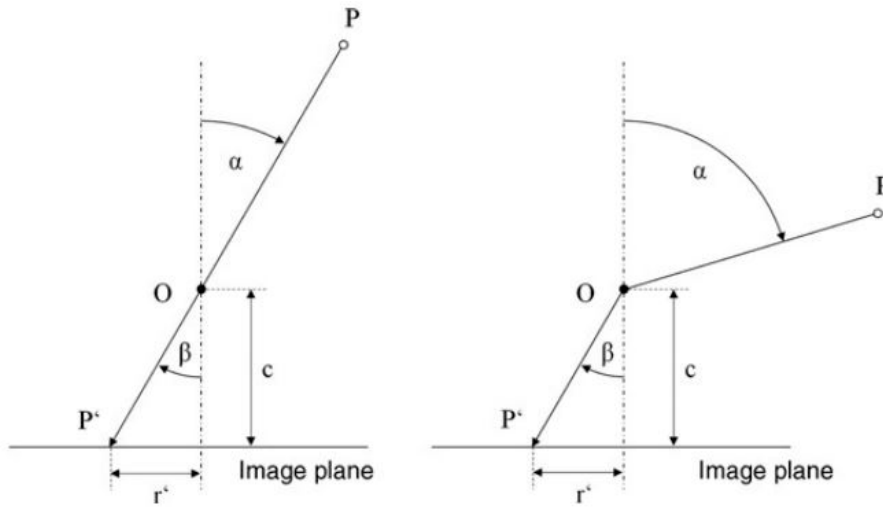


Figure 25 Schematic representation of central perspective geometry (left) and fisheye projection geometry (right). (Source: Schneider et al., 2009)

The relation between incidence angle  $\alpha$  and reflection angle  $\beta$  for central perspective projection can be written as:

$$\alpha = \beta \quad r' = c * \tan \alpha$$

where  $r'$  is the image radius and  $c$  is the focal length

In all fisheye projection incident angle  $\alpha$  is different from reflection angle  $\beta$  and rays are refracted in the direction of the optical axis.

In equidistant projection:

$$\alpha \neq \beta \quad r' = c * \alpha$$

angles of incidence are translated linearly into radial distances within the image.

In equisolid-angle projection:

$$\alpha \neq \beta \quad r' = 2c * \sin \frac{\alpha}{2}$$

the ratio between incident solid angle and its resulting area on the image is constant.

Geometrical modelling of fisheye cameras started from the definition of three coordinates systems, as shown in Figure 26: object coordinate system, camera coordinate system and image coordinate system. Object coordinates are transformed into camera coordinates system:

$$x = R^{-1}(X - X_0)$$

$X$  is the coordinate vector in the object coordinate system,  $x$  the coordinate vector in the camera coordinate system,  $R$  the rotation matrix and  $X_0$  the translation between object and camera coordinate system.

Incidence angle  $\alpha$  in camera coordinate system is defined as:

$$\tan \alpha = \frac{\sqrt{x^2 + y^2}}{z}$$

The radius  $r'$  is defined as function for image coordinated:

$$r' = \sqrt{x'^2 + y'^2}$$

Image coordinates can be described as function of object points coordinates in camera coordinates system:

$$\frac{x'}{y'} = \frac{x}{y}$$

Projection equations can thus be derived as:

$$x' = \frac{r'}{\sqrt{\left(\frac{y}{x}\right)^2 + 1}} \quad y' = \frac{r'}{\sqrt{\left(\frac{x}{y}\right)^2 + 1}}$$

Is now possible to insert these equations into the different types of fisheye projection extended by the coordinates of principle point  $x'_0$  and  $y'_0$  and the correction terms  $\Delta x'$  and  $\Delta y'$  that contains additional parameters for systematic effects:

For the equidistant projection:

$$x' = c * \frac{\arctan \frac{\sqrt{x^2 + y^2}}{z}}{\sqrt{\left(\frac{y}{x}\right)^2 + 1}} + x'_0 + \Delta x'$$

$$y' = c * \frac{\arctan \frac{\sqrt{x^2 + y^2}}{z}}{\sqrt{\left(\frac{x}{y}\right)^2 + 1}} + y'_0 + \Delta y'$$

For the equisolid-angle projection:

$$x' = c * \frac{\sin \left( \frac{1}{2} * \arctan \frac{\sqrt{x^2 + y^2}}{z} \right)}{\sqrt{\left(\frac{y}{x}\right)^2 + 1}} + x'_0 + \Delta x'$$



be achieved from time to time and different strategies can be employed (further details in section 4.2.2).

All the intrinsic parameters retrieved from the calibration allow to reconstruct the image points in their ideal position, the parameters involved in the process will be described in the following sections.

### 3.1.1 Focal Length (or principal distance)

As already reported, focal length is defined as the distance along the optical axis from the perspective centre of the lens to the image plane. If the camera is focused at infinity, the value of focal length is equivalent to the focal length  $f'$  of the lens. If the focus is set more closer, the focal length will increase. Changes in the focus or zoom creates new calibration states. In CV, after the affine transformation from the camera reference system to the object reference system, the focal length computed is expressed in two values (one for horizontal and one for vertical pixels); in the standard case in which the pixels are squared the two values are identical and usually the second parameters is negligible.

### 3.1.2 Principal Point

Principal Point (PP) can be defined as the intersection of the optical axis of the lens system with the plane of the sensor or film (Figure 27). The position of this point can change with different zoom settings but is always near the image centre.

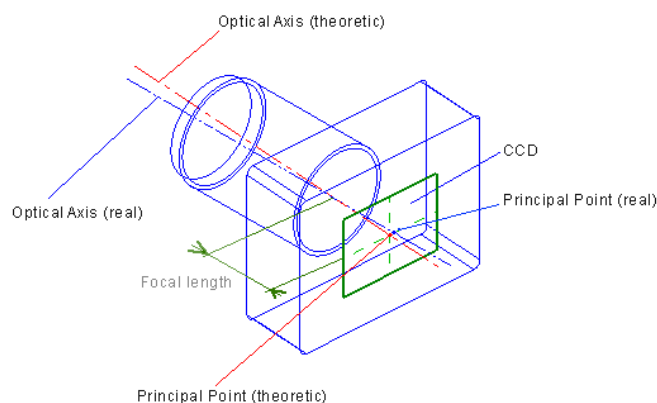


*Figure 27 Schematic representation of the shift between theoretical PP and real PP*

### 3.1.3 Radial Distortion

This distortion is the central symmetrical component of lens distortion and is present along radial lines from the principal point. This type of distortion is unavoidable, and especially in commercial cameras is quite significant, and thus needs to be modelled.

In analytical photogrammetry radial distortion is usually represented as an odd ordered polynomial series (D. Brown, 1971):

$$\Delta r = K_1 r^3 + K_2 r^5 + K_3 r^7$$

$K_i$  terms represent the coefficients of radial distortion and  $r$  is the radial distance from the principal point:

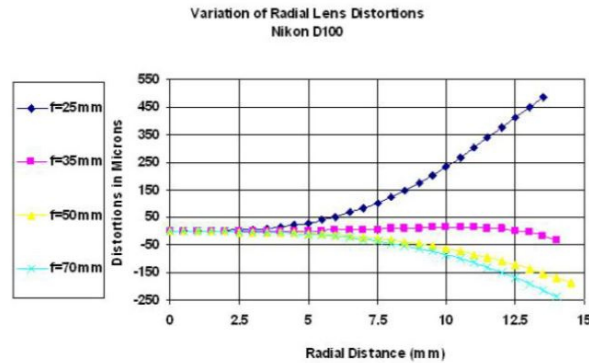
$$r^2 = \bar{x}^2 + \bar{y}^2 = (x - x_0)^2 + (y - y_0)^2$$

Image coordinates  $x, y$  are then corrected with:

$$\Delta x_r = \bar{x} \frac{\Delta r}{r} \quad \text{and} \quad \Delta y_r = \bar{y} \frac{\Delta r}{r}$$

Generally, one to four  $k$  parameters are used to describe this distortion, however, the estimation of  $K_1$  term is sufficient for medium accuracy applications with digital commercial cameras,  $K_2$  and  $K_3$  are accounted for high accuracy applications or in case of wide-angle lenses. Radial distortion profile  $\Delta_r$  is associated with the focal length and is defined as Gaussian distortion. As a consequence, radial distortion is directly influenced by the focusing and the field of view.

The given  $k$  parameters can have both positive (Barrel distortion - Figure 23, C) and negative (pincushion distortion - Figure 23, B) values. An example of the variation of radial distortion profiles at different focal lengths is reported in the following Figure 28.



*Figure 28 Example of the variation of radial distortion profile at different focal lengths from: (Guidi & Remondino, 2012)*

### 3.1.4 Decentering Distortion

On the other hand, the presence of the phenomenon of decentering (or tangential) distortion is caused by a misalignment of the elements composing the lens.

The decentering distortion can be modelled by the following equation (D. Brown, 1966):

$$\Delta x_d = P_1(r^2 + 2\bar{x}^2) + 2P_2\bar{x}\bar{y}$$

$$\Delta y_d = 2P_1\bar{x}\bar{y} + P_2(r^2 + 2\bar{y}^2)$$

The magnitude of decentering distortion can be represented through the function  $P(r)$ :

$$P(r) = (P_1^2 + P_2^2)^{\frac{1}{2}} r^2$$

Usually, compared with the tangential component, decentering distortion has a lower influence in the analytic photogrammetry process, and can be often neglected. However, this distortion is common in commercial lens system, with variable zoom or focus. An example of the variation of decentering distortion profiles at different focal lengths is reported in the following Figure 29.

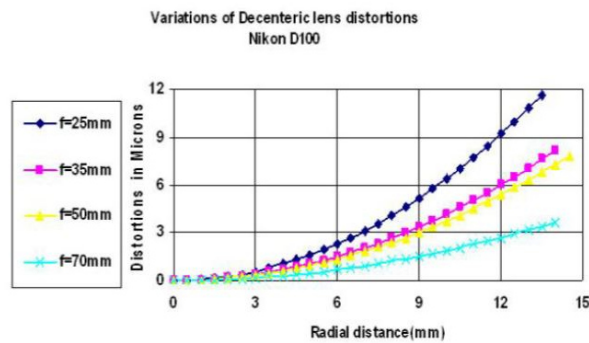
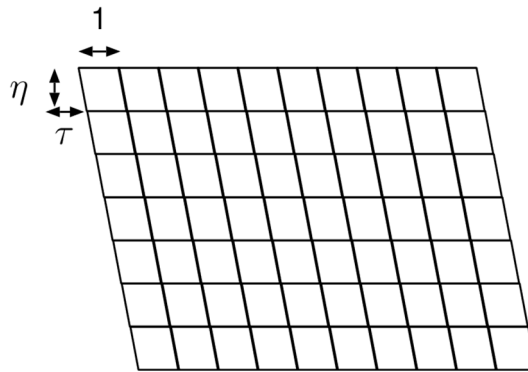


Figure 29 Example of the variation of decentering distortion profile at different focal lengths from: (Guidi & Remondino, 2012)

### 3.1.5 Other Parameters

Furthermore, other camera characteristics can be modelled and calibrated. The so-called *skew* (or shear) is one of these parameters and it represent the affinity in the image plane (Figure 30); due to some manufacturing errors pixels may not be rectangular. In the use of film cameras, almost disappeared for photogrammetric purposes, also the unflattens of the film plane need to be considered.

Another important element that need to be considered is the *pixel size* defined as: “The size of the individual radiation-sensitive elements (e.g. CCD or CMOS) of a digital camera or scanner” (Granshaw, 2016).



*Figure 30 Non-ideal image sensor*

### 3.2.3 Exterior Orientation (E.O.)

Exterior Orientation is the process of establishing relationship between image coordinate system and an exterior coordinate system (local object coordinates or global coordinates depending on the case). During the exterior orientation, position and orientation of the camera, when the images were acquired, are defined. The position of the camera is defined with x, y, z coordinates of the focal point, while the orientation is defined with a set of three rotation angles: defined with the attitude omega (rotation of the x axis), phi (rotation of the y axis) and kappa (rotation of the z axis). A total of six parameters is therefore needed to estimate the exterior orientation.

In the era before the advent of digital photogrammetry, the phase of E.O. was distinctly separated from the I.O. phase. Today, thanks to the processes of automatization that involved the field of photogrammetry, these two parts of the process are solved simultaneously, thanks to the so-called Bundle Block Adjustment (BBA), (Grun, 1982). It is however important to define and described them separately, to better underline their contribute inside the photogrammetric process.

An overview of the different approaches, both derived from photogrammetry and CV, for E.O. can be found in (Grussenmeyer & Al Khalil, 2002).

The process of orientation can be also aided through the use of direct measurement of the sensor position through the use of Inertial Measurement Unit (IMU) and Global Navigation Satellite System (GNSS) receiver; a wide literature is available on the topic (Christian Heipke, Karsten Jacobsen, 2002; Cramer, 1996; Cramer, Haala, & Stallmann, 2000; Jacobsen, 2000).

### **3.3 The SfM based photogrammetric workflow adopted in this research**

Generally, the photogrammetric workflow can be divided into five main steps:

1. Acquisition phase
2. Pre-processing
3. Processing
4. Validation of the process
5. Delivery of the products

The acquisition phase (that will be described in the following section 3.3.1) is obviously the first operation to be achieved directly on the field and its probably one of the most delicate, because it represents the moment in which images are created and can highly influence all the further phases of the process.

The pre-processing includes all the operations that is possible to perform on the images before starting the processing, it gathers procedures like radiometric correction or image enhancement; however, it will not be in depth analyse in this work.

The processing phase is composed by different steps:

- Orientation (Tie Points (TPs) extraction, I.O., E.O.)
- Dense Matching and point cloud generation
- Derivation of other products

The fundamentals behind the TPs extraction and matching phases (i.e. the correspondence problem) will be analysed in section 3.3.2, while the definition of I.O. and E.O. phases have been already provided in section 3.2.

After the processing phase, and before the delivery of the final products, it is mandatory to assess the quality of the overall photogrammetric process. Several quality assessments can be performed through all the photogrammetric process, as reported for example in (ASPR, 2014; JCGM, 2012; Remondino, Nocerino, Toschi, & Menna, 2017), moreover also 3D models derived from other sensors can be used as validating elements.

In this case, it is difficult to provide general rules or standards, however it is important to introduce some definitions of the methods that will be used to validate the adopted procedures and the achieved results. Despite the different technique employed it is possible to set some a common reference language to verify if the chosen approach satisfies the requirements previously defined for each specific case.

The reliability of a set of measurements can be defined and evaluated using different statistical parameters and variables, as for example:

-**Accuracy**: “closeness of agreement between a measured quantity value and a true quantity value of a measure” (JCGM, 2012) or an accepted ground truth value. It is generally described with **Root Mean Square (RMS)** or **Root Mean Square error (RMSe)**. RMS is the square root of the mean of the squared differences between the variable and its most probable value. RMSe is computed using a reference and independent measurement. In case of photogrammetric approach, RMS is computed for the residual in image space (re-projection error) as:

$$RMS_x = \sqrt{\frac{1}{n} * \sum_{i=1}^n (x_i - \bar{x}_i)^2}$$

$$RMS_y = \sqrt{\frac{1}{n} * \sum_{i=1}^n (y_i - \bar{y}_i)^2}$$

$$RMS = \sqrt{RMS_x^2 + RMS_y^2}$$

$x_i$  and  $y_i$  are the image coordinates

$\bar{x}_i$  and  $\bar{y}_i$  are the re-projected values of the computed coordinates

Or it can be computed for check points as:

$$RMSe_x = \sqrt{\frac{1}{n} * \sum_{i=1}^n (X_{Comp_i} - X_{Ref_i})^2}$$

$$RMSe_y = \sqrt{\frac{1}{n} * \sum_{i=1}^n (Y_{Comp_i} - Y_{Ref_i})^2}$$

$$RMSe_z = \sqrt{\frac{1}{n} * \sum_{i=1}^n (Z_{Comp_i} - Z_{Ref_i})^2}$$

$$RMSe = \sqrt{RMSe_x^2 + RMSe_y^2 + RMSe_z^2}$$

*Comp* indicates the computed coordinates values

*Ref* indicates the reference coordinate values

**-Precision:** “closeness of agreement between indications or measured quantity values obtained by replicate measurements on the same or similar objects under specified conditions” (JCGM, 2012). It is generally described with **Standard Deviation** (St. dev.):

$$St. dev = \pm \sqrt{\frac{\sum_{i=1}^n v_i^2}{n-1}}$$

$n$  is the number of measurements and  $v$  is the residual

**-Noise:** random error related with the repetition of measurements

**-Bias:** “estimate of a systematic measurement error” (JCGM, 2012)

**-Ground Sample Distance (GSD):** “the pixel size expressed in ground (object space) units by reference to the image scale” (Granshaw, 2016)

The products derived from the photogrammetric process can be grouped in four main categories (point clouds, meshes, DTM/DSM and orthoimages) and will be described in section 3.8.

### 3.3.1 Acquisition strategies

Considering the fact that all the photogrammetric process is based on the images acquired on the field, the acquisition phase is crucial to achieve good results in the overall process. It is thus useful to recall some principles and guidelines to be followed on the field. The first thing that need to be mentioned is that all the guidelines that will be reported below needs to be adapted considering several factors, like the object geometry, the camera system used, the environmental conditions, etc. It is clear that the experience of the operators is crucial in this phase of the process; all these different issues need to be considered and the available instrumentations need to be employed at its best possibilities. First, it is important to select the correct photographic set up of the camera, that won't be in deep discuss here, in order to obtain good quality images (in terms of sharpness, focusing, radiometry, exposure, etc.).

After completing the setting up of the camera it is crucial to correctly project the geometry of acquisition:

- Camera parameters need to be held fix for the whole acquisition (colour profile, zoom setting, etc.). The geometry of the camera need not to be changed in order not to variate the I.O. parameters of the camera.

- In case of indoor acquisitions or low light condition a tripod can be used in order to ensure a good quality of the images.
- In case of artificial light, it is better to try to obtain a diffuse illumination and not to have punctual sources of light. For outdoor acquisitions avoiding hours with incident sunrays can prevent different illumination areas and the presence of shadows.
- Each part of the object that need to be reconstructed need to be imaged from at least 2 – 3 images and a good coverage of the whole object needs the be achieved.
- Base to depth ratio (B/D ratio) is another key element to consider, it indicates the relation between the distance from camera to camera stations and the object to camera distance. Small bases between camera station lead to a bigger overlay between images, however, also the incidence of the rays from multiple cameras need to be considered and evaluated. Thus, the real challenge is to find the balance between these two requirements: generally, images should be convergent and an optimal convergent angle between images should be ensured. Network geometry of the acquisition is thus a fundamental element, as reported from different authors (Clarke et al., 1998; Fraser, 2001; Gru'n and Beyer, 2001; El-Hakim et al., 2003 ); few other consideration can be reported: network accuracy will increase with the increment of B/D ratio, accuracy will improve dependently of the number of images in which a point is recorded (after four images correspondences increments are less significant), accuracy will also increase with the number of points measured on each images (if the geometric configuration is strong and the point measured are well defined - like targets – and well distributed the improvement is not particularly significant), pixels image resolution influences the accuracy of the retrieved object coordinates (especially on natural features).
- Insert metrical references on the scene before the acquisition. Both GCPs or known distances (such as scale bars of precisely known length) can be used to solve the scale ambiguity during the process.
- Images should be stored in organized archive and possibly with some rough indication associated with the location of the images on the field.

### **3.3.2 The correspondence problem (Tie Points extraction and matching)**

As already reported, the central part of the photogrammetric process is represented by the conversion of 2D measurements of images into 3D measurements; this process consists in the task of finding the correspondences of the same points in different images and is defined

as the *correspondence problem*. To solve this problem is mandatory to define the geometrical relations that occur between two cameras stations; this is done adopting the principles of epipolar geometry, that are illustrated in Figure 31.

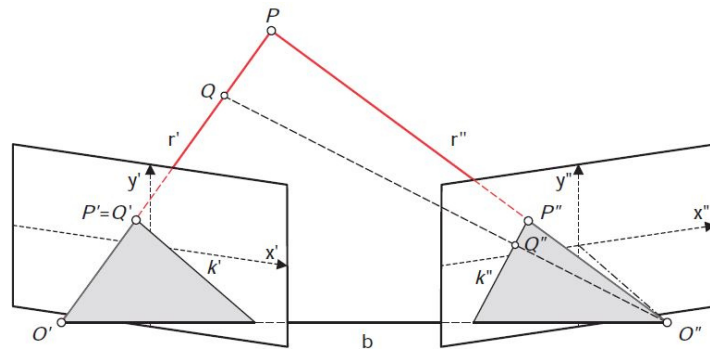


**Figure 31 Epipolar geometry. Epipolar plane for convergent images. (Source: Luhmann et al., 2006)**

The epipolar plane is defined by the base  $b$  (from the two perspective centres of the images) and the projected rays  $r'$  and  $r''$  to an object point  $P$ . Furthermore,  $k'$  and  $k''$  are the lines created from the intersection of the epipolar plane and the image plane, defined as epipolar lines. Image point  $P''$ , that corresponds to image point  $P'$ , must lie on the epipolar plane and on epipolar line  $k''$ . This relation is very useful because the time and resources for the research of correspondences can be drastically reduced from the whole image area to the epipolar line.

The epipolar relations can be represented by the Fundamental matrix ( $F$ ), defined as function of the two-perspective projection matrix of the two cameras, and it contains all the information related to the epipolar geometry. It is possible to calculate the Fundamental matrix knowing the correspondence between (at least) 8 points in the two images, putting in relations the pixel coordinates of the homologous points. Knowing the I.P. ( $K$ ) of the used camera, and considering two images of the same camera, it is possible to put in relations the normalized coordinates of the homologous points using the Essential matrix ( $E$ ), assuming as reference system the one of the first camera.

Since both  $F$  and  $E$  describe the rigid transformation between two cameras, they are related by the following:

$$F = K'^{-T} E K^{-117}$$

Independently on the methods used to solve the Fundamental Matrix or Essential Matrix, linear or non-linear, the set of correspondences between two images can include also inliers or outliers and thus the results estimated can include also incorrect matches. To deal with

<sup>17</sup> Source: (Fusiello, 2018)

these outliers, statistic techniques can be employed: among the more used today are Random Sample Consensus (RANSAC - Foley, Fischler, & Bolles, 1981), Least Median Squares (Massart, Kaufman, Rousseeuw, & Leroy, 1986) and A Posteriori Sample Consensus (MAPSAC - Torr, 2002).

The correlation problem and thus the research of correspondences between two or more images, can be solved adopting two main solutions (a more detailed description of the two approaches can be found in for example Chiabrando & Spanò, 2013; Nex, 2009; Remondino, El-Hakim, Gruen, & Zhang, 2008):

- Correlation-based methods
- Feature-based methods.

*Correlation-based method*, i.e. the more traditional approach, based on the continuity assumption. This assumption states that, when image matching is performed, at a certain level of resolution of the images the major part of the image windows represents a portion of a planar and continuous surface element. Following this approach it is possible to say that adjacent pixels in the windows represents continuous point in the object space. A reference image is then selected, each point is the centre of a small window of pixels that is compared with equal size pixels windows in a target image. This approach provides high accuracy in case of well textured images, however, it requires high computational resources because the searching range between images is quite small. If the continuity assumption is not respected, repetitive or lack of texture are present this approach can encounter some issues.

*Feature-based methods* determine the image correspondences using image features. These methods usually follow a two steps approach: 1) features and their attributes are detected in all images and 2) correspondences between features are then determined. Three different types of features can be determined:

- 1) *Interest Points*: generally these features are extracted using contour-based methods, template fitting methods or signal-based methods. Usually point detectors are accurate, stable (detect the same feature also in case of image transformations), sensitive (detect the same feature also in case of bad contrasted images), rapid and controllable.
- 2) *Edges*: edges features are detected through the intensity change. The process usually follows these steps: smoothing, edge enhancement, selecting a threshold and finally edge tracing. Generally, edges provide more geometric information than interest points.

- 3) *Regions*: regions are defined as homogenous areas of the images with an intensity variation below a defined threshold.

Research in the field of features detection algorithms is still a central point in both CV and photogrammetry community, and several algorithms have been developed over the years. One of the most employed is for sure the Scale Invariant Feature Transform (SIFT): the main characteristic of this algorithms is that it provides features that are invariant to image translation, rotation and scaling. A detailed description of this operator can be found in (Lowe, 2004), briefly it is possible to say that it operates in four main steps: 1) scale space extreme detection, 2) Keypoints localization, 3) Orientation assignment and 3) Keypoints descriptor.

Another diffused algorithm for image features extraction is the Speeded-Up Robust Feature (SURF), described in detail in (Bay, Ess, Tuytelaars, & Van Gool, 2008). This algorithm returns similar results compared to the SIFT algorithm, however it requires lower computational resources and is thus faster.

### **3.3.3 3D reconstruction**

Thereafter, it is necessary to deal with the so-called 3D reconstruction problem, i.e. the retrieval of the position of an object point after the recognition of its corresponding points; this operation aim at the reconstruction of the geometry of a scene. The different approaches to the resolution of this problem are strictly related with the a-priori knowledge of the camera setup. As reported in (Moons, Vergauwen, & Gool, 2015; Toschi, 2014) four main approaches can be described based on this a-priori knowledge:

*Euclidean 3D reconstruction*: requires intrinsic and extrinsic parameters of the cameras to be known, i.e. relative position of cameras is known, and camera are calibrated. Generally absolute orientation in world coordinate system is missing.

*Metric 3D reconstruction*: cameras are calibrated but distances between cameras is unknown. Reconstruction of object points will be solved to an unknow scalar factor, thus the overall scale of the scene will be unknown.

*Affine 3D reconstruction*: in this case also camera calibration is unknown. This method employs the theory of the vanishing point to create a system of affinity equations for the scene reconstruction.

*Projective 3D reconstruction*: in this case no knowledge about the camera configuration or the scene are provided. It is still possible to extract image correspondences and to achieve a reconstruction of the scene through a projective approach. The 3D structure of the scene

is known only up to an arbitrary projective transformation and is thus impossible to obtain indication about the scene dimensions.

These four approaches are described for a standard two-view configuration, the next two sections will address this issue for traditional stereo approach and the SfM approach.

### 3.3.4 The traditional approach: stereo digital plotting

It is not surprising that a set of two images, that have recorded the scene from two different viewpoints, is sufficient to reconstruct the scene without having a pre-knowledge about it, because this configuration is similar to our visual system that can recover a 3D reconstruction of a scene based on two viewpoints provided by our eyes.

The correspondence problem and its possible solution have been already addressed in section 3.3.2, the solution of this problem for couples of images imposes strong constraints on the relative position of the two cameras: the projection rays of points from the two cameras need to intersect or be coplanar (Figure 32). The corresponding point measured between images are called Tie Points (TPs): they must cover a sufficient area in the object and image space to provide a robust connection between images. Tie Points can be identified manually, both in monoscopic and stereoscopic viewing, or using a feature-based approach (again section 3.3.2). Applying this constraints, and knowing enough corresponding point between two images, the relative orientation of the cameras can be obtained both for calibrated or uncalibrated cameras, up to the scale factor. Thus, the relative orientation derives all the 3D corresponding points between images and the relative pose of the two cameras in a local coordinate system. The absolute orientation transforms the scene system into global object coordinate system, using reference points. This is the traditional two-steps solution adopted to solve this problem

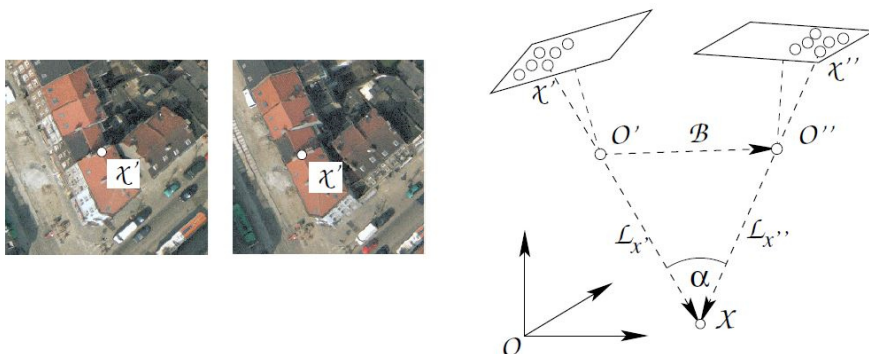


*Figure 32 Example of a stereo-configuration.  $X'$  and  $X''$  are the two corresponding point of the object point  $X$ .  $L_{x'}$  and  $L_{x''}$  are the image rays from the projection centres  $O'$  and  $O''$  (that forms the baseline  $B$ ). Source:(Förstner & Wrobel, 2016)*

To provide aid to the operators, devices that allows the comparison of two images through separated eyepieces were developed: the stereocomparators. Corresponding object points are then located on the two images and thus their spatial position is computed through collinearity principle. Stereocomparators were among the earliest photogrammetric measurement systems and undergone several development during times, an overview of their history can be found in (Luhmann, Robson, Kyle, & Boehm, 2013)

### **3.3.5 The innovative approach: SfM**

The Structure from Motion (SfM) approach is required when images are acquired from a single moving camera (Förstner & Wrobel, 2016; Häming & Peters, 2010; Özyeşil, Voroninski, Basri, & Singer, 2017; Pollefeys, 2003). In an SfM approach the camera relative poses and 3D reconstruction of the scene are achieved simultaneously (Figure 33). Generally, the scene is assumed as static and without moving objects, and thus this approach can be divided in two parts:

- The correspondence problem (3.3.2)
- Camera motion and 3D reconstruction problem

If moving objects are present in the scene the issue of segmentation can be added to the two problems previously cited, however, this case won't be considered in this work and the recorded scene will be assumed as static.

These two issues can be solved following two different approaches, one more traditional and another that was subsequently developed and is the most diffused today.

In the first approach the fundamental matrix is computed matching at least eight features between the different poses, and a projective 3D reconstruction of the scene could be achieved. In order to upgrade the fundamental matrix into the essential matrix, and thus achieve a 3D metric reconstruction, camera I.O. parameters need to be known. The different approach available to solve this task have been already described in section 4.2.1, generally a self-calibration approach is the most diffused between the operators. In this case the scene will be reconstructed up to a scale factor, the use of known measurements will lead to a 3D in scale metric reconstruction.

A ground-breaking approach to SfM was developed by the BBA method, derived from photogrammetric community and now widely used also in CV. Thomas Luhmann (Luhmann et al., 2013) define BBA as “[...] a method for the simultaneous numerical fit of an unlimited number of spatially distributed images (bundles of rays). It makes use of

photogrammetric observations (measured image point), survey observations and an object coordinate system [...]”.

In this approach TPs are used to merge the images in a global model that allows to reconstruct the object surface in three dimensions. Global object coordinate system can be connected to the global model using a number of reference points. It is important to notice that all corresponding image rays should intersect in the corresponding object point with a good consistency. The success of adjustment techniques resides in the fact that all the needed parameters (3D object coordinates, image orientation parameters, additional parameters and statistical information about accuracy and reliability) are estimated in a simultaneous calculation and this provide also a “[...]strong geometry for a dense, high accuracy measurement network” (Luhmann et al., 2013). Furthermore, the development of BBA needs to be related with the increase of the computational power of computers. All this factors considered, it is possible to see BBA as a combination of well-known elements (photogrammetric and geodetic triangulation, space resection and camera calibration), and thus the issues of this approach can be found in the number of unknowns in the system of equations, in the creation of approximate values for the unknowns and finally in the detection and elimination of gross errors.

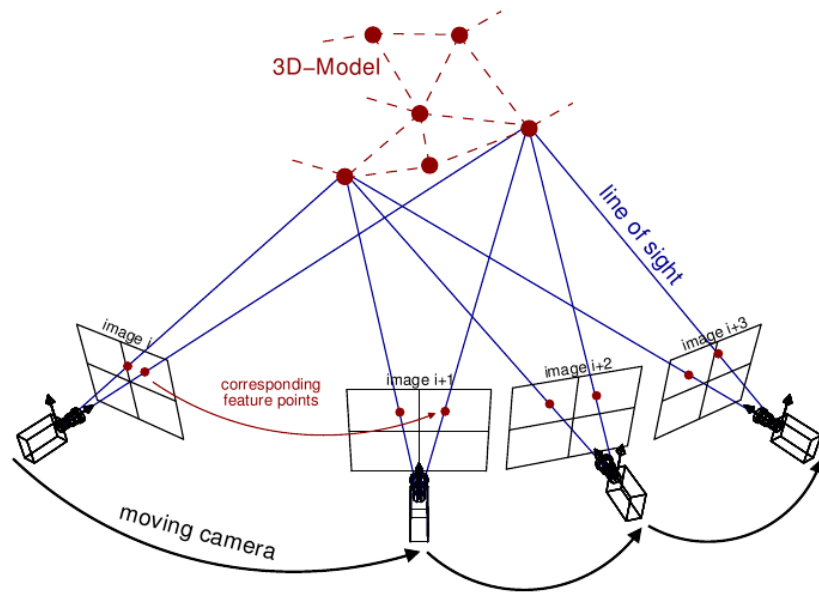


Figure 33 SfM triangulation pipeline. Source: <http://theia-sfm.org/sfm.html#chapter-sfm>

BBA is an iterative process that redefines the camera parameters and the 3D structure through the bundle of rays, to minimize the re-projection errors. Re-projection errors can be considered as the Euclidean distance between a feature in the image and its re-projection in the image plane, starting from its computed position and the camera poses.

## 3.5 Spherical images

As often happens for technological innovation, the attempt to represent the space surrounding the observer is gathered from a transposition of nature and human behaviour. As reported in an interesting text of Thomas Luhmann (Thomas Luhmann, 2004), the FoV of a human eye is limited to 176°, rotating the head is possible to achieve approximately a 330° FoV, while for a complete 360° observation of the environment a rotation of the whole body is mandatory. Needless to say, orientation in the surrounding space and navigation are made easy by a 360° view of the environment.

Nowadays the interest in spherical images, or more in general, in panoramic images is enhanced by the easiness on the use of digital cameras and in the development of automated and simple stitching solutions. This kind of images can be successfully employed in different fields of application: monitoring for safety reasons, video conferences, weather forecasts, tourism, entertainment, mobile mapping and photogrammetry. A brief overview of the historical evolution of this kind of representations of reality will be reported in the following sections, starting for the first experiments of an immersive representation of the environment, through the enhancements provided by the invention of photography and finally till the digital revolution.

### 3.5.1 Historical notes on panoramic images

As reported in the Oxford dictionary of word origins (Cresswell, 2010) the origin of the word *panorama* can be ascribed to the painter Robert Barker and dates back to the late XVIII century. The English painter created this word merging two Greek terms, *pan* (παν - all) and *horama* (ὄραμα - view), in order to describe its aquatint of Edinburgh (Figure 34). In a short time, the most accepted meaning of the word *panorama* was widely recognize as: “An unbroken view of the whole region surrounding an observer” (Cresswell, 2010). Nowadays, the use of the word panorama is intended for wide-angle view, up to 360° panoramas (Luhmann, 2004).



*Figure 34 Robert Barker, view of Edinburgh from Calton Hill (source: City of Edinburgh Council – Libraries)*

Thus, the panorama was conceived as a form of art for the entertainment of people and at the beginning of the XIX it gathered an enormous success. More specifically its success was related with the creation of *ad hoc* temporary structures that allow to the visitors to stand in the centre of a circular platform to enjoy a sort of embryonic immersive experience (often defined as *cyclorama*).

However, the conception of panoramas techniques was already existing and in cartography, panoramas techniques were used for centuries to transpose 3D dimensional objects into 2D representation. The geometric transformation present in cartography were thus successfully transposed in panoramic photography and is possible to identify four main type of projection for this kind of images: cylindrical, equirectangular, cubic and prospective. Today, for photogrammetric application, the most diffused projection is the equirectangular as will be describe in section 3.6.1.

### 3.5.2 First analogic revolution

The daguerreotype was the first successful process in the history of photography and was named after its inventor Louis-Jacques-Mandé Daguerre. After the announcement and introduction in 1839, the daguerreotype was widely used in Europe for the first photographic images of Europe and its citizens. The base of the daguerreotype is a highly polished metal plate, consisting of a thin layer of silver on a copper support. A daguerreotype is created through direct exposure in the camera and delivers a unique image from which no further photographic prints can be made.

Based on this technology, the first panoramic camera invented was probably thanks to the effort of the Austrian Joseph Puchberger in 1843, it was composed by a swing lenses that impressed a field of view of around 150 degrees on a daguerreotype. One of the first examples where a panorama is composed by a set of separated frames that imagined the environment is ascribable to William S. Porter and represent a view of Cincinnati<sup>18</sup>. This idea was later developed in more professional panoramic cameras, like the Al-Vista system showed in the following Figure 35.

---

<sup>18</sup> An interactive visualization of the panorama can be found at <http://1848.cincinnati.library.org/>

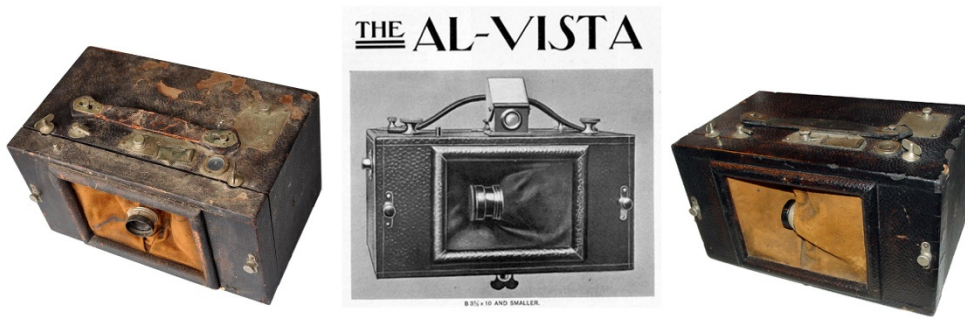


Figure 35 Al-vista panoramic camera. Source: <http://historiccamera.com/>

With the development of photography also the sector of panoramic cameras was subjected to several innovation and analog panoramic cameras were manufactured.

These types of cameras can be divided basically in three categories, following three different technical solution for the generation of the panoramic images:

1. *Cameras equipped with a swing lens:* in these cameras the lens is projected to swing around a vertical axis. The film is placed on a cylindrical surface and is exposed through a small fissure. An example of this type of camera is showed in Figure 36.



Figure 36 Camera equipped with a swing lens. The Horizon 202 (Source: <http://www.sovietcams.com/>)

2. *Rotating cameras:* in this kind of system a motor rotates the camera while the film is moved at the same time. A 360° on the horizontal axis can be achieved with these kinds of cameras. An example of this system is showed in Figure 37.

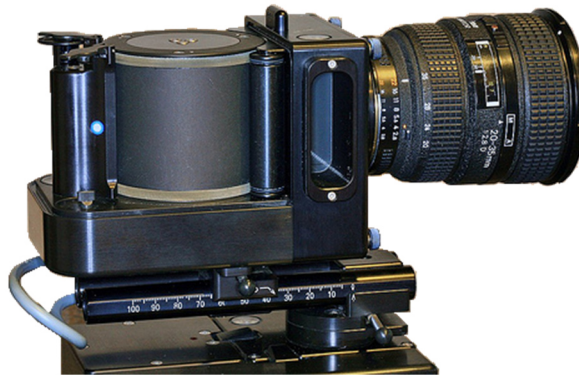


Figure 37 Example of a rotating camera manufactured by Seitz (Source: <https://www.roundshot.com>)

3. *Cameras equipped with a spherical lens:* these systems are equipped with a spherical fisheye lens that provide a panoramic view without a process of “scanning” of the scene. These images are more difficult to interpret and the resolution decrease at the increasing of the radius. As will be described in the following section, the use of this kind of lenses and the digital revolution led to the possibility of obtaining full spherical images of the environment. An example of this lens and of the type of images that can be recorded is reported in Figure 38.



Figure 38 The 8mm F3.5 Circular fisheye manufactured by Sigma (on the left. Source: <https://www.sigmaphoto.com/>). An example of images acquired from a circular fisheye lens – GoPro Fusion (on the right. Source: Author elaboration)

### 3.5.3 Second digital revolution

The digital revolution that interested the world of photography had an impact also on the sector of panoramic images. The possibility to post-process digital images allowed the creation of image stitching algorithms (that will be more in depth described in the following section 3.5.4 ). Moreover, other two key factors can be identified to explain the growing interest in recent time for the recording and use of immersive contents: the development and diffusion of COTS digital cameras and secondly to the simplified and almost automatic

workflow for the generation of panoramic images/videos. The stitching algorithms, developed in the field of CV, are embedded by default in low cost digital cameras and personal devices (such as smartphones and tablets) and the digital production of immersive contents is accessible to everyone. An impressive example is the Street View application for mobile devices distributed by Google (Figure 39): through a step by step procedure the user is guided into the generation of 360° images (the user just shoot the images in the indicated points and the device's processor perform the stitching of the images with quite good results in term of quality).



*Figure 39 Example of the quality of a spherical image (here represented in an equirectangular projection) achievable using the Google Street View application and a commercial smartphone. Basilica di San Nicola, Tolentino (MC), Italy. Source: Author's photo*

Moreover, the distribution through the internet of these kind of images has become easier and quicker. Another factor that need not to be underestimated is the increasing in the use of cameras for surveillance purposes in public and private buildings, allowing the development of ultra-wide angle or spherical cameras also in this sector.

### **3.5.4 Stitching of images (approaches derived from the CV domain)**

Image stitching is defined as the technique that allows to combine multiple singular images into a composite virtual image (an example of this process is reported in Figure 40). Singular images should have sufficient overlapping FoV and the stitched images should possess at least two main requisites: “[...] *should be as similar as possible to the input images, both geometrically and photometrically* [...] *the seam between the stitched images should be invisible*”(Levin, Zomet, Peleg, & Weiss, 2004).



*Figure 40 Example of multiple images stitched into a single panorama, Rainbow bridge, Tokyo. Source: Author's photo*

The turning point in the procedures of image stitching can be traced in the work developed by Szeliski and Shum at the end of the '90s, for Microsoft research (Szeliski & Shum, 1997) and further developed in the following years (M. Brown & Lowe, 2007; Herrmann et al., 2018; Suman, Rastogi, & Tiwari, 2016; Szeliski, 2006), adding also a global alignment of the images composing a panorama through bundle alignment algorithms. The ground-breaking innovation proposed by these two researchers resides in the fact that this system doesn't require controlled motion or camera constraints for the generation of the panoramic images (as long as no strong parallax motion occurs); thus, images can be acquired using hand held cameras. This technique offers the possibility to obtain panoramic images merging planar images acquired from the "same" point of view and with sufficient overlap. What is interesting of this new procedure, if compared with previous image stitching techniques, is the fact that images do not need to have exactly the same projection centre. Another advantage of the approach proposed by Szelinski and Shum is that the generation of panoramic images became available with low-cost and COTS equipment, leading to a great diffusion of these kind of products.

The software that were developed for image stitching starting from this turning point became able to compensate both radial and decentring distortion and complete an almost full camera calibration, estimating the I.O. parameters during the process of stitching. The

virtual image derived from the process of stitching can thus be considered distortion free, this characteristic became really useful for photogrammetric applications, as will be reported in section 3.6.

The process of image stitching can be generally divided into five principal phases:

- *Image acquisition*: during this phase some cautions are needed. It is necessary to ensure enough overlap between images, it is a good practice also to ensure the most uniform exposure between images and, when possible respect to the camera characteristics, to adopt a High Dynamic Range (HDR) approach during the acquisition.
- *Computation of transformation between the second image and first image*: this phase is completed through the detection and match of key points between images (e.g. using the SIFT or SURF algorithms). Homography is then computed using DLT and excluding the outliers using the RANSAC algorithms.
- *Translation of the overlapping area of second image to the first*: the two images are then projected on a common plane and the second image is translated onto the first on their overlapping area.
- *Blending of the two images*: in this phase the pixels that will contribute to the final image are selected and the best approaches to minimize aberrations (seamlines, blur and ghosting) are chosen. Several approaches can be adopted in this phase: average weighting of pixels, optimal seam placement, blending (pyramidal, gradient domain), etc. A more detailed description of these approaches can be found in (Szeliski, 2006).
- *Repeat for all the images that need to be stitched*: the whole process described above can successfully be solved also through bundle adjustment algorithms, performing a global processing of all the images together.

In recent years the approaches for image stitching have also been moved in the field of videography allowing the possibility of creating immersive video from the combination of video recorded from different cameras.

The main issues that can occur during the phase of image stitching are related with parallax effect, images exposure and ghosting effect.

The parallax effect is caused by the use of different cameras, change of position of the camera itself or the movement of objects in the scene. If a non-uniform exposure is achieved in the stitched image the issues generally reside in the different exposures present in the images that compose the panorama. This problem can be solved acquiring the images

in the shorter time possible or adopting an HDR strategy. Ghosting effect happens when moving objects are present on the scene (i.e. people, clouds, waves, etc.).



*Figure 41 Examples of ghosting (left) and parallax (right) errors in the stitching process.*

*Source: author's photo*

### 3.5.5 Software solution for the stitching

Due to the rapid growth of the use of panoramic images for several applications also the number of software available for this purpose has grown as well, they can be grouped in two main categories: commercial (the major part) and freeware.

The commercial packages available are often linked with a camera system, generally the manufacturers provide their physical systems with a dedicated software for the stitching of the digital products. A list of the currently available cameras on the market will be reported in the section 3.6.2, some of the most diffused packages are reported in the following Table 1:

| Software name       | Producer | Website   |
|---------------------|----------|---|
| GoPro Fusion Studio | GoPro    | <a href="https://it.shop.gopro.com/EMEA/softwareandapp/gopro-fusion-studio-app/fusion-studio.html">https://it.shop.gopro.com/EMEA/softwareandapp/gopro-fusion-studio-app/fusion-studio.html</a> |
| Immersive Studio    | NCTech   | <a href="https://www.nctechimaging.com/immersive-studio/">https://www.nctechimaging.com/immersive-studio/</a>   |
| LadybugCapPro       | Ladybug  | <a href="https://www.ptgrey.com/ladybug-sdk">https://www.ptgrey.com/ladybug-sdk</a>   |
| ...                 | ...      | ...   |

*Table 1 Example of dedicated stitching software for commercial cameras*

The list reported above do not include the software, desktop or mobile, in which the stitching is performed automatically and the user is not able to interact in the different phases of the stitching.

Other commercial software packages instead can be used for almost all different camera models and allow the users to generate panoramic images even without a specific camera.

The list reported in the following Table 2 indicates the most diffused software in this category, the list is constantly updating due to the new available solution on the market, software packages still existing but no longer updated are not included:

| Software name           | Producer                   | Website   |
|-------------------------|----------------------------|---|
| <b>AutoPano Giga</b>    | Kolor                      | <a href="http://www.kolor.com/">http://www.kolor.com/</a> <sup>19</sup> |
| <b>GigaPan</b>          | GigaPan System             | <a href="http://www.gigapan.com/">http://www.gigapan.com/</a>           |
| <b>PanoramaStudio</b>   | tshsoft                    | <a href="https://www.tshsoft.de/en">https://www.tshsoft.de/en</a>       |
| <b>Panoweaver</b>       | Easypano                   | <a href="http://www.easypano.com/">http://www.easypano.com/</a>         |
| <b>PTGui</b>            | New House Internet Service | <a href="http://www.ptgui.com/">http://www.ptgui.com/</a>               |
| <b>WidsMob Panorama</b> | WidsMob                    | <a href="https://www.widsmob.com/">https://www.widsmob.com/</a>         |
| ...                     | ...                        | ...   |

*Table 2 Examples of commercial software packages for stitching of images*

Up to date, few freeware and open source solutions exists for this task, the most known are Hugin and ICE, as reported in the following Table 3.

| Software name                       | Producer   | Website   |
|-------------------------------------|------------|---|
| <b>Hugin</b>                        | OpenSource | <a href="http://hugin.sourceforge.net/">http://hugin.sourceforge.net/</a>   |
| <b>ICE (Image Composite Editor)</b> | Microsoft  | <a href="https://www.microsoft.com/en-us/research/product/computational-photography-applications/image-composite-editor/">https://www.microsoft.com/en-us/research/product/computational-photography-applications/image-composite-editor/</a> |
| <b>Google Photos</b>                | Google     | <a href="https://photos.google.com">https://photos.google.com</a>   |
| ...                                 | ...        | ...   |

*Table 3 Examples of freeware and opensource software for the stitching of images*

Despite the small number of freely available software, it is interesting to underline that the major part of the above-mentioned commercial solutions offers trial licences with almost complete features and allow the user to deeply test the software before purchasing a licence. The workflow of these software is almost the same and follows the steps of image stitching procedure described in the previous section. The main difference between the different software is related to the possibility of the user to act in the different phases of the process and to define constrains, parameters and operations. Usually the software provided with a peculiar system are markedly user friendly, but on the other hand, allow few controls over the stitching parameters for the user. On the contrary, software that are dedicated to the stitching of images from different cameras need to include the control over a bigger number of parameters and to allow the user intervention over different phases of the processing.

---

<sup>19</sup> The author became aware during the writing of the work that unfortunately the company has closed; thus the software won't be developed in the future.

The choice of the software to employ depends mainly on the set up of the acquisition phase and from the characteristics of the camera system used: on the other hand, it is true that the software designed for a specific camera do not offer many options for the user's intervention, but on the other hand they generally produce a good stitched images, knowing the parameters of the camera employed. However, in general terms, it is always a good option to have access directly on the raw files recorded from the camera system, to be able to freely decide which software solutions adopt for the stitching phase and eventually minimize aberrations produced during the stitching phase.

### 3.6 Spherical Photogrammetry

The first analog panoramic cameras were not successfully used for photogrammetry for two main reasons: first, as reported in section 3.5.2, the rotation mechanism of the cameras was not precise enough and secondly, the image modelling was more complicated to be used during the restitution process. It is possible to state that the first real use of these cameras for metric purposes was thanks to their combination with theodolites, in the so-called photo-theodolites. With the digital revolution and the development of new solutions for the creation of panoramic and immersive images, also the photogrammetric use of these images was subjected to major changes. The efforts in this field were devoted to solve two main issues: the development of ad hoc instrumental solutions and the refinement of the mathematical modelling of these cameras. The first experiences in these field were related with cylindrical images and a detailed description of the problems related with the modelling of these cameras can be found in (Luhmann et al., 2006, 2013; Luhmann & Tecklenburg, 2004). However, in this research the focus will be only on the use of spherical images and other panoramic representations will not be considered.

Two main approaches can be followed for a photogrammetric use of spherical images:

- *Multi-Image Spherical Photogrammetry (MISP)*, defined also as *Panoramic Spherical Photogrammetry (PSP)* or *Spherical Photogrammetry (SP)*: was developed mainly by the Italian group of the Università Politecnica delle Marche led by Prof. Fangi (Barazzetti, Fangi, Remondino, & Scaioni, 2010; Fangi, 2007, 2015). One of the reasons that led to the development of this approach was connected with the idea to stress the main advantages connected with the use of spherical images instead of normal frames. The main benefits, as reported in (Fangi & Nardinocchi, 2013), are thus connected to: the plotting of the object main features that can be performed with simple direct measurements, it is low-cost, it is rapid and it is complete. PSP is defined as an analytical approach for the

processing of spherical images represented in an equirectangular projection. The mathematical and geometrical modelling of spherical images will be discussed in the following section 3.6.1, however is possible to introduce a schematic representation of the workflow (reported in Figure 42) as described in (Fangi, 2015).

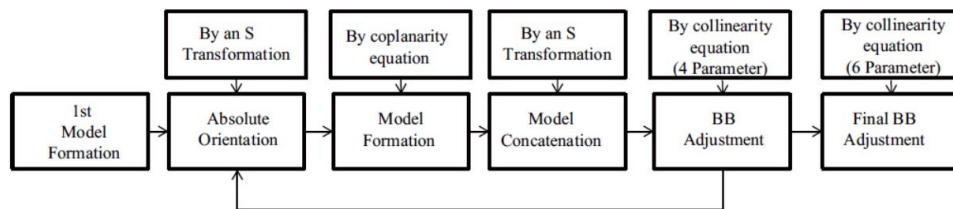


*Figure 42 Schematic representation of PSP processing phase (Source: Fangi, 2015)*

The first part of the process is initialized with the model formation of two spherical images, which absolute orientation is then computed, transforming the model system into an absolute reference system. The adjacent models are then formed and concatenated with the first one, until a final BBA that allows the estimation of the final orientation parameters and object point coordinates. The software developed by Fangi was updated and implemented during the years, e.g. introducing a self-calibration of the panoramas in order to estimate the radius of the sphere.

- *SfM*: the development and diffusion of SfM algorithms in the photogrammetric community result also in a second new life for spherical photogrammetry. In the last years the community of researchers (Abate, Toschi, Sturdy-Colls, & Remondino, 2017; Barazzetti, Previtali, & Roncoroni, 2017a, 2018; Fangi, Pierdicca, Sturari, & Malinverni, 2018; Kwiatek & Tokarczyk, 2014, 2015; Pagani & Stricke, 2011) started investigating issues related with the processing of these images through a SfM approach and also software solution that embed this possibility became available. The research in this field has just began and a lot of issues need to be analysed and solved, however the first results are significantly promising.

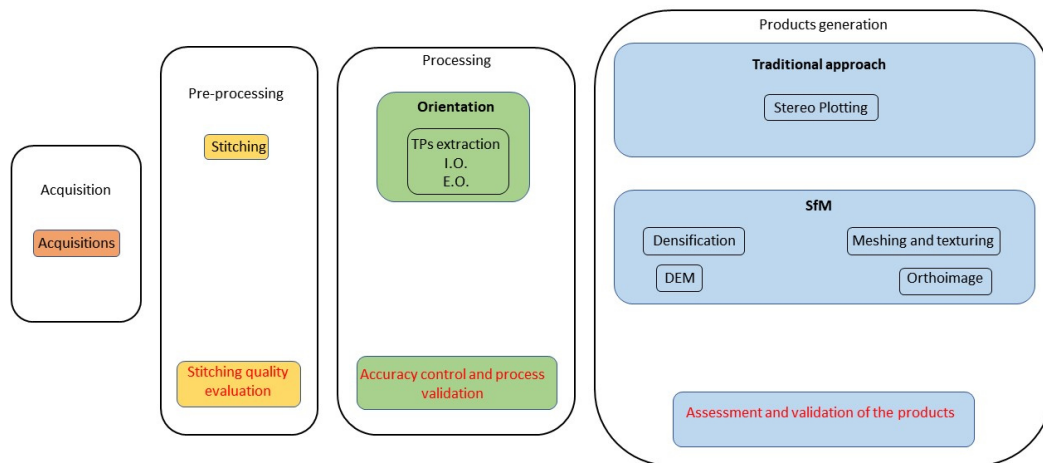


**Figure 43 Schematic representation of the PSP workflow. Source: author's elaboration**

In Figure 43 a schematic representation of the SP workflow as it is configured nowadays is reported. The first phase is connected with the acquisition of the spherical images that involves a series of considerations and requires *ad hoc* strategies, as it will be further reported in section 4.3. The pre-processing of the images is devoted mainly to the stitching of the single images acquired on the field from the 360 system into the spherical panorama. The problems derived from the process of image stitching have already been addressed in section 3.5.4, in this phase of the workflow it is necessary to maintain an overall control of the stitching quality of the images derived from the 360 system. The phase of the processing can be achieved following the traditional workflow described by Fangi in (Fangi, 2015b) or adopting other solution derived from the SfM approach, solving I.O. and E.O. phases trough BBA approaches. The SfM approach is the one that is adopted in this research, as it will be described in section 4.3.2. Finally, there are two main approaches to derive the products at the end of the processing: following a traditional stereo-plotting approach or completing different phase of the SfM process. The photogrammetric products used in this research are the one derived with the SfM approach and have been already described in section 3.8.

Since its first developments PSP was conceived as a precious tool for the survey and documentation of CH (Abbey, Theatre, Pisa, Zeppa, & Fangi, 2010; D'Annibale, 2011; D'Annibale & Fangi, 2009; D'Annibale et al., 2011; D'Annibale, Tasseti, & Malinverni, 2013; Gottardi & Guerra, 2018; Ramos & Prieto, 2016; Wahbeh & Nardinocchi, 2015; Wahbeh, Nebiker, & Fangi, 2016) for several reasons already partially reported: it can be successfully achieved without traditional topographic measurements or pre-signalized targets on the field, the cost of the equipment is quite low and the documentation produced is complete and with high quality radiometric contents

Moreover, compared to “standard” photogrammetry, a smaller number of images is required to cover all the scene and thus is possible to drastically reduce the time to spend on the field for the acquisition phase. Furthermore, the use of a smaller number of images allows a simplification of the BBA phase. Generally, thanks to spherical view of a panoramic camera or system the operator is free from the constrain derived from the use of a fixed FoV of traditional cameras.

All these reasons considered, the deployment of spherical photography and photogrammetry was especially successful in the field of the documentation of CH. Apart from the advantages already reported, it is possible also to record data that can be successfully used for the creation of immersive contents and thus for dissemination and valorisation purposes (Kwiatek, 2012) .

### **3.6.1 Modelling and Calibration of Spherical Cameras**

Epipolar geometry has been already described for “standard” photogrammetry (section 3.3.2) and the same considerations can be transferred to spherical photogrammetry, despite the fact that the epipolar line will not be represented by a linear equation. Back in the 2004 the epipolar line for cylindrical images have been already studied and analysed by (Luhmann & Tecklenburg, 2004) that demonstrated that it can be plotted as a sinusoid. Geometric constrains of two- and three-view geometry of spherical cameras and construction of epipolar geometry for these kind of cameras have been described by (Torii & Imiya, 2007; Torii, Imiya, & Ohnishi, 2005).

The mathematical modelling of spherical cameras and their orientation is deeply described in (Fangi & Nardinocchi, 2013) and will be briefly reported here. As will be described this modelling is based in the conversion of pixel coordinates into horizontal and vertical angles, on the correction of the verticality of the z axis and into bundle adjustment of different camera stations, similarly to geodetic networks.

More specifically, the modelling of spherical cameras is mainly based on two steps: first spherical points are projected into an equirectangular projection and secondly two angular corrections are applied in order to the z axis of the sphere to be vertical.

The possibility of mapping spherical images into different projections have been already described in section 3.5.1, generally an equirectangular projection is adopted for photogrammetric applications: in this case meridians and parallels are represented as equally spaced straight lines (vertical and horizontal) and the two poles are represented as straight lines with a length equal to the equator. A schematic representation of this model of projection is reported in the following Figure 44 :

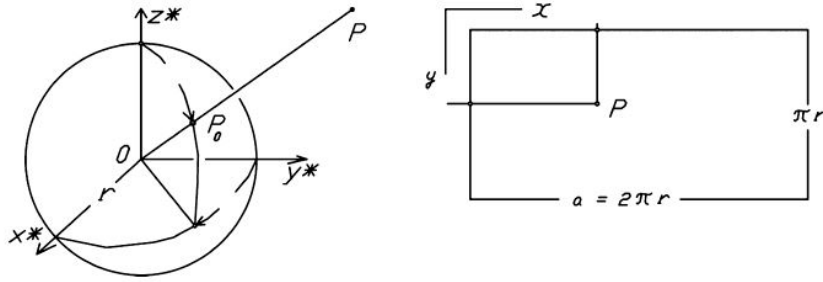


Figure 44 Schematic representation of the equirectangular projection (Source: Fangi & Nardinocchi, 2013)

The projection is represented by two simple equations:

$$x = r\vartheta$$

$$y = r\varphi$$

Where  $\vartheta$  is the longitude,  $\varphi$  is the complement of latitude and  $r$  is the radius of the sphere. What is interesting of this kind of projection is the fact that it establishes a simple relation between image pixel position as  $p(x,y)$ , which are the pixel coordinates of the image and its corresponding point on the spherical image (Fangi & Nardinocchi, 2013).

The collinearity equations (section 3.2) need to be modified for spherical photogrammetry as described in (Fangi & Nardinocchi, 2013) and as will be reported here:

considered a spherical images  $S$  with centre in  $O(X_0, Y_0, Z_0)^T$  and radius  $r$ ,

considered a clockwise reference system having origin in the centre of the sphere and the  $Z^*$  axis coincident with its vertical axis ( $Y^*$  axis passes through the meridian that represents the border of the image);

A point  $P(X, Y, Z)^T$  at a given distance from the centre of the sphere ( $d = \sqrt{(X - X_0)^2 + (Y - Y_0)^2 + (Z - Z_0)^2}$ ) has coordinates  $(X^*, Y^*, Z^*)^T$  in the spherical reference system.

The spherical reference system can be derived from its spherical coordinates  $(d, \vartheta, \varphi)$ , using the following relation:

$$X^* = d \sin \varphi \sin \vartheta; \quad Y^* = d \sin \varphi \cos \vartheta; \quad Z^* = d \sin \varphi$$

As already reported  $\vartheta, \varphi$  are derived from the pixel image coordinates.

To simplify, in an equirectangular projection is possible to see each pair of image coordinates as vertical and horizontal angles that can be measured with a theodolite and scaled of a factor  $r$  that is the radius of the sphere. Differently from a theodolite the vertical axis of the spherical reference system needs to be corrected through two rotation angles  $(\alpha_x, \alpha_y)$  around  $X^*$  and  $Y^*$  axes (Figure 45).

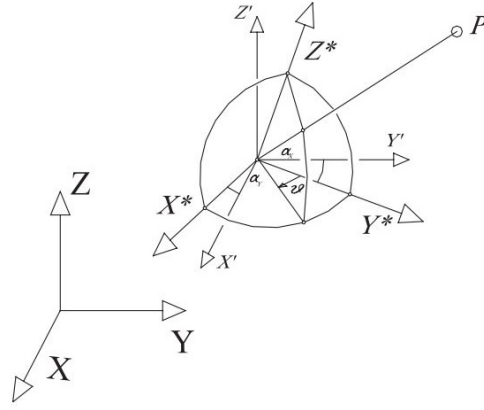


**Figure 45 Schematic representation of the relation between spherical and terrestrial coordinate systems**  
 (Source: Fangi & Nardinocchi, 2013)

The transformation of the spherical reference system in the terrestrial reference system is performed in two steps: first the angles  $\alpha_x$  and  $\alpha_y$  are used to align  $Z^*$  axis to the terrestrial  $Z$  axis and then the rotation around the  $Z$  axis is solved, introducing the spherical orientation angle. Relations of spherical and terrestrial reference system can be described as:

$$\begin{bmatrix} X^* \\ Y^* \\ Z^* \end{bmatrix} = \Delta R(\alpha_x, \alpha_y) \begin{bmatrix} X' \\ Y' \\ Z' \end{bmatrix} = \Delta R(\alpha_x, \alpha_y) \begin{bmatrix} X - X_0 \\ Y - Y_0 \\ Z - Z_0 \end{bmatrix} = \begin{bmatrix} d \sin \varphi \sin \vartheta \\ d \sin \varphi \cos \vartheta \\ d \cos \vartheta \end{bmatrix}$$

where  $(X', Y', Z')^T$  are the coordinates of point P in the terrestrial centre and transferred to the centre of the sphere and  $\Delta R(\alpha_x, \alpha_y)$  is a rotation matrix defined as:

$$\Delta R(\alpha_x, \alpha_y) = \begin{bmatrix} 1 & 0 & d\alpha_y \\ 0 & 1 & -d\alpha_x \\ -d\alpha_y & d\alpha_x & 1 \end{bmatrix}$$

After this correction the spherical reference system need to be oriented with respect to the terrestrial system by an angle  $\theta_0$ . A clockwise rotation is applied to  $\vartheta$  such as  $\theta = \theta_0 + \vartheta$ . Using the collinearity equation is possible to express the relation between image point  $p(x,y)$  and object point P  $(X, Y, Z)^T$ :

$$\theta = \theta_0 + \arctan \left( \frac{(X - X_0) + d\alpha_y(Z - Z_0)}{(Y - Y_0) - d\alpha_x(Z - Z_0)} \right)$$

$$\varphi = \arccos \left( \frac{-d\alpha_y(X - X_0) + d\alpha_x(Y - Y_0) + (Z - Z_0)}{d} \right)$$

In a nutshell, these two equations define the horizontal direction  $\theta$  and the vertical angle  $\varphi$ , corrected in order to account also the correction to the verticality of the sphere.

Using again the coplanarity principle for which two projective rays to a point P and the optical base  $b$  lie on the same epipolar plane and thus the approximate coordinates values of all tie points and orientation parameters can be retrieved. The coplanarity condition can be expressed as:

$$g = x'R'^TBR''x'' = 0$$

$R'$  and  $R''$  are the rotation matrix of the two panoramas,

$B$  is the matrix that contains the components of the baselines between to panorama stations:

$$B = \begin{bmatrix} 0 & -b_z & b_y \\ b_z & 0 & -b_x \\ -b_y & b_x & 0 \end{bmatrix}$$

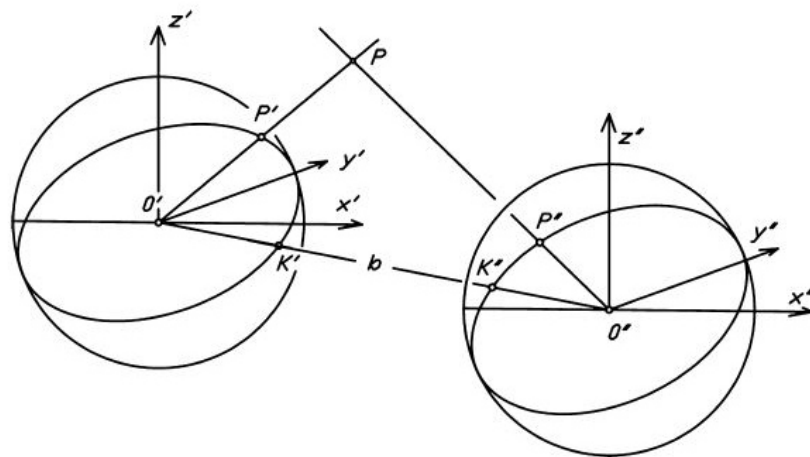


*Figure 46 Epipolar geometry of two spherical images (Source: Fangi & Nardinocchi, 2013)*

As is possible to see from Figure 46, the epipolar geometry (i.e. the geometrical relation between corresponding points on a pair of images) of two spherical images is defined like the one of “standard” photogrammetry. In case of spherical images, the epipolar line is defined as a great circle that passes on the images, due to the fact that it lies on the plane that passes through the centre of the sphere.

If two spherical images are considered ( $S_1$  with origin in  $O_1$  and  $S_2$  with origin in  $O_2$ ) and an image point  $P_0$  is selected in  $S_1$ , the epipolar plane  $\pi_{12}$  is defined between  $S_1$  and  $S_2$  and described by three points:  $O_1$ ,  $O_2$  and  $P_0$ . The epipolar line  $l_2$  is then described from the set of points that belongs to plane  $\pi_{12}$  and images  $S_2$  and correspond to a circle (Figure 47). It is then useful to manage this 3D line in 2D and this can be achieved following two different procedure: 1) defining a reference system  $(x, y)$  on the epipolar plane, having the  $z$  axis

following its normal (Figure 47 - left) or 2) using curvilinear coordinates expressed in the sphere system (Figure 47 - right). In case 1 the points that describe the epipolar line are identified by spanning  $x$  (or  $y$ ) interval of  $[-r; +r]$  to find the other ones. In case 2 angular components  $\vartheta$  or  $\varphi$  are used and by means of the angular space of  $\vartheta$   $[0, 2\pi]$  is possible to find the corresponding value.

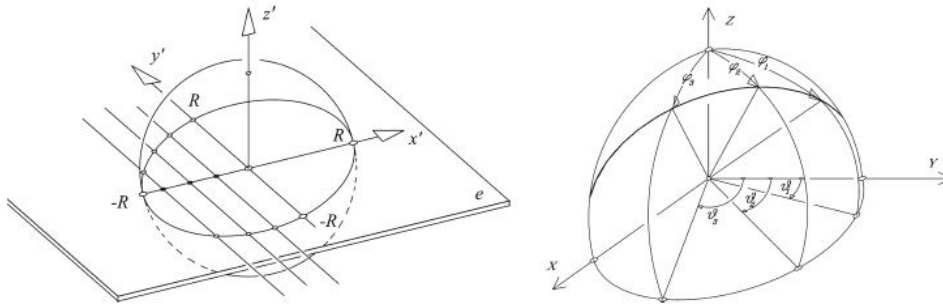


**Figure 47 Epipolar plane on a spherical image and extraction of a set of point for the construction of epipolar line (Source: Fangi & Nardinocchi, 2013)**

After having extract the spherical coordinates of a point  $P_0$  is possible to obtain its corresponding cartesian coordinates following this relation:

$$X = r \sin \varphi \sin \vartheta ; Y = r \sin \varphi \cos \vartheta ; Z = r \sin \varphi$$

$r$  is the radius of the sphere

$\varphi$  is the complement of the latitude

$\vartheta$  is the longitude

The equation of the epipolar plane passing through  $O_1$ ,  $O_2$  and  $P_0$  can be expressed as:

$$Z = aX + bY + cZ$$

$a$ ,  $b$  and  $c$  are the direction cosines of the plane

Finally, the epipolar equation can be written as:

$$\varphi = \arctan\left(-\frac{c}{a \sin(\vartheta) + b \cos(\vartheta)}\right)$$

Thus, the point on the sphere is mapped with the two directions  $\alpha$  and  $\vartheta$ , according to the equirectangular representation, and the epipolar line on the spherical panorama can be extracted (an example of plotting of epipolar line for SP is reported in Figure 48).

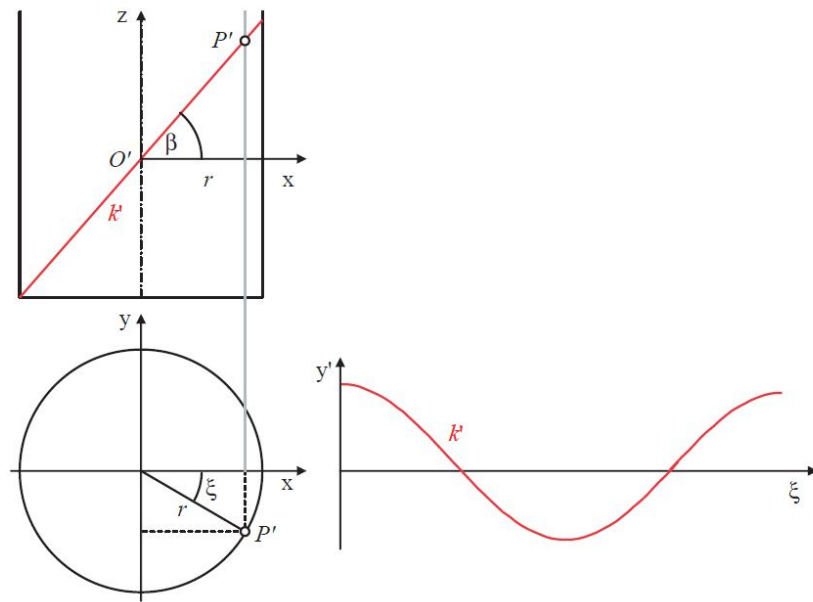


Figure 48 Example of plotting of the epipolar line for SP (Source: Luhmann et al., 2006)

### 3.6.2 Spherical camera systems: Single camera, Dual camera, Multicamera

Spherical camera system can be divided mainly in three categories, depending on the number of camera/lens embedded in the physical device: Single camera, Dual camera and Multiple cameras. Among these three categories it is possible to identify another categorization: Self built system (Do It Yourself - DIY) and COTS. The DIY systems are generally more unstable and need more efforts from the user to reach good results, but are less expensive and more flexible, allowing a higher customisation. On the contrary, COTS cameras are often more expensive and limit the user intervention in the different phases of the process but are more stable and produce higher quality results with less efforts.

*Single camera system:* these systems are usually equipped with a single fisheye super wide lens. The main advantage of these camera is the fact that using a single image is possible to avoid the stitching phase and consequently also the stitching errors that can derive from this phase. The drawback resides on the impossibility to reach a fully 360x180 degrees panorama and generally the FoV is thus limited. Example of these cameras are reported in the following Table 4.

| System image  | System name    | Price (euro – November 2018) |
|---|----------------|------------------------------|
|  | 360FLY 4K      | 300-430                      |
|  | Kodak SP360 4K | 380-480                      |
|  | Omi Omicamera  | 310                          |
|  | DIY systems    | variable                     |
| ...   | ...            | ...                          |

*Table 4 360 cameras. Examples of Single camera system*

These cameras are however the less diffused ones among the users, especially for the limited FoV issue previously reported.

*Dual camera systems:* these systems are composed by two cameras facing two opposite directions and with two FoV partially overlapping. The lens employed in these systems are generally super wide-angle fisheyes or circular fisheyes, that are able to guarantee sufficient overlap between the images. In general, these systems are quite low-cost and with reduced dimensions, due to the fact that they are often conceived as an evolution of action cameras for the recording of sports or other activities.

| System image  | System name       | Price (euro – November 2018) |
|---|-------------------|------------------------------|
|  | Garmin VIRB 360   | 800                          |
|  | GoPro Fusion      | 610-720                      |
|  | Insta360 ONEX     | 440-460                      |
|  | Kodak ORBIT360 4K | 400-450                      |

|   |                      |          |
|---|----------------------|----------|
|    | Nikon KeyMission 360 | 260-300  |
|    | Ricoh THETA V        | 380-440  |
|    | Samsung Gear 360     | 140-170  |
|    | Vuze XR              | 440      |
|    | Yi 360 VR            | 310-350  |
|  | DIY                  | variable |
| ...   | ...                  | ...      |

*Table 5 360 cameras. Examples of Dual camera systems*

*Multiple cameras systems:* these systems are composed by a variable number of cameras looking in different directions. The design of these system can vary in different shapes and configuration and also the range of price varies a lot, from few hundred euros till some thousands.

| System image  | System name       | Price (euro – November 2018) |
|---|-------------------|------------------------------|
|  | Aurovis Argus 360 | 4000                         |
|  | Bubl BublCam      | 700                          |

|   |                    |           |
|---|--------------------|-----------|
|    | GoPro Omni         | 1500-5000 |
|    | Insta360 Pro II    | 4000      |
|    | Kandao QooCam      | 355-435   |
|    | Kandao Obsidian R  | 6000      |
|    | Kandao Obsidian Go | 2200      |
|   | Panono 360° Pro    | 1300-1600 |
|  | Vuze +             | 1200      |
|  | Z Cam S1 pro       | 9000      |
|  | Z Cam V1 pro       | 34000     |
| ...   | ...                | ...       |

*Table 6 360 cameras. Examples of Multiple camera systems*

In this overview of 360 system, catadioptric and in general systems that use mirrors to widen the camera's FoV are not considered due to the fact that they introduce other distortions that are not easy to model and need to be separately considered and analysed. Another way to obtain spherical images, the first one that was developed, is through the stitching of images recorded with a single camera (usually a Digital Single-Lens Reflex - DSLR) rotating around a nodal point. This approach was the most popular until the recent

development and launch on the market of COTS 360 systems; it is the one used in the major part of the researches about SP and is still a valid approach for Spherical SfM. The acquisition phase of this approach is faster than traditional one, however, the new camera systems described above are faster, at the cost of sacrificing a part of the resolution of the final images.

In this research two different systems for the acquisition of spherical images were employed: a Multiple camera system (the Freedom 360) and a Dual camera system (GoPro Fusion). In the following sections the two systems will be described and analysed and some considerations on their calibration and use for photogrammetric purposes will be presented as well.

### **3.7 Unmanned Aerial Vehicle: UAV's**

UAVs were born and developed on military contexts as platforms for training, recognition missions, surveillance, mapping and war actions (Dalamagkidis, Valavanis, & Piegler, 2012; Keane & Carr, 2013); however their potentialities in the field of mapping were rapidly understood; early examples can be found in (Wester-Ebbinghaus, 1980).

The roots of UAVs development can be traced in the wider sector of aerial observation through flying vehicles. Cameras started being used from balloons and first images from the air were then captured already in the second half of XIX century (Gaspard-Félix Tournachon in 1858 acquired several photographs of Paris from a hot air balloon). Other interesting experiments were performed in the following years using other flying platforms such as kites, rockets and also birds as a manner to transport and use standard cameras from the sky. These first experiments were then not pursued for some decades, due to the invention of the airplane and the rapid development of manned airborne photography that took the whole scene of aerial photography starting from 1903 (from the first flight of the Wright brothers). The aerial photography from aeroplane rapidly became a fundamental tool in military applications and in the late XX century times were ripe for the study on the remote control of aerial platforms to be started again, thanks also to the technological evolution. The history on the origin and evolution of UAVs is wide and well-studied, only few notes are reported in this research and it is possible to find more detailed information in (Dalamagkidis, Valavanis, Piegler, Dalamagkidis, Konstantinos; Valavanis, Kimon P.; Piegler, & Valavanis, Kimon P.; Oh, Paul; Piegler, 2009; Eisenbeiß, 2009); a schematic overview of the different evolution phases of UAVs use, both in military and civilian sector, is showed in the following Figure 49.

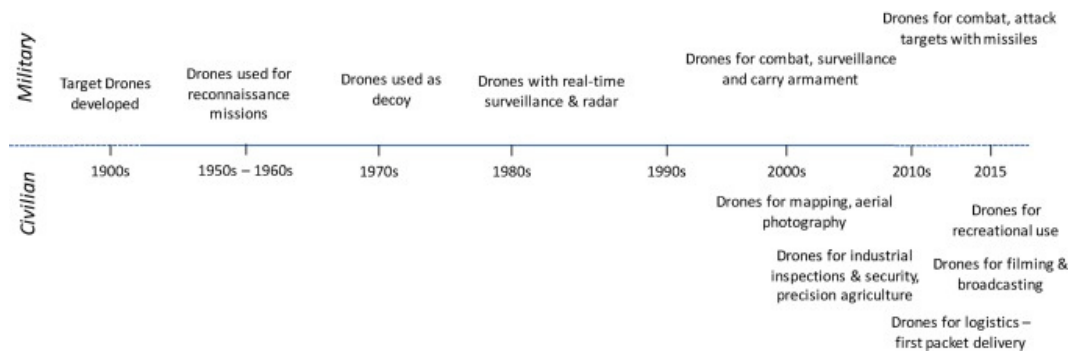


**Figure 49** Timeline of military and civilian evolution of UAVs use (Source: Giones & Brem, 2017)

The success of UAVs among citizens, professional organisations and researchers can be read through different keys: it is possible to analyse the number of registered platforms in a specific state, e.g. as in the work of (Everaerts, 2009), to evaluate the growth of the economic sector related with the production and sell of UAVs, e.g. as in (Giones & Brem, 2017), or to analyse the growth of the research works connected to these platforms in the scientific literature, as in (Colomina & Molina, 2014).

In the work of (Giones & Brem, 2017) is possible to find a lucid and complete analysis on the rise and evolution of the UAVs industries, that was worth \$2 billion in 2016 and is expected to be \$127 billion in 2020.

Despite the chosen key of interpretation, one point is fixed: the growing rates of this sector and of all the connected activities was impressive and the process is not finished yet.

In the Geomatics community UAVs had an explosive success, thanks to the facts that they opened new scenarios of application in close-range aerial domain and rapidly became a low-cost alternative to traditional airborne manned photogrammetry.

### 3.7.1 Definition of UAVs and their components

In general terms an UAVs can be defined as “[...] a system of systems - that is, a set of complementary technologies brought together to fulfil a specific task - [...]”, as reported by Colomina and Molina (Colomina & Molina, 2014).

Still nowadays, there is no widely recognize and accepted definition for this class of systems; among the geomatics community the most used definitions are UAVs (Unmanned Aerial Vehicle) and UAS (Unmanned Aerial Systems), while the International Civil Aviation Authority (ICAO) has introduced the definition of Remotely Piloted Aerial System (RPAS). Moreover, other definitions can be found in the literature: Remotely Piloted Vehicle (RPV), Remotely Operated Aircraft (ROA), Remote Controlled (RC) Helicopter. In this research these platforms will be addressed as UAVs.

The intrinsic diversified nature of these systems led to a difficulty also in the creation of well-defined general categories for UAVs. They have been divided in classes following different characteristics (Eisenbeiß, 2009; Everaerts, 2009; Nex & Remondino, 2014): if they are powered or not, their size, their weight, their range, their price, their payload, etc. To shed light on this topic, it can be useful to define which are the components that describe a top-level UAVs, in order to categorize the different types of platforms starting from these components. The three main components are:

- *The unmanned aerial vehicle*: the physical structure of the system. It includes all the component that allow the platform to fly, communicate with the GCS and all the sensors that are necessary to navigate in the space.
- *The ground control station (GCS)*: is the hardware and software part that allow to monitor and control the vehicle. This component is crucial in order to avoid or correct errors during the flight operations and can reach different levels of complexity depending on the employed platform.
- *The communication data link*: it ensures the communication between the GCS and platforms. It is critical in terms of system control and also for safety reasons.

In modern platforms, especially low cost and COTS, GCS and data link are combined in the handheld remote controller.

Obviously, each of these three categories can be subdivided in a series of other group and several other components need to be considered and analysed, more details can be found in (Colomina & Molina, 2014). In this research the categorisation provided by UVS international and reported also in (Remondino, Barazzetti, Nex, Scaioni, & Sarazzi, 2012) will be followed, thus UAVs platforms are divided in the following three categories:

- *Tactical UAVs*: which include micro, mini, close-, short-, medium-range, medium-range endurance, low altitude deep penetration, low altitude long endurance, medium altitude long endurance systems. The mass ranges from few kilograms - or less- up to 1,000 kg, the range from few kilometers up to 500 km, the flight altitude from few meters to 5 km, and the endurance from some minutes to 2-3 days
- *Strategical UAVs*: including high altitude long endurance, stratospheric and exo-stratospheric systems which fly higher than 20,000 m altitude and have an endurance of 2-4 days
- *Special tasks UAVs*: like unmanned combat autonomous vehicles, lethal and decoys systems

Non-powered system, such as balloons or kites, are not considered for the aims of this research, and they are part of another class of platforms.

A further classification can be done dividing fixed-wing and multi-rotors platforms. Fixed-wing are usually able to guarantee a longer flight autonomy and consequently can cover wider areas of territory, on the other hand they require higher flight altitude and more space for take-off and landing. Multi-rotors allow more manoeuvrability and stability, can work at lower altitude, are easier to deploy for take-off and landing, and can work at low distances from inaccessible objects. On the other hand, multi-rotors systems are generally more complex and require higher resources and effort for the maintenance. Moreover, the flight time is reduced if compared to fixed-wing UAVs.

Thanks to the evolution of the sensors mounted on board (such as GPS/GNSS receiver, gyroscope, compass, IMU, etc) it is nowadays possible for UAVs to perform autonomous pre-programmed flight, enhancing the operation on the field and the overall acquisition phase (a more detailed analysis on this aspect and on the different approaches to program the flight plans will be described in section 4.1.1).

On modern platforms, also COTS and low-cost, the number of secondary on-board sensors has grown as well and especially sensors that can enhance the navigation of the platform and the avoidance of obstacle. The systems that are most employed in the field of mapping from geomatics experts can be included in the first categories of platforms, tactical UAVs, and usually their weight is comprehend between few hundred grams up to 25/50 kilograms. A critical issue that have grown as well in the past years is related with the legislation connected with the use of UAVs. The growth of the sector was rapid and the national and international regulations were not able to promulgate laws with the same speed, this resulting in differentiate regulations from state to state and in confused and complicated laws that have a high impact on the users of UAVs for professional purposes.

In the USA the rules vary from state to state and the situation is similar in the EU, nevertheless an effort to unify the laws of the different member states is currently in action. Generally, the regulations influenced also the type of platforms to deploy (weight and equipment) and the limits of the mission to complete (area covered, maximum flight altitude and distance from the operator), as shown by (Haarbrink, 2012).

An exhaustive overview on the national and international regulations regarding UAVs deployment can be found in (Colomina & Molina, 2014; Everaerts, 2009; Stöcker, Bennett, Nex, Gerke, & Zevenbergen, 2017) and in the texts promulgated by the national authorities, in this work only the national laws of Italy and Turkey (the two nations were UAVs were used for this research) will be described.

In Italy the regulation for UAVs are promulgated by the Italian Civil Aviation Authority – ENAC with a regulation that have been updated six times in the last five years<sup>20</sup>. The regulation is divided in eight sections: Section I reports the general definition adopted in the text, Section II reports the norms for platform with Maximum Take Off Weight (MTOW) under 25 kg, Section III the norms for platforms with MTOW over 25 kg, Section IV define the norms that define a UAV pilot and the certification needed to operate these systems, Section V reports the rules for UAVs circulation and use of airspace, Section VI reports the indication of the documentation that need to be updated during the lifetime of the platforms, Section VII indicates the general norms for the non-professional use of UAVs and finally Section VIII indicates the fees and charges for infractions and the final disposition of the regulation. The main disposition that need to be followed for professional operations with UAVs are:

- The person in charge of performing the flight operations need to possess a valid certificate and need to record all the flight performed
- The UAVs employed need to be registered and certificate from the ENAC authorities and the *Certification of the Design* of the platform need to be present
- A valid insurance for the platform should be present
- Operations should be conducted following the norms reported on the regulation, safety conditions need to be guarantee and all the needed pre-authorizations should be present when required. There are limits for maxim flight altitude and horizontal distance of the UAV depending on the operative scenario
- Data protection and privacy issues need to be considered as well

For the purposes of this research all the requirements issued by ENAC were respected depending on the type of fieldwork that needed to be achieved. Moreover, it needs to be reported that a great effort was carried out by the European Union Aviation Safety Agency (EASA) in the last years to harmonise the regulations of the European States. The new European UAVs regulation will probably enter into force in the end of 2019 and the member states will have a 2 years' time to adapt their local regulation to the new norms. The main changes that will be introduced from the new EASA regulations can be summarised as:

- An overall simplification of the regulation

---

<sup>20</sup>An English version of the regulation is available at:  
[https://www.enac.gov.it/sites/default/files/allegati/2018-Lug/Regulation\\_RPAS\\_Issue\\_2\\_Rev\\_4\\_eng.pdf](https://www.enac.gov.it/sites/default/files/allegati/2018-Lug/Regulation_RPAS_Issue_2_Rev_4_eng.pdf)

- A revision of the categories of operations that can be completed on the field based on the level of risk connected with the operation
- The new categories of operations will also set up the different limitations to respect and the type of platform that can be used
- A revision of the procedures to obtain the certificates that are needed for flying a drone

Concerning the regulations exiting for Turkey, the situation is slightly different, and it changed recently. The authority in charge for the control over UAVs norms is the Directorate of Civil Aviation (SHGM). The documentation is unfortunately available almost only in Turkish language, a summary in English language can be found on SHGM website<sup>21</sup>. The import of UAVs in Turkey is regulated as follow: *“Any persons, operators/companies or entities, intending to import an unmanned aerial vehicle from any country to Turkey, shall make an application for technical conformity regarding importation, in order to be submitted to the concerned Customs Office, in compliance with the requirements of Article 5 (2) of the SHT-IHA Instruction”* with some exemptions. The exemptions are:

- UAVs with MTOW less than 20 kg, without autonomous flight capabilities that are used outdoors in the line of sight of the pilot and only for sports and entertainment
- Flying toys or vehicles manufactured to be used indoor
- UAVs with MTOW less than 4kg, maximum speed lower than 50 km per hour and maximum flight altitude lower than 100 m to the ground

In the other cases the process of importation needs to follow several steps and several documents need to be presented and approved from Turkish authorities. For the purposes of this research drones respecting the characteristics to be included in the exemptions were used.

### **3.7.2 UAVs deployment in the field of heritage documentation**

In the community of geomatics UAVs have been deployed in different fields of application, this work will focus on CH application, it is however useful to recall the classification of

---

<sup>21</sup> <http://web.shgm.gov.tr/en>

the different application fields of UAVs as reported for example by (Nex & Remondino, 2014):

- *Agriculture*: UAVs can support the decision process of producers (Gómez-Candón, De Castro, & López-Granados, 2014; Honkavaara et al., 2013; Zheng et al., 2018), in order to optimize resources and time, monitoring the health of the cultivation, etc.
- *Archaeology and Architecture*: the deployment of UAVs in this field will be exploited later in the text.
- *Emergency management*: UAVs have proven their efficiency in emergency scenarios so far already (Boccardo et al., 2015; Calantropio et al., 2018; Duarte et al., 2017). They can be deployed both for early impact assessment, rescue planning and in all the different phases of the disaster management cycle, ensuring the safety of the operators.
- *Environment*: environmental elements (e.g. water, land, rocks, volcanos, etc) can be monitored through a multi-temporal UAVs approach. At the same time, manmade artefacts can be mapped (e.g. road, bridges, or other infrastructures, pollution, etc.), (Manfreda et al., 2018; Toro & Tsourdos, 2018; Tripolitsiotis et al., 2017).
- *Forestry*: in this field UAVs can be deployed in case of fires, monitoring on the different species of vegetation, and other tasks (Guerra-Hernández et al., 2018; Hartley, 2017; Thiel & Schmullius, 2017) .
- *Industrial*: another sector where UAVs can be successfully deployed is the one of industrial application, e.g. for infrastructures inspection, building site monitoring, etc. (Ham, Han, Lin, & Golparvar-Fard, 2016; Morgenthal & Hallermann, 2016).
- *Traffic monitoring*: in this sector UAVs can be used for surveillance, estimation of trajectories, travel time information, incidence response and other connected tasks (Ke, Li, Tang, Pan, & Wang, 2018; Sutheerakul, Kronprasert, Kaewmorachoen, & Pichayapan, 2017).

Even this brief list can justify why UAVs have developed a dedicated methodology in the geomatics community and why they represents an autonomous field of research that need to be combined with other geomatics researches.

Of particular success was the use of UAVs in the field of CH documentation both in the field of archaeology and architecture (Bolognesi, Furini, Russo, Pellegrinelli, & Russo, 2015; Chiabrando, Nex, Piatti, & Rinaudo, 2011; Georgopoulos, Oikonomou, Adamopoulos, & Stathopoulou, 2016; Lo Brutto, Garraffa, & Meli, 2014; Nikolakopoulos, Soura, Koukouvelas, & Argyropoulos, 2017; Sauerbier & Eisenbeiss, 2010; Stek, 2016).

The success of UAVs in these sectors can be underline thanks to different elements:

- Decreasing of the cost if compared to traditional aerial systems
- Reduction of the object-sensor distance
- Easiness of deployment and transport on the field in different contexts
- Improvement of the COTS cameras mounted on the platforms
- Change of the “point of view”

Integration of data derived from UAVs and data from other sensors have been a topic stressed by a lot of researchers in the last years (Balletti et al., 2015; Chiabrando, Spanò, et al., 2017; Grussenmeyer et al., 2008; Peinado Checa, Fernández Morales, & Agustín Hernández, 2014; Xu et al., 2014). In the following section some best practices will be reported while in section 4 open issues related with the deployment of UAVs on archaeological/architectural sites will be analysed and strategies to overcome these issues will be described.

The payload of UAVs can be really variable, and many different sensors can be used (multi-spectral, LiDAR, thermal cameras, etc). In this research only RGB COTS cameras were employed and analysed.

### **3.7.3 UAVs photogrammetry: best practices**

As already reported the interest of the geomatics community in the use of UAVs and in the development of different research topics connected to it covered a wide part of the literature in the last years (Everaerts, 2008; Fernandez Galarreta, Kerle, & Gerke, 2015; Gini et al., 2013; Murtiyoso, Grussenmeyer, & Freville, 2017; Nex & Remondino, 2014; Thoeni et al., 2016).

Generally, the pipeline for UAVs deployment involve five main phases: flight planning, planning and measurement of GCPs, acquisition of images, photogrammetric processing and products delivery. This typical pipeline is showed in Figure 50 where the different phases of the process are drawn in yellow while the input parameters are in green. Nevertheless, there are also other operations that need to be fulfilled before the acquisition phase, i.e. all the issues related with the maintenance and upgrade of the system that need to be completed, as well as all the administrative documentation for the flight authorization; all these shrewdness are fundamental to guarantee a safety finalisation of the acquisition phases.

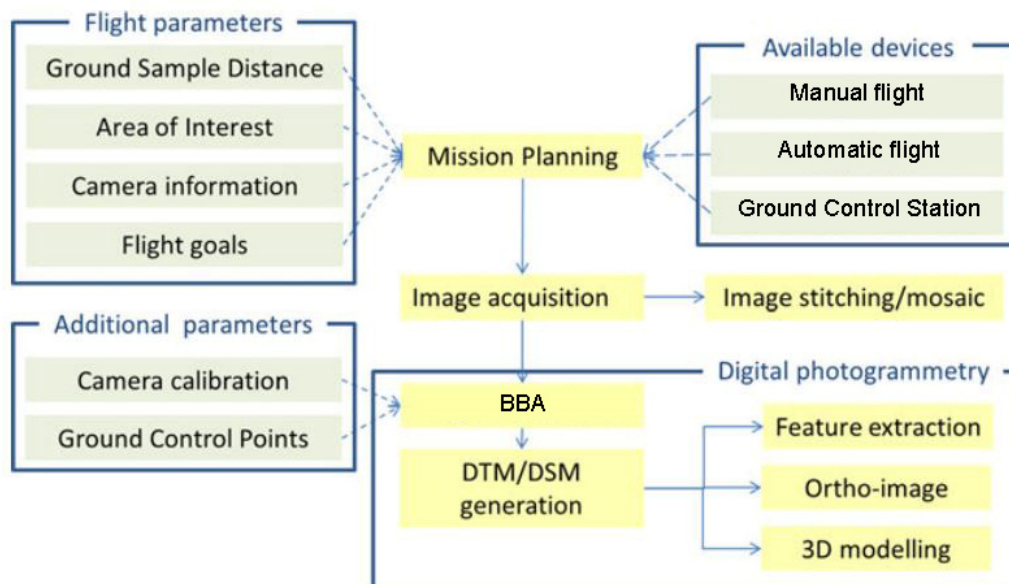


*Figure 50 Schematic representation of the UAV's pipeline (Source: adapted from Nex & Remondino, 2014)*

The mission phases, i.e. the manually or automatic flight that allow the acquisition of images, is probably the phases can mostly demark a good or a bad result of the whole photogrammetric process. As already reported, the flight can be fully autonomous, manual or a combination of the two. Autonomous flight can be planned in the laboratory or directly on the field, this choice is related with the prior knowledge of the area where the flight will be performed. If the area is well known, or a previous inspection of it have been completed, is possible to plan the flight in the laboratory. This decision is related with the knowledge of different factors that can influence the flight operations and that are not always identifiable from a satellite image or a map: presence of trees (and their height), development of the ground, presence of people or inhabited building, presence of other structures (e.g. high voltage cables), etc. If it is not possible to achieve a previous inspection of the area but there is sufficient documentation of it, is possible to perform a tentative flight plan that will then be partially adjusted and modified before the flight, to be adapted to punctual elements highlighted on the field. If also this solution can't be followed, the flight plan needs to be projected directly on the field and the time necessary for this phase need to be included in the overall management of the survey operations.

It has already been reported that this is a crucial phase for the whole photogrammetric process, but it needs to be carefully considered also for safety reasons. What needs to be remarked is the fact that the experience of the flight crew and the pilot is a key element, due to the fact that the factors that need to be considered are many and also the smaller forgetfulness can result in a bad acquisition or, in the worst scenario, in a crash of the platform.

There are nowadays plenty of solution to achieve this task, both open source and commercial, and the general pipeline of mission planning software is structured as follow: the area of interest is outlined, the desired GSD and consequently the flight altitude is estimated (thanks to the knowledge of part of the camera parameters), the waypoints (position of camera centres for the acquisitions) are computed fixing longitudinal and transversal overlap and also the speed of the UAVs is fixed in this phase as well as the shape and direction of the flight lines and the orientation of the camera (a more detailed overview of this topic will be reported in section 4.1.1).

As it is possible to see also from this brief list, the parameters involved in the phase of flight planning are many and they need to be defined also according to the aims of the flight, the operational situation in the field and the accuracy requested for the final products of the survey.

The flight can also be performed in manual mode, if required: this choice is however more critical if compared to the autonomous flight and need to be choose if no other options are available and if the flight crew and pilot experience are sufficient. This type of flight can be performed if the distance object-platforms need to be drastically reduced, if positioning systems are not providing an accurate data, if whether and environmental conditions are not good enough, etc. Generally, a manual flight will produce a more irregular flight grid and it's more difficult to ensure a correct overlap between images and the collection of the right quantity of data (both overabundant or underabundant quantity of data are possible). In other cases, a mixed approach can be used, and the operators can decide to perform an autonomous flight but to maintain the control over specific parts of the flight, mainly take-off and landing.

The planning and measurement of GCPs is another important phase of the whole pipeline of UAVs deployment. The first issue is related with the type and dimension of the pre-signalized target on the ground, if they are used, or in the selection of natural points visible in the aerial images acquired during the flight. The number and position of the targets is another factor that need to be analysed and evaluated; positioning and measuring of GCPs is probably the most time consuming operation conducted on the field, that's the reason why a lot of effort have been spent in the last years in order to reduce the number of measured points and optimize this phase of the pipeline. Real Time Kinematic (RTK) and Post Processed Kinematic (PPK) are two of the solution tested to enhance the phase of E.O. solution in UAVs photogrammetry; an analysis on the different strategies developed in the last years and some test conducted in the framework of this research will be reported in section 4.1.2.

After the acquisition of the images, the focus is then moved on the processing phases. Camera calibration and image orientation are important phases in UAVs photogrammetry

as they are for Close Range Photogrammetry (CRP) (section 3.2.1). In case of higher accuracy requirements these two steps are processed separately, however, especially thanks to the developments of SfM algorithms they have been solved in the last years through a self-calibrating bundle adjustment, maintaining a good accuracy.

## **3.8 Products derived from the CV photogrammetric approach**

If all the processing phases, both for terrestrial and aerial photogrammetry, are achieved with adequate metric control, it is possible to obtain several products depending on the survey requirements. In general, the photogrammetric approach provides three-dimensional object coordinates that can be employed to derive other products. In the following sections the main products that can be derived from a photogrammetric survey will be briefly introduced, they will be later evaluated in connection with their use in archaeological contexts.

### **Point Cloud derived from dense matching**

If camera orientation parameters are known, with a priori calibration or with self-calibration approaches, it is possible to digitally reconstruct a scene with iterative procedures or dense matching techniques. Both commercial and opensource algorithms are available today for performing the dense image matching step, a review of the different algorithms can be found in (Remondino, Spera, Nocerino, Menna, & Nex, 2014) and have been already briefly described in section 3.3.2.

Despite the employed strategy the output of the process is generally a sparse or a dense cloud, describing at least the salient features of the object of interest. What need to be considered is also the points density in relation with the object geometry: in order to preserve the main features of the object without having too many points in flat areas.

### **Mesh**

After the generation of the point cloud is possible to obtain another product: the polygonal model (mesh or Triangulated Irregular Network - TIN). This product can be generated for different purposes: better visualisation of the object, texturing, etc. An overview of the different algorithms that can be used for the mesh generation can be found in (Berger, Levine, Gustavo Nonato, Taubin, & Silva, 2011). The process is generally divided in sub-steps that can be completed in different orders depending on the source data. If source data is composed by a sparse cloud the mesh is generally created following an iterative procedure: creating first lines, then polygons and finally surfaces. When the source data is

a dense point cloud and the data is unstructured a specific process is required, like the one proposed by Delaunay. In this case, the 3D points are projected on a plane or another primitive surface, a search of the shorter point to point correspondences and a generation of potential triangles in performed and finally the triangles are re-projected in 3D and topologically verified. The steps for mesh generation from an unstructured point cloud are generally:

- merging the 2.5D point clouds in order to reduce overlapping areas and creating a uniform full resolution 3D cloud
- meshing with a solution more complex than the one proposed by Delaunay. Two main approaches can be followed: 1) interpolating a surface that build more triangles than the ones needed and then remove triangles without a connection with the surface. 2) approximating surfaces where the output is often a triangulation of a best-fit function of the raw 3D points

### **DEM/DSM/DTM**

Generally speaking three main terms are employed to define these products: Digital Elevation Model – DEM, Digital Surface Model – DSM and Digital Terrain Model – DTM. DEM is defined as a general surface representation where a couple of x,y coordinates is associated with the corresponding z value, it is possible to state that it includes both DSM and DTM.

DSM is a representation of the earth surface with the elements that reside on it while a DTM is a representation of the bare earth. A schematic representation of the difference between DSM and is showed in Figure 51.

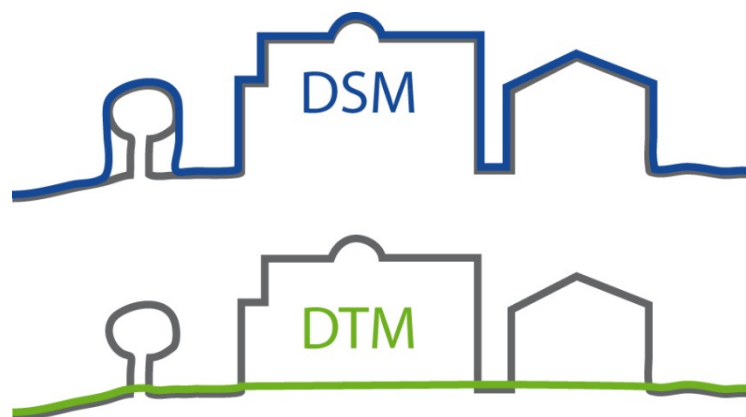


*Figure 51 Schematic representation of DSM and DTM features. (Source: <https://3dmetrica.it/dtm-dsm-dem/>)*

These products can be derived following traditional techniques (e.g. ground surveys, digitisation of already existing data, satellite images, etc.) or directly from a previously computed point cloud and can be achieved following different procedures.

For the purposes of this research the DSM/DTM were derived from set of points (point cloud generated through an image-based approach) with known coordinates, mathematical models were then used to create the surface. DEM can be structured in two different ways:

- Grid Structure: the elevation component  $Z$  is recorded only at each node of the grid and not all the features of the surface are recorded in the cells of the grid. It's easy to retrieve and analyse.
- Triangulated Irregular Network (TIN). Accurate surface models are provided joining points in order not to form overlapping triangles.

### **Orthoimages**

Traditionally the process of orthorectification was employed to correct image perspective and resample the original image to specific geometrical properties. Thanks to the developments of photogrammetry the process of orthoimages generation became easier, both for terrestrial and aerial photogrammetry.

An orthoimage is an image of the object surface in orthogonal parallel projection of each pixels onto a cartographic plane or a local reference plane and thanks to its proprieties it is possible to extract measurements of distances, angles, areas, etc. As reported in (Biasion, Dequal, & Lingua, 2004) an orthoimage can be considered as “[...] *a metrically correct photographic representation of the territory, with the same accuracy as a traditional topographic map*”, containing also other information that are not present on a traditional map.

The orthoimage generation is an automatic process in recent photogrammetric suites and these elements need to be known:

- One or more images of the object/surface
- I.O. and E.O. parameters of the images
- A 3D model (DSM or mesh) of the surface/object

Moreover, thanks to the introduction of the concept of true orthophoto (Biasion et al., 2004; Dequal & Lingua, 2003) it became possible to correctly reproduce the geometry of the entire image, despite surfaces discontinuities caused by occlusions and hidden areas.

## 3.9 Employed software solutions for the photogrammetric approach

The availability of software solution to perform a full photogrammetric process have grown in the last years and at impressive rates. A number of authors have analysed and compared different available solutions (Alidoost & Arefi, 2017; Grussenmeyer & Khalil, 2008; Niederheiser et al., 2018; Schöning & Heidemann, 2015) and the number of available packages is growing every years. In this research a complete overview of the different available solutions will not be reported, more details can be found in the cited literature. In the following sections a brief description of the photogrammetric software used in this work will be reported; the software have been divided in two categories depending on the type of licence of use: commercial and opensource.

### 3.9.1 Opensource

**MicMac:** among the different available opensource solution the one of the most developed and diffused is the MicMac suite (<https://micmac.ensg.eu/index.php/Accueil>). Starting from 2003 it has been developed from the National Institute of Geographic and Forestry Information (IGN) and the National School of Geographic Sciences (ENSG) and it constantly evolved over the years (Rupnik, Daakir, & Pierrot Deseilligny, 2017). In 2005 the different tools previously developed where interface via an XML framework, and it became possible for the users to configure different parameters in the processing steps. In 2007 IGN started distributing the software under opensource licence (CECILL-B). In 2010 XML framework was replaced by a simplified command line interface, allowing more users to start using MicMac (Pierrot-Deseilligny & Clery, 2012).

The general workflow of MicMac is similar to other commercial software solution, however some main differences can be underlined. In general terms, this opensource solution allows more control over a set of different parameters of the photogrammetric process and is possible for the user to maintain a major control over the overall quality of the process. On the other hand, for non-expert users is more difficult to learn the basic command of the software and to interact with the different phases.

For this reason, different projects have been developed in order to provide the users with the MicMac experience but in a more friendly environment and with a proper Graphical User Interface (GUI). Among this various projects the two more recent efforts are the Graphically Enhanced MicMac's New Interface (GEMINI -Calantropio, Deseilligny,

Rinaudo, & Rupnik, 2018)<sup>22</sup> and the inteGRATED PHOtogrammetric Suite (GRAPHOS - Gonzalez-Aguilera et al., 2018)<sup>23</sup>

### 3.9.2 Commercial

Among the several commercial software solutions available on the market two software where used in this research: Agisoft Photoscan and Pix4D mapper.

**Agisoft Photoscan** (<http://www.agisoft.com/>) is for sure one of the most known and used photogrammetric suite both among researchers and non-professional users (Gini et al., 2013; Koutsoudis et al., 2014; Verhoeven, 2011). Despite being considered a black box one button solution from several researchers, with a partial degree of reason, it needs to be reported that the software allows expert users to have control over a set of advanced parameters, especially if the python console is used. The Russian company was founded in 2006 and in few years it gained the upper hand in the market of commercial software for photogrammetry. The processing steps of the Photoscan are similar to other photogrammetric suites: the first phase of the process is dedicated to the estimation of I.O. and E.O. parameters of the images imported in the software and to the extraction of the TPs that will constitute the first sparse cloud generated. In the subsequent steps is possible to go through the densification of the point cloud, the generation of the mesh and finally the creation DSM and orthomosaics. The model can be georeferenced and scaled through the use of images geotag or with the import of points with known coordinates that need to be individuated on the different images. As already reported, the software incorporates some advanced functions such as the possibility of split the computation process on different machines connected to the same network or perform several actions through the python console.

**Pix4D** (<https://pix4d.com/>) was founded in 2011 as a spinoff of the EPFL (École Polytechnique fédérale de Lausanne) and since its establishment the main efforts of the company were focused on the development of photogrammetric software solutions for the processing of images acquired from UAVs (Strecha, 2014). The company is constantly growing, and the proposed software solutions are growing as well, both connected with UAVs and with other applications fields (including also the processing of multispectral images for precision agriculture and the integration of data extracted from RGB images in BIM platforms). In this research the Pix4D mapper pro solution was used; the software follows the standard SfM workflow providing traditional output such as point cloud, mesh,

---

<sup>22</sup> <https://github.com/GAMHer/GEMINI>

<sup>23</sup> <https://github.com/itos3d/GRAPHOS>

DSM and orthophotos. The steps provided by the software are: initial processing, point cloud densification and mesh creation, DSM and orthomosaic generation. In the initial processing I.O. and E.O. parameters of the cameras are computed, and a sparse TP cloud is created.

The model can be referenced and scaled following different approaches: direct georeferencing through images geotag or importing real world coordinates of known points recognizable on the images.

In the second step the densification process is performed through a dense matching approach and a textured mesh can be generated as well. Finally, DSM and orthomosaic are created. This software was chosen due to the fact that, in the authors' experience, it proved to be one of the best solutions for the processing of UAV data (Calantropio, Chiabrando, Rinaudo, & Teppati Losè, 2018; Chiabrando, Lingua, et al., 2017; Chiabrando & Teppati Losè, 2017; Spanò, Chiabrando, Sammartano, & Teppati Losè, 2018).

## Chapter 4

### Aerial and terrestrial sensors and techniques deployment on selected CH test sites

In the following sections the main issues encountered during the development of the methodological framework adopted in this research will be reported, both in case of aerial and terrestrial sensors and techniques. Different tests have been performed on CH sites to tackle the different issues for each sensor employed. The main aim was to deeply test each approach on different contexts before performing more specific analyses on two selected archaeological test sites. The two archaeological sites (Figure 52), where the products of these techniques were more in deep analysed, are the site of Rocca San Silvestro (Tuscany, Italy) and the site of Hierapolis (Denizli, Turkey).



*Figure 52 Aerial views of the archaeological site of Rocca San Silvestro (left) and some structures of the archaeological site of Hierapolis (right)*

All the other sites were selected in respect to some common features that can stress the adopted techniques to their limits. First of all, all the sites are classified as CH sites; this is crucial due to the fact that, as reported in section 2.2, CH documentation has its own rules and procedures that need to be considered and respected. Moreover, another important aspect was connected with the vertical development and the state of conservation of the structures of this site. The two archaeological sites where these approaches were more in deep deployed present an overall good state of conservation of the archaeological remains and thus a good vertical development of the historical structures. The other sites where thus selected as test sites also for this reason and the geometrical configuration of their structures allows to deepen the analyses on the deployment on the field of the investigated sensors and their performances.

For example, the methodologies connected with the deployment of UAVs were more in deep tested on these other two sites (Figure 53): the San Giuliano chapel in Savigliano (CN - Italy) and the Giuseppe Galliano barrack in Mondovì (CN – Italy), while some tests with the 360 systems were performed on the court of the Valentino Castle (TO – Italy).

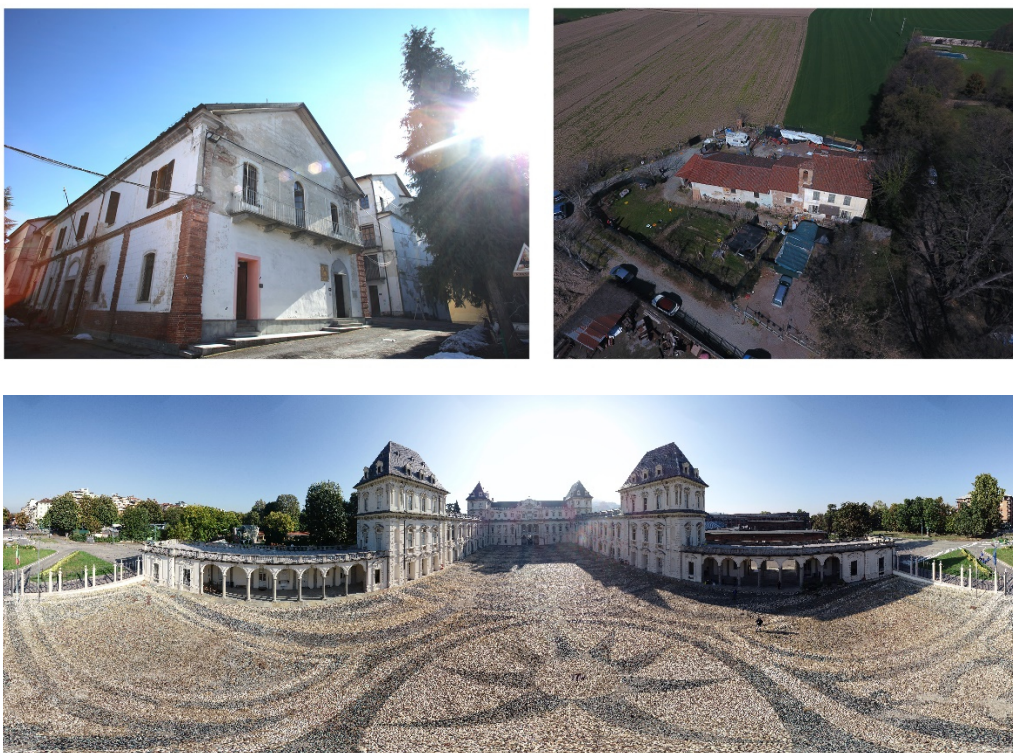


*Figure 53 San Giuliano chapel in Savigliano (top-right), the Giuseppe Galliano barrack in Mondovì (top-left) and the Valentino Castel (bottom)*

## 4.1 Aerial Sensors and techniques

### 4.1.1 Flight Plan and Camera Orientation

The importance of the flight planning phases has been already underlined in section 3.7.3 and will be further analysed in this section. A wide literature is available on this topic (e.g. Hernandez-Lopez, Felipe-Garcia, Gonzalez-Aguilera, & Arias-Perez, 2013; Nex & Remondino, 2014; F. Remondino et al., 2012), however there are still some issues related with this phase of the UAVs photogrammetry pipeline that need to be investigated and solved. A first approach of the author's research group to this topic was proposed in a work presented in the 2017 at the 3D ARCH conference organised in Nafplio with the support of ISPRS (Chiabrandò, Lingua, et al., 2017). This first test was carried out using a UAVs platform that is not ascribable to the COTS and low-cost categories, however the aim of this research was mainly to set up the methodological framework that was then implemented in the following years and is further extended in this thesis work. As will be further report, the aims of this research were to test different flight plans and camera set up in relation with the integration of nadiral and oblique images and the number and distribution of control points. A second research (Chiabrandò & Teppati Losè, 2017), presented in 2017 at the UAV-g conference held in Bonn and again supported by ISPRS, proposed an extension of the previously cited methodological framework to the sector of low-cost and COTS platforms. A third contribute (Calantropio, Chiabrandò, et al., 2018) was presented in 2018 at the ISPRS TC I Midterm Symposium held at the Karlsruhe Institute of Technology in Germany, extending the previous works to other sensors. The experience gained from these three works was included and further implemented in the research developed in this thesis. An extension of part of the work presented in these contributes will be detailed in the following sections and new applications of these methodologies will be reported as well.

The development of UAVs platforms and particularly of the on-board sensors equipped allows the possibility to exploit in the most useful way the intrinsic characteristics of these systems, i.e. their ability to be remotely piloted. Several researches were conducted in the last years (Chunhua, Yong, Zhihong, Jihong, & Zengqi, 2006; J. He, Li, & Zhang, 2012; Hernandez-Lopez et al., 2013; Mangiameli, Muscato, Mussumeci, & Milazzo, 2013) and nowadays automatic navigation of UAVs based on a pre-programmed flight paths is achievable also for COTS and low-cost systems. Moreover, in photogrammetric applications, the navigation task of UAVs is also connected to other parameters, such as camera set up, images geotagging, flight lines, etc., in order to enhance the data acquisition phase. In general terms, flight planning is defined as the fulfilment of a task that complete

a pre-programmed operation considering all the involved parameters. Two types of parameters are generally taken into account in geomatics applications: parameters connected with the platforms and parameters connected with the photogrammetric application. The parameters connected to the platform are responsible of the actual navigation of the aircraft and involve the cruise speed, the attitude of the system on its three axes, its ability to avoid obstacle, its positioning in relation with a global or local coordinates system, the interactions with the GS, etc. The parameters connected with the photogrammetric application gain control over the camera set up, the adherence to a predetermined GSD, the control of the overlap between images, etc.

The major part of flight planning solutions works in the following way: first the area to cover within the flight is selected on an available cartography (e.g. Google Maps, Bing, Open Street Map, etc.), then the flight altitude is selected based on the desired GSD and on the environmental conditions, then all the parameters related with the acquisition of images are set (e.g. camera orientation angle and overlap between images) and finally all the parameters related with the navigation of the platform are defined (cruise speed, flight direction, etc.). All these operations lead to the creation of a grid of waypoints, which can vary in shape and configuration and that represents the network of navigation points on which the UAV will move. Depending on the parameters set by the operator, images can be acquired having the platform stopping on preselected waypoints or eventually during the flight without hovering on the point. This choice is connected also with the camera mounted on the UAV and the time available for the flight operations (e.g. if a rolling shutter camera is used the modelling of the camera parameters can be more complicated if the platform is moving during the acquisition: Chia-Kai Liang, Li-Wen Chang, & Chen, 2008; Oth, Furgale, Kneip, & Siegwart, 2013). Some examples of different flight grids are reported in the following Figure 54.

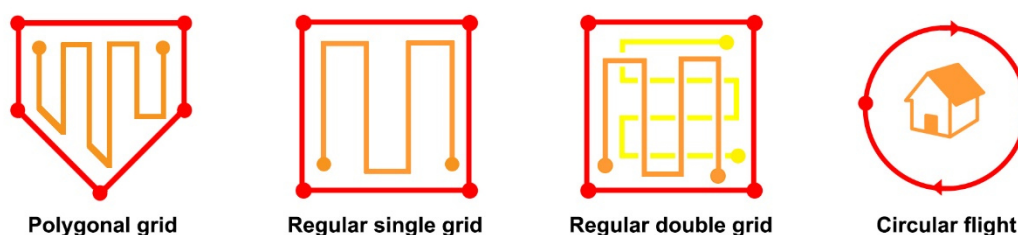


*Figure 54 Examples of different flight grids typologies that can be projected with the dedicated software solutions*

The operations of flight planning need also to consider all the possible issues connected with the safety, thus almost all the available software solutions developed different options to fulfil these tasks. These options are generally related with procedure of automatic return

to home and landing in case of problems during the flight (e.g. battery failure, obstacle, loss of connection with the ground station, etc.).

Nowadays, several software solutions are available to achieve this phase of the photogrammetric process. The choice of the solution to employ is generally related with several factors, e.g. the type of aerial platform used, the conformation of the scene to survey, the experience of the operator, etc. A brief (surely not complete) list of the most diffused solutions and their main characteristics is reported below.

*DJI GS PRO* (<https://www.dji.com/it/ground-station-pro>): commercial, available only for iPad, support part of DJI platforms. This solution is designed only for part of the DJI platforms and is enhanced to work with these devices. It presents a simplify interface that allows the creation of complex flight missions through the use of waypoints. Moreover, it allows to synchronize flight data derived from different operators in a single cloud space and grant a control over large fleets of platforms. One of the most interesting features is connected with the possibility to import .kml and .shp files allowing the users to consider the elevation of the terrain in the phase of flight planning, in order to enhance the flight operations. The user can also set a virtual cage that need to be respected by the platform during the flight, in order to guarantee adequate safety levels.

*DroneDeploy* (<https://www.dronedeploy.com/>): commercial, available both for android and iOS devices, support the major part of DJI drones. Like other solutions described, it allows the generation of flight plans through the use of preselected waypoints. Probably, the most interesting feature of this solution is related with the so-called *live map* tools. This tool allows to generate a 2D map in real time while performing the flight. Another point emphasized by the company that developed this solution is the possibility to work with the acquired data in a collaborative cloud environment and to export these data to a series of third part applications.

*Drone Harmony* (<https://droneharmony.com/index.html>): commercial, works with most of DJI platforms, only on android devices. This software was developed particularly with the aim of performing industrial applications in the easiest way, and its projected mainly for the inspection of cell tower. However, it also allows to import terrain data into the software and to use them to enhance the flight planning. It also presents some interesting alternative flight schemes for the mapping of large areas (e.g. a flight scheme composed by several overlapping orbits to cover the geometry of complex areas).

*Litchi* (<https://flylitchi.com/>): commercial, works with most of DJI platforms, available for mobile devices and for desktop. The peculiarity of this software for flight planning is the possibility to control all the sets of parameters that are involved in the flight plan, not only the ones related with the platform, but also the one of each single waypoint. It is

implemented both for the acquisition of video and photos and for the generation of complex photogrammetric mapping projects.

*Measure* (<https://www.measure.com/ground-control>): commercial, works with most of DJI platforms, available for iOS systems. This solution is particularly devoted to the management of large fleet of UAVs and large numbers of missions and pilots. The software allows to control all the pre-flight checklists and all the parameters of every completed flight. It offers options as well both for semi-automatic and fully automatic flight missions.

*Mission Planner* (<http://ardupilot.org/planner/docs/mission-planner-overview.html>): opensource, works with platforms with specific autopilot board, windows systems only. This solution is developed for the autonomous navigation of several types of vehicles, not only aerial. It is less user friendly compared to other solutions and requires some basic training before using the software. Its biggest utility resides in the fact that it is fully customizable, but on the other side only few platforms are supported and generally COTS solutions are not included.

*Pix4D Capture* (<https://www.pix4d.com/product/pix4dcapture>): commercial, only on mobile devices, support DJI, Parrot and Yuneec platforms. This solution is developed from the Pix4D company and is strictly related with the photogrammetric suite already describe in section 3.9.2. It run on Android and iOS operative systems and allows the control of different flight parameters over a series of multi-brand platforms. It allows to define the altitude of the flight based on the desired GSD, to set camera orientation angle and manage different navigation parameters of the platforms (e.g. flight speed, flight line direction, etc.). It also offers different flight schemes for the definition of the mission area of coverage, the overlap between stripes, etc. The app also provides a cloud service for the processing of images, related with the Pix4D photogrammetric suite.

*Precision Flight* (<https://www.precisionhawk.com/precisionflight>): freeware, support most of DJI, Mikrokopter and Parrot platforms, works on mobile devices (bot android and iOS). This solution includes different flight schemes, allows an advanced control over the camera parameters and it grant the possibility to import the terrain model.

*UGCS* (<https://www.ugcs.com/>): commercial, support most of DJI, Mikrokopter and Yuneec platforms, works on desktop system (bot windows and iOS) and on android devices. This solution allows to import several types of files to define the terrain surface and enhance the flight planning. It allows also the management and creation of no-fly zones, in order to improve the safety conditions of the mission.

Finally, another possible solution is to create a flight planning tool starting from zero. This solution is quite difficult but is followed by researchers that want to achieve a full customisation of all the involved parameters in the flight planning phases.

### **Set up and validation of the methodological framework with a commercial platform**

After a survey of these software solutions, the first issue that was investigated was related with the flight planning and camera orientation phases and how they can affect the photogrammetric survey. A part of this research was presented in the already cited work (Chiabrando, Lingua, et al., 2017) and was further extended in this thesis. The UAVs data collected in 2016 at Rocca San Silvestro, were used for these tests. In this first experimentation a multi-rotor platform, specifically built for the Politecnico di Torino, was used; the tests completed with this platform were crucial to set up the methodological framework with a more customizable and controllable system. The results obtained with these tests were then the base for additional analyses on COTS and low-cost platforms, as will be further described in this work. The datasets were projected to consider different camera orientation set up and different directions of the flight lines and the dataset were processed combined in different levels, in order to exploit the results achievable following different approaches.

This multi-rotor platform (*UBIK DIATI MK01* - Figure 55) is equipped with the Pixhawk flight controller. The system is composed of six motors and it mounts all the electronic equipment required for both remote control and automatic flight. The ground station is composed by a computer connected with the platform.



*Figure 55 The UBIK DIATI MK01 platform and an image of the fieldwork at Rocca San Silvestro*

The payload of the platform is of about 1 kg and it has a maximum flight time of about 12–15 min at a nominal cruise speed between 3 and 5 m/s. In this case the payload was constituted of a Sony Alpha 5100 digital mirror less camera with the following main characteristics: 24.3 MPixel CMOS sensor, 6000x4000 max image size, sensor size 23.5 x 15.6 mm, pixel size 3.92  $\mu\text{m}$ , weight 283 g (batteries included) and it was equipped with a 20 mm lens. The digital camera is mounted on a servo-assisted support that grants electronically-controlled rotations along the principal axes. This system allows to set up the different camera configurations and orient the lens axis during the acquisition phases.

Several factors were considered during the phases of flight planning: the extension of the area to survey, the development and shape of the terrain, the level of conservation of the structures to survey and thus their elevation from the ground and finally the expected results achievable from the survey (representation scale, metrical accuracy, geometrical reconstruction accuracy, radiometric information, etc.). The integration of oblique images with nadiral acquisition have been a topic of high interest in the last years and several researcher focused their attention on these “non-conventional” views (Chiabrandò, Spanò, et al., 2017; Høhle, 2008; Lingua, Noardo, Spanò, Sanna, & Matrone, 2017; Remondino, Toschi, et al., 2017; Rupnik et al., 2014). In the case of Rocca San Silvestro, the use of oblique images was particularly stressed due to the morphological conformation of the site, that presents a conical development from the bottom of the site till the top of it, where the main defensive structure of the site insists. Other standard set up for the flight planning phases were considered as well, such as the ones related with weather and wind conditions, cruise speed, presence of obstacle, camera exposure, white balance, etc.

A large overlap between the different flight lines was also ensured (>80% longitudinal overlap, >70% transversal overlap). The software employed for the flight plan was in this case Mission Planner, created by Michael Osborne, that allows to connect a computer, used as ground station, with the platform and to set up all the parameters for the flight mission. The flight plans were created defining a set of waypoints and creating different flight schemes as reported in the following list and in Figure 56:

1. Nadiral configuration of the camera. Flight lines direction North-South.
2. Nadiral configuration of the camera. Flight lines direction West-Est.
3. Oblique configuration of the camera ( $\approx 45^\circ$ ). Flight lines direction North-South.
4. Oblique configuration of the camera ( $\approx 45^\circ$ ). Flight lines direction West-Est.
5. Oblique configuration of the camera ( $\approx 45^\circ$ ). Circular flight lines with the centre of the circle in the middle of the site

Each flight had a duration of around 15 minutes, they were performed at an altitude between 30 and 40 meters from the ground and a total of 1119 images were acquired, divided as:

- Nadiral configuration (North-South): 118 images
- Nadiral configuration (West-Est.): 153 images
- Oblique configuration (North-South): 278 images
- Oblique configuration (West-Est): 177 images
- Circular: 393 images

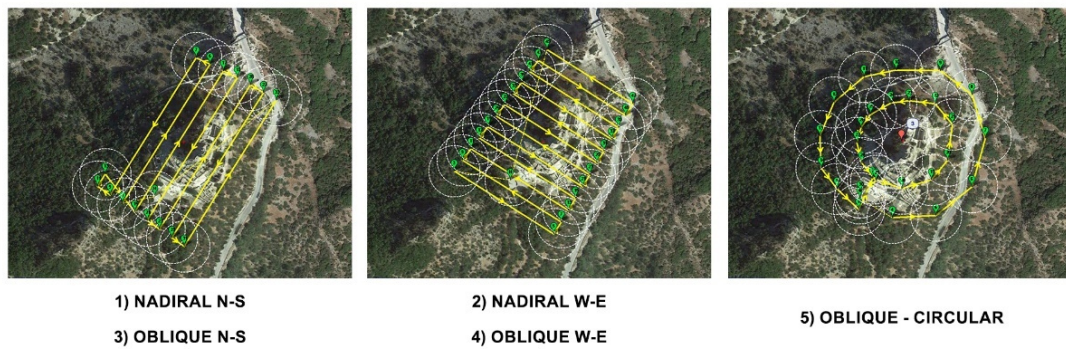


*Figure 56 Rocca San Silvestro. Flight plans and camera configuration*

The data collected on the field were then processed combined together in several blocks using Pix4D mapper, following the standard photogrammetric pipeline: camera I.O and E.O. and TPs extraction through a BBA and the use of GCPs, evaluation of the metric accuracy through Check Points (CPs) and generation of the photogrammetric products (dense cloud, mesh, DSM and orthomosaic).

The five acquisition were combined and processed in the following blocks:

1. The two nadiral acquisitions
2. The two oblique acquisitions
3. The circular acquisition
4. The two nadiral and the circular acquisitions
5. The two oblique and the circular acquisitions
6. The two nadiral and the two oblique acquisitions
7. All the five flights

All the projects were processed using the same set of GCPs and CPs (six point were used to assess the metric accuracy of the process) and the parameters of the processing were fixed for all the projects. The RMSe value for the six points used as CPs is reported in the following Figure 57 for all the seven projects:

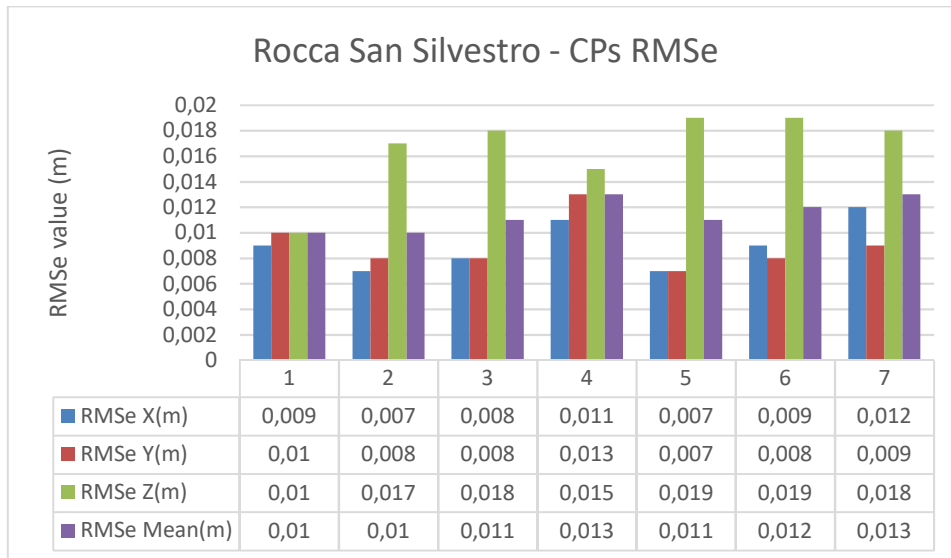
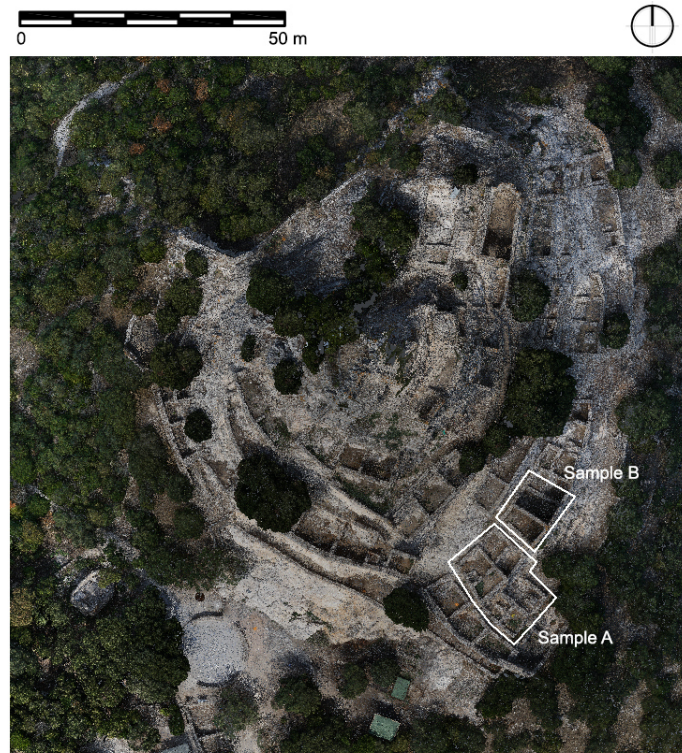


**Figure 57** *Rocca San Silvestro, graphical representation of the mean RMSe of the CPs in the seven projects*

According to the value of RMSe on the CPs, all the seven projects can be considered suitable for the production of the typical image-based products in terms of metric accuracy, with a mean RMSe value always near 1 centimetre. It is interesting to report some observations for the z components which value seems to be directly linked with the type of images used: it increases with the use of oblique cameras. On the other hand, oblique cameras create an improvement for the values of x and y components, that as expected present always a lower value than the z. These data indicate how the use of oblique cameras can enhance the overall metric accuracy of the process, however it is clear that the integration with nadiral acquisition is mandatory and should also be well balanced in terms of numbers of images. With this configuration of GCPs the impact of oblique cameras is particularly relevant in project 4, where the circular flight is combined with the two nadiral acquisitions, as will be reported in the following section 4.1.2 results can be different if other configurations of GCPs and CPs are adopted, especially if the number of GCPs is reduced and other flights and camera configuration can allow to achieve better results in term of accuracy.

The next step in this test on flight plans and camera configuration was focused on the quantitative/qualitative analyses performed on one of the products: the point cloud. The main aim was to assess how the parameters of flight plan and camera orientation influenced the production of the 3D models. Two specific sample areas were chosen to be in depth analysed, as shown in the following Figure 58. The two areas were chosen to represent peculiar features of the site, with marked horizontal and vertical developments of the walls and development of the terrain, in the lower part of the site where the ancient residential area insisted.



**SAMPLE A**

**SAMPLE B**

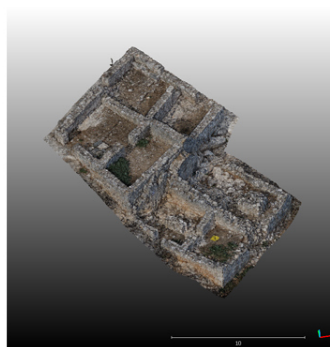
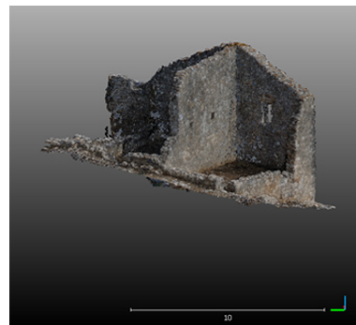
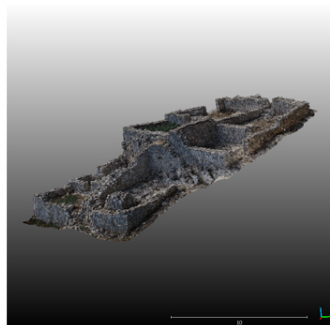


*Figure 58 Rocca San Silvestro. The two sample areas that were chosen to perform further analyses and their location indicated on an orthoimage of the site (left).*

In sample A different residential blocks are enclosed, they develop on two different levels and also some remains of the ancient road systems are present. The structures are not really

well preserved, and their height is quite reduced, however the buildings are close to each other and the urbanistic system is quite dense and complex in this part of the residential area. Sample B is composed by a well-preserved structure; one of the façades is still standing from the ground level till the ancient roof supports. The overall quality of the dense cloud derived from the seven projects was evaluated using two approaches: the density analysis tool implemented in the CloudCompare software and through a semiautomatic generation of vertical section of the different models.

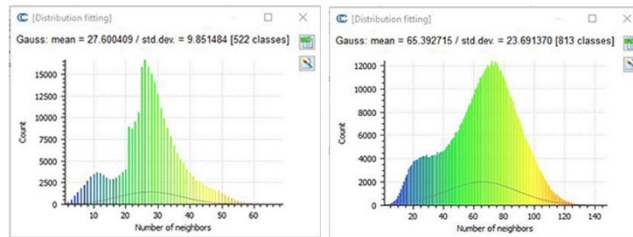
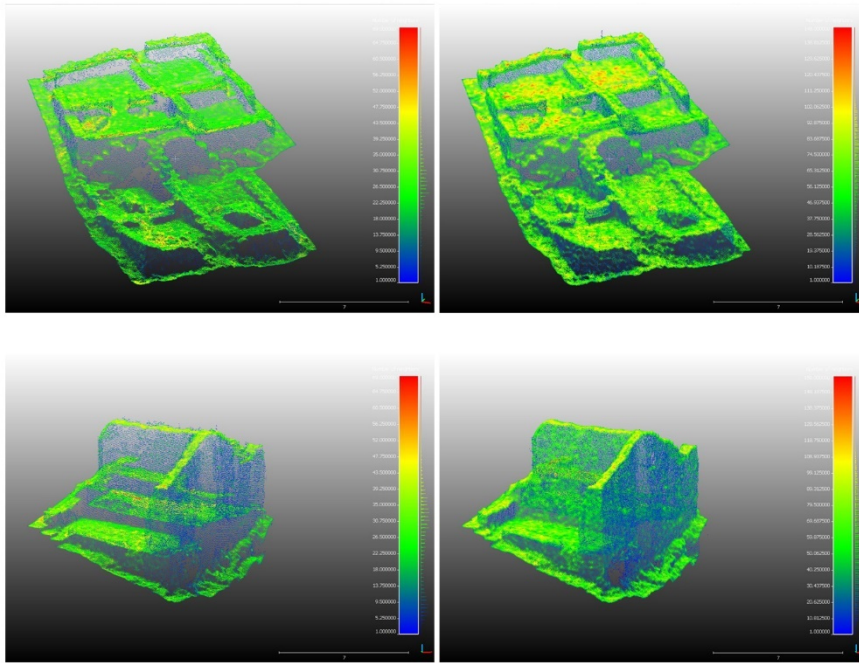
The two sample areas were first segmented to be included in the same bounding box, in order to obtain a more reliable analysis. The density analysis was then completed in CloudCompare, the analysis method was set as precise (the radius of research around a single point was set to a value of 0.1 m for all the analyses achieved) and the number of neighbors method was chosen (an overview of some of the algorithms implemented in CloudCompare for this kind of analyses can be found in Lague, Brodu, & Leroux, 2013). Adopting this approach, the density is computed estimating for each point the number of neighbors inside a sphere of predetermined radius. The results of the performed analysis are reported in the following Table 7.

| Flight configuration                            | SAMPLE A  |                     |           | SAMPLE B  |                     |           |
|---|-----------|---------------------|-----------|-----------|---------------------|-----------|
|   | N° of pts | Number of neighbors |           | N° of pts | Number of neighbors |           |
|   |           | Mean                | Std. Dev. |           | Mean                | Std. Dev. |
| 1. Two nadiral acquisitions                     | 271.588   | 27.6                | 9.8       | 193.590   | 24.8                | 12.5      |
| 2. Two oblique acquisitions                     | 313.132   | 29.5                | 10.5      | 240.319   | 25.5                | 12.6      |
| 3. Circular acquisition                         | 465.440   | 45.7                | 16.9      | 342.856   | 40.7                | 20.8      |
| 4. Two nadiral and the circular acquisitions    | 660.229   | 65.4                | 23.7      | 446.123   | 54.4                | 28.1      |
| 5. Two oblique and the circular acquisitions    | 645.592   | 61.4                | 21.6      | 470.977   | 52.8                | 25.6      |
| 6. Two nadiral and the two oblique acquisitions | 435.267   | 42.5                | 16.5      | 306.818   | 34.9                | 17.9      |
| 7. All the five acquisitions                    | 784.729   | 76.2                | 27.5      | 540.091   | 63.8                | 31.9      |

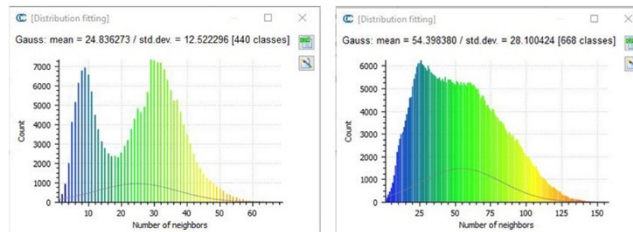
*Table 7 Rocca San Silvestro. Density analysis on the two selected sample A and B*

The information collected in this table can lead to further analysis and consideration. The dataset 1, including only the two nadiral flight, is the one generating the lower number of points of the two selected areas. This is an expected data in two areas that present a marked elevation component of the structures. On the other hand, it is true that the number of neighbors is lower than in the other projects, but it is also true that the standard deviation of this samples of data is quite low if compared to other configurations. The values for the

configuration number 2 are similar, with a small improvement of the point density but also a small growth of the standard deviation. It is interesting to observe the behaviour of configuration 6, that confirmed that nadiral and oblique configurations work in an optimized way if combined together. In the case of Rocca San Silvestro, due to the conformation of the site, it is worth to report also the performances of the circular flight. This dataset, even if considered alone as in project 3, can return good density values, with a quite low standard deviation value. If processed together with the nadiral flights, as in projects 4, the achieved results are quite promising. These considerations are also confirmed in the analyses through sections that will be presented hereafter. Moreover, the density analyses derived with this tool can be represented in different forms. Using a scalar representation in false colours is possible to graphically characterize the distribution of this values on the considered samples; an example of this representation is reported in Figure 59. Using this representation is possible to evaluate the density of the points generated through the photogrammetric approach in relation with the geometry of the surveyed object. Furthermore, the data extracted from the analyses can be represented through a Gaussian distribution graph, allowing more considerations on the data extracted from the process.



**Sample A. Project 1 (left) and Project 4 (right)**



**Sample B. Project 1 (left) and Project 4 (right)**

*Figure 59 Rocca San Silvestro. Graphical representation of the density analysis on the two selected samples A and B for project 1 and 4*

As showed in the figure above, the use of oblique images is crucial to improve the quality of the generated model, especially in determined areas of the samples. The contribute of oblique images is particularly clear on the corner between the intersections of the walls and on the vertical development of the masonries. It also provides a good informative contribute in the connection between ground and walls. In sample B these aspects are more evident, due to the configuration of the area chosen and of the height of the standing structures. On

the other hand, in sample A, oblique images can result really important for an accurate definition of the development of the terrain.

The second analysis performed was achieved using the 3D Reshaper software of Hexagon and was aimed at evaluating the geometrical reconstruction provided by the seven different projects. All the seven models were imported in the software and semiautomatic vertical sections were created in the same point of the model (the position of the section in the two sample areas is showed in Figure 60) and using the same set of parameters. In this case a model derived from a Terrestrial Laser Scanning (TLS) acquisition was used as ground truth to compare the performances of the photogrammetric process with a more consolidated sensor (similar approaches were methodologically tested and described in previous works: A Calantropio, Chiabrando, Rinaudo, et al., 2018; Calantropio, Patrucco, et al., 2018; Gruszczyński, Matwijn, & Cwiąkała, 2017; Vallet, Panissod, Strecha, & Tracol, 2012). In the following Figure 61 the sections extracted from sample A are reported while the sections extracted from sample B are reported in Figure 62.

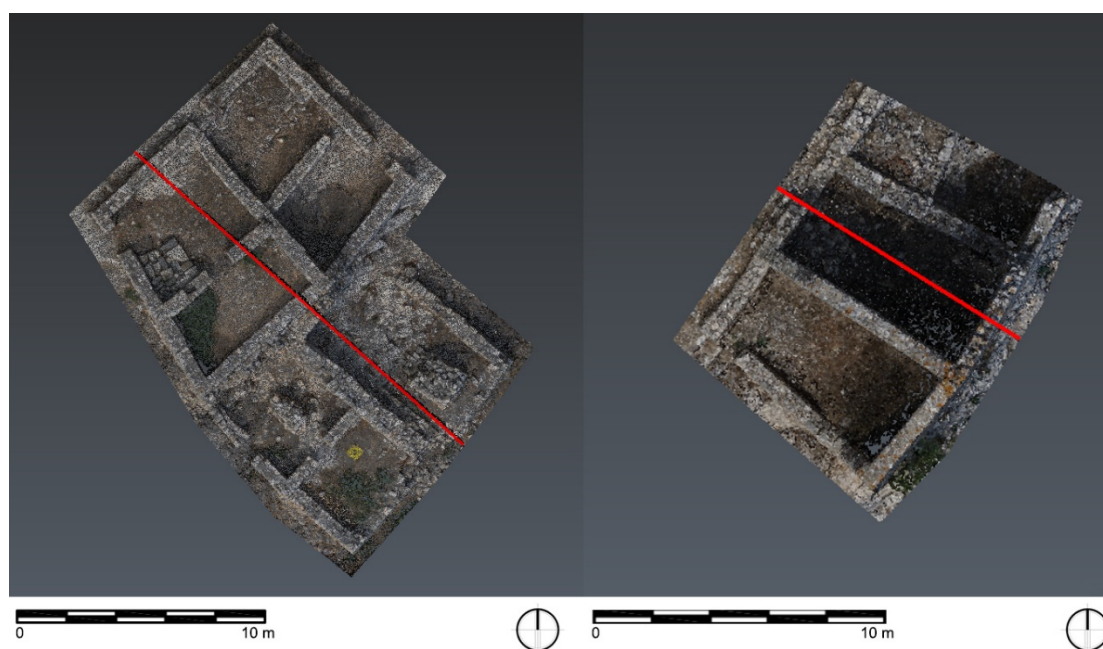


*Figure 60 Rocca San Silvestro, Sample A (left) and Sample B (right). Position of the vertical sections extracted for the two sample areas.*

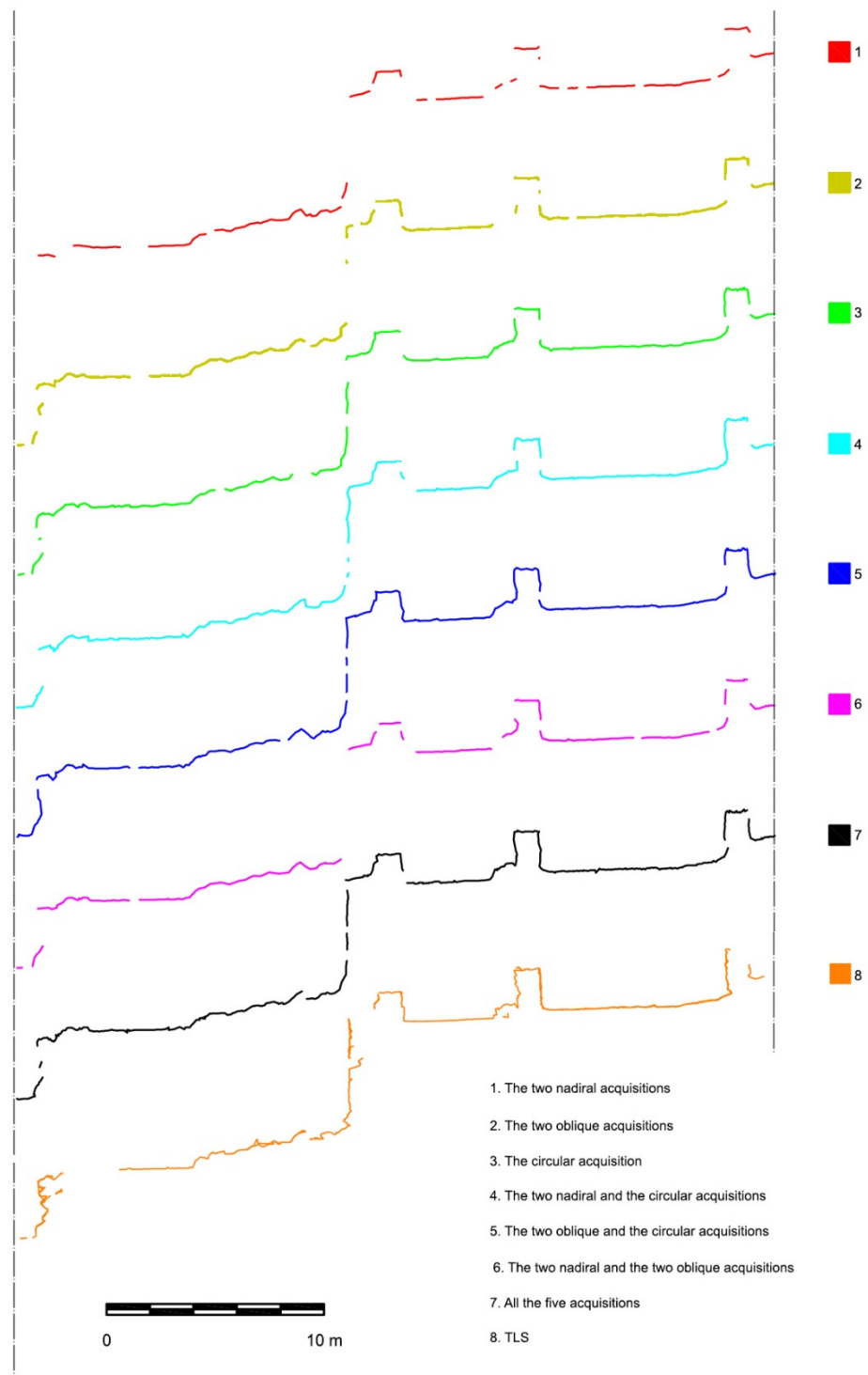


*Figure 61 Rocca San Silvestro, Sample A. Semiautomatic sections extracted from the seven photogrammetric point clouds and from the TLS reference point cloud*

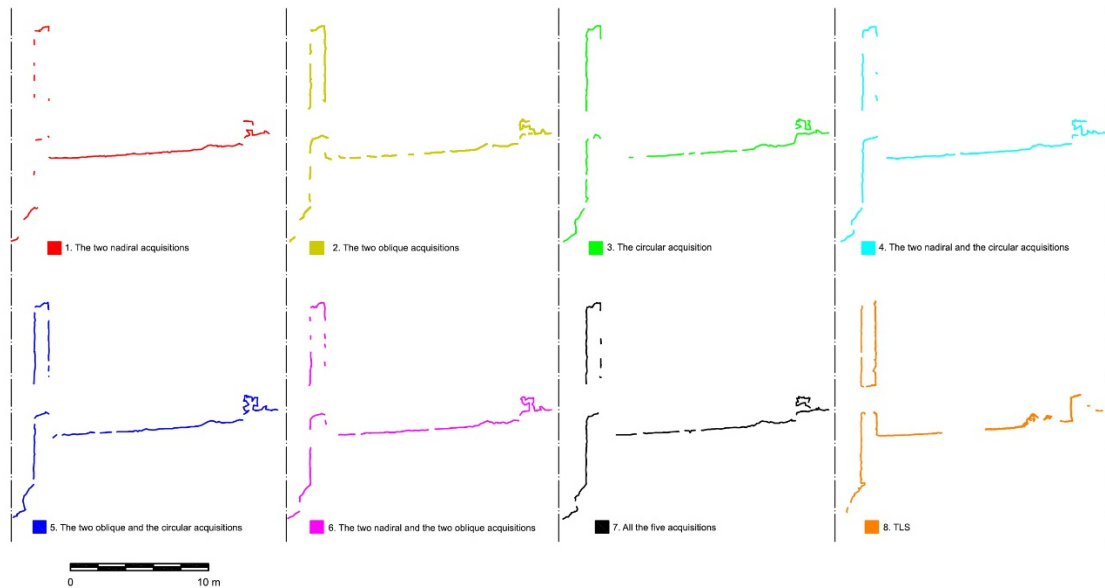


**Figure 62** *Rocca San Silvestro, Sample B. Semiautomatic sections extracted from the seven photogrammetric point clouds and from the TLS reference point cloud*

In this analysis it is again clear in both the sample areas considered the impact of oblique images, as already reported in other researches (Aicardi, 2017). Moreover, it is interesting to notice also in this case that the circular configuration of the flight is performing better than the regular grid of oblique images. This fact can be attributed to the geometrical configuration of Rocca San Silvestro, as previously reported. Another well-known, but still interesting factor is related with the better geometrical description of certain features of the object, provided by the UAVs data if compared with the TLS. Despite the large number of scans acquired on the field, UAVs acquisition was able to better represent some portions of the archaeological structures, especially the upper part of the walls. This fact, combined with the faster acquisition time on the field, demonstrate once again the competitiveness of UAVs in respect to more consolidated techniques (Guerra-Hernández et al., 2018; Lo Brutto et al., 2014; Murtiyoso et al., 2017; Nikolakopoulos et al., 2017).

### **Adapting and validating the methodological approach to different platforms: flight planning and camera orientation with COTS and low-cost platforms employed in this research**

The tests presented in the above section were further developed in the past two years and the results of these researches are included in this thesis work, with the specific aim of stressing the methodological framework adopted at Rocca San Silvestro using COTS and low-cost platforms. In the experiences that were carried out in these researches, the test sites were represented by CH artefacts which documentation needs are similar and comparable with the ones of archaeological heritage. These works allow to ulteriorly deepen the issues connected with the use of these platforms for the documentation of CH artefacts and to refine the methodology connected with this use. Five COTS and low-cost

platforms by DJI were employed for this work: the Mavic Pro, the Phantom 4, the Phantom 4 Pro, the Spark and the Inspire 2 (main specifications of these platforms are reported in the following Table 8).

|   |  |   |
|---|--|---|
| 1 |  <p>Mavic Pro<br/>(Source: <a href="https://www.dji.com">https://www.dji.com</a>)<br/>≈ 1300 euro</p>       | <p>The peculiarity of this platform resides in its foldable propeller mechanism, its small dimension and low weight (734 g). Equipped with a 4K camera and a 3-axis gimbal that allows the device to capture stabilized video and images. The camera shoots in cinematic 4K and snaps 12.7 MP stills.</p>   |
| 2 |  <p>Phantom 4<br/>(Source: <a href="https://www.dji.com">https://www.dji.com</a>)<br/>≈ 1200 euro</p>       | <p>The Phantom 4 is a small quadcopter, one of the most popular products of DJI. It is equipped with a 4K video camera that has a 1/2.3" CMOS sensor, 94-degree field of view, 12.4 MP, 20 mm (35 mm equivalent) with a focus to infinity. It weighs 1.38 kg, has a maximum flight time of 28 minutes.</p>  |
| 3 |  <p>Phantom 4 Pro<br/>(Source: <a href="https://www.dji.com">https://www.dji.com</a>)<br/>≈ 1600 euro</p> | <p>Phantom 4 Pro presents a number of small but significant improvements comparing to the previous model. It is equipped with a 5 direction obstacle avoidance system and it mounts a new camera with a 1" CMOS sensor (four size larger compared to the Phantom 4), this camera is able to acquire 20 MP images and 4K video up to 30 frames per second.</p> |
| 4 |  <p>Spark<br/>(Source: <a href="https://www.dji.com">https://www.dji.com</a>)<br/>≈ 650 euro</p>          | <p>Spark is a mini drone (300g) with a 12 MP camera and a CMOS sensor of 1/2.3". FoV 81.9°, 4,5 mm (25 mm in 35 mm format equivalent). It is capable to capture images in 4K (4:3) and videos in full HD (16:9). It is equipped with a stabilized 2-axis mechanical gimbal, with a controllable range of pitch going from 0° to -85° (nadir).</p>             |
| 5 |  <p>Inspire 2<br/>(Source: <a href="https://www.dji.com">https://www.dji.com</a>)<br/>≈ 14200 euro</p>    | <p>Inspire 2 is one of the top range platforms of the Chinese company. It weights 3440 g without the payload and allows around 25 minutes of flight time. It can mount different sensors and in this research it was equipped with a Zenmuse X5 camera (4/3 CMOS sensors, 16 MP, 30 mm equivalent) able to acquire 4K videos.</p>                             |

*Table 8 Main specifications of the DJI platforms used in this research*

The platforms presented in the above table represent different segments of the actual drone market and have different characteristics: they vary in size and weight, operational range, on board sensors equipment, etc. The Spark is the smallest one, it is conceived as a personal portable drone for a non-professional use and it embed several characteristics to be attractive for large segment of the market. The Mavic Pro is slightly bigger than the Spark but can compensate its dimensions with the foldable propellers. It adds a third axis of rotation on the camera gimbal, a slightly bigger sensors and also the flight time is enhanced. The Phantom series is probably the most famous line of the DJI products. The drones of this series are a good compromise both for the professional and amatorial operators. The main difference between Phantom 4 and Phantom 4 Pro is the type of camera mounted on the platform that is significantly more performing on the Pro series. The Inspire 2 is the top platform in the COTS segment of DJI. This drone is projected mainly for cinematographic shootings and can mount different type of cameras. All of these 5 platforms were deployed in this research considering their characteristics, both from the platforms side and both from the sensors side. One of the aims of the research was to assess the use of this platform in different context connected to the documentation of CH and then on archaeological sites. The five platforms were then stressed in different working scenarios and the acquired data were then carefully processed and evaluated. The idea was also to define which platforms is more suitable depending on the operational context and on the desired output of the survey.

#### **The Savigliano test site. Platform 1, 2 and 3**

Following the procedural scheme implemented at Rocca San Silvestro the first three platforms were tested on a small medieval Church in Savigliano (Cuneo - Italy). For each of the three platforms five different flights have been planned and completed as follows:

- Two flights with a regular grid of flight lines East-West (parallel with the main development of the structure). One with a nadiral configuration of the camera and one with an oblique configuration of the camera ( $\approx 45$  degrees).
- Two flights with a regular grid of flight lines North-South (perpendicular with the main development of the structure). One with a nadiral configuration of the camera and one with an oblique configuration of the camera ( $\approx 45$  degrees).
- One circular flight with the centre of the circle set on the middle of the structure. This flight was completed with an oblique configuration of the camera ( $\approx 45$  degrees).

How is possible to notice from the flight schemes reported in Figure 63 the flights achieved with the oblique configuration of the camera were slightly extended if compared with the

nadiral ones, in order to ensure a good overlap between images and an acceptable coverage of the whole structure. This shrewdness was derived from the experience gained after the data acquisitions performed at Rocca San Silvestro. The flights were planned and completed using the Pix4D capture app (version 3.7.1) directly on the field and setting a regular flight altitude of 40 meters for all the fifteen flights.



**Figure 63** Flight planning for platforms 1,2 and 3 for the test performed at Savignano

The first issue that need to be reported about these tests is connected with some problems that occurred during the acquisition phases with these platforms; some failures happened with the Mavic Pro (platform 1) and Phantom 4 (platform 2). Four out of five set of images of the Mavic were acquired without problem, while one of the sets presented blurry images. After contacting the Pix4D support it resulted clear that this problem represented a known issue related with the internal parameters of the flight planning software and with the platforms firmware. The limit of the software in this case is connected with the phase of camera set up, that is performed at ground level before take-off, and that can result in a bad configuration if the camera axis is rotated or if some close occlusions are present. After these acquisitions the platform was used several other times with the Pix4D app and this problem repeated again, confirming this software failure. A backdoor solution was developed by the author's research group to avoid this issue and it consisted in a two steps approach. First the take-off of the platform is achieved using the native DJI app (DJI GO)

for the manual control of the UAV that is moved to the desired altitude for the automatic flight that need to be performed. In the second step a switch between DJI GO and Pix4D capture app is completed on the mobile device that is controlling the system and then the flight plan is uploaded on the UAV and initialised. This solution allows the camera setting up to be performed at the altitude that will be maintained during the flight, resulting in more correct parameters of the camera. However, this approach does not represent the best solution to adopt for different reasons: first of all, the higher the distance between ground station and platform, the higher the possibility of data corruption during the transfer phase; secondly this approach lead to an undue battery consumption that frustrate the battery optimisation achievable thanks to the automatic flight planning.

Instead, the issue that occurred with the Phantom 4 is different and also in this case it repeated in other previous and subsequent missions. During the final phases of the circular flight the platform missed the landing point of around 10/15 meters, despite the correct setting of the landing point in the app and the good satellite signal coverage at the moment of the flight. Thanks to a good planning of the buffer area before the flight neither people or object were harmed and the aircraft landed safely, however this issue can results in really dangerous implication for the safety of the operations.

These issues during the acquisition phases confirmed that the limits of COTS and low-cost solution, both from the software and hardware side, reside in the lower number of parameters that the operators can control and modify in the phase of mission planning and during the fulfilment of the task. On the other hand, the deployment of these platforms can be much more rapid than other non-commercial solution, reaching at the same time good results during the operations development.

In this case study the methodological framework set up in the Rocca San Silvestro test was stressed for this commercial platforms and further tests were implemented to evaluate the different cameras performances in the TPs extraction phase and in the BBA. The datasets were processed using two software solutions (MicMac - opensource and Pix4D mapper - commercial) and were combined as follows:

- A. All the flights (available only for the Phantom 4 and Phantom 4 Pro)
- B. Nadiral and Circular (available only for the Phantom 4 and Phantom 4 Pro)
- C. Nadiral and Oblique (available for all the platforms)
- D. Only the two strips of the nadir image (available for all the platforms)

Further tests were achieved to stress different configuration of GCPs in order to evaluate the impact of different flight schemes on the accuracy of the overall model, the results connected with these issues will be reported in the following section 4.1.2.

### The Mondovì test site. Platform 4 and 5.

Platform 4 (Spark) and platform 5 (Inspire 2) were tested on another CH site (Giuseppe Galliano Barrack, Mondovì, Italy). The Inspire 2 was used to produce a general model of the structure and the area surrounding it, while the Spark was tested in order to verify its ability to produce more detailed models of smaller portions of the building. The flight plans for the Inspire were created using the Pix4D Capture app (version 4.2.0) and following the acquisition scheme consolidated in the work previously described. In this case the geometrical structure of the building to survey was quite simple and only three different flight plans were considered necessary to achieve the desired detail. As shown in the following Figure 64, one nadir flight (with flight lines parallel to the main development of the building) and two oblique flights (with flight lines parallel and perpendicular to the main development of the building) were completed: the altitude of the flights was around 40 meters, with an expected GSD of 1.1 cm/pix.

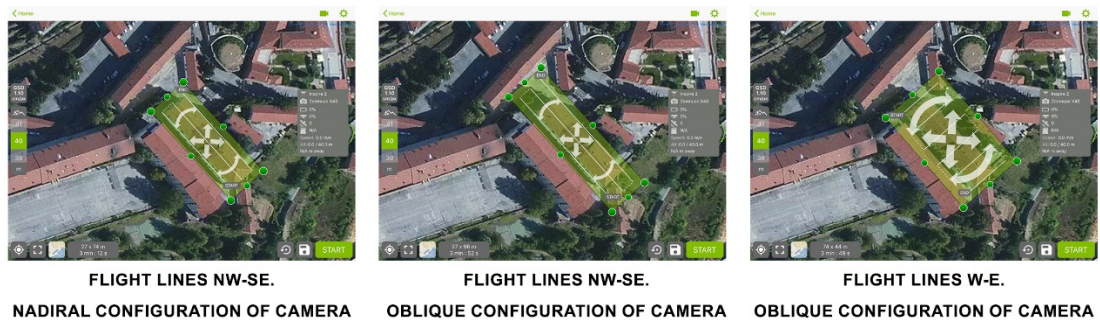


Figure 64 Giuseppe Galliano Barrack. Flight plans of the three flights completed with the Inspire 2

As for the Mavic Pro at Savigliano, even in this case and with this platform some problems occurred in the focusing parameters of the camera and some of the flights need to be repeated. The three datasets were processed together using Agisoft Photoscan (version 1.4.4), following the standard photogrammetric pipeline. The main parameters of the processing of this dataset are reported in the following Table 9.

| Inspire 2 dataset |         |                           |               |              |                    |
|-------------------|---------|---------------------------|---------------|--------------|--------------------|
| N° images         | N° TPs  | Reprojection error (mean) | RMSe GCPs (m) | RMSe CPs (m) | Dense cloud pts N° |
| 228               | 531,666 | 0,655 pix                 | 0,012         | 0,033        | 94,501,646         |

Table 9 Giuseppe Galliano Barrack. Inspire 2 dataset parameters

At the time when the test in Mondovì was performed there were no existing applications that supported fully automatic flight for the DJI Spark. This platform was developed specifically for the mass market distribution and its application for photogrammetric purposes was tested only on a second time. This issue has been partially solved by third part applications that allow an autonomous navigation of the Spark, however, other

limitations, such as the range of the radio controller need to be considered. In order to evaluate different solutions for the acquisition of images with the Spark, three approaches were created and tested:

1. Semi- automatic flight with Pix4D capture app at a medium altitude
2. Manual flight with photogrammetric strips for the survey of the façades
3. Manual flight for the survey of the facades (but recording videos in order to extract and process frames in a second time)

The use of Pix4D app allowed to include some automation in the process of acquisition, the app permits to select an acquisition interval (measured in meters of movement of the UAV both in the horizontal and vertical direction) between one shot and the subsequent. The advantage of this modality is that it allows the operator to focus only on the flight of the UAVs, while the acquisition of the images is demanded to the software. The drawback of this practice resides in the risk of collecting redundant data, especially in case of complex geometries of the scene that requires a lot of UAVs movements. On the other hand, manual flight can avoid this risk but requires more efforts from the operator side and longer time of flight, due to the higher number of tasks that are demanded to the manual intervention of the pilot. The main characteristics of the three flights that were completed with the Spark are reported in the following Table 10:

| <b>ID</b> | <b>N° of images</b> | <b>Camera set up</b> | <b>Acquisition distance</b> | <b>Acquisition time</b> |
|-----------|---------------------|----------------------|-----------------------------|-------------------------|
| <b>1</b>  | 230                 | Forward and Oblique  | 5 m                         | 21 min                  |
| <b>2</b>  | 190                 | Forward              | 5 m                         | 16 min                  |
| <b>3</b>  | 150 (frames)        | Forward              | 5 m                         | 5 min                   |

*Table 10 Giuseppe Galliano Barrack. Main specifications of the flight performed with the Spark*

The data collected on the field with the Spark were processed also in this case testing the two different software solution described above: Pix4D mapper and MicMac. Among the different dataset available the north façade has been selected to conduct further analyses. Peculiar analyses were performed on the dataset number three (the one achieved through the acquisition of a full HD video), the position of camera stations and control points for this flight is reported in Figure 65. This dataset was selected for different reasons: it was at the same time the fastest acquisition strategy and the one that can stress the platform performances (a crop factor is automatically applied during the video recording and the resolution is slightly lower if compared to image acquisition).



*Figure 65 Giuseppe Galliano Barrack, Acquisition with the Spark (flight ID 3). Camera station positions (left) and control point position (right)*

Both the processing with the two software were completed following the standard photogrammetric pipeline; the first evaluation of the accuracy of the generated model was achieved through an analysis of the RMSe on GCPs and CPs. The points used in this process were constituted both from codified target and natural features that were measured using a traditional topographic approach with TS. RMSe values for GCPs and CPs estimated from both the software are reported in the following Figure 66.

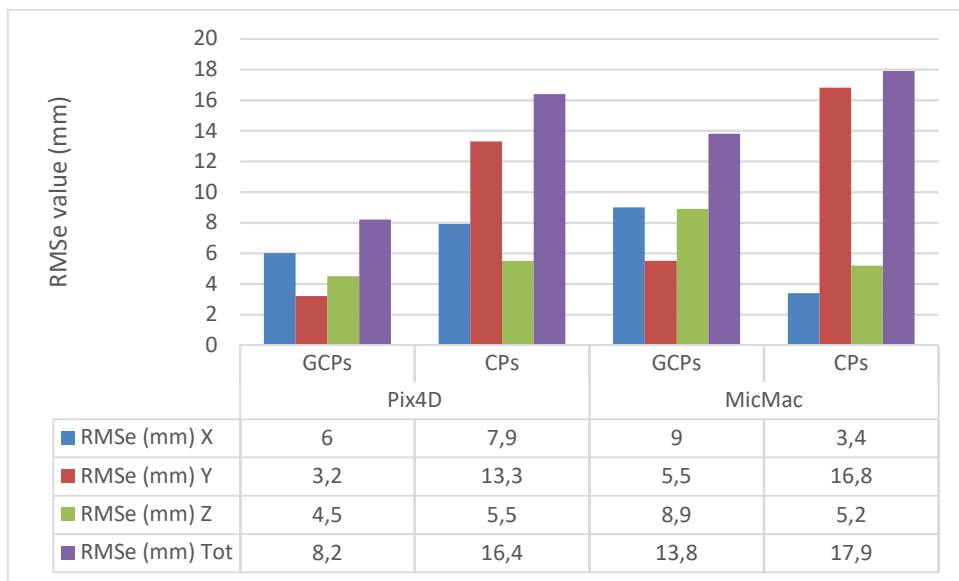


*Figure 66 Giuseppe Galliano Barracks, flight ID 3. RMSe comparison for GCPs and CPs computed in the two software solutions tested*

The data contained in the previous table show a slightly better performance of Pix4D software, however both the software were able to achieve an accuracy of the data that can be considered coherent with the desired scale of the products for this survey (1:100).

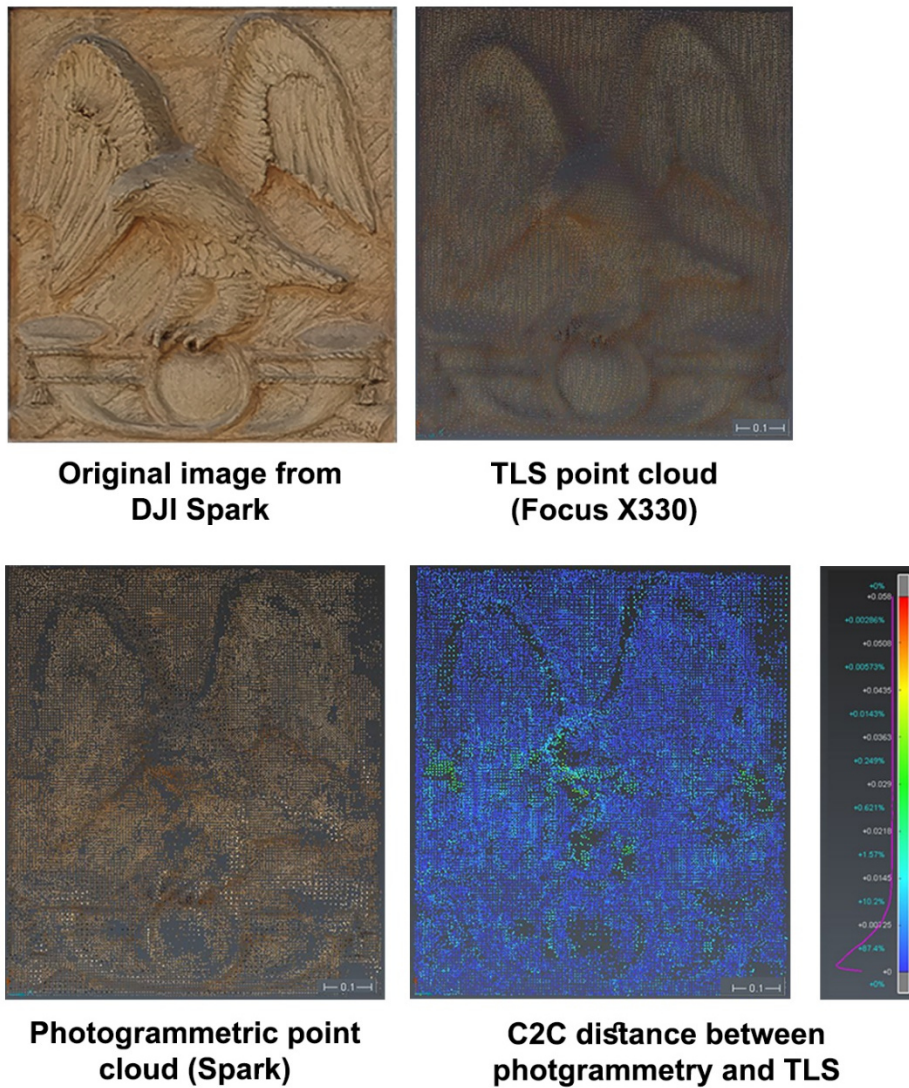
Another analysis was performed on the self-calibration parameters estimated by the two software, part of the I.O. parameters was thus evaluated more in detail. Considering the fact that the two software use different mathematical models for the estimation of radial and decentring distortion, this analysis was achieved only on focal length and PP parameters. The data considered in this evaluation are reported in Table 11.

| Software | Value     | I.O. parameters |        |        |
|----------|-----------|-----------------|--------|--------|
|          |           | F (px)          | PP     |        |
|          |           |                 | X (px) | Y (px) |
| Pix4D    | Estimated | 1.831,45        | 964,38 | 537,43 |
|          | RMSe      | 2,59            | 1,25   | 1,59   |
| MicMac   | Estimated | 1.844,27        | 959,87 | 543,10 |
|          | RMSe      | 3,42            | 0,72   | 1,00   |

*Table 11 Giuseppe Galliano Barrack, comparison of focal length a PP coordinates estimated from the two considered software for flight ID 3*

In the phase of the I.O. parameters estimation the two software solutions are performing in a similar way, confirming the good degree of confidence achievable, both with open source and commercial solution, and the overall good metric performances of this COTS sensor. A second step of the tests performed at Giuseppe Galliano Barracks was devoted to the assessment of the geometric quality of the model generated through the image-based approach with the Spark. In this case, two TLS dataset were acquired as ground truth elements: one with the Faro Focus X330 by Cam2 and one with the BLK 360 by Leica. Several strategies for the acquisition and treatment of the laser data were also analysed and evaluated, all the considerations derived from this part of the research won't be reported in this thesis work, reader can refer to the published contribute for further details on this subject (Calantropio, Chiabrandò, et al., 2018).

The first analysis consisted in a C2C distance computation between the model generated by the TLS (the Focus X330 was chosen for this analysis) and the one by the Spark. A portion of the building was selected and segmented (a decorative element of 0,9 x 0,8 meters as shown in Figure 67) and the point density of the two segmented cloud were normalised in order to achieve a more reliable comparison between the two (as expected the laser dataset was way more information redundant in comparison with the image-based one).



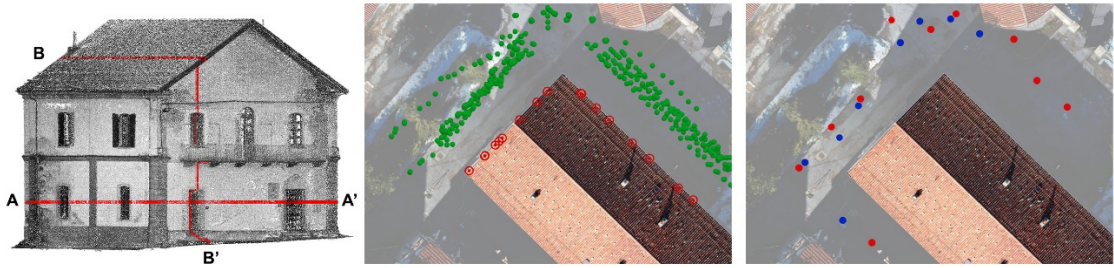


*Figure 68 Giuseppe Galliano Barrack, Key Plan of the extracted section (left), camera stations of the UAVs flight (centre) and position of the acquired scan with the two lasers (right)*

The same methodologies already described for the analyses performed at Rocca San Silvestro have been applied also on the Giuseppe Galliano Barrack, considering the general aim of an architectural survey that require the realization of traditional sections, plans and façade. Sections have been semi automatically extracted from the three point clouds using 3D Reshaper and the results have been compared has shown in Figure 69. Considering the results derived from this analysis and from the C2C comparisons presented above is possible to state that the model derived from the Spark is suitable for the realisation of the traditional survey products, both in terms of metric accuracy and accuracy of the reconstruction of the geometry of the surveyed object, considering a scale of representation of 1:100. Obviously, the automatic extraction of these sections is just a preliminary phase of the production of these survey products that will need further intervention from the involved operators.

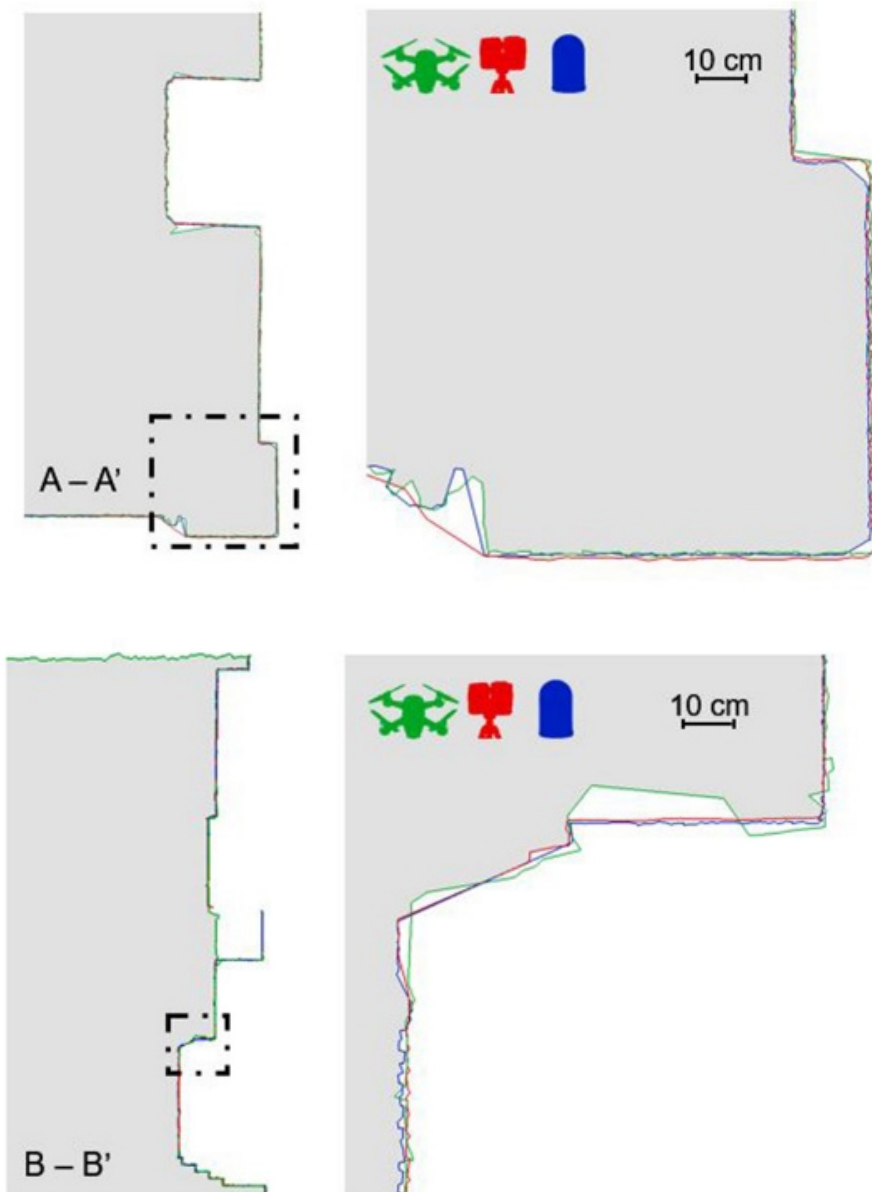


*Figure 69 Giuseppe Galliano Barrack. Comparison of the Semiautomatic sections extracted with the 3D Reshaper software*

A further test was performed in order to evaluate the integration between the two different UAVs platforms tested in Mondovì. The data derived from platform 4 (Spark) and platform 5 (Inspire 2) were separately processed, the processing parameters for these two datasets have been already reported and discussed in the text and were then integrated thanks to the common reference system adopted for both the dataset. The models derived from the two sensors were firstly segmented and then integrated as reported in Figure 70.



*Figure 70 Giuseppe Galliano Barrack, Example of integration of datasets: the final model (left), the Inspire 2 model (centre - blue) and the Spark model (right - blue)*

As is possible to see from the image, the dataset derived from the Inspire 2 was used for the reconstruction of the rooftop, while the one derived from the Spark was used for a more detailed reconstruction of the façades. This choice was influenced from two main factors: the two different resolutions of the employed sensors and the object-sensor distance. The flight with the Inspire 2 was performed at a bigger altitude but it was possible to achieve a small GSD thanks to the Zenmuse X5 specifications (Table 8), while to compensate the lower performances of the Spark it was necessary to reduce the object-sensors distance to reach a similar GSD. Likewise, the density of the final point cloud is influenced, among the other factors, also from the resolution of the acquired images: the same strategy of object-distance reduction was adopted to achieve similar results, also for the generation of this product.

### **Adopting the methodological framework for archaeological heritage: automatic flight planning in the Northern Necropolis of Hierapolis**

The possibilities offered by these COTS platforms for mapping purposes were further investigated with several other tests during the development of this research. In the archaeological site of Hierapolis, different COTS systems have been deployed in the field campaigns. The possibility to deploy these systems for the mapping of large archaeological areas in short amounts of time have been particularly stressed in the 2017 campaign. More expensive systems, especially fixed-wing UAVs, have already been used in the site for these kind of applications (Chiabrando, D'Andria, Sammartano, & Spanò, 2017), on the other hand, the use of multi-rotors COTS and low-cost platforms for this kind of tasks still need to be partially validated, and the methodologies to be refined. In 2017 the Phantom 4 (platform 2) was deployed to achieve the survey of the Northern Necropolis (Figure 71) of the Turkish site, that wasn't covered by previous aerial campaigns.



*Figure 71 Overall map of Hierapolis, in blue the area of the Northern Necropolis acquired in the 2017 and in red the area acquired in 2018 (source: D'Andria, Scardozzi, & Spanò, 2008)*

The phase of flight planning was projected following the experience gained in the test conducted at Rocca San Silvestro and resulted in the generation of the five flight plans reported in Figure 72. It is interesting to notice how with this approach it was possible to cover a wide area of the site in a short amount of time; the effective time of the flight was of 36 minutes, plus around 30 minutes for the operation of set up and deployment of the platforms (batteries changes included). It is also necessary to include the time that was dedicated to the positioning and measurement of the control points that will be better discussed in the following section 4.1.2. The area covered by the acquisitions was of around 0.2 km<sup>2</sup>.

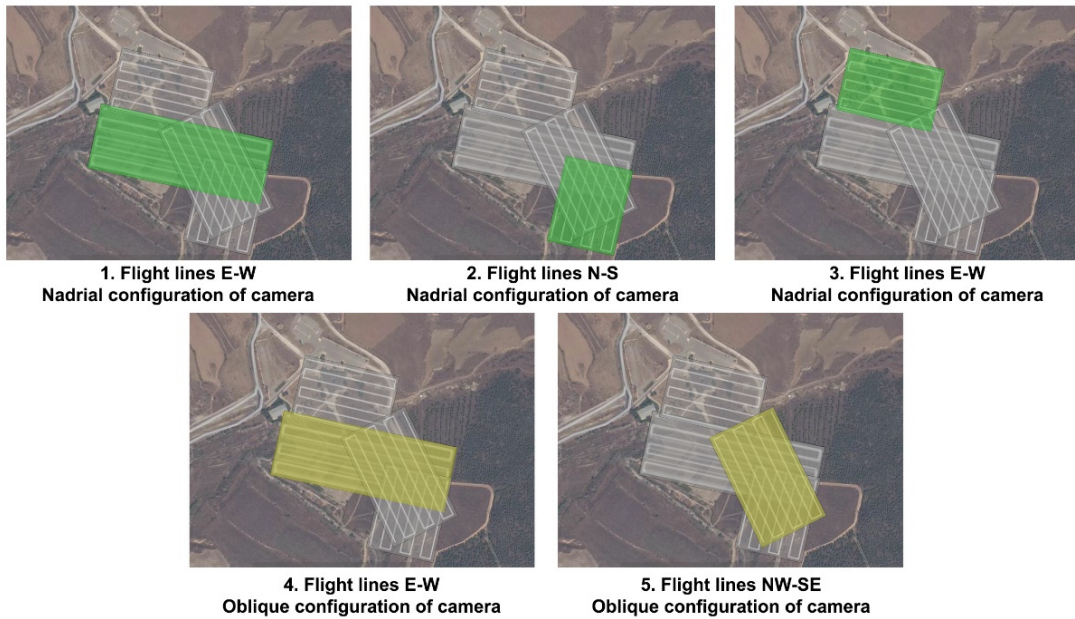


*Figure 72 Northern Necropolis of Hierapolis. Flight planning and camera orientation of the missions completed in 2017 with the Phantom 4 (platform 2)*

The main characteristics of the five flights performed are reported in the following Table 12. Three nadiral flights were completed following the developments of the necropolis and of the main viability that crosses the area. Two oblique acquisitions were added to better define the area where the concentration of the monuments is bigger and flight lines were projected to be interconnected with the other flight grids.

| Flight ID | N° images | Camera configuration | Flight time | Flight altitude |
|-----------|-----------|----------------------|-------------|-----------------|
| 1         | 215       | Nadiral              | 10 min      | 40-50 m         |
| 2         | 115       | Nadiral              | 6 min       | 40-50 m         |
| 3         | 127       | Nadiral              | 6 min       | 40-50 m         |
| 4         | 159       | Oblique              | 8 min       | 40-50 m         |
| 5         | 126       | Oblique              | 6 min       | 40-50 m         |

*Table 12 Northern Necropolis of Hierapolis. Main characteristics of the flights completed in 2017 with the Phantom 4 (platform 2)*

For this survey, all the five flights were processed together following the standard photogrammetric pipeline, the evaluation of the RMSe errors on the GCPs and CPs is reported in Table 13.

| Northern Necropolis 2017 flights |                           |              |               |              |                    |
|----------------------------------|---------------------------|--------------|---------------|--------------|--------------------|
| N° images                        | Reprojection error (mean) | GSD (cm/pix) | RMSe GCPs (m) | RMSe CPs (m) | Dense cloud pts N° |
| 742                              | 0,25 pix                  | 2,9          | 0,033         | 0,036        | 153.643.158        |

*Table 13 Hierapolis, Northern Necropolis. Phantom 4 flights processing main characteristics*

What is important to stress about these flights is the fact that in a reduced amount of time it was possible to deploy a COTS platform and to cover a wide area of the site. The result achieved allows to generate products with a scale of 1:200.

**When automatic flights are not possible: manual flight planning in part of the Northern Necropolis and in in the Apollo Sanctuary of Hierapolis**

As reported in section 3.7.3, the automatic flight based on previously projected missions is not always achievable and in specific situations manual flight should be preferred. These issues have been partially tackled with the tests performed with the Spark at Giuseppe Galliano Barrack, however they need to be further exploited. In the archaeological site of Hierapolis, the choice of performing (often) fully manual flights was dictated from four main reasons:

- The site is a major tourist destination in Turkey, it is not closed during the works of the Archaeological Italian Mission and the safety of the visitors must be ensured.
- Weather condition can have and high impact on the flights performed in this area and especially the wind may vary during daytime quite rapid and manual flight can guarantee a better control over the platform in these cases. GPS/GNSS signal doesn't always offer a good coverage and in case of low altitude flight is better to maintain more control over the UAV.
- The conformation of the scene or objects that need to be surveyed and the desired scale of the survey can have a high impact on the type of flight that need to be performed and on the altitude that need to be maintained. If a more detailed survey is requested, the object-sensor distance need to be reduced.
- The satellite images database embedded in the app used for flight planning do not offer a good resolution for this area and is thus difficult to programme more detailed flights on smaller portions of the site.
- The presence of unauthorized UAVs, piloted from the visitors is not uncommon, despite the strict prohibitions active on the area encompassing the archaeological site.

During the 2018 campaign, a portion of the Northern Necropolis was part of a more extensive and detailed survey. To integrate the aerial dataset acquired in 2017 further UAVs acquisitions were achieved, in a smaller area (in red in Figure 71). In this case, depending on the two platforms available on the field, from the desired details and finally from the conformation of the area that present a lot of different structures located on different levels of the terrain and a high density of archaeological remains. These reasons considered, the flights were fully manually performed following some criteria: the grids of waypoints,

shown in Figure 75, were executed following the methodology previously described and the cameras orientation were set considering the different developments of the structures present on the area and the conformation of the area itself. The flights were performed using two different platforms, the Mavic Pro and the Spark. This choice was undertaken to optimize the operational time of the batteries and with the idea to combine two systems that mount a similar sensor. Four flights were achieved with the Mavic and three with the Spark. The altitudes are slightly different in relation with the sensor's specifications: to achieve the same GSD the flights with the spark were performed at a lower altitude. The main characteristics of the flights are reported in the following Table 14.

| Northern Necropolis 2018 flights |           |  |             |                 |
|----------------------------------|-----------|--|-------------|-----------------|
| Mavic Pro (platform 1)           |           |  |             |                 |
| ID                               | N° Images | Flight and camera configuration                      | Flight time | Flight altitude |
| 1                                | 127       | Nadiral. Flight lines N-S                            | 11 min      | ≈25 m           |
| 2                                | 91        | Nadiral. Flight lines N-S                            | 7 min       | ≈25 m           |
| 3                                | 130       | Oblique. Flight lines N-S. Camera direction: E       | 13 min      | ≈25 m           |
| 4                                | 195       | Oblique. Flight lines N-S. Camera direction: W       | 15 min      | ≈25 m           |
| Spark (platform 4)               |           |  |             |                 |
| 5                                | 86        | Oblique. Flight lines W-E. Camera direction: E       | 10 min      | ≈15m            |
| 6                                | 81        | Oblique. Flight lines W-E. Camera direction: W       | 8 min       | ≈15m            |
| 7                                | 122       | Oblique. Flight lines N-S. Camera direction: N and S | 10 min      | ≈15m            |

*Table 14 Hierapolis, Northern Necropolis. Flight planning and camera orientation of the missions completed in 2018 with the Mavic Pro (platform 1) and Spark (platform 4)*

All the seven flights were processed together following the standard photogrammetric pipeline, the evaluation of the RMSe errors on the GCPs and CPs is reported in Table 15.

| Northern Necropolis 2018 flights |                           |              |               |              |                    |
|----------------------------------|---------------------------|--------------|---------------|--------------|--------------------|
| N° images                        | Reprojection error (mean) | GSD (cm/pix) | RMSe GCPs (m) | RMSe CPs (m) | Dense cloud pts N° |
| 829                              | 1,08 pix                  | 0,7          | 0,008         | 0,011        | 24.228.836         |

*Table 15 Hierapolis, Northern Necropolis. Mavic Pro and Spark flights processing main characteristics*

A similar approach was adopted for the flight performed in the 2017 and 2018 campaigns regarding the area of the Nymphaeum of the Apollo Sanctuary (located in the central area of the city as showed in Figure 73), manual flight was chosen as the best solution to adopt.



**Figure 73 Overall map of Hierapolis, in blue the area of the Apollo Sanctuary (source: D'Andria, Scardozzi, & Spanò, 2008)**

The flights in the area of Apollo Sanctuary and in particular on the Nymphaeum were performed both in the 2017 (with platform 2), both in 2018 (with platform 1 and 4). In both the campaigns the flights were achieved manually. Nevertheless, also in this case, data were not randomly acquired but precise guidelines and strategies were followed. First of all, an attempt to achieve a regular grid of camera positions was made, reproducing acquisitions schemes similar to the one implemented with the automatic flights. Secondly, the flight altitude was preselected after having decided the desired GSD and was maintained constant. Finally, a good overlap between images was ensured. The network of images acquired with this approach is definitely less regular than an automatic flight and the effort and time to spend on the field are more demanding, however it was possible to achieve the desired results. Main information of the flights performed in 2017 are reported in Table 16 and Figure 74, while for 2018 in Table 17 and Figure 75.

| Apollo Sanctuary 2017 flight |                           |                                    |               |              |                       |                    |
|------------------------------|---------------------------|------------------------------------|---------------|--------------|-----------------------|--------------------|
| Flight planning              |                           |                                    |               |              |                       |                    |
| Flight ID                    | N° images                 | Flight and camera configuration    |               |              | Flight time           | Flight altitude    |
| 1                            | 71                        | Nadiral – Flight lines W-E         |               |              | 10 min                | ≈ 25m              |
| 2                            | 80                        | Nadiral – Flight lines N-S         |               |              | 9 min                 | ≈ 25m              |
| 3                            | 91                        | Oblique – Flight lines W-E and N-S |               |              | 15 min                | ≈ 25m              |
| Processing                   |                           |                                    |               |              |                       |                    |
| N° images                    | Reprojection error (mean) | GSD (cm/pix)                       | RMSe GCPs (m) | RMSe CPs (m) | Sparse cloud (TPs) N° | Dense cloud pts N° |
| 242                          | 0,77 pix                  | 1,17                               | 0,009         | 0,008        | 445,516               | 42,475,111         |

*Table 16 Hierapolis, area of the Apollo Sanctuary. Flight planning, camera orientation and processing parameters of the missions completed in 2017 with the Phantom 4 (platform 2)*

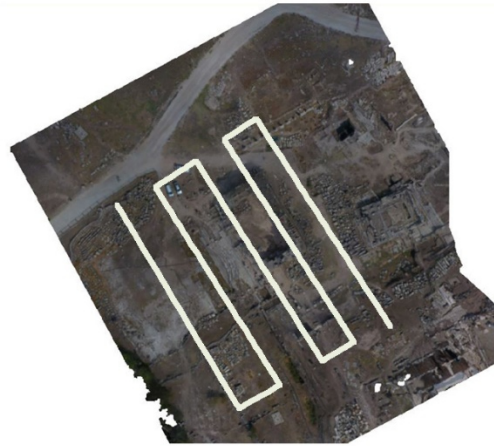
In 2017 two nadiral flights covering the area of the Apollo sanctuary were completed: one with flight lines perpendicular with the main development of the Nymphaeum and one with flight lines parallel with the main development of this building. A third flight with an oblique configuration of the camera was achieved projecting the flight lines around the structure with the camera always oriented on its centre. The RMSe value is always slightly below 1 centimetre both for GCPs and CPs, the points were measured with a traditional topographic approach with TS.

**ACHIEVED FLIGHT PLAN**

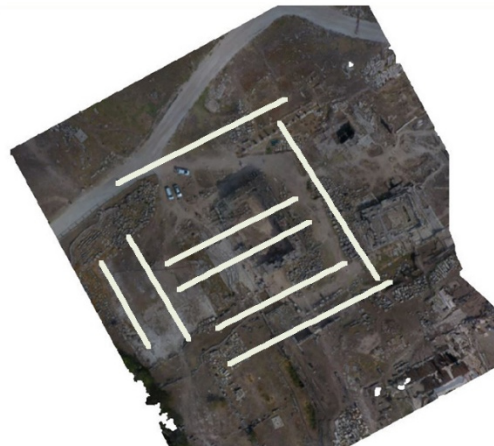
**PROJECTED FLIGHT PLAN**



**Flight 1. Nadiral configuration of camera. Flight lines W-E**



**Flight 2. Nadiral configuration of camera. Flight lines N-S**



**Flight 3. Oblique configuration of camera. Flight lines W-E and N-S**

*Figure 74 Hierapolis, area of the Apollo Sanctuary. Flight planning and camera orientation of the missions completed in 2017 with the Phantom 4 (platform 2)*

The 2018 flights were projected in a slightly different way, in particular due to the progress of the Italian team of archaeologist in the excavation of the area. More flights were achieved and with a bigger overlap between single images. Two nadiral flights were completed with flight lines perpendicular with the main development of the Nymphaeum and three oblique flights with different flight lines direction were achieved as well. Finally, a lower flight with a mixed configuration of camera and flight line set up was carried out in the basin of the Nymphaeum, that was one of the areas investigated through the archaeological excavation.

| <b>Apollo Sanctuary 2018 flight</b>         |                  |  |                    |                        |
|---|------------------|--|--------------------|------------------------|
| <b>Flight planning (Mavic – platform 1)</b> |                  |  |                    |                        |
| <b>Flight ID</b>                            | <b>N° images</b> | <b>Flight and camera configuration</b> | <b>Flight time</b> | <b>Flight altitude</b> |
| <b>1</b>                                    | 120              | Nadiral – Flight lines W-E             | 14 min             | ≈ 25m                  |
| <b>2</b>                                    | 176              | Nadiral – Flight lines W-E             | 16 min             | ≈ 25m                  |
| <b>Flight planning (Spark – platform 4)</b> |                  |  |                    |                        |
| <b>3</b>                                    | 95               | Oblique – Flight lines W-E             | 12 min             | ≈ 15m                  |
| <b>4</b>                                    | 89               | Oblique – Flight lines W-E             | 10 min             | ≈ 15m                  |
| <b>5</b>                                    | 65               | Oblique – Flight lines N-S             | 7 min              | ≈ 15m                  |
| <b>6</b>                                    | 114              | Mixed free flight - detailed           | 8 min              | ≈ 10 m                 |

*Table 17 Hierapolis, area of the Apollo Sanctuary. Flight planning and camera orientation parameters of the missions completed in 2018 with the Mavic Pro (platform 1) and Spark (platform 4)*

**ACHIEVED FLIGHT PLAN**

**PROJECTED FLIGHT PLAN**



**Flight 1. Nadiral – Flight lines W-E**



**Flight 2. Nadiral – Flight lines W-E**



**Flight 3. Oblique – Flight lines W-E**

**ACHIEVED FLIGHT PLAN**

**PROJECTED FLIGHT PLAN**



**Flight 4. Oblique – Flight lines W-E**



**Flight 5. Oblique – Flight lines N-S**



**Flight 6. Mixed free flight - detailed**

*Figure 75 Hierapolis, area of the Apollo Sanctuary. Flight planning and camera orientation of the missions completed in 2018 with Mavic Pro (platform 1) and Spark (platform 4)*

## 4.1.2 Georeferencing strategies and GCPs

Among the different phases of the photogrammetric pipeline one of the most time consuming, both in the acquisition phases on the field, both during the data processing, is the one related with the georeferencing and scaling of the model. Three main strategies can be adopted to complete this process:

- Direct Georeferencing
- Use of GCPs
- Co-registration of the dataset

### **Georeferencing strategies: direct georeferencing**

The direct georeferencing of the dataset can be reached if the coordinates of the different camera positions are known a-priori. This situation can be achieved if a GPS/GNSS sensor is mounted on the aerial platform and if the data collected by this sensor can somehow be used and treated after the phases of data acquisition. Two main techniques can be employed to reach these results: Real Time Kinematics (RTK) and Post-Processed Kinematic (PPK). There are several differences between the two techniques, in general terms the RTK process happens in real time (as the name suggest), while the PPK is completed in a separate phase. During an RTK UAVs acquisition the aerial platform's GNSS is connected with another receiver that works as base station, the data received from the satellites are corrected in real time and the global coordinates are embedded in the Exchangeable image file format (Exif) metadata of the images, with a process known as geotagging. On the other hand, PPK process works in a different way: again, two GNSS receiver are involved in the process, one mounted on-board the platform and one serving as ground station, but for this approach no connection between the two receivers is needed. The data derived from the two receivers are recorded in raw formats and are then processed afterwards with dedicated solutions. The geotagging of images is then performed after having applied the needed corrections of the GNSS data recorded on the field. Several researches have been conducted during the last years regarding these approaches (e.g. Benassi et al., 2017; Gerke & Przybilla, 2016; Rieke, Foerster, Geipel, & Prinz, 2012), however their implementation in COTS and low-cost platforms is not fully achieved yet, despite the fact that drone industries are stressing a lot this possibility and new solutions contemplating these approaches are now being launched on the market. A third procedure is related with the direct tagging of the acquired images with the onboard GNSS receiver, without applying any correction to the positioning data collected. In term of accuracy and easiness of deployment on the field, PPK is the best solution while the instant geotagging of the images is the one providing the worst accuracy.

Some tests with other commercial and more expensive solutions have been performed by the authors research group (Calantropio et al., 2018) providing good results; the situation is quite different for the COTS platform presented in section 4.1.1 and employed in this thesis.

Some preliminary tests have been performed with these COTS platforms, however, the precision of the GNSS receiver mounted on the platform is not always satisfying and, especially when working with different platforms, some gross errors can be clearly visible. In Figure 76 an example of the processing, using a direct georeferencing approach, of two datasets of the Nymphaeum acquired at the same time with two different platforms is reported. From this image is clear that the two systems are recording the GPS/GNSS signal in an inconsistent and incoherent way, confirming that this strategy is not always adoptable in case of COTS platforms and the positioning data derived from these sensors need to be carefully controlled.

This issue is probably ascribable to the different quality of the GPS/GNSS sensors embedded in the different platforms; in the case of the Nymphaeum of Apollo this issue resulted in a systematic shift of camera positions along the z direction.

Due to the category of platforms selected and the weakness still present on this approach for this kind of UAVs, this solution was not adopted in this research.

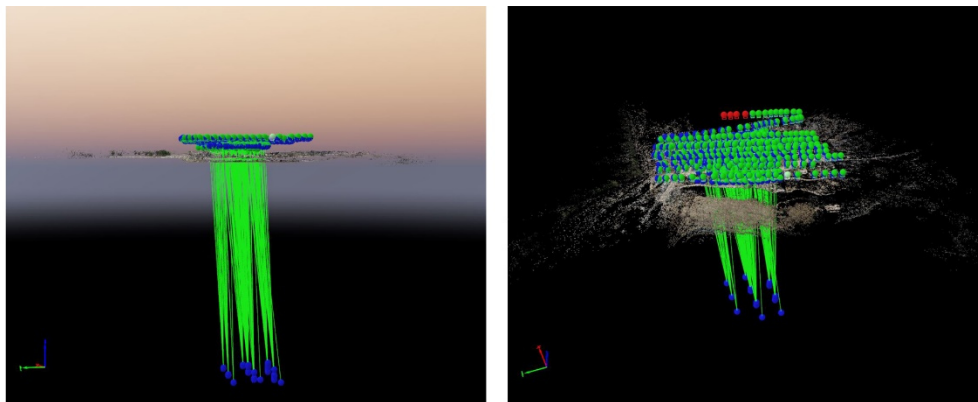


*Figure 76 Hierapolis, Nymphaeum of Apollo. Gross error on direct georeferencing derived from two different platforms*

### **Georeferencing strategies: the use of GCPs**

The use of GCPs is by far the most employed techniques and, at the same time, the most time and resources consuming. In the traditional approach both pre-codified markers and natural features can be used in this approach. The distribution of these point in the area to survey must be carefully projected and completed: both the number and the position of the points are factors that need to be considered. The distribution of the points should be

homogenous, and all the area of interest must be comprehended, moreover, it must be ensured that every marker is acquired by multiple images.

The size, shape and colour of the codified target are other factors that need to be evaluated depending on the altitude of the flight, the light condition of the scene recorded and the colour of the surface on which the marker is attached. If natural/man made features are chosen as points to be measured the same shrewdness described for the target must be applied and it must be ensured the recognizability of the feature on the acquired images. After the selection and positioning of the point the phase of measurement must be completed; two traditional topographic techniques are generally employed to measure the selected points: TS or GNSS techniques. The choice of which techniques to adopt is related with the conformation and dimension of the area interested from the survey, the time available on the field and finally the desired accuracy. TS generally provides a better accuracy of the measurements but requires also more time on the field for this phase. On the other hand, GNSS technique allows to cover wider areas in a shorter time but sacrificing some accuracy of the measurements. Despite the employed techniques, the overall phase dedicated to the positioning and measurement of the control points is for sure the one that mostly impact the fieldwork. For these reasons, a lot of efforts have been put by the different geomatics research teams to improve this phase.

The first tests on this research topic were achieved at Rocca San Silvestro and the main idea was to evaluate if and how the use of oblique images and different flight configurations can impact on the use of control points, as tested by other authors (Dall'Asta et al., 2015; Nocerino, Menna, & Remondino, 2014). The seven projects were first processed following the standard photogrammetric pipeline and 6 out of the 24 measured point were used as CPs, as already reported in Figure 57. In a second phase only 4 point were chosen as GCPs, while all the other 20 were used as CPs, the position of these 4 points was chosen based on the conformation of the site and is reported in the following Figure 77.

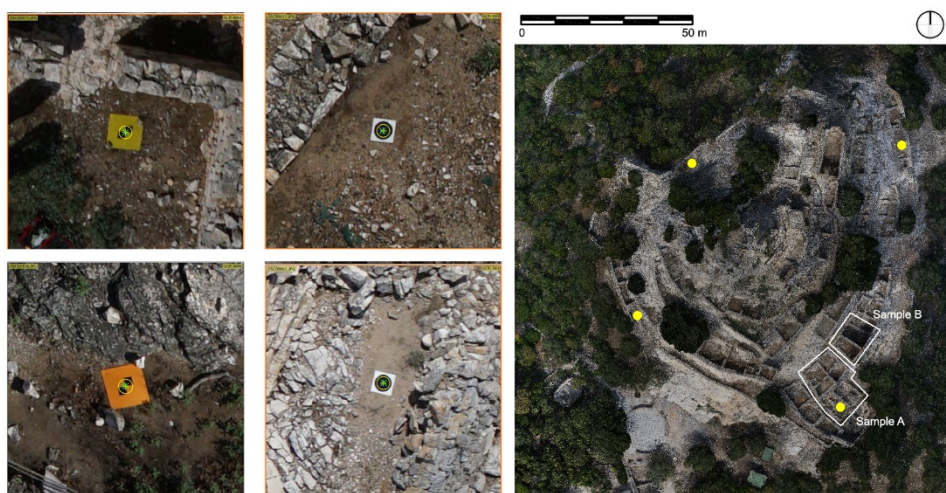


*Figure 77 Rocca San Silvestro, 4 GCPs configuration. Position and type of GCPs*

All the seven projects were then processed again adopting this configuration and the results are reported in the following Figure 78.

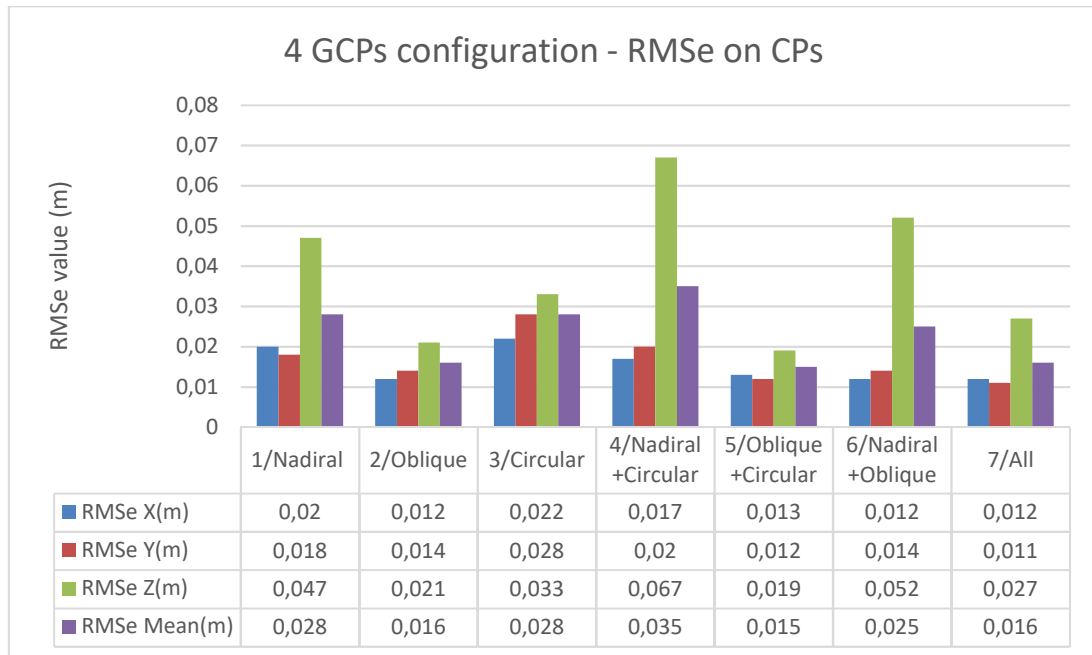


**Figure 78 Rocca San Silvestro, Graphical representation of the mean RMSe of the CPs in the seven projects, using only 4 GCPs**

Camera and flight configuration surely have an impact on the BBA as is possible to see from the data extracted from the seven different project configurations. A general reduction of the RMSe is visible on the projects where oblique images are used. It is interesting to notice that in terms of accuracy the performances of the circular flight are below the expectations. While this configuration was producing good results in the analysis previously performed concerning the geometrical reconstruction, its impact is lower with this kind of GCPs and CPs configuration, especially in the z component.

The test on GCPs and CPs configuration were further developed and extended to COTS platform in the research conducted at Savigliano. In this case, the 4 combinations of datasets were processed with three GCPs configuration for each of the three platforms employed. As reported in the following Table 18 flights A,B,C and D were processed with three different GCPs configurations: 12 GCPs and 0 CPs (GCPs I), 6 GCPs and 6 CPs (GCPs II) and finally 4 GCPs and 8 CPs (GCPs III), as shown in Figure 79.

| Flights and camera configuration   | GCPs and CPs configuration   |
|--|--|
| A. All the flights (available only for the Phantom 4 and Phantom 4 Pro)      | GCP I (12 GCPs and 0 CPs)<br>GCP II (6 GCPs and 6 CPs)<br>GCP III (4 GCPs and 8 CPs) |
| B. Nadiral and Circular (available only for the Phantom 4 and Phantom 4 Pro) |  |
| C. Nadiral and Oblique (available for all the platforms)                     |  |
| D. Only the two strips of the nadir image (available for all the platforms)  |  |

**Table 18 Savigliano, processing configurations. On the left the combination of the five flights described at page 135 together, on the right the different GCPs configurations**

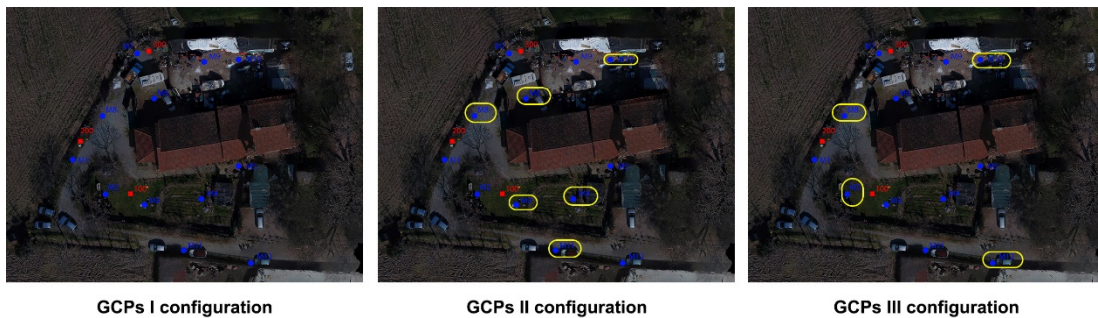


**Figure 79 Savigliano, the three GCPs configurations adopted in the processing of the four datasets. In yellow the points used as GCPs**

The datasets just described were processed both with MicMac and Pix4D, a detailed comparison between the results achieved with the two different software solutions can be found in the already cited work (Chiabrando & Teppati Losè, 2017). Due to the fact that Pix4D was in the end slightly better performing than MicMac, the results of the first will be reported here. The following three tables (Table 19, Table 20 and Table 21) report the mean RMSe values for both GCPs and CPs in the for combinations of datasets and in the three GCPs configurations. The values are reported for the three platforms.

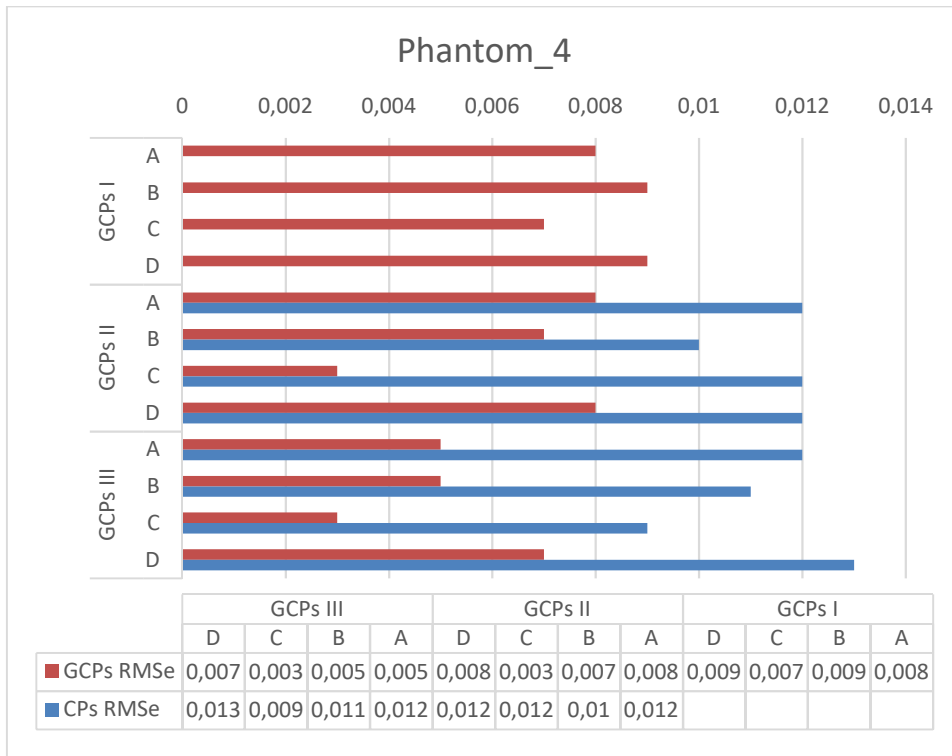


**Table 19 Savigliano, mean RMSe value on GCPs and CPs for the 4 projects in the three GCPs configuration with the Phantom 4**

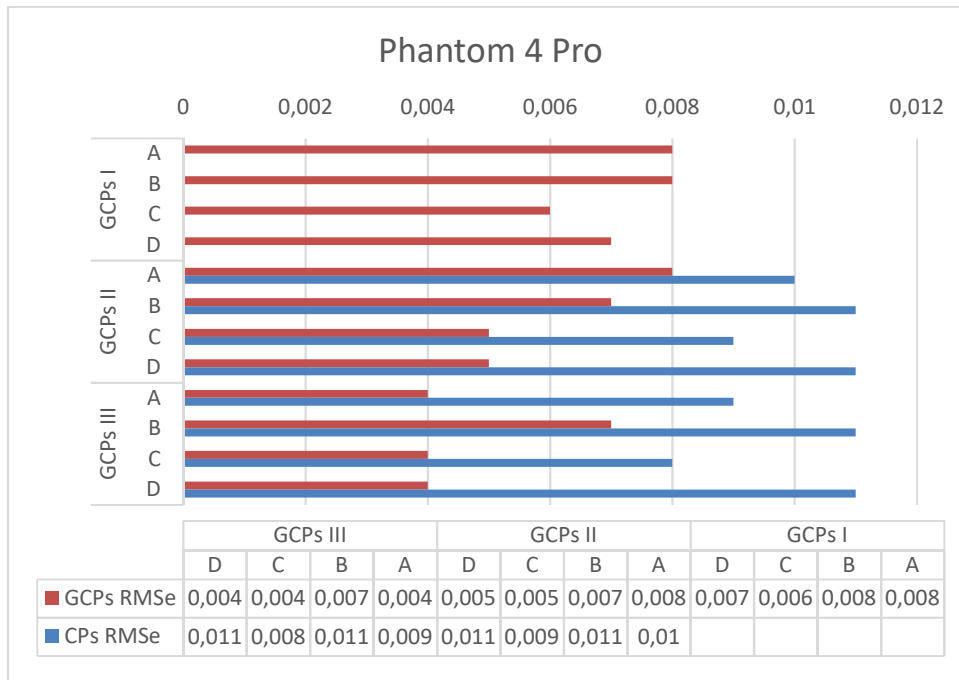


**Table 20 Savigliano, mean RMSe value on GCPs and CPs for the 4 projects in the three GCPs configuration with the Phantom 4 Pro**

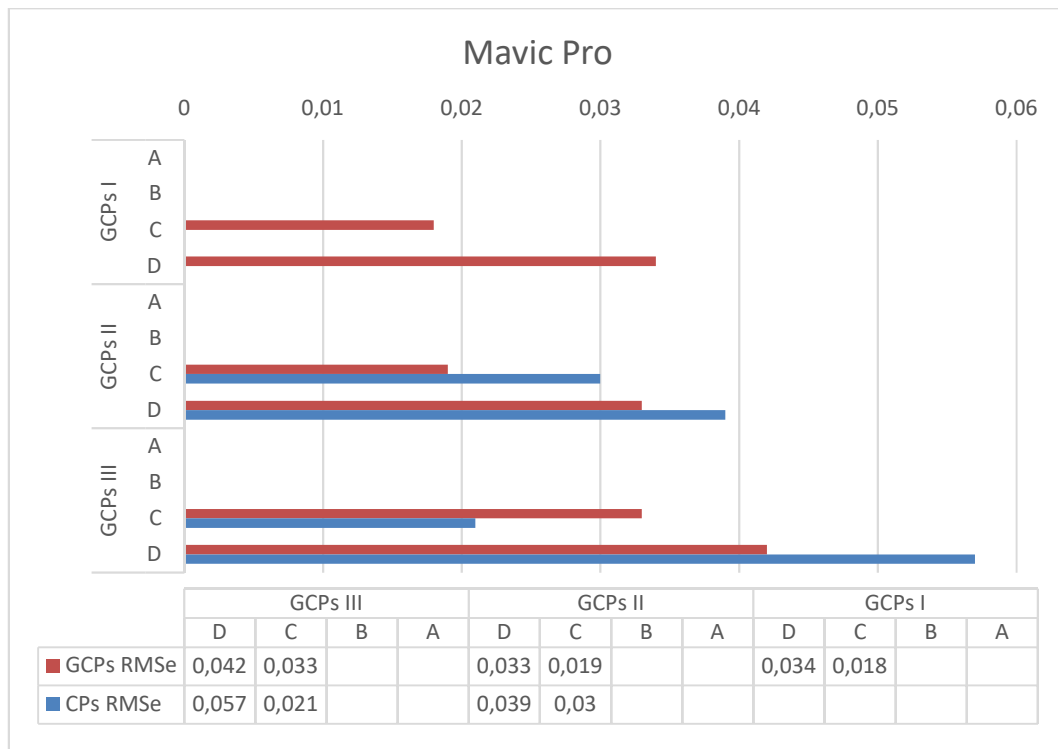


*Table 21 Savigliano, mean RMSe value on GCPs and CPs for the 4 projects in the three GCPs configuration with the Mavic Pro*

It is possible to underline that the three platforms, according to these values, can be considered suitable for architectural large-scale documentation purposes. It is interesting to notice that Phantom 4 and Phantom 4 Pro presents similar performances, with a slightly better behaviour of the Phantom 4 Pro thanks to the more performing camera mounted on the platform. The use of oblique images can highly contribute in the overall strategies of reducing the number of needed GCPs; project C, that integrate nadiral and oblique flights, seems to be one of the best solutions in this sense. This project is returning good RMSe value in all the three GCPs configurations, even in GCPs III, that is using only 4 point as ground control points. The Mavic Pro is, on the other hand, the worst performing platform. This is due to different reasons: the lower performances of this UAVs sensor and the failure in the acquisition of the circular flight. Due to the lack of the circular flight it was not possible to achieve a complete analysis of this UAVs. In the Savigliano test, the contribute of the circular flight is, however, less impacting compared with the Rocca San Silvestro tests, this is especially dependant to the geometry of the surveyed object that in this case is more suitable for the standard grid of oblique cameras.

**Georeferencing strategies: co-registration approach**

The third approach for the scaling and georeferencing of the data collected on the field is the co-registration of different datasets. This approach has been developed in the last years to monitor dynamic scene reducing the use of GCPs and thus the manual intervention of the operator involved in the process. This approach is also defined as image-based co-



| <b>Nymphaeum, 2017 datasets</b> |                                  |                     |                      |                     |                              |                           |
|---------------------------------|----------------------------------|---------------------|----------------------|---------------------|------------------------------|---------------------------|
| <b>N° images</b>                | <b>Reprojection error (mean)</b> | <b>GSD (cm/pix)</b> | <b>RMSe GCPs (m)</b> | <b>RMSe CPs (m)</b> | <b>Sparse cloud (TPs) N°</b> | <b>Dense cloud pts N°</b> |
| <b>242</b>                      | 0,77 pix                         | 1,17                | 0,009                | 0,008               | 445,516                      | 42,475,111                |

*Table 22 Nymphaeum of Apollo, main parameters for the processing of the UAVs dataset collected in 2017*

For the processing of these datasets and to develop the co-registration approach described above, Agisoft Photoscan was preferred to Pix4D; indeed, the Russian software allows to manage and organize the project in different layers (chunk), function that is not implemented in the Swiss software. This feature allows also a better management of the different images, that can be imported in the software during different steps of the processing, can be grouped in different layers (chunk) and, depending on the operator decision, selectively included or excluded from the processing. Thus, the 2018 images were added in a new camera group created in the already processed 2017 projects: thanks to the processing already performed the project was already georeferenced and scaled with known point coordinates and the overall metric accuracy of the photogrammetric process has been already assessed.

The 2017 camera stations group was used as a rigid block to complete the phases of TPs extraction and camera orientation for the 2018 dataset. The aim was to estimate the 2018 camera stations position and orientation in real world coordinates, in order to complete this phase of the processing without the use of control points. In a second step the 2017 images were then disabled, and the processing was completed following the standard photogrammetric pipeline and generating the desired products.

This approach was validated using the coordinates of some natural features extracted from a TLS reference dataset. It was chosen to extract the coordinates of some recognizable natural features from a laser dataset acquired in the 2017 and georeferenced in the same coordinate system adopted for the photogrammetric processing. The TLS dataset was composed by 45 scans and was processed following the consolidated LiDAR data processing workflow: first the different scans are registered using a cloud to cloud approach based on an ICP (Iterative Closest Points) algorithm and in a second phase control points are used to georeference the scans block and evaluate its accuracy; the main parameters of this processing of the laser dataset are reported in Table 23, while an overview of the scans positions is showed in Figure 81. Concerning the Nymphaeum of Apollo, the scans were acquired using a Faro Focus X330 and the processing of the dataset were achieved using the Faro Scene software.

| N° of scans | Cloud to cloud                      |  | Target based                    |                         |
|-------------|-------------------------------------|--|---------------------------------|-------------------------|
|             | Average tension on scan points (mm) | Average tension on scan points (<4 mm) | Average tension on targets (mm) | Standard deviation (mm) |
| 45          | 3,04                                | 62,6 %                                 | 9,56                            | 4,81                    |

*Table 23 Nymphaeum of Apollo, accuracy of the TLS dataset processing*

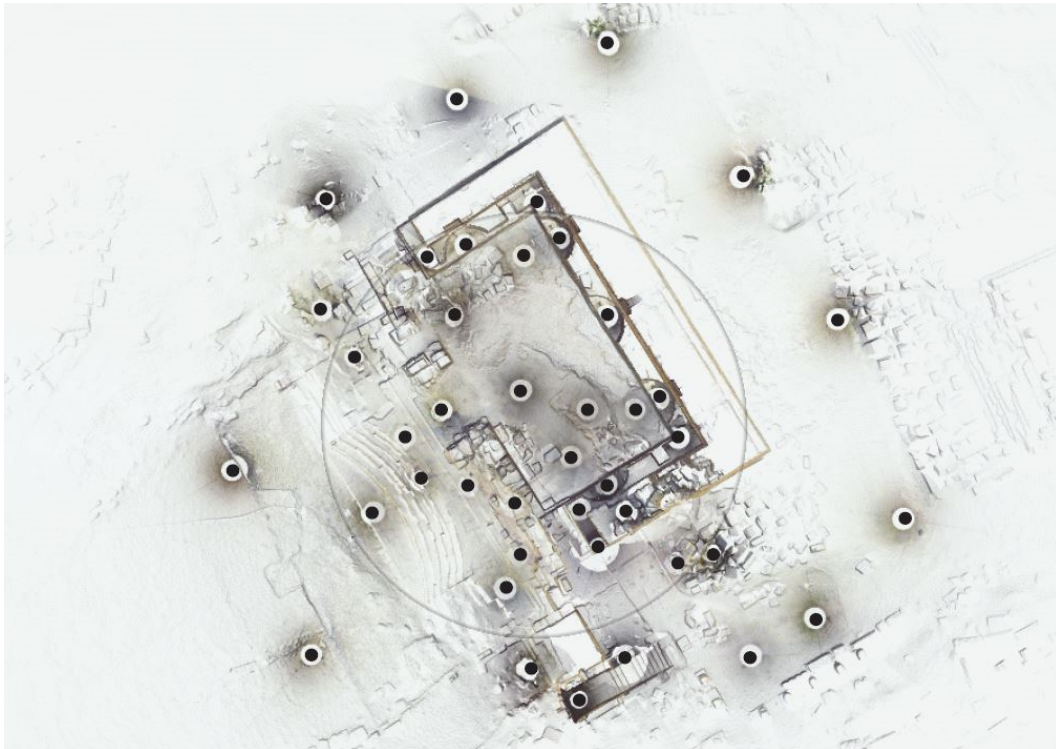


*Figure 81 Nymphaeum of Apollo, position of the scans acquired in the 2017 campaign*

Eight natural features homogenously distributed over the structure were chosen in this dataset and their coordinates were extracted, they are reported in the following Figure 82. These features were chosen both on horizontal and vertical surfaces of the structures and in areas that have not been modified in the time between the two acquisitions.



*Figure 82 Natural features selected to be used to validate the co-registration approach*

The same natural features were then identified in the 2018 photogrammetric project and were located in the oriented set of images in order to have their coordinates to be computed

by the software as manual TPs. The coordinates extracted through this approach were then compared with the ones obtained from the TLS dataset, as reported in the following Table 24.

|          | 2017 TLS |          |          | 2018 CO-REGISTERED |          |         | 2017-2018 COMPARISON |                   |                   |                      |
|----------|----------|----------|----------|--------------------|----------|---------|----------------------|-------------------|-------------------|----------------------|
|          | X (m)    | Y (m)    | Z (m)    | X (m)              | Y (m)    | Z (m)   | $\Delta X$<br>(m)    | $\Delta Y$<br>(m) | $\Delta Z$<br>(m) | $\Delta MEAN$<br>(m) |
| <b>A</b> | 1929,332 | 2016,974 | 376,260  | 1929,285           | 2016,939 | 376,223 | 0,047                | 0,035             | 0,037             | <b>0,040</b>         |
| <b>B</b> | 1918,555 | 2029,502 | 369,1894 | 1918,551           | 2029,453 | 369,195 | 0,004                | 0,049             | -0,006            | <b>0,016</b>         |
| <b>C</b> | 1913,27  | 2029,484 | 376,1985 | 1913,326           | 2029,431 | 376,205 | -0,056               | 0,053             | -0,006            | <b>-0,003</b>        |
| <b>D</b> | 1917,197 | 2002,628 | 368,7316 | 1917,164           | 2002,586 | 368,720 | 0,033                | 0,042             | 0,012             | <b>0,029</b>         |
| <b>E</b> | 1919,031 | 1995,98  | 367,8873 | 1918,993           | 1995,980 | 367,910 | 0,038                | 0,000             | -0,023            | <b>0,005</b>         |
| <b>F</b> | 1901,766 | 2024,52  | 368,2193 | 1901,755           | 2024,517 | 368,250 | 0,011                | 0,003             | -0,031            | <b>-0,005</b>        |
| <b>G</b> | 1933,965 | 2009,669 | 378,8114 | 1933,998           | 2009,569 | 378,803 | -0,033               | 0,100             | 0,008             | <b>0,025</b>         |
| <b>H</b> | 1929,572 | 2024,431 | 375,2932 | 1929,573           | 2024,437 | 375,265 | -0,001               | -0,006            | 0,028             | <b>0,007</b>         |

*Table 24 Nymphaeum of Apollo, comparison between TLS extracted coordinates and photogrammetric computed coordinates*

As is possible to notice from the value reported in the previous table, this approach can be considered valid from a metric point of view. The overall deviation of the estimated coordinates of the selected points is acceptable and ranges from few millimetres to few centimetres. Moreover, also an analysis on the values separated in the three coordinates components doesn't seem to underline any particular trends: the values are quite homogeneously distributed and a major deviation in one of the three components seems not to be present.

According to the experience gained in these tests, this strategy is not always practicable, and some conditions need to be fulfilled. First of all, the scene or the object recorded in the two datasets must not change too much or move during time and in the space comprehend

between the different acquisitions. Otherwise it won't be possible to co-register the two datasets and it won't be possible to find correlations between the images. Secondly, if different sensors are used, they main characteristic need to be similar, e.g. in term of resolution, radiometric profile, etc. Further tests are still on development to deepen the possibilities connected with this approach, both enhancing the acquisitions phases, both the processing phases. From the acquisition phase further tests will be devoted to the standardisation of the flight planning to be repeated for the multitemporal approach in the documentation of archaeological excavations. Secondly, new strategies to co-register and validate the multitemporal dataset will be experimented. One of the possibilities is connected to the set-up of fixed materialised points around the excavation to be used both in the processing and in the metric control of the results. Another possibility to investigate is related with the use of masks inside the photogrammetric software during the processing, this can allow to exclude from the orientation phase of cameras the areas that undergone some modification and enhance this phase of the processing. These strategies can really lead to appreciable results but is definitely a time-consuming operation.

#### **4.1.3 Use of the photogrammetric derived products. The multitemporal approach in the site of Hierapolis**

According to the results and to the literature previously presented, it is possible to state that the possibility to deploy COTS and low-cost UAVs platforms for photogrammetric application is nowadays consolidated. These platforms can be used for 3D modelling and metric survey purposes and especially the field of CH documentation can benefit from their deployment. Nevertheless, as previously stressed, there are still many issues to be solved and many research topics to exploit; both connected with these platforms alone, both with the integration of UAVs derived data with the ones from other sensors. In the following sections, some of the available products derived from this approach will be better analysed and some of the uses connected to them will be better exploited. Nevertheless, these products have proven to be really successfully used in the generation of traditional 2D drawings. Standard architectural sections and plans can be produced starting from these data, with a strong intervention of the operator involved. However, in the following sections, the attention will be focused on the contribute that these products can provide both during the excavation phases both during the subsequent phases of study and interpretation. The multi temporal dataset of the Nymphaeum of Apollo was chosen to be more in-depth analyses in the following sections. This choice was led to the fact that the availability of two co-registered dataset acquired in two different years allows to perform some interesting analyses on the changes that occurred in this span of time.

## Point Cloud

The first products considered is the point cloud derived from the densification phase of the photogrammetric processing. This analysis was performed on the two point clouds generated from the two flights performed in 2017 and 2018 on the Nymphaeum. The two models were first segmented to be included in the same area and the number of points between the two was normalised, the 2018 point cloud was slightly richer in term of number of generated points, due to the fact that a bigger number of images was acquired in 2018 and later processed. This analysis was performed in the CloudCompare software, using the C2C distances analysis tool. In this case the 2017 dataset was used as reference elements and the 2018 as compared one. This tool was used to underline the major discrepancies between the models generated in the two different campaigns. Indeed, in the period that interurred between the two acquisitions some major changes happened in the area, due to the archaeological excavations. An overview of the main changes detected from this analysis is reported in Figure 83.

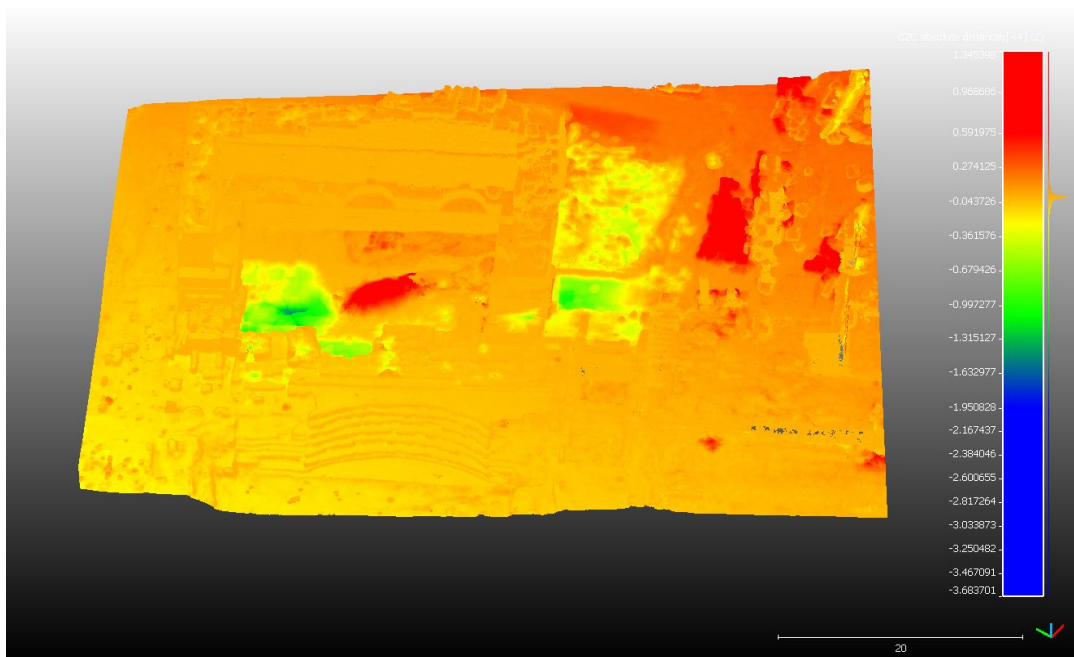


*Figure 83 Nymphaeum of Apollo, General overview of the C2C analyses. The areas where major changes occurred are underlined in red and green*

It is possible to notice two major areas where these discrepancies are located, corresponding to the excavation areas of the Italian team of archaeologists, the basin of the Nymphaeum and the area adjacent to the southern walls of the structure. These discrepancies have been validated also from other products of the photogrammetric process. In order to deepen the analyses onto these two areas, the point clouds were further segmented considering the borders indicated in following Figure 84.



*Figure 84 Nymphaeum of Apollo, the two areas selected to deepen the analysis between 2017 and 2018 dataset*

The first area includes the basin of the Nymphaeum, in 2017 it was excavated in the south portion, while in the 2018 the northern part was under investigation. The second area is located in the southern part of the building and was excavated in different steps both in 2017 and 2018. The adopted approach was conceived in order to evaluate if it was possible to automatically detect the major changes between the models generated from the data acquired in the two years. After some tests of the settings available for the C2C distance tool, it was chosen to set the maximum research distance to 2 meters. Moreover, it was also decided to split the analysis on the different three components (x, y and z) in order to better evaluate the available outputs. In this case it was particularly important to evaluate the z component of the datasets, that was the one that can better underline the major changes occurred in the area due to the archaeological excavations.

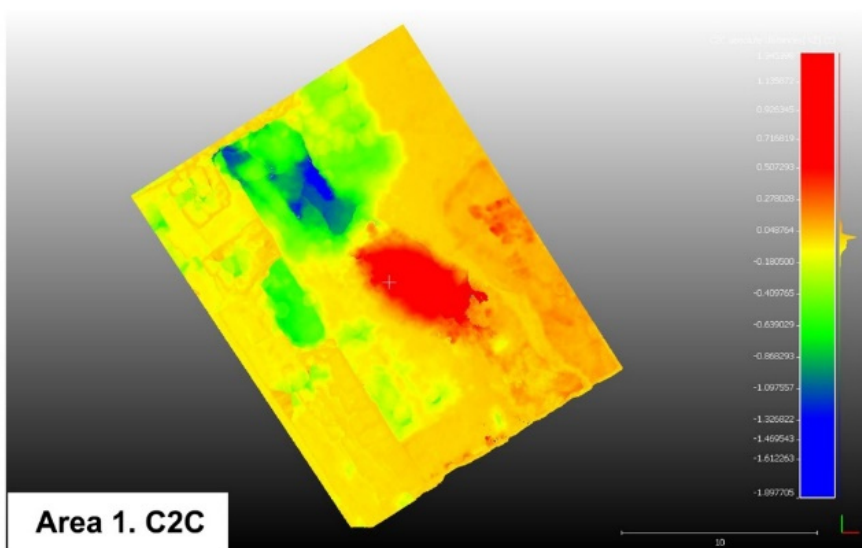
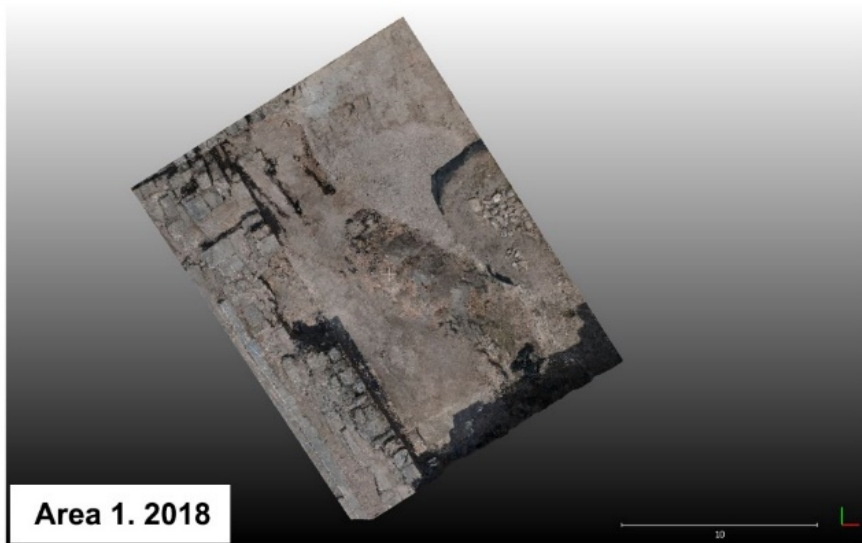




*Figure 85 Nymphaeum of Apollo, Area 1, C2C analysis between the models derived from 2017 and 2018 UAVs dataset*

The analysis performed in the Area 1 sample, reported in Figure 85, allow to identify several changes:

- In the northern part of the area is possible to underline the portion that was excavated in 2018. Values from green to blue indicate a removal of ground from 0 up to minus 1,9 meters.
- Another small excavation area in the centre-left of Area 1 is underlined with value from 0 to minus 0,8 meters.
- Finally, the portion of the model on the southern part of the area, indicated with orange and red values ranging from 0 to plus 1,4 correspond to an accumulation of the ground removed from the nearby excavation area.
- Finally, another small excavation can be located in the south-west part of the area, with green coloured values ranging from 0 to minus 0,7 meters.

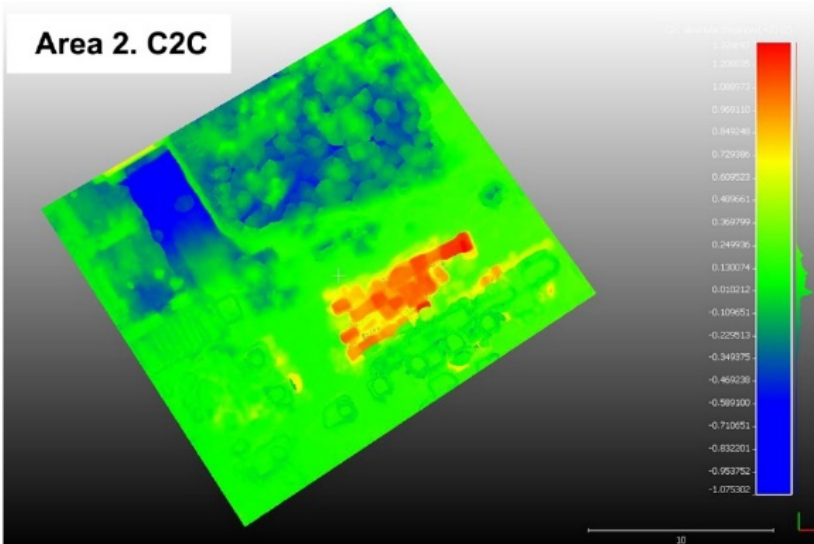
Area 2. 2017



Area 2. 2018



Area 2. C2C



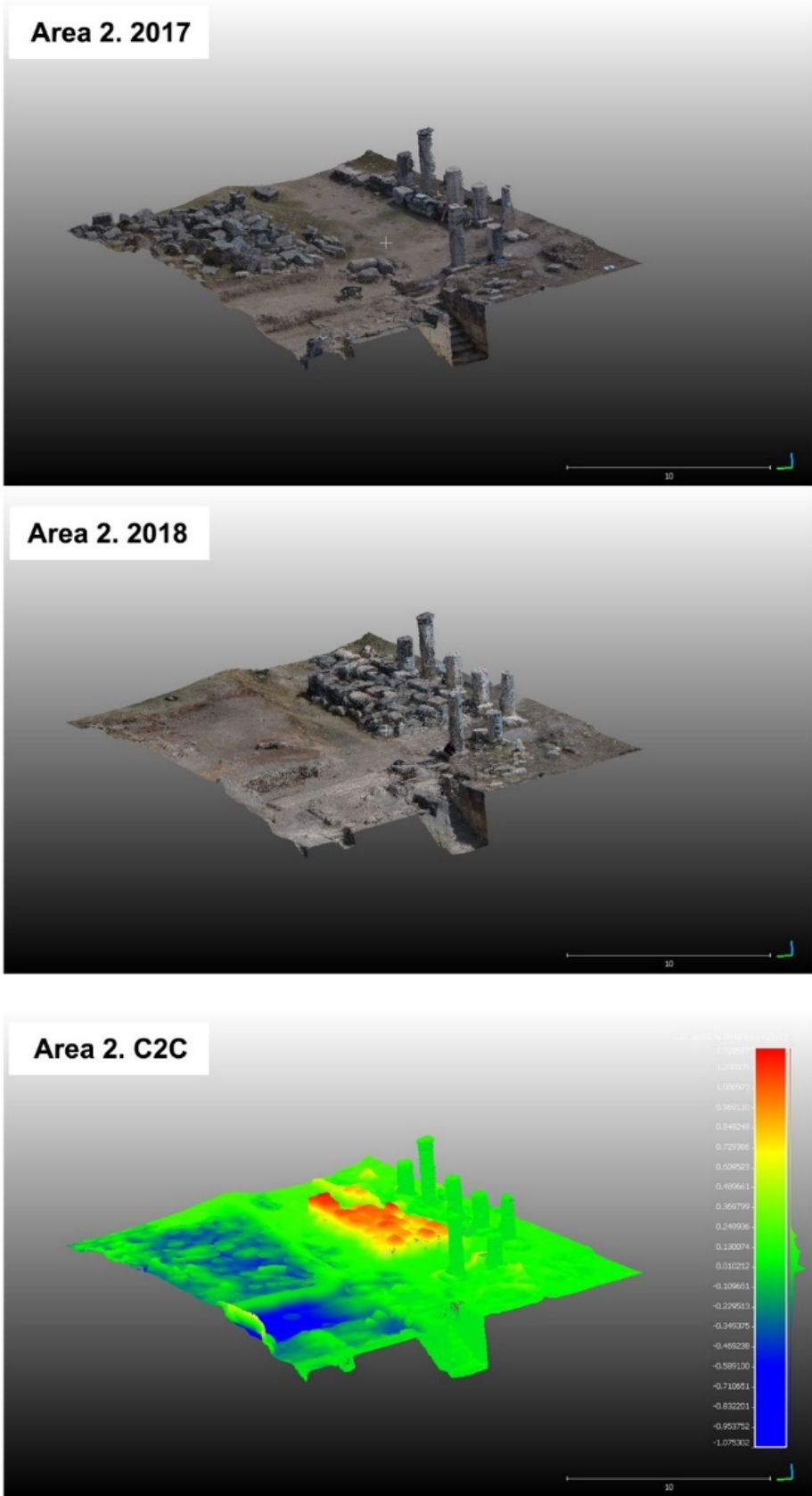


Figure 86 Nymphaeum of Apollo, Area 2, C2C analysis between the models derived from 2017 and 2018 UAVs dataset

Likewise, the same analysis was achieved for Area 2, Figure 86, allowing to detect different changes between the two datasets:

- In the east part of the area is possible to locate a regular rectangular excavation area, blue coloured, and that comprehend values starting from minus 0,1 to minus 1 meter.
- In the northern part of the area, the point cloud is not coloured in a homogenous way, indicating that different blocks and rubble have been moved, creating changes indicated with green and blue colours, and ranging from 0 to minus 0,5 meter.
- Finally, in the southern portion of the area, a growth of material is present. Again, it is not a uniform material, but the shapes of different block can be identifiable. Changes in this area vary from 0 to plus 1,3 meters and are indicated with colours from yellow to red.

The discrepancies derived from these analyses have been compared with the images and the data of these two areas acquired in the two years, in order to validate the procedure and underline eventual failures. In general terms, the results achieved have proven to be quite accurate in locating the area where archaeological works were actually completed. However, an issue was found in the analysis achieved in Area 1. In this case the ground removed from the new excavated areas was accumulated on the central part of the basin. This area was excavated in 2017, and acquired from the UAVs acquisitions of that year, but was covered at the end of the 2017 archaeological campaign and in 2018 was temporary not visible due to the mound of ground. Due to this situation it was not possible to detect with the analysis performed on the 2018 dataset this excavation area. This issue is related with the fact that a reference dataset before the beginning of excavation is not available and the 2017 dataset was used as the reference time to compare the 2018 acquisitions. This type of analysis can definitely benefit from the existence of a model derived from an acquisition performed before the beginning of the excavation works.

In Area 2 it is interesting to notice that the discrepancies underlined in the northern and southern parts are derived from the relocation of the stone blocks from the north to the south parts to proceed with the excavation. However, at the actual state of the research, it is not possible to link the two discrepancies areas using this approach, and it was necessary to integrate the performed analyses with other available data and information to confirm this relation.

### **Mesh**

The second product that was analysed is the 3D continuous model derived from the photogrammetric approach. Several operations can be performed on a mesh and in this case

the use of this products was stressed in order to perform computations on the volume of different elements. In a first phase, these tools were used to compute the volume of elements related with the archaeological excavation. The main idea was to focus on the aspects: the volume of the area already excavated and the volume of the materials that need to be removed from the excavation area (ground and rubble). This analysis was performed both on the 2017 mesh and the 2018 mesh (Figure 87); two area were selected from the 2017 (Figure 88) and two for the 2018 (Figure 89).

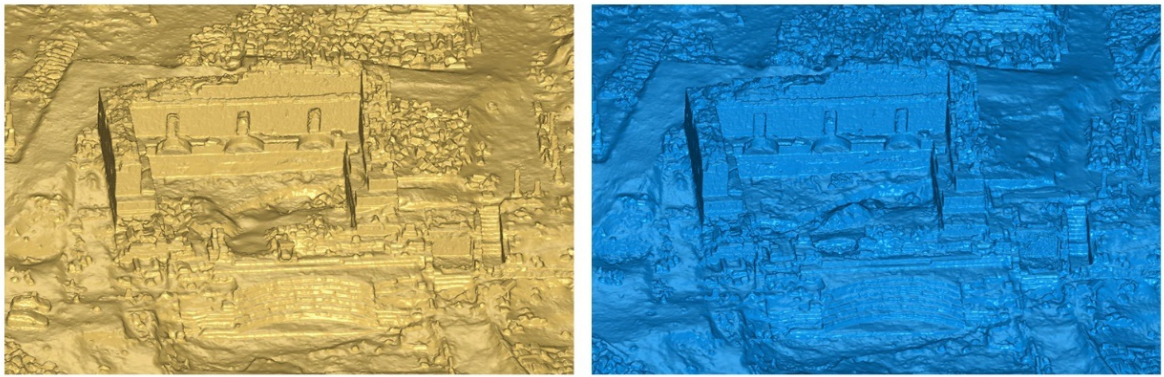


*Figure 87 Nymphaeum of Apollo, mesh derived from the photogrammetric approach. In yellow 2017 dataset and in blue 2018 dataset*

The analysis was performed using the 3D Reshaper software and following this steps: first the model was segmented extracting the limits of the area of interest, secondly the segmented portion of the model was closed interpolating a plane between the extracted limits of the single areas and creating a new part of the mesh (this step is mandatory to perform the volume computation) and finally the volume was computed through the tool implemented in the software.

The first area of the 2017 represent the excavation area that was not possible to map on the C2C analysis performed on the point cloud, while the second area is located south of the Nymphaeum and is composed by the blocks of stone removed in the 2018.

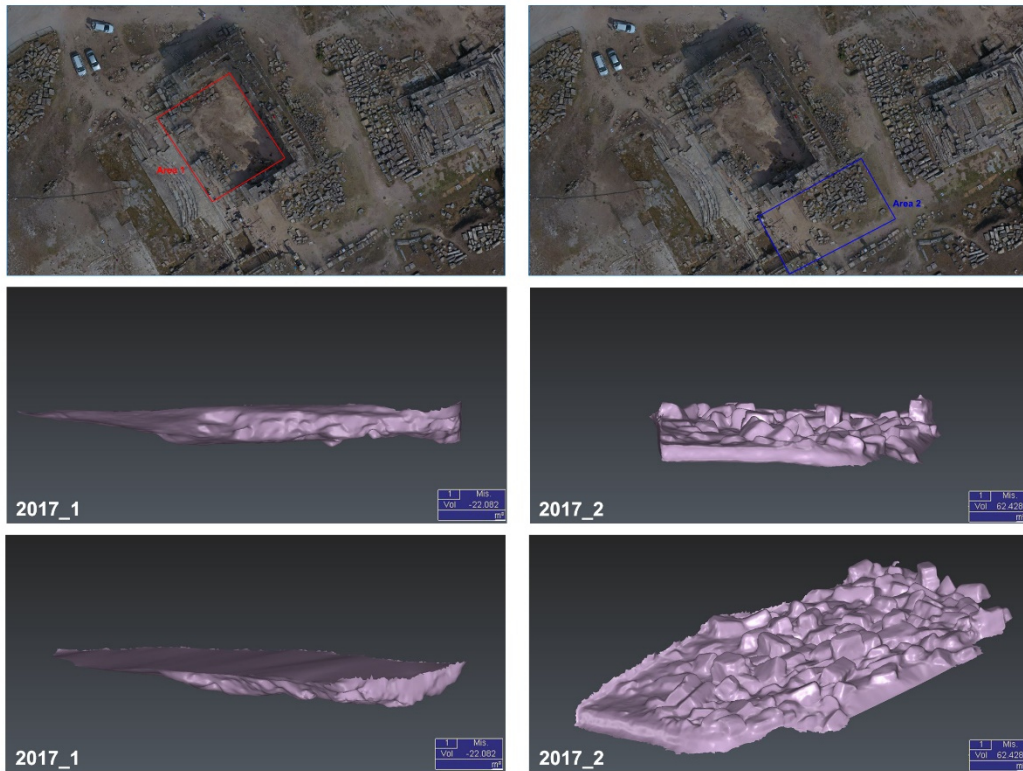


*Figure 88 Nymphaeum of Apollo, volume computation on two samples of 2017 dataset*

In the first area considered, 2017\_1, represent one of the areas excavated in 2017 and the computed volume is of  $\approx -22 \text{ m}^3$ . The second area, 2017\_2, is composed by stone blocks and ground and the volume is of  $\approx 62 \text{ m}^3$ .

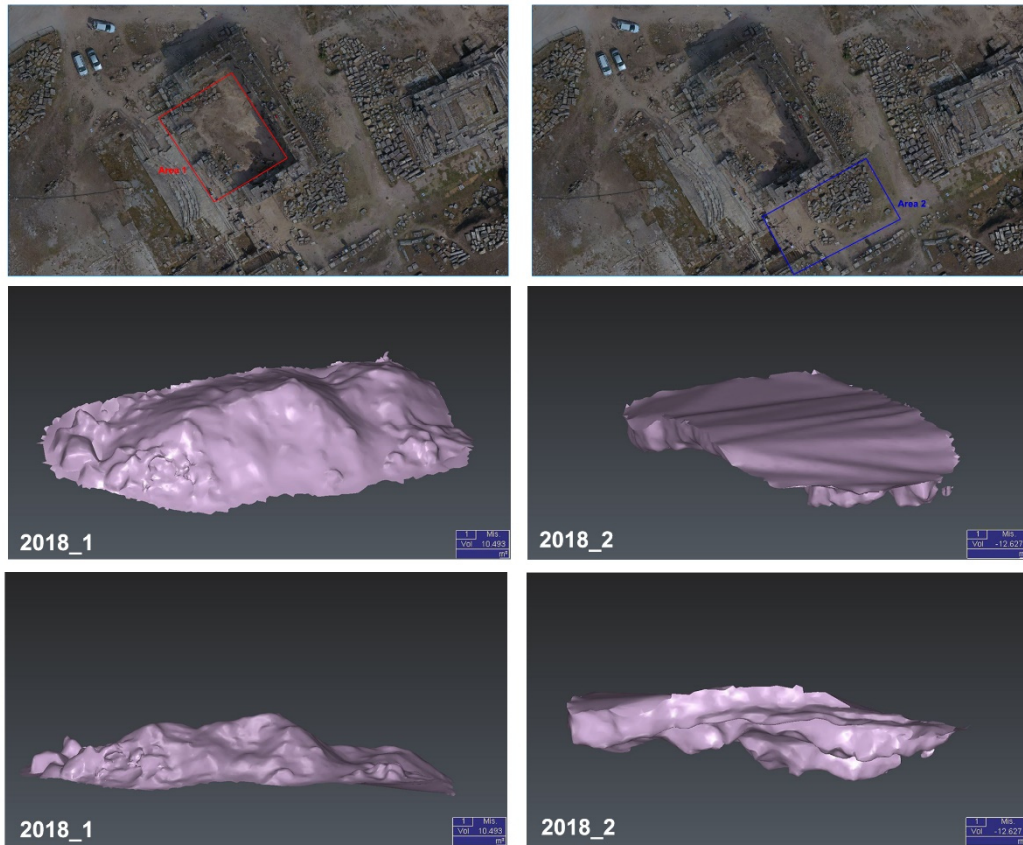


*Figure 89 Nymphaeum of Apollo, volume computation on two samples of 2018 dataset*

The first sample of 2018, 2018\_1, is composed by the mound of ground that need to be removed after the operations of excavation in the surrounding areas and has a volume of  $\approx 10 \text{ m}^3$ . The second sample, 2018\_2, is the excavation area on the northern part of the basin and has a volume of  $\approx -13 \text{ m}^3$ . These analyses can be quite useful for several aspects of the archaeological works, both during the field operations (if a rapid acquisition and processing of data is performed), both afterwards during the study of the evidences collected on the field. The volume of the mound of ground to remove can be used to plan the operations on the field, to decide when remove it and which means to use. These aspects can be really useful also for emergency excavation scenarios, where this kind of data need to be carefully considered and the operation on the field precisely organised. The volume computed for the excavated area can be used in the subsequent phases of archaeological research and study for the interpretation of the site. This approach can be used to compute the volume of specific features unveiled during the excavation and can be also adopted to perform more precise analyses from the archaeological point of view.

The same approach can be also developed to examine the architectural features of the considered structures. In the case of the Nymphaeum of Apollo this workflow was used to compute the volume of one of the niches present on three of the main walls as showed in Figure 90.

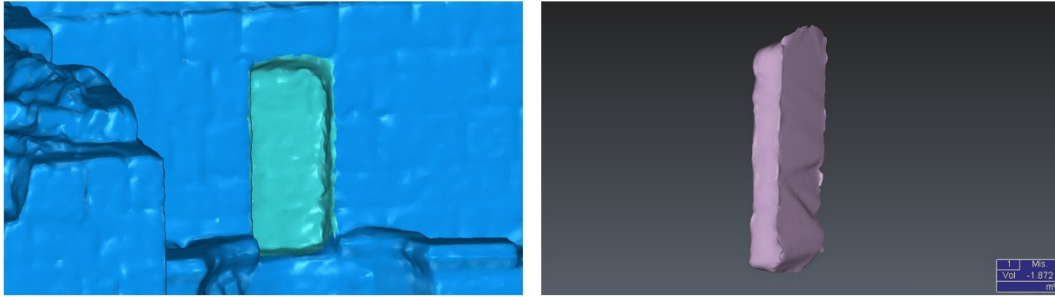


*Figure 90 Nymphaeum of Apollo, volume computation on a niche of 2018 dataset*

The integration of oblique images and thus the creation of a detailed 3D model, allows to generate a detailed 3D model also of the standing parts of the Nymphaeum. This approach was can also be stressed to directly represent on the 3D model the different building phases of the structure.

### **DSM**

Some analyses were also implemented in a GIS environment using the two DSM generated from the 2017 and 2018 datasets. The two DSM were processed using the raster calculator implemented in the opensource software QGIS and the 2017 DSM was subtracted to the 2018 DSM. The result is a new DSM, showed in Figure 91, underlining the discrepancies between the two datasets. This analysis allows to confirm the data that were already extracted from the test performed on the other datasets: the area of changes between the two years are visible also on the 2.5 representation and, through a false colour scale, it is possible to visualise also a dimension of this changing.

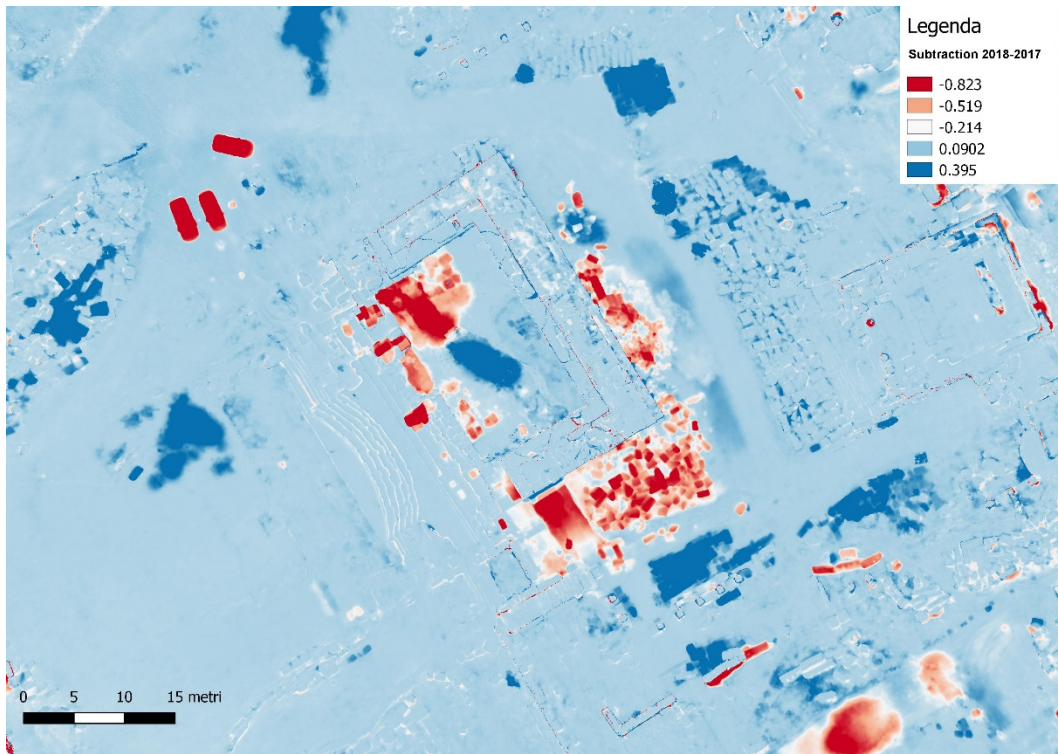


*Figure 91 Nymphaeum of Apollo, results of the analysis performed on the two DSM*

Other analyses were performed on the UAVs dataset of the 2018, acquired in the northern Necropolis. The DSM of this area of the Necropolis was used to automatically extract contour lines, that are reported on a shaded representation of the DSM of the area in Figure 92; the step between contour lines is 0,5 m.

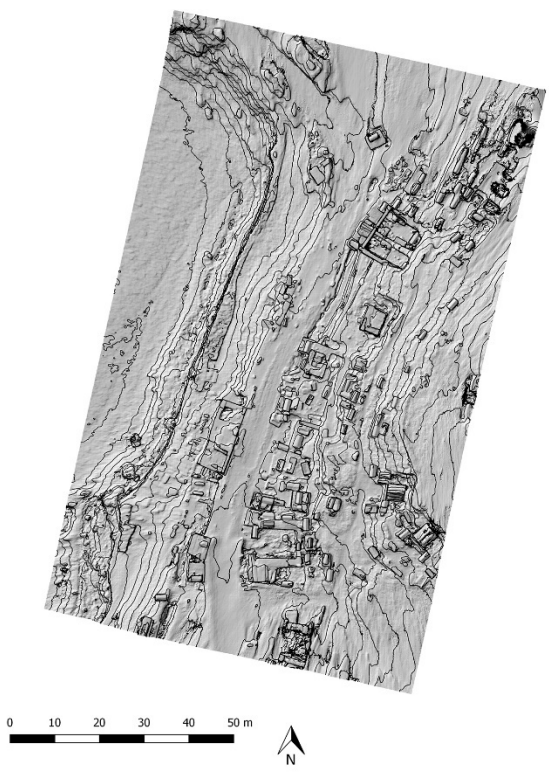
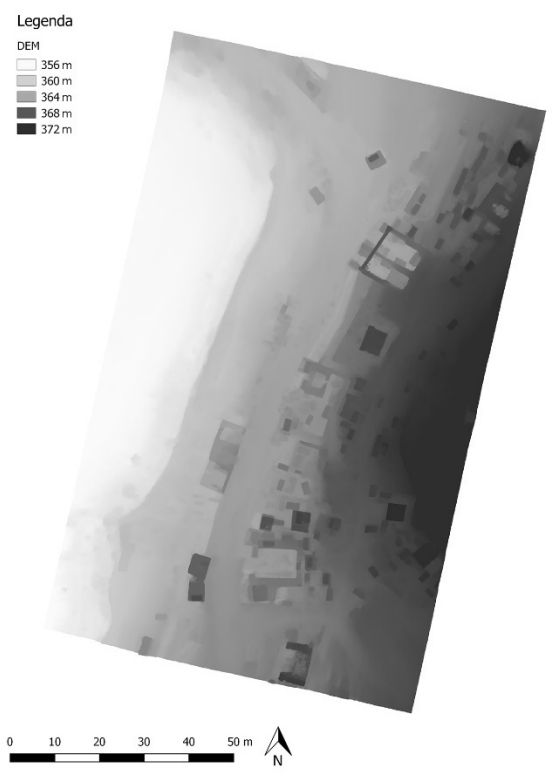


**Figure 92 Hierapolis, Northern Necropolis. DEM derived from UAVs 2018 dataset (left) and overlay of the automatically extracted contour lines on the shaded model (right)**

Moreover, through the raster processing tools implemented in Qgis, it was possible to perform a slope analysis on the DSM, the results of this analysis are reported in the following Figure 93.

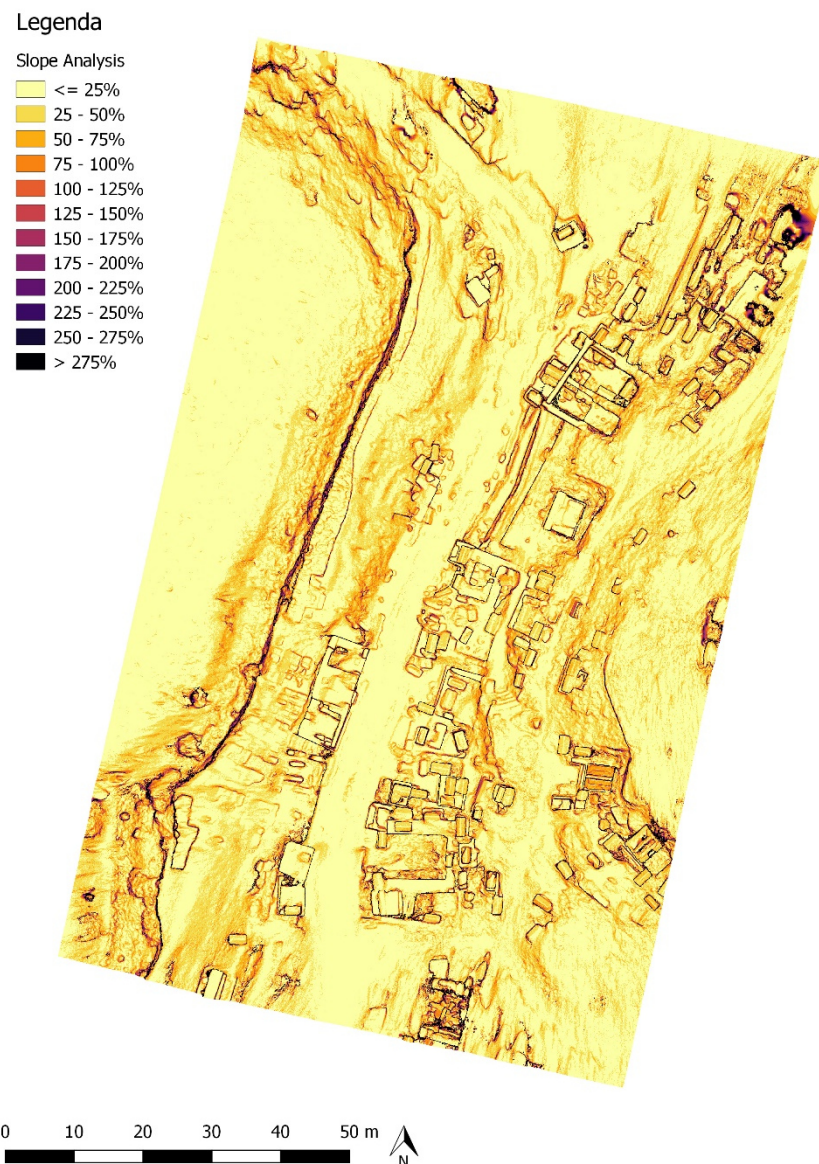


*Figure 93 Hierapolis, Northern Necropolis. Slope analysis of the area acquired in with the UAVs flights of the 2018*

Finally, thanks to the qProf plugin developed for Qgis<sup>24</sup>, height and slope profiles were automatically extracted from the selected area of the DSM, as shown in Figure 94; in this case the analysis was replicated also on the 2017 dataset. In order to evaluate the differences in the resolution achievable thanks to datasets with different intrinsic resolutions.

<sup>24</sup> <https://github.com/mauroalberti/qProf>

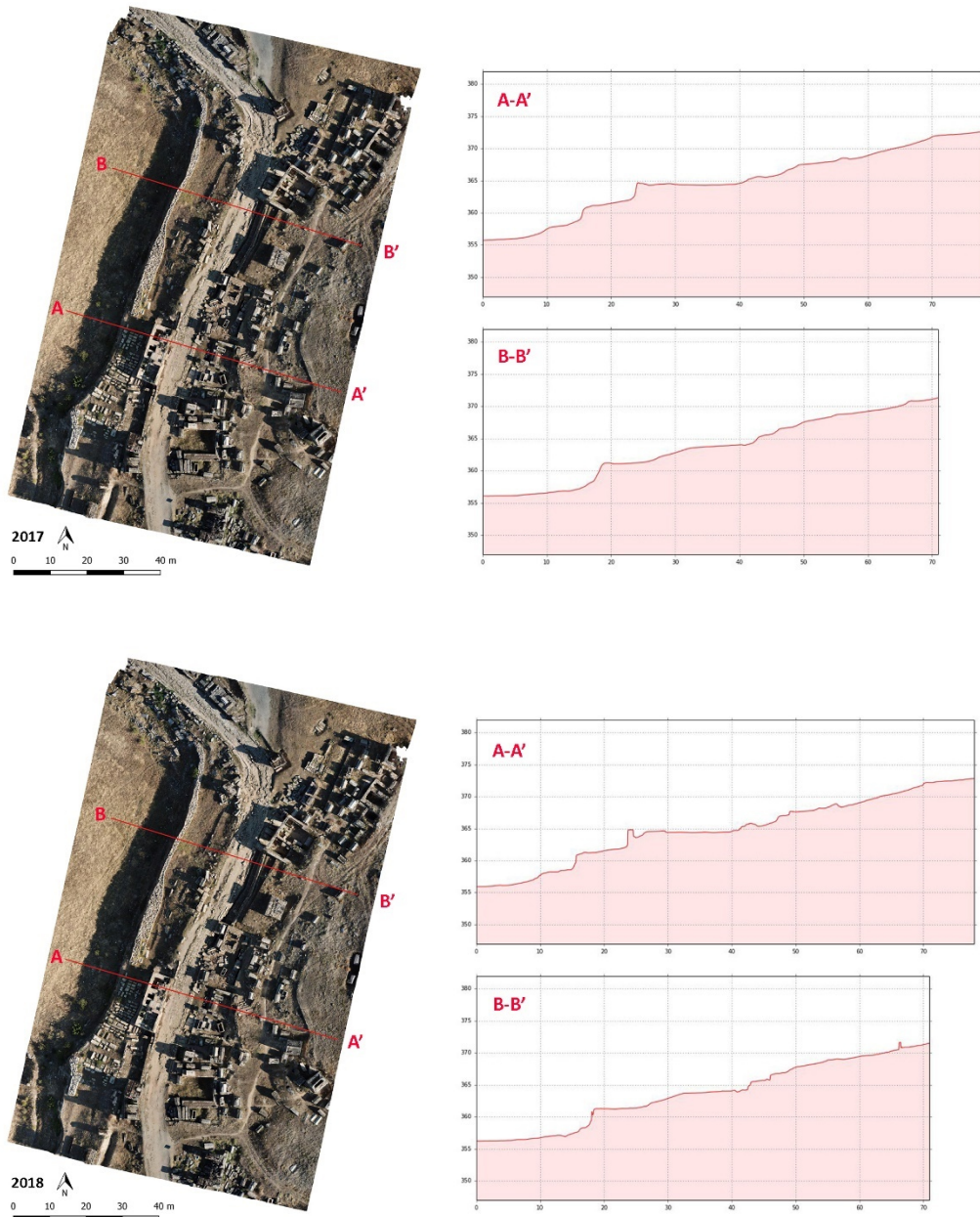


**Figure 94 Hierapolis, Northern Necropolis. Terrain profiles extracted in Qgis with the qProf plugin. Comparison between 2017 (top) and 2018 (down) datasets**

As is possible to notice in both the profiles extracted from the DSM, the different resolution achieved in the two flights is highly impacting also on the detail that can be extracted from the DSM. As already reported, lowering the flight altitude in the acquisition phase allows to obtain a more detailed geometric reconstruction of the surveyed scene and thus also the analysis that can be performed can reach a higher degree of detail. The 2017 dataset is able to guarantee a 1:200 scale of representation, while the 2018 a 1:50 scale.

## Ortophoto

Finally, also the orthophotos generated from the two datasets were produced and more in depth analysed. As is possible to see from Figure 95 the two products present a different radiometric content, due to the different time of the acquisitions in the two years. This issue is also evident from the different position of shadows in relation with the buildings and their overall impact on the scene.



*Figure 95 Nymphaeum of Apollo, general orthophoto of the area in 2017 and 2018*

Starting from this general ortophoto, two areas were more in depth analysed in the 2017 and 2018 dataset, as showed in Figure 96. These areas are the same of the analyses of detail already achieved on other products and through the orthophotos is possible to confirm what already partially underlined in the previous analyses. In the Area 1 of the Nymphaeum, Figure 96 top, is possible to notice the new excavation areas that were opened between 2017 and 2018, the blocks of stone that were removed and the mound of ground created in the centre of the basin. In Area 2, Figure 96 down, is possible to see the advancements of the excavation. The stone blocks present in 2017 were moved on the southern part of the area and on the west part is possible to see the new archaeological features unveiled by the excavation.



*Figure 96 Nymphaeum of Apollo, details of the produced orthophotos on two specific areas*

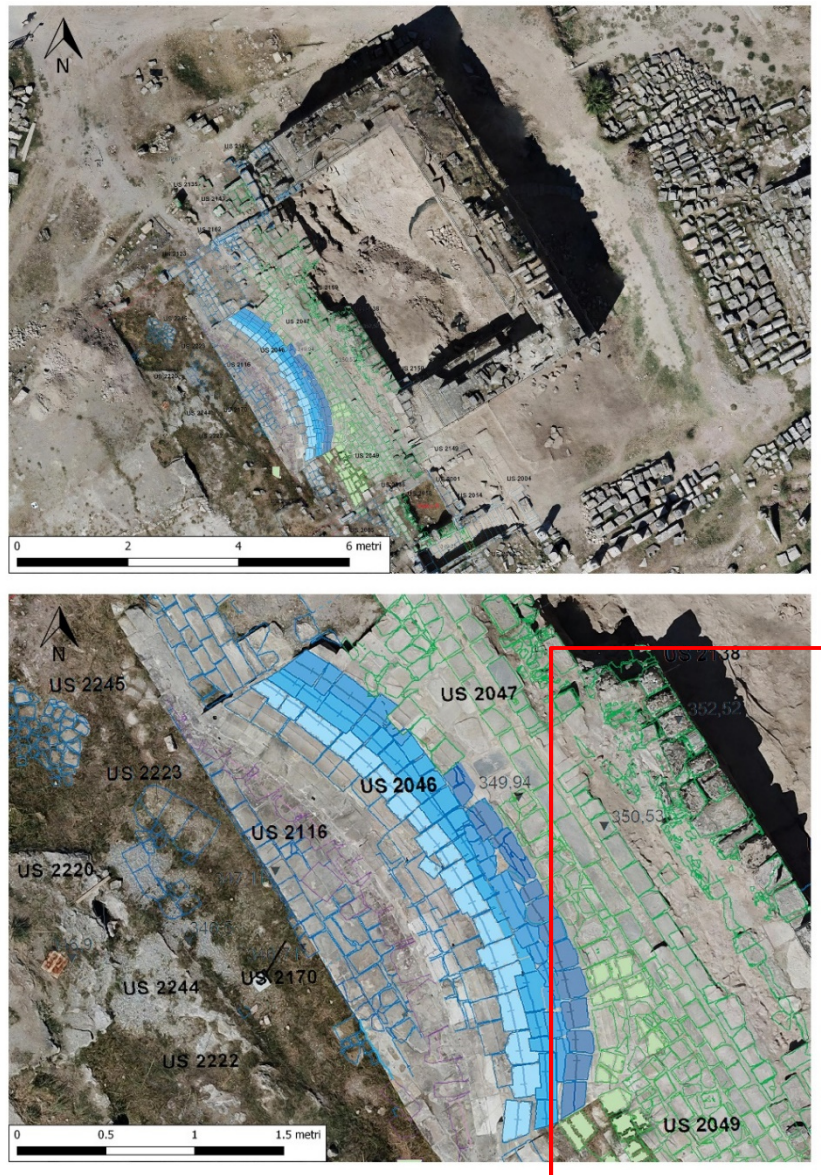


*Figure 97 Nymphaeum of Apollo, integration of data derived from the archaeological documentation of the past years and the orthophoto produced with the 2018 UAVs data*

Furthermore, these products can enhance also the update of the documentation of the archaeological excavations. An example is reported in Figure 97, where the data derived from the archaeological excavation conducted between the years 2007-2011 were integrated in the orthophoto produced from the 2018 data. This approach can lead to really interesting results that can help the team of archaeologists in the phases of interpretation during and after the excavation. In the area presented it is interesting to focus on the portion highlighted in red, that was excavated in the last two years of field campaigns. The overlay of the data derived from the previous archaeological survey can be integrated on the more recent orthophoto, allowing an easier process of interpretation of the data. This kind of products, as well as the other derived from the photogrammetric approach, can become a new standard in the archaeological documentation procedures. If the wide spreading use of

UAVs will be guided from a mature methodological reflexion, both in the geomatics and archaeological community, it will be possible to set up standardise procedures and guidelines and these powerful instruments will become a common practice in the documentation of archaeological heritage. This is already happening, however the exploitation of the possibilities connected with these platforms and with the “real-time” deployment in the archaeological documentation process still need to be pushed to their maturity.

What is important to consider in these cases, is the planning of the flight’s main characteristics, due to the fact that they can highly impact the resolution of the overall photogrammetric approach. As previously reported, the 2017 and 2018 flights in the Northern Necropolis of Hierapolis were performed adopting different approaches, this choice is also leading to different resolution of the delivered photogrammetric products. The 2017 flights were performed adopting automatic flight planning solutions at an altitude of 40-50 meters (Table 12) while the 2018 flights were performed manually at an altitude of 15-25 meter (Table 14) in a smaller area of the necropolis, where a bigger detail of the products was needed. These different flights configurations led to the generation of products at a different resolution, as reported in Table 13 and Table 15. Concerning the two ortophotos derived from these datasets it is interesting to notice how the 2018 acquisitions can provide a GSD that is around 4 time lower than the 2017 dataset, allowing more detailed analyses of the area of interests, till a scale comprehend between 1:50 and 1:100. An example of this feature is reported in the following Figure 98, where two extracts of the same area of the Necropolis are compared in the two orthophotos.



*Figure 98 Hierapolis, Northern Necropolis. Comparison between the ortophotos derived from the 2017 (high flight altitude) and 2018 (low flight altitude) datasets*

## 4.2 Terrestrial Sensors and techniques. Calibration and analyses on two spherical systems

### 4.2.1 Camera Calibration

As already stated, camera calibration has always been a central point in the photogrammetric process and has become more important after the diffusion of consumer grade non-metric cameras, in order to obtain a mathematical parameterization of these departures from collinearity. Especially, because it is quite uncommon and rare for the users to obtain such parameters from the producers of these kinds of cameras. Extract reliable and precise metric information is a nodal point in the photogrammetric workflow and through a brief survey of the recent (and non-recent) research products concerning this topic (Abraham & Hau, 1997; D. Brown, 1971; Clarke & Fryer, 1998; Fraser, 2013; Fraser & Remondino, 2006; Luhmann, Fraser, & Maas, 2016; Salvi, Armanguè, & Batlle, 2002; Zhang, 2000) it is possible to underline the centrality of the problem for both CV and photogrammetry experts.

A camera can be considered calibrated when: “*principal distance (focal length), principal point offset and lens distortion parameters are known*” (Fraser & Remondino, 2006), as reported in section 3.2 these parameters are fundamental to solve the collinearity equations. In the photogrammetric community two main approaches are used for camera calibration, adopting two different camera models:

- A **perspective projection** model derived from collinearity equations and that includes the modelling of all the departures from collinearity. At least five points correspondences are needed in a multi-image network. Parameters are approximated within a least-squares bundle adjustment.
- A **projective** model characterized by the Essential and the Fundamental matrix that can accommodate variable and unknown focal length but needs six-eight points correspondences.

The work already cited (Fraser & Remondino, 2006) defines also other criteria to classify camera calibration approaches:

- *Implicit versus explicit models*: Implicit calibration is the process of calibration of a camera without explicitly computing its physical parameters, while explicit

calibration consists in the process of computing the physical parameters of the camera (Guo-Qing Wei & Song De Ma, 1994).

- *Methods using 3D rather than planar point arrays:* Methods used both in CV and photogrammetry. One of the most famous examples can be found in (Zhang, 2000).
- *Point-based versus line-based methods:* Point based methods are the more used in photogrammetry with the exception of plumbline calibration, that is a line-based method.

More specifically, another classification can be made according to the technique employed for the parameters' estimation and optimization:

- *Linear techniques:* simple and fast. Can't handle lens distortion and need a control point array of known coordinates. Usually simplify the camera model and lead to low-accuracy solution. The DLT (Direct Linear Transformation), described in (Abdel-Aziz, Karara, & Hauck, 2015) is part of this techniques.
- *Non-linear techniques:* accurate modelling of the camera I.O. and lens distortion using an iterative least-squares estimation process. The extended collinearity equation model (that is the base of the self-calibration process) is part of these techniques (D. Brown, 1971).
- *Linear and non-linear techniques combined together:* two stage approach where linear techniques are used to estimate an initial value of the parameters and a non-linear approach is used to iteratively refine it (Heikkila & Silven, 1997).

Using different model for camera calibration will results in slightly different defined coefficients for the definition of the camera system, in general term the following coefficients are used in the literature:

- $f$  to define the focal length (in pixels or millimetres)
- $c_x$  and  $c_y$  to define the principal point offset (its definition depends on the convention used to define the origin of the sensor's system)
- $K_1, K_2, K_3, K_4$  are the coefficients used to model the radial distortion
- $P_1, P_2, P_3, P_4$  are the coefficients used to model the decentring or tangential distortion
- $B_1, B_2$  are the skew coefficients

## 4.2.2 Camera Calibration approaches

Several methodologies and approaches have been defined over the years to perform the calibration of cameras and retrieve the I.O. parameters of the optical system. It can be useful to recall an article of Roger Tsai (Tsai, 1987) in which the author has defined five general criteria to be respected in the process of camera calibration, it should be:

1. *Autonomous*: should not require the operator intervention.
2. *Accurate*: should meet the accuracy requirements of the applications. Theoretical modelling of the camera should be accurate.
3. *Reasonably Efficient*: should be quite rapid and optimized.
4. *Versatile*: should be feasible for multiple applications and with different levels of accuracy.
5. *Need only common Off The Shelf cameras and lenses*: should be implemented also for Commercial Off The Shelf (COTS) sensors, that are versatile, low-cost and user-friendly.

These five assumptions were made at the beginning of the development of the self-calibration techniques (that will be described in the following sections) and were part of the debate around this new technique, that opened the way for the new world of SfM. This text is also of particular interest because it highlights some of the points that would have been developed in the following years. There is a first address to automatization of the photogrammetric process, the introduction of a scale factor related with the required accuracy depending of the application and finally a strong overlook to the possibilities offered by the development of new digital COTS cameras.

Nevertheless, a large number of authors have investigated the issue of camera calibration and a wide literature is available both from photogrammetry and CV communities (Brito, Angst, Köser, & Pollefeys, 2013; D. Brown, 1966, 1971; Clarke & Fryer, 1998; Fraser, 1997, 2001, 2013; Fraser & Remondino, 2006; J. G. Fryer & Brown, 1986; Gruen & Beyer, 2001; Kenefick, Gyer, & Harp, 1972; Luhmann et al., 2016; Nowakowski, 2018; Salvi et al., 2002; Zhang, 2000).

Thus, the process of calibration can be performed following different procedures and adopting different approaches, in this research the definition provided by Luhmann (Luhmann et al., 2006) will be adopted. According to this author, three main methods can be distinguished, characterized by the object used as reference and by the time and location of the procedure:

**Laboratory calibration:** requires a high effort and adequate laboratory equipment to be performed. In this case one or more characteristics of the camera are analysed in carefully controlled conditions; optical techniques such as collimators are used. This approach is generally used only for metric and semi-metric cameras and cannot be performed by the user.

**Calibration with a known test field:** in this case the I.O. parameters are determined through the relation that exists between the points of the test field and the images acquired of the field itself. Usually test fields are composed by a set of points (with known coordinates or distances), arranged in a grid or set of lines. If the test field is known a small set of images is usually needed to determine the intrinsic parameters, however, some shrewdness needs to be followed during the acquisition phase: good ray intersections must be ensured, and the test field needs to fill the image format as much as possible. Acquisition should be performed shooting both perpendicular and oblique images of the test field and a relative rotation of  $90^\circ$  (roll angles) around the optical axis of the camera is recommended. A scheme of the geometry of the acquisition and an example of acquired images is reported in Figure 99 – left. In general terms, the size and design of the test field should be representative of the volume of the object that needs to be further measured, and this can represent an issue in the case of medium and large projects of acquisition.

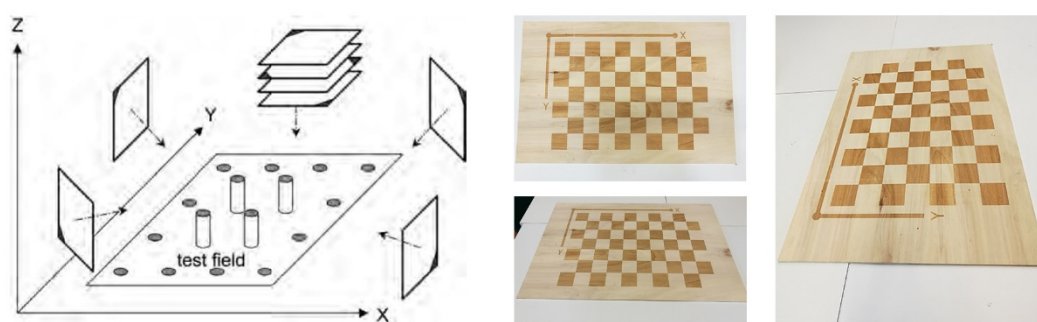


*Figure 99 Geometry of image acquisition of the test field on the left (Luhmann et al., 2006). On the right example of some images of the checkboard panel*

**Self-calibration:** in this case the test field for the calibration is constituted by the object that needs to be measured and estimation of I.O. parameters can be performed simultaneously with the measurements of the object itself. The parameters are determined using a large set of images and adopting a self-calibration bundle adjustment; in contrast with the previous method, the 3D coordinates of the test field need not to be known. The use of reference points, such as a codified target, allows to define also the global coordinate system of the object, and thus to perform simultaneously I.O. and E.O. of the scene acquired. Also in a self-calibration scenario the geometry of acquisition of the images is a crucial point, beside the shrewdness already reported for the previous approach, some other

attentions need to be followed (a brief overview of the best practices for image acquisition will be described in section 3.3.1). Self-calibration is generally more adaptable and rigorous if compared with test-range calibration, however it requires higher computational resources. Self-calibration is more reliable if object points presents a good three-dimensional distribution. Thus, this approach can present some issues:

- Correlation between the parameters. The intrinsic parameters can be mutual influenced by their correlation, this issue is usually neglectable but need to be considered and evaluated in case of weak camera geometry during the acquisitions.
- Absence of images relative roll angles. If the test field doesn't provide a good distribution of reference points, or a sufficient number of convergent images is acquired, images with relative roll angles are necessary. This kind of images are especially important to determinate the principal point coordinates, if the previously cited conditions are not respected.
- Incomplete use of image format. To determinate distortion parameters valid across the whole image dimension is necessary to use all the image format during the acquisition phase.
- Use of high distortion lenses. The use of these lenses causes high distortion in the image corners and distortion models can result in low accuracy estimation of I.O. parameters, especially if others issues between the ones described are present.
- Camera stability. The camera stability, especially in case of consumer grade cameras, is not constant over time. For this reason, also the calibration of the camera can be considered valid only for a certain period of time.
- Depth variation. Enough depth variation of the scene must be guaranteed in order to correctly estimate the focal length of the camera.

A further definition of the process of calibration can be provided based on the time when the calibration is performed:

- **Pre-calibration:** if the calibration is performed before the survey phases is possible to define it as a pre-calibration. The intrinsic parameters are estimated prior to the acquisition phase and are considered stable for a determined amount of time, time in which the survey of the object is performed.
- **In situ (on the job) - calibration:** if the calibration is performed simultaneously with the acquisition phase of the survey is possible to define it as *in situ* or *on the job* calibration.

Both these two processes can be performed following both the 3D test field and the self-calibration approach, however, while it is quite common to use both the approaches for a pre-calibration stage, it is more usual to perform the *in situ* calibration through a self-calibration approach.

### **4.2.3 Camera calibration approaches adopted in this research**

In this research, aside for the laboratory calibration, the other two main approaches for camera calibration were tested and evaluated. Some preliminary analyses on this topic were presented in an article published in The International Archives of the Photogrammetry, Remote Sensing and Spatial Information Sciences (Calantropio et al., 2017) and will be extended in the following sections. The calibration with a test field was performed using an Matlab tool, Camera Calibrator<sup>25</sup>, while for the self-calibration approach different software solutions (both commercial and open source – more details in section 3.9) were tested.

### **4.2.4 Calibration with a known 2D test field**

Among the different solutions available to perform the calibration with a known 3D test field (Fraser & Remondino, 2006), the Single Camera Calibrator app of Matlab was used. This tool was developed inside the CV community (Heikkila & Silven, 1997; Zhang, 2000) and is intended as a rapid instrument to automatically retrieve intrinsic, extrinsic and lens distortion parameters. A specific calibration pattern (Figure 100) is imaged from 10 to 20 camera stations and the data are then processed inside the Matlab tool. In this case the pattern was replicated on a wooden table using a Computer Numerical Control (CNC) laser-cutting machine, this choice was accomplished in order to have a clean and plane surface presenting a high precision of the geometric features and to avoid deformation of the test field.

This tool, despite being almost automatic and really fast can be successfully used for a preliminary estimation of lens distortion parameters for photogrammetric purposes. However, it is fundamental to adopt some cautions during the acquisition phase in order to achieve appreciable results (as already reported in section 3.2.1): the pattern should be imaged in every portion of the sensor, focus and zoom should be maintained fixed and distance and orientation between pattern and sensors must change. The calibration requires a minimum of three images (a number between 10 and 20 is suggested) but is a good

---

<sup>25</sup> <https://www.mathworks.com/help/vision/ref/cameracalibrator-app.html>

practice to acquire around 30 images. This is useful especially because the tool allows to exclude part of the images based on the reprojection errors estimated during the process. The software allows also to plot the locations of the calibration pattern in the camera's coordinate system, or vice-versa the locations of the camera in the pattern's coordinate system. Each parameter of the calibration is thus plotted with its relative uncertainty, expressed as the standard error  $\sigma$  for each estimated camera parameters.



**Figure 100** *The wooden checkboard panel used for the calibration procedure. On the left the CNC machine during the cutting phase*

Another tool similar to Camera Calibrator, Agisoft Lens, were also used to perform a preliminary calibration of some of the cameras used in this research, as will be better reported in section 4.2.7. This software solution for camera calibration is developed by Agisoft and is generally provided together with the Photoscan photogrammetric suite. Similarly to the Matlab tool, Lens use a known 2D test field for the estimation of the I.O. parameters of the selected camera. Generally, the software projects the pattern on the computer screen in order to allow the user to record it with the camera. This approach is thus limited from two main factors: the dimensions of the screen and its reflectivity; these two issues can generate some problems in the phase of images acquisition. To overcome this problem, it was decided to adopt a slightly different solution and to create and print an ad hoc 2D test field. This test field was composed of a chessboard pattern (with alternate black and white squares of 5 cm side) that was printed on a 1189 x 841 mm paper support. The pattern was then acquired following the same procedure already described for the Matlab calibration tool. Lens is able to estimate the following I.O. parameters: focal length ( $f_x$ ,  $f_y$ ), principal point coordinates ( $c_x$ ,  $c_y$ ), radial and decentring distortion coefficients, using Brown's distortion model ( $K1$ ,  $K2$ ,  $K3$ ,  $P1$ ,  $P2$ ,  $P3$ ,  $P4$ ) and the skew coefficients ( $B1$ ,  $B2$ ).

## 4.2.5 Self-Calibration

A different approach was adopted to perform the self-calibration. A specific 3D calibration test field was projected and created by the Laboratory of Geomatics for CH of the Politecnico of Turin, at the Galileo Ferraris building in Turin, Italy. The calibration field was created specifically to respond to some requirements for the calibration of multi-camera systems (section 3.6.1), however it can be used also for other sensors calibration. The calibration field needed to respect some conditions:

- Present marked three-dimensional features and volumes
- Need to have marked texture materials and features
- Good illumination conditions
- Simulate both indoor and outdoor conditions
- Allow short to medium distances of acquisition

Before projecting and creating the test field used for this research several tests were performed to identify the main characteristics that it need to respects and set up the methodological framework to follow. Different test performed in the indoor environments of the building underlined several factors that need to be carefully considered when projecting this kind of test. The illumination of the environment is a first issue that need to be considered, followed by the reflectivity of the material that will be recorded from the camera. These two issues can highly impact the performances of the photogrammetric approach during I.O. and E.O. phases and thus highly affect the overall results of the calibration through this approach. Moreover, the maximum acquisition distance achievable in the chosen environment was another key-factor that was considered, due to the fact that one of the main aims of the research was to stress the operational range of the tested sensors. Some of the issues encountered during the definition of the test field are reported in the following Figure 101.



*Figure 101 Examples of non-suitable environments for the creation of a calibration field. In the left and central images, it's not possible to complete a correct photogrammetric process due to the lack of features in the scene. In the right image the coating of the walls is too reflective. In all the three cases the overall illumination of the scene was not good enough*

After the above mentioned attempts the calibration field was created using a portion of an external concrete stairs, built near the façade of the building. In this environment 14 plastic coated codified targets were homogenously distributed. The choice of this solution allowed to obtain a hybrid 3D calibration test field that can satisfy both the requirements to simulate indoor and outdoor environment, presents a good diffused illumination and a good surface texture of the wall that enhance the feature recognition phase of the photogrammetric process and allow to freely select the desired acquisition distance.



*Figure 102 The calibration field and a detail of some of the target distributed on its surface*

The targets were measured using a traditional topographic approach: two points forward intersection to obtain with a good accuracy the coordinates of the points. A Leica Viva TS16 Total Station was used: accuracy of 1" (0.3 mgon) on angular measurement and distance accuracy on prism of 1mm+1.5 parts per million. To obtain the best accuracy and precision as possible in the measurement of the distance a circular mini-prism were used during the topographic survey of the targets. The data collected on the field were then adjusted using MicroSurvey STAR\*NET software where the planimetric and altimetric components of the forward intersection were separately considered. According to the acquisition geometry, distances and adopted strategy the residual on the 14 targets for both the components planimetric and altimetric is less than 2 mm.

The final 3D coordinates were then used in the photogrammetric approach both as GCPs (Ground Control Points) and CPs (Check Points) to precisely estimate and control the camera interior parameters and to scale and georeference the generated models. The calibration field was also recorded through Terrestrial Laser Scanner (TLS), in order to have a 3D models acquired with a more consolidated sensor, in order to use it as ground truth for further analyses on the 3D models.

## 4.2.6 Multicamera systems: Freedom 360

The considered system, the Freedom 360<sup>26</sup> *classic mount*, is a multi-camera mount produced and marketed by Freedom 360, an American company located in Long Island City (New York). The company began projecting 360 systems in the late 2012 and since the beginning was devoted to the conversion of already commercialised action cameras, instead of using *ad hoc* customizable products. More specifically, the *classic mount* (Figure 103) is intended for a combined use with six GoPro action cameras (Hero 3 or Hero 4).

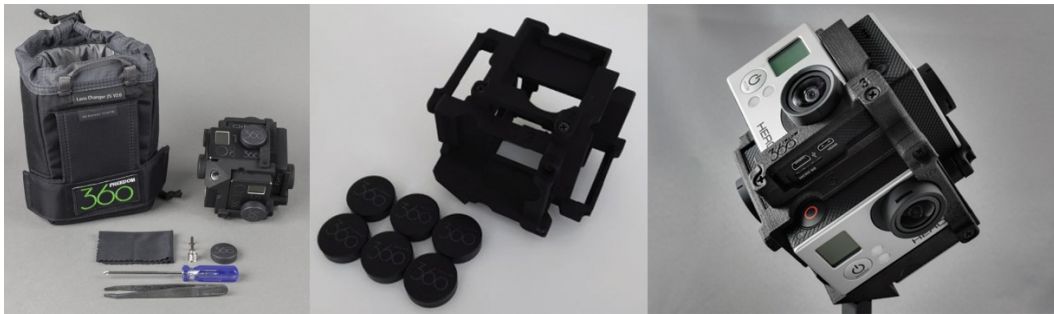


*Figure 103 The classic mount by Freedom 360. The complete kit (left), the 3D printed rig (centre) and the complete system with the six GoPro*

It is composed by a 3D printed mount design to hold the six action cameras coupled in opposite positions to record full spherical immersive videos or images. The main attractive features of the *classic mount*, and of other similar products, can be traced in: the relative low cost compared with other similar systems, its portability, the possibility of controlling individually and independently the six cameras and consequently to have the chance to manage and process the data recorded from the six cameras both separately or together. The drawbacks in the use of this system are: the acquisition and processing of the data collected by this system is less controlled, compared to other more expensive solutions, and is not always easy to reach good results during the creation of 360 contents. Moreover, the overall quality is directly influenced by the characteristics of the single camera. Due to the reasons reported above one of the main aims of the research was to assess and verify the consistency of the six action cameras, and consequently of the system itself, before performing some tests in the contest of the documentation of a real Built Heritage environment.

The main characteristics of the system are reported in the following Table 25:

---

<sup>26</sup> <https://freedom360.us/>

| Classic mount main specifications |                            |
|-----------------------------------|----------------------------|
| Weight with cameras               | 525 gr                     |
| Weight without cameras            | 85 gr                      |
| Size                              | 10x10x10 cm (lens to lens) |
| Price                             | \$ 425                     |

*Table 25 Main specifications of the classic mount by Freedom 360*

Nevertheless, the available output of the system is determined by the camera's model mounted on the rig. In the present research the *classic mount* was equipped with six Hero 4 silver edition by GoPro (Figure 104), which main characteristics are reported in the following Table 26:

| GoPro Hero 4 main specifications |                               |
|----------------------------------|-------------------------------|
| Weight                           | 84 gr                         |
| Size                             | 54x41x30 mm                   |
| Sensor                           | CMOS – 12 MP                  |
| Sensor size                      | 1/2.3"                        |
| Focal length                     | 2.92 mm                       |
| Video resolution                 | Up to 4K (up to 30 fps in 4K) |
| Image resolution                 | Max 4000x3000                 |
| Price                            | \$300-400                     |

*Table 26 Main specifications of GoPro Hero 4 silver*



*Figure 104 The basic Hero 4 kit (left) and the front/back of the action cam (right)*

This system was deeply tested in the past years in order to exploit all the possible issues related to its use both for photogrammetric and entertainment purposes. A preliminary report of the analyses conducted can be found in (Teppati Losè, Chiabrando, & Spanò, 2018) and the research will be extended in the present work.

The technical issues that involves this system are related with two different research topics: on the one hand the problems related with the use of action cameras for photogrammetric purposes need to be considered and on the other hand, all the researches connected to the world of spherical cameras need to be exploited. Action cameras have been a topic of interest in the geomatics community in the last years (Balletti et al., 2014; Barazzetti, Previtali, & Roncoroni, 2017b; Markiewicz, Lapiński, Bienkowski, & Kaliszewska, 2017; Perfetti, Polari, & Fassi, 2017; Schneider et al., 2009; Strecha & Glassey, 2015) and the issues considered are different: influence of shorth focal length, modelling of fisheye lens distortion, etc. In this case, all these research topics need to be combined with the problems related with spherical cameras (Holdener, Nebiker, & Blaser, 2017; Kossieris, Kourouniotti, Agrafiotis, & Georgopoulos, 2017; Perfetti, Polari, & Fassi, 2018; Teo, Shih, Yu, & Tsai, 2016). It is well known among the community of researchers that in general terms low cost commercial cameras are less stable in terms of I.O. parameters stability over time (Akkaynak et al., 2014; Balletti et al., 2014; Chandler, Fryer, & Jack, 2005; Habib & Morgan, 2003; Läbe & Förstner, 2004) and thus they need to be carefully investigated and analysed in order to use these devices in a photogrammetric approach. The retrieval and the control over the cameras interior parameters can be useful for the generation of spherical products and as reported in section 3.2.1 they are crucial in the photogrammetric process. To cope with these issues for the Freedom 360 a self-calibration approach was chosen, and the 3D test field described in section 4.2.2 was used. The first step, preliminary to the acquisition phase contemplate the assignment of a univocal identification letter to the six cameras in order to maintain the control over the parameters of each camera. Two main acquisition strategies were then followed:

- Each one of the six cameras was detached from the 360 rig and inserted in an ad-hoc support that was previously 3D printed (Figure 105 - left). The single cameras were then mounted on a photographic tripod for image acquisition. With this configuration, a dense set of images was acquired (Figure 105 - right) for each camera (with different camera orientation and relative position). An average number of 150 images were obtained for each of the six cameras.

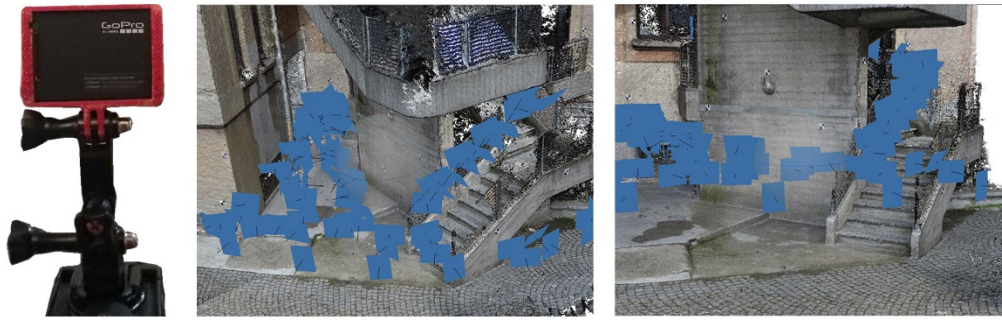


*Figure 105 The 3D printed support design to hold the Hero 4 (left) and the network of the acquired images of the 3D calibration field (right)*

- All the six cameras attached onto the Freedom 360 rig (Figure 106 - left) and used in the time-controlled modality for the shoot. The system was then moved in different preselected positions to acquire the whole calibration field (Figure 106 - right). The images were then manually selected and only the images acquired in the desired positions were considered. A total of 258 images were acquired with the 360 configuration, corresponding to 43 preselected position of the rig.

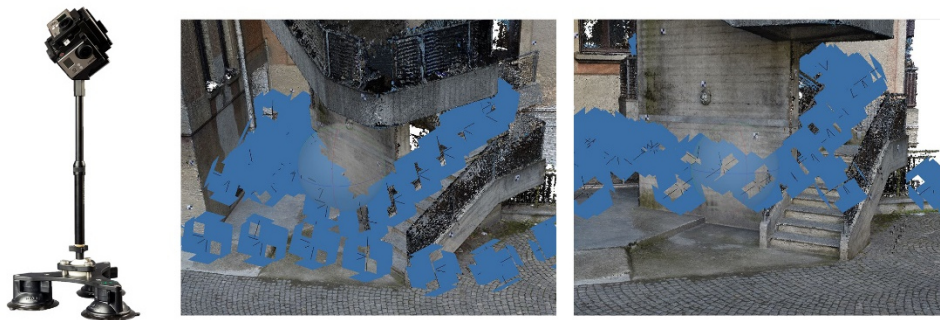


*Figure 106 The 6 cameras on the Freedom 360 rig (left) and the network of the acquired images of the 3D calibration field (right)*

For the processing of these data the well-known commercial software solution for SfM Agisoft Photoscan was used (an overview of the photogrammetric software solutions used in this research can be found in section 3.9). The two set of acquisitions were processed in eight different projects:

- Six projects were dedicated to the individual action cameras mounted on the photographic tripod.
- One project for the images acquired with the 360 rig, using the native Exif metadata embedded in the cameras.
- One last project, again for the images acquired with the 360 rig, but applying a modification on the Exif metadata, in order to have the software recognizing the six cameras as different.

The eight projects were then processed, and some analyses were achieved. A first analysis was performed on the GCPs (Ground Control Points) and CPs (Control Points): in each project 8 of the measured targets were used as GCPs while 6 were used as CPs, Figure 107 reports the RMSe (Root Mean Square error) of these points.

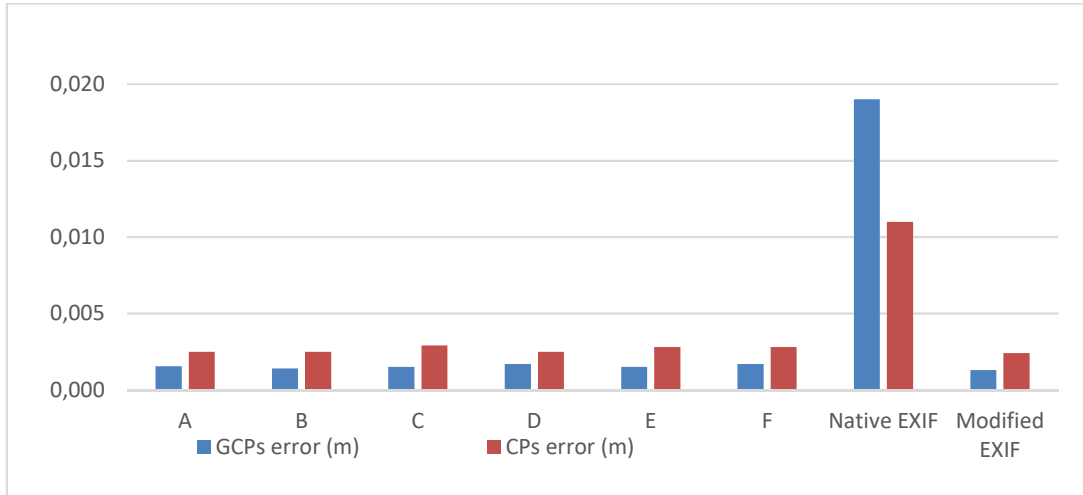


*Figure 107 RMSe on GCPs and CPs in the eight different photogrammetric projects*

These values indicate an almost identical situation for the six individual projects, a lower value for the processing of the rig acquisition with the modified Exif, while it is worth notice that with the native Exif a big growth of the RMSe value is present, both for GCPs and CPs. All the projects were processed using the same parameters for I.O. and E.O. estimation, tie point extraction and BBA: the value of the accuracy of alignment was set as high in order to estimate at least three coefficients for the radial distortion and two for the tangential, plus the focal length, the principal point coordinates and the skew transformation coefficients. Key/tie points limit was set at 0 in order to extract as many points as possible. As already reported, the six action cameras of the 360 system were marked with letters (A, B, C, D, E, F) to provide a unique identification between each camera and its position on the rig. After achieving the I.O. parameters estimation for each camera, the data were collected and organize in order to be compared and analysed. The parameters estimated for the six cameras are reported in the following Table 27: focal length in pixels and millimetres (f), principal point coordinates in pixels (cx and cy), radial distortion coefficients in millimetres (k1, k2, k3), skew coefficients in pixels (b1 and b2) and tangential distortion coefficients in millimetres (p1 and p2) are reported.

| Estimated interior orientation parameters of the six cameras separately considered and processed |            |            |            |             |            |            |
|--|------------|------------|------------|-------------|------------|------------|
|  | A          | B          | C          | D           | E          | F          |
| f(focal length -mm)  | 3,049      | 3,042      | 3,040      | 3,040       | 3,044      | 3,035      |
| f(focal length -px)  | 1761,739   | 1757,888   | 1756,620   | 1756,499    | 1758,889   | 1753,511   |
| cx (px)  | -59,928    | -76,449    | 21,457     | -1,514      | 48,974     | 50,579     |
| cy (px)  | -23,881    | -30,115    | -44,285    | -6,173      | 54,031     | 22,681     |
| k1 (mm)  | 0,00533    | 0,00523    | 0,00496    | 0,00518     | 0,00518    | 0,00521    |
| k2 (mm)  | 0,00018    | 0,00017    | 0,00021    | 0,00020     | 0,00019    | 0,00018    |
| k3 (mm)  | -7,820E-06 | -7,684E-06 | -8,792E-06 | -8,3076E-06 | -8,068E-06 | -7,652E-06 |
| b1 (px)  | 0,0528     | -0,4354    | 0,2083     | -0,0041     | -0,0546    | -0,0416    |
| b2 (px)  | -0,0820    | -0,0213    | 0,0472     | 0,2613      | 0,0571     | 0,0862     |
| p1 (mm)  | -2,640E-05 | 1,6157E-05 | -8,781E-06 | 2,110E-05   | 1,993E-05  | 5,325E-06  |
| p2 (mm)  | 3,470E-05  | -1,490E-07 | 1,640E-06  | -1,131E-06  | -1,470E-07 | 1,667E-06  |

Table 27 Estimated I.O. parameters of the six action cameras separately considered and processed

The estimated focal length of the six cameras can be considered consistent and similar, some issues can be traced in the estimation of the PP coordinates of the different sensors, i.e. coordinates of lens optical axis interception with sensor plane (expressed in pixels with cx and cy coefficients). The estimated principal points of the six cameras sensors is graphically represented in the following Figure 108.

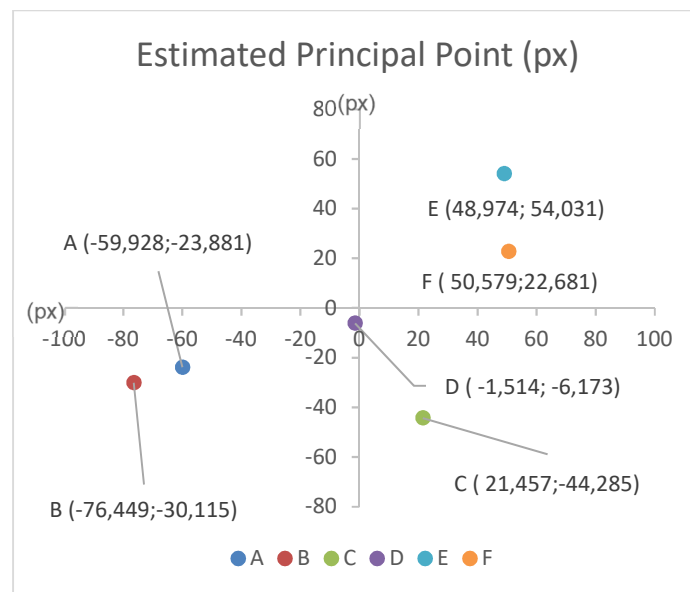


Figure 108 Graphical representation of Estimated principal point coordinates of the six cameras separately considered and processed

The PP coordinates of five out of six cameras are comparable (the deviation from the ideal principal point of coordinates 0,0 has the same order of magnitude but located on different quarter of the sensor) while the camera D presents a completely different position, almost in the ideal intersection of the two principal axes. This camera, which value is theoretically

closer to the ideal PP, can create some issues when working together with the other five sensors, due to its different interior parameters. This can be considered an issue both for the stitching of the six images in a single spherical image, both in the photogrammetric process.

In a second phase of the study the images acquired by the six cameras mounted on the rig were processed in two different ways: following the *automatic workflow* implemented in Photoscan and subsequently applying a *manual editing* to better control the camera parameters.

Following the *automatic workflow*, the software uses the information derived from the Exif metadata as initial parameters for the I.O. phase and for the further camera parameters estimation. Due to the information embedded in the Exif, the software assumed that only a camera was used and performed all the phases of the photogrammetric process considering all the cameras as identical. This wrong assumption lead to different problems in the phases of I.O. parameters estimation and TPs extraction. This issue explains the computed values of GCPs and CPs errors (Figure 107). Also, in this case is interesting to analyse the values estimated for the PP coordinates (Figure 109) that are similar to the ones of camera D individually considered. The values of the deviation of the six different cameras from the PP coordinates that were evident with the previously reported approach (Figure 108) were not considered by the software in this case.

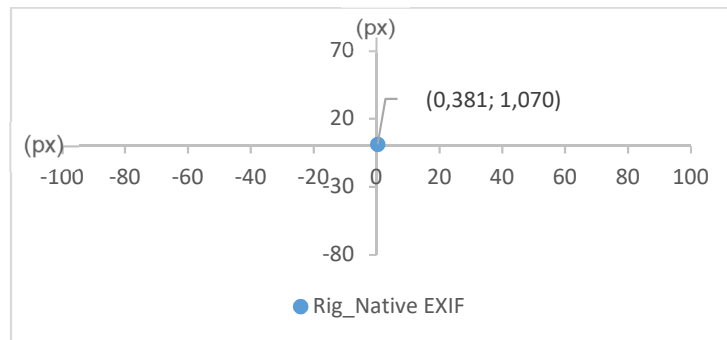


**Figure 109** Graphical representation of the estimated principal point coordinates of the six cameras mounted on the rig and automatically processed with the native Exif information

This issue is also evident if the plotting of the image residuals is analysed, as shown in Figure 110.

RIG 360  
NATIVE EXIF

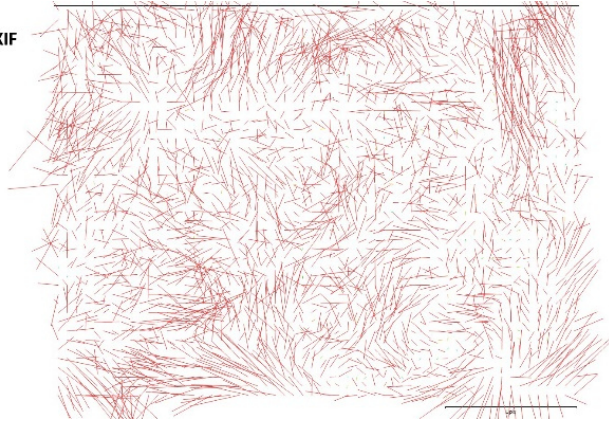


*Figure 110 Image residuals for the 360 configuration automatically processed with the native Exif*

From the analysis of these two elements it is clear that the I.O. parameters estimated for the camera are not reporting consistent results and that performing a single calibration for the six cameras, following an automatic approach, is not a successful and satisfying solution. The other estimated parameters of the I.O. for this configuration are reported in the following Table 28 .

| <b>360 Rig. Native Exif. Interior orientation parameters</b> |            |
|--|------------|
| <b>f(focal length -mm)</b>                                   | 3,038      |
| <b>f(focal length -px)</b>                                   | 1755,593   |
| <b>cx (px)</b>   | 0,381      |
| <b>cy (px)</b>   | 1,070      |
| <b>k1 (mm)</b>   | 0,00499    |
| <b>k2 (mm)</b>   | 0,00021    |
| <b>k3 (mm)</b>   | -8,878E-06 |
| <b>b1 (px)</b>   | 1,0267     |
| <b>b2 (px)</b>   | 0,4841     |
| <b>p1 (mm)</b>   | 1,273E-05  |
| <b>p2 (mm)</b>   | -9,230E-07 |

*Table 28 Estimated I.O. parameters of the six cameras mounted on the rig and automatically processed with the native Exif*

Finally, a *manual editing* of the Exif metadata of the six cameras was achieved to evaluate if it was possible to contemporary calibrate, and with satisfying result, the six cameras mounted on the rig. Before the processing, the information embedded in the Exif files were modified and the name of the camera model was changed, in order to independently process the six cameras during the workflow. The estimated I.O. parameters are reported in Table 29, while the estimated coordinates of the six principal points are shown in the images below, Figure 111.

| 360 Rig. Modified Exif. Estimated interior orientation parameters of the six cameras |              |             |            |            |            |            |
|--|--------------|-------------|------------|------------|------------|------------|
|  | A            | B           | C          | D          | E          | F          |
| f(focal length - mm)   | 3,050        | 3,038       | 3,040      | 3,041      | 3,045      | 3,035      |
| f(focal length - px)   | 1762,37711   | 1755,30797  | 1756,610   | 1756,98423 | 1759,15712 | 1753,58122 |
| cx (px)  | -59,740      | -76,220     | 21,893     | -1,884     | 48,956     | 50,620     |
| cy (px)  | -24,235      | -30,213     | -44,387    | -6,310     | 54,120     | 22,333     |
| k1 (mm)  | 0,00526      | 0,00620     | 0,00503    | 0,00516    | 0,00512    | 0,00521    |
| k2 (mm)  | 0,00019      | 0,00001     | 0,00020    | 0,00020    | 0,00019    | 0,00018    |
| k3 (mm)  | -0,00001     | 0,00000     | -0,00001   | -0,00001   | -0,00001   | -0,00001   |
| b1 (px)  | -0,1357      | -0,1955     | 0,1670     | -0,2115    | -0,0670    | 0,0277     |
| b2 (px)  | -0,0682      | -0,2481     | -0,0361    | 0,2873     | 0,1400     | -0,0095    |
| p1 (mm)  | -4,89731E-07 | 1,33023E-05 | -1,009E-05 | 2,237E-05  | 2,316E-05  | 1,340E-06  |
| p2 (mm)  | 4,20493E-07  | 4,505E-07   | 1,868E-06  | -9,839E-07 | -2,416E-07 | 2,162E-06  |

Table 29 Estimated I.O. parameters of the six cameras mounted on the rig and processed after the Exif modification

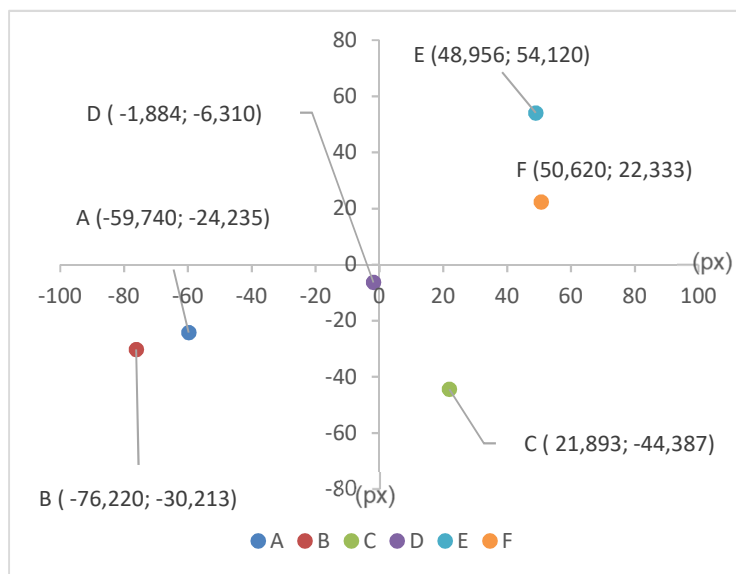


Figure 111 Graphical representation of the estimated principal point coordinates of the six cameras mounted on the rig and processed after the Exif modification.

As shown in Figure 107, adopting the last solution presented it is possible to achieve an RMSe on the GCPs and CPs that can be compared with the one achieved with the six cameras separately processed, even with smaller values.

Further analyses were then conducted on the data extracted from the different approaches for the estimation of I.O. parameters of the cameras, in order to evaluate also the quality of the different derived 3D models.

It had already been stressed the fact that low-cost cameras, and sensors in general, can present deformation derived from their mass market production. The six action cameras mounted on the rig have nominally the same exact specifications, thus, as demonstrated, each camera has different characteristic and, in particular, one of the cameras presented a set of completely different I.O. parameters that can lead to an inconsistency of the 360 system considered as a whole. This issue can be negligible if the camera is used as a standalone, as generally happens in most of the applications, but can be a critical element if the sensor is used together with other ones. Photogrammetry must not be considered as a black box solution, and also in the most diffused commercial solutions, such as Agisoft Photoscan, it is possible for the operator to maintain the control of several parameters during the different steps of the processing. However, especially in case of low cost and COTS sensors, some best practices need to be followed: it is important during the acquisition phases to achieve a strong network geometry with a good overlap between cameras stations; a control and an intervention of the operator, such as the Exif modification, can have a strong impact on the quality of camera calibration and TPs extraction and consequently on the generated 3D model; finally, the use of well distributed GCPs and CPs is really important.

Some further consideration can be done analysing the parameters of I.O. estimated for the eight projects (Table 27, Table 28, Table 29). The six projects of the cameras individually processed are considered as the most reliable and thus the other two approaches were compared to them. It is again clear that using a fully automatic uncontrolled procedure led to poor results in terms of camera calibration, while the Exif modification approach can be definitely considered as accurate.

Moreover, the impact of the different calibration approaches on the phase of TPs extraction was also analysed. The two approaches related with the jointed uses of the six cameras together, native and modified Exif, were further examined. In Photoscan it is possible, through a Python script launched by command line, to directly extract from the photogrammetric project a *.txt* file containing some precious information. This file is composed by four columns of information related to the sparse cloud of the computed TPs, the first three columns are dedicated to the spatial coordinates of each TP while the last one contains their reprojection error. The points were manually filtered, excluding the so-called outliers, and all the points with a reprojection error higher than 10 pixels were not considered. The script was applied to the two photogrammetric projects and the obtained data were imported and classified in CloudCompare software, applying a scale of false colours based on the reprojection error of each TP. An example of these analyses is reported in Figure 112, where is clearly visible the impact of a correct calibration on the quality of the TPs extracted in the photogrammetric process.

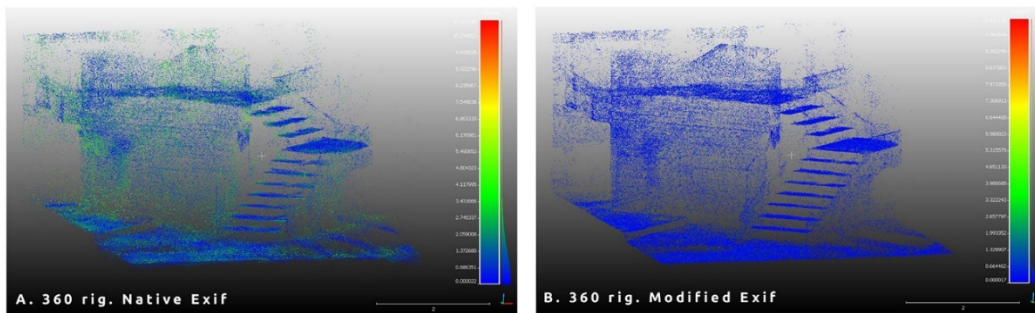


**Figure 112** Sparse cloud. Tie point quality based on reprojection error. 360 configuration: automatic process with native Exif (A), process with modified Exif (B)

It is possible to notice that in the A configuration only the 24% of points presents a reprojection error value minor of 0.5 pixels, while for the B configuration the 72% of points are comprehend in the same range of values. If we move the observation to the value of 1 pixel of reprojection error the ratio between A and B is 40% to 90%.

After performing these analyses, some other considerations were achieved for the 3D models generated with the two different approaches, the difference in quality between the two models is already evident for a visual inspection, as shown in Figure 113.

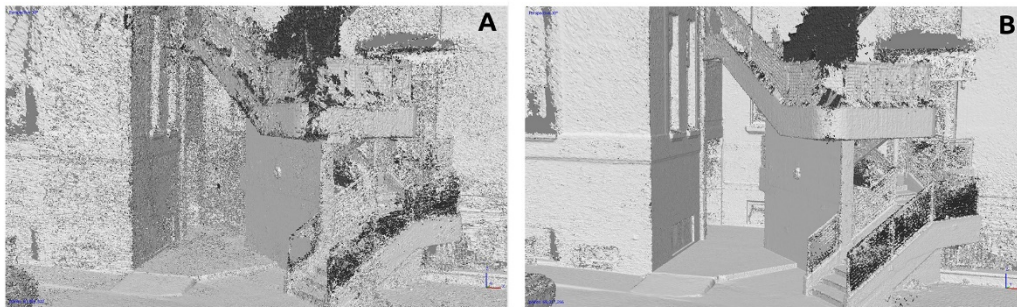


**Figure 113** Visual inspection of the Dense Cloud generated in Photoscan. 360 configuration: automatic process with native Exif (A), process with modified Exif (B)

In order to perform a more reliable analysis on the overall quality of the generated 3D models a ground truth LiDAR model was acquired. A Faro Focus X120 by CAM2 was employed, following the consolidated workflow for acquisition and post-processing phases, the scans were registered using a cloud to cloud approach and then georeferenced with the same dataset of control points used for the photogrammetric acquisitions. Afterwards, a small sample area was chosen, and the two photogrammetric clouds were compared with the one derived from the laser scanner, using the C2C (Cloud to Cloud) distances tool implemented in CloudCompare (Lague et al., 2013). The results of these analyses are reported in Figure 114: it is clear in the A configuration that the geometry of the object have been poorly reconstructed (only the 4% of the selected points present a deviation minor of 0.003 m compared to the TLS point cloud) while in the B configuration the results

are much better (the 60% of points present a deviation minor of 0.003 m compared with the TLS point cloud). In the A configuration it is also worth to notice that several gaps are present on the reconstruction of the geometry of the object.

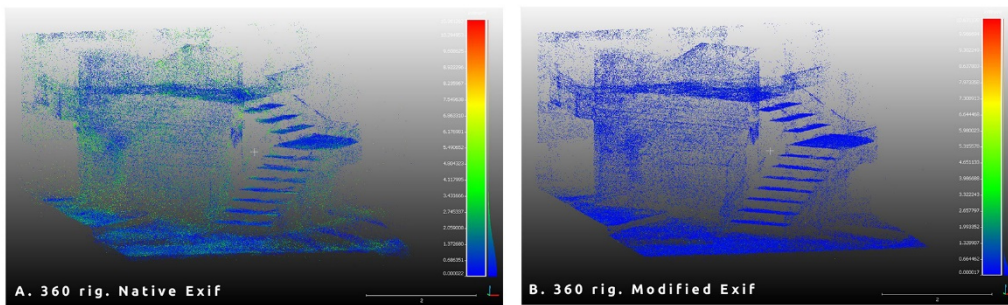


*Figure 114 C2C distances analysis performed in CloudCompare with LiDAR data set as ground truth. Max distance set at 0.01 m. 360 configuration: automatic process with native Exif (A), process with modified Exif (B)*

All the elements presented in the above sections can have an impact also in the phase of image stitching. In Figure 115 an example of how the images acquired from the Freedom 360 system are stitched together is shown, the different colours underline the contribute of the different images to the final spherical panorama and the overlapping areas between images.

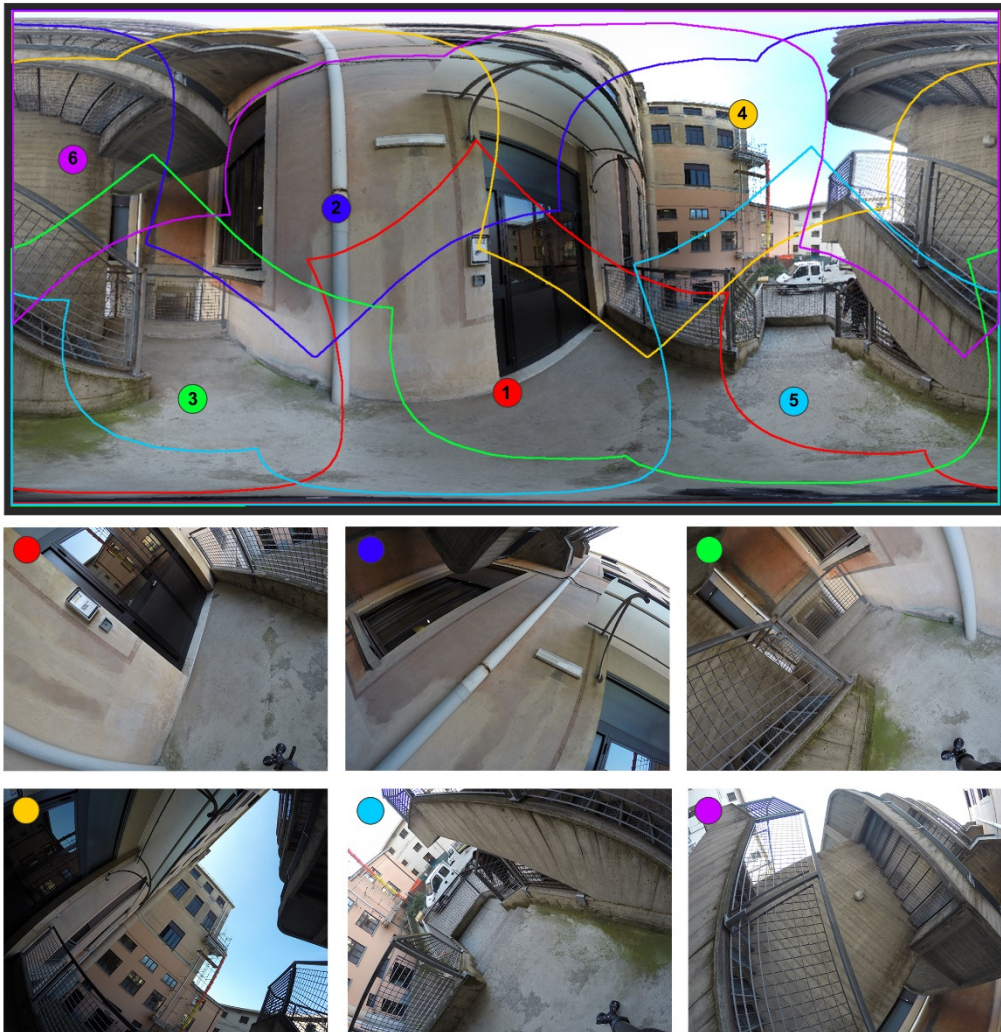


*Figure 115 Freedom 360. Stitching of the six cameras and overlapping areas between images*

Among the different software solution existing on the market for the processing of these digital contents (section 3.5.5) the commercial solution tested in this case is AutoPano Giga (v. 4.2), by Kolor. The algorithms and the workflow embedded in these software have been already presented in section 3.5.4 and how the I.O. parameters estimated for the different cameras can influence the process has been already underlined. AutoPano Giga take into consideration a set of three parameters during the process of stitching: focal length,  $k_1$ ,  $k_2$  and  $k_3$  coefficient for radial distortion and the coordinates of the principal point and these parameters are partially read from the Exif metadata (focal length) and partially extracted from the software database (all the other parameters). Also in this case is possible to apply some manual editing to modify the information embedded in the Exif file to let the software consider separately the six cameras. Furthermore, the calibration parameters extracted in the self-calibration performed in Photoscan were used. The stitching process was then completed following these three approaches: fully automatic, Exif modification and use of

I.O. parameters as shown in Figure 116, and the results were evaluated through a visual inspection as shown in Figure 117.

| Nome                | Focale   | Velocità | Apertura | Iso | Imbardata | Beccheggio | Rollio  | FOV     | Focale calcolata | K1    | K2     | K3    | Offset X | Offset Y |
|---------------------|----------|----------|----------|-----|-----------|------------|---------|---------|------------------|-------|--------|-------|----------|----------|
| (1) A_G0033063.J... | 15.00... | 1/120    | F2.8     | 136 | -0.000    | -37.580    | 44.334  | 146.792 | 16.888mm         | 0.119 | -0.019 | 0.000 | -6.90    | 6.00     |
| (2) B_G0028686.J... | 15.00... | 1/370    | F2.8     | 100 | 179.910   | 36.818     | -44.643 | 146.792 | 16.888mm         | 0.119 | -0.019 | 0.000 | -6.90    | 6.00     |
| (3) C_G0023138.J... | 15.00... | 1/120    | F2.8     | 120 | -60.095   | 33.629     | -43.707 | 146.792 | 16.888mm         | 0.119 | -0.019 | 0.000 | -6.90    | 6.00     |
| (4) D_G0022604.J... | 15.00... | 1/175    | F2.8     | 100 | 118.856   | -33.500    | 45.262  | 146.792 | 16.888mm         | 0.119 | -0.019 | 0.000 | -6.90    | 6.00     |
| (5) E_G0012426.J... | 15.00... | 1/100    | F2.8     | 132 | -122.312  | -31.141    | 46.696  | 146.792 | 16.888mm         | 0.119 | -0.019 | 0.000 | -6.90    | 6.00     |
| (6) F_G0022994.J... | 15.00... | 1/756... | F2.8     | 100 | 57.166    | 33.278     | -46.575 | 146.792 | 16.888mm         | 0.119 | -0.019 | 0.000 | -6.90    | 6.00     |

**Native Exif**

| Nome                | Focale   | Velocità | Apertura | Iso | Imbardata | Beccheggio | Rollio  | FOV     | Focale calcolata | K1    | K2     | K3    | Offset X | Offset Y |
|---------------------|----------|----------|----------|-----|-----------|------------|---------|---------|------------------|-------|--------|-------|----------|----------|
| (1) a_g0033063.J... | 15.00... | 1/120    | F2.8     | 136 | -0.000    | -35.695    | 44.042  | 149.124 | 16.624mm         | 0.158 | -0.062 | 0.000 | -71.79   | 24.10    |
| (2) b_g0028686.J... | 15.00... | 1/370    | F2.8     | 100 | -179.912  | 35.317     | -43.869 | 145.552 | 17.032mm         | 0.111 | -0.012 | 0.000 | -47.85   | -2.81    |
| (3) c_g0023138.J... | 15.00... | 1/120    | F2.8     | 120 | -61.453   | 33.590     | -46.062 | 148.687 | 16.673mm         | 0.116 | -0.025 | 0.000 | -26.73   | -19.29   |
| (4) d_g0022604.J... | 15.00... | 1/175    | F2.8     | 100 | 118.395   | -32.945    | 46.823  | 144.860 | 17.113mm         | 0.027 | 0.055  | 0.000 | -8.17    | 35.67    |
| (5) e_g0012426.J... | 15.00... | 1/100    | F2.8     | 132 | -118.543  | -34.919    | 45.573  | 147.476 | 16.809mm         | 0.228 | -0.099 | 0.000 | 107.17   | -5.10    |
| (6) f_g0022994.J... | 15.00... | 1/756... | F2.8     | 100 | 59.635    | 35.945     | -45.771 | 145.928 | 16.988mm         | 0.138 | -0.024 | 0.000 | 33.48    | -0.28    |

**Modified Exif**

| Nome                | Focale   | Velocità | Apertura | Iso | Imbardata | Beccheggio | Rollio  | FOV     | Focale calcolata | K1    | K2    | K3     | Offset X | Offset Y |
|---------------------|----------|----------|----------|-----|-----------|------------|---------|---------|------------------|-------|-------|--------|----------|----------|
| (1) a_g0033063.J... | 16.42... | 1/120    | F2.8     | 136 | 0.408     | -34.385    | 43.749  | 150.516 | 16.470mm         | 0.050 | 0.016 | -0.006 | -59.93   | -23.88   |
| (2) b_g0028686.J... | 16.42... | 1/370    | F2.8     | 100 | -179.723  | 35.336     | -43.691 | 151.011 | 16.416mm         | 0.048 | 0.015 | -0.006 | -76.45   | -30.11   |
| (3) c_g0023138.J... | 16.42... | 1/120    | F2.8     | 120 | -60.204   | 33.658     | -45.516 | 151.011 | 16.416mm         | 0.046 | 0.018 | -0.007 | 21.46    | -44.29   |
| (4) d_g0022604.J... | 16.42... | 1/175    | F2.8     | 100 | 119.204   | -33.916    | 46.477  | 151.011 | 16.416mm         | 0.048 | 0.017 | -0.007 | -1.51    | -6.17    |
| (5) e_g0012426.J... | 16.42... | 1/100    | F2.8     | 132 | -120.154  | -35.110    | 46.590  | 151.011 | 16.416mm         | 0.048 | 0.016 | -0.006 | 48.97    | 54.03    |
| (6) f_g0022994.J... | 16.36... | 1/756... | F2.8     | 100 | 58.347    | 35.946     | -46.500 | 151.510 | 16.362mm         | 0.048 | 0.015 | -0.006 | 50.58    | 22.68    |

**Modified Exif and camera parameters**

*Figure 116 Camera parameters used in three different approach in AutoPano Giga*



**Native Exif**

**Modified Exif**

**Modified Exif and camera parameters**

*Figure 117 Stitching aberration related with the use of different approach for camera interior parameters estimation*

Finally, it has been decided not to calibrate the Freedom 360, i.e. the relative spatial position between the cameras, for one main reason: the system stability over time. The material of the rig and the fact that the cameras are detachable are two key factors that are

not able to guarantee the system stability over time, thus a calibration of the rig as a system will result in a waste of effort and time.

#### 4.2.7 Dual camera systems: GoPro Fusion

Among the different dual camera systems available on the market, the GoPro Fusion was the device tested in this research. This camera is the first COTS 360 system commercialised by GoPro, after the semi-professional solution GoPro Omni. The system was launched at the end of the 2017, presenting some new interesting features in the panorama of immersive low-cost and COTS devices. The GoPro Fusion is composed by two cameras, two circular fisheyes, mounted on the same body in opposite position as shown in Figure 118. The main attractive features of this camera reside in its small size and weight and in the easiness of use. The camera is easy to set up and use and the aim of the company is to make also the stitching process as easier as possible. The main specifications of the camera are reported in Table 30.



*Figure 118 GoPro Fusion, 360 camera*

Another interesting feature of the camera is its resolution, thanks to the stitching of the data collected by the two sensors, the camera is able to provide video up to 5.2 K and stitched images with a maximum resolution of 5760 X 2880. The camera can be directly controlled with the physical buttons embedded on the body of the device, or through a dedicated app for smartphone and tablet. Moreover, the camera is equipped with a GPS/GNSS sensor and it is able to provide geoinformation embedded in the images.

| <b>GoPro Fusion main specifications</b> |                                     |
|---|-------------------------------------|
| <b>Weight</b>                           | 220 gr                              |
| <b>Size</b>                             | 74 x 75 x 40 mm                     |
| <b>Sensor</b>                           | 2x (CMOS, 1/2.3" – 9.3 MP)          |
| <b>Focal length (From EXIF)</b>         | 3 mm                                |
| <b>Video resolution</b>                 | Up to 5.2 K (up to 30 fps in 5.2 K) |
| <b>Image resolution</b>                 | Max 5760 X 2880                     |
| <b>Price</b>                            | 610-720 euros                       |

*Table 30 GoPro Fusion main specifications*

As will be further reported, the value for the focal length embedded on the Exif file is not correct, the real focal length of the two fisheye cameras have been estimated in the calibration process and converted in 35mm equivalent. The obtained value is of  $\approx 6.80$  mm that related with the FoV led to a value greater than  $180^\circ$  (as graphically shown in Figure 21). This is not surprising and is connected to the fact that the two cameras are coupled with opposite direction views on parallel planes and a sufficient overlap between the acquired images need to be ensured to perform the stitching process (Figure 119).



*Figure 119 Example of two images acquired by back (left) and front (right) cameras of the GoPro Fusion in the same moment*

This 360 camera was deeply analysed in this research and its use and main features were evaluated as well. The 3D calibration field described in section 4.2.2 was again employed to estimate the interior parameters of the two sensors composing the system, the configuration of cameras in relation with the stitching of the spherical images and the photogrammetric use of these data.

The acquisitions were achieved with the camera mounted on a photographic tripod, following a pre-projected schema and adopting varying roll angles, to achieve a more precise estimation of the I.O. parameters, especially of the PP. For each of the two sensors embedded in the GoPro Fusion the acquisition was performed following a traditional

approach: a first acquisition with the camera axis perpendicular to the object and other two acquisitions with the camera axis with an angle of incidence of around  $45^\circ$  degrees on the left and right views of the cameras. The distance between the camera stations was around 1 meter and the camera object distance was around 5 to 7 meters. Finally, a fourth acquisition was completed in order to improve the network of camera stations. This last acquisition was performed with the same shrewdness of the other three but with a reduced distance between camera and object and exploiting the omnidirectional view of the system, the fire stair and the portions of the building surrounding it were acquired more in detail in this case. An example of the acquisition phase is reported in Figure 120, while a scheme of the network of cameras and some of the images acquired are reported in Figure 121.



*Figure 120 Some phases of acquisition of the 3D calibration field with the GoPro Fusion*



*Figure 121 Acquisition scheme of the 3D calibration field achieved with the GoPro Fusion and example of acquired images*

The first approach that was tested for the estimation of the I.O. parameters of the two cameras was through a self-calibration approach. Using Agisoft Photoscan (version 1.4.0)

the dataset of the two cameras, marked as *back* and *front*, were separately processed. Before processing the two dataset, GoPro customer service was contacted to obtain some missing information that was not possible to retrieve elsewhere: the sensor size and the pixel size of the two cameras. However, the test performed with this approach alone were not able to produce valid results. The data collected were processed following two approaches: one without using GCPs and the other using the measured control points. However, the results derived from both the approaches were not able to perform a correct extraction of features between the images and the estimated I.O. parameters could not be considered reliable. Through this approach only a small part of the images was aligned (a number comprehend between 30 and 50 %). Moreover, the so-called bowl effect (Tournadre, Pierrot-Deseilligny, & Faure, 2015) was clearly visible also from a visual inspection, as shown in Figure 122. Another clear indicator of the issues encountered in this preliminary approach is the reprojection error on the GCPs, that presented high values (generally bigger than 10 pixels).

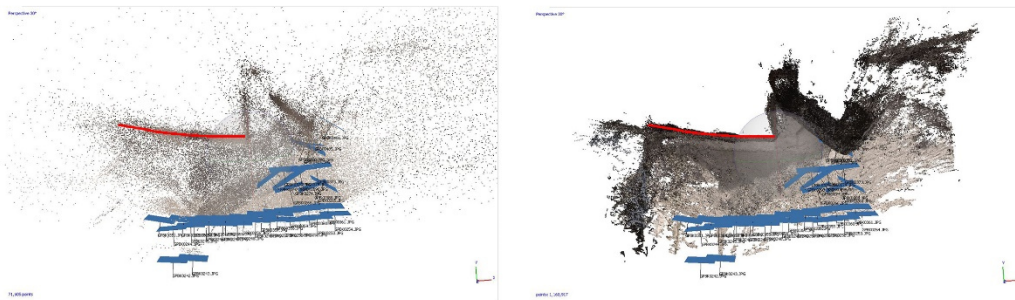


**Figure 122 Bowl effect on the back camera of the GoPro Fusion. Red lines should be straight walls. Top view of sparse cloud (left) and dense cloud (right)**

To overcome these issues and perform a valid self-calibration a further preliminary step was needed, an a-priori estimation of I.O. parameters of the cameras through a calibration with a known test field. The procedural workflow described in (Calantropio et al., 2017) was firstly adopted. Several images of the wooden checkboard shown in Figure 100, with varying roll angles and orientations, were acquired and the data collected were processed in Matlab, with the Camera Calibrator tool<sup>27</sup>. Unfortunately, the mathematical model embedded in this tool was not able to correctly estimate the parameters for the two circular fisheyes that compose the Fusion system and it became necessary to adopt another tool. Thus, a solution implemented in Agisoft photogrammetric suite was used, Agisoft Lens. A different type of checkboard was printed with a size of an ISO A0 format and applied on a rigid support. Several images (Figure 123) were then acquired following the standard

<sup>27</sup> <https://www.mathworks.com/help/vision/ug/single-camera-calibrator-app.html>

procedure (again varying roll angles, different orientations, etc.) and were then processed in the dedicated software. This procedure allows to estimate the I.O. parameters for the two cameras with a certain degree of confidence. This approach is derived from the CV community and is usually adopted to estimate I.O. parameters in a rapid way but with a lower degree of confidence. In this case however the idea wasn't to obtain a definitive certificate of calibration of the considered cameras, but to achieve a preliminary estimation of I.O. parameters in order to enhance the self-calibration process to complete a more accurate estimation.

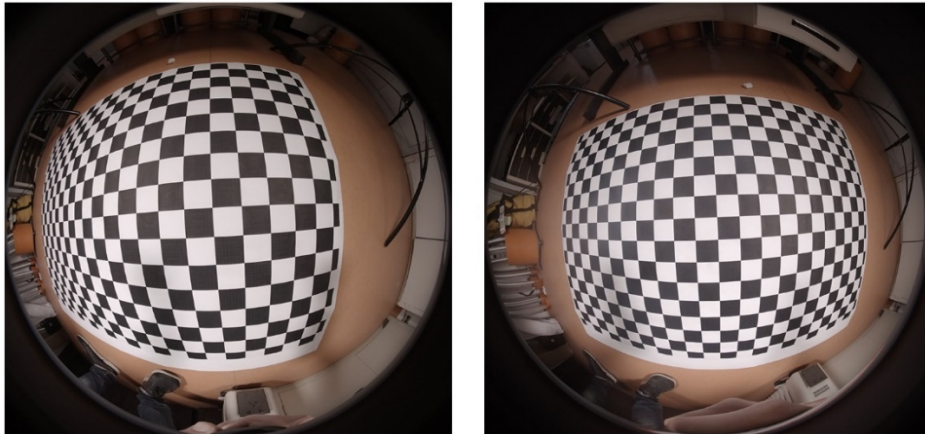


*Figure 123 Examples of the images acquired of the printed checkboard for the calibration with Agisoft Lens*

The images acquired were then processed in Agisoft Lens and the parameters reported in the following Table 31 were estimated. The results achieved confirmed that the previous self-calibration approach was not reliable. In this case the parameters of the two cameras were quite similar, and the differences were comprehended in an order of magnitude that can be considered acceptable for two identical model of mass marketed sensors.

| <b>Estimated I.O. parameters of the two cameras composing the GoPro Fusion trough Agisoft Lens</b> |              |             |
|--|--------------|-------------|
|  | <b>Front</b> | <b>Back</b> |
| <b>f(focal length -px)</b>   | 1091,751     | 1087,957    |
| <b>cx (px)</b>   | -5,364       | -3,728      |
| <b>cy (px)</b>   | -4,709       | -4,662      |
| <b>k1 (mm)</b>   | -0,057       | -0,066      |
| <b>k2 (mm)</b>   | 0,005        | 0,044       |
| <b>k3 (mm)</b>   | -0,001       | -0,056      |
| <b>b1 (px)</b>   | -1,218       | -1,831      |
| <b>b2 (px)</b>   | 0,018        | -0,016      |
| <b>p1 (mm)</b>   | 0            | 0           |
| <b>p2 (mm)</b>   | 0,001        | 0           |

*Table 31 GoPro Fusion. Estimated I.O. parameters trough Agisoft Lens*

The parameters estimated with the procedure described above were then used to optimize the self-calibration approach: the values reported in Table 31 were set as initial parameters for the two cameras in Agisoft Photoscan and the dataset were processed again. The first improvements were manifest also from a preliminary inspection of the results after the processing and two issues that were evident in the previous projects were corrected: all the cameras were aligned, and the bowl effect was no longer present. Furthermore, the data were deeply analysed: a first validation was performed on the RMSe on the GCPs and CPs used in the two self-calibration projects, as reported in the following Table 32.

| <b>RMSe on GCPs and CPs in the Self-calibration project</b> |               |               |               |                 |
|---|---------------|---------------|---------------|-----------------|
| <b>CAMERA FRONT</b>   |               |               |               |                 |
|   | <b>X (mm)</b> | <b>Y (mm)</b> | <b>Z (mm)</b> | <b>TOT (mm)</b> |
| <b>GCPs</b>   | 0,412         | 1,421         | 0,621         | 1,605           |
| <b>CPs</b>  | 0,488         | 0,926         | 1,116         | 1,047           |
| <b>CAMERA BACK</b>  |               |               |               |                 |
|   | <b>X (mm)</b> | <b>Y (mm)</b> | <b>Z (mm)</b> | <b>TOT (mm)</b> |
| <b>GCPs</b>   | 3,916         | 2,977         | 0,812         | 4,985           |
| <b>CPs</b>  | 1,437         | 6,206         | 1,481         | 6,540           |

*Table 32 RMSe in mm of GCPs and CPs on the two cameras projects for self-calibration. Seven measured points were used as GCPs and seven as CPs*

As is possible to notice from the RMSe values reported in the previous table the overall photogrammetric process can be considered reliable, with slightly different values for the back camera. This is probably due to a weaker geometry of the acquisitions, however also the RMSe for the back cameras is always less than a centimetre.

In the following Table 33 the estimated I.O. parameters through the self-calibration approach, after the insertion of the initial values extracted from Lens, are reported. It is possible to notice that the different parameters are congruent between the two cameras and that the P1 and P2 coefficient of decentring distortion are not computed through this approach. This can be probably reconducted to the mathematical model that the software uses for fisheye cameras.

| <b>Estimated I.O. parameters of the two cameras composing the GoPro Fusion through a self-calibration approach</b> |              |             |
|--|--------------|-------------|
|  | <b>Front</b> | <b>Back</b> |
| <b>f(focal length -px)</b>   | 1086.856     | 1089.578    |
| <b>cx (px)</b>   | -5.378       | -3.256      |
| <b>cy (px)</b>   | -1.104       | -2.138      |
| <b>k1 (mm)</b>   | -0.053       | -0.096      |
| <b>k2 (mm)</b>   | -0.001       | 0.082       |
| <b>k3 (mm)</b>   | -0.001       | -0.062      |
| <b>b1 (px)</b>   | -0.429       | -0.158      |
| <b>b2 (px)</b>   | 0.030        | -0.038      |
| <b>p1 (mm)</b>   | 0            | 0           |
| <b>p2 (mm)</b>   | 0            | 0           |

*Table 33 GoPro Fusion. Estimated I.O. parameters through the self-calibration approach*

Thereafter, some analyses already performed for the Freedom system and described in section 4.2.6 and in (Teppati Losè et al., 2018) were achieved also for the Fusion system. Through a python script the reprojection errors of the TPs of the two self-calibration projects were extracted, filtered and analysed. The data reported in Table 34 summarize the results extracted through this process.

| <b>TPs reprojection error</b> |                     |                    |
|-------------------------------|---------------------|--------------------|
| <b>Reprojection error</b>     | <b>Camera Front</b> | <b>Camera Back</b> |
|                               | <b>% below</b>      | <b>% below</b>     |
| <b>0.5 pix</b>                | 77,22 %             | 48,70 %            |
| <b>1 pix</b>                  | 95,55 %             | 81,73 %            |
| <b>2 pix</b>                  | 99,30 %             | 97,21 %            |
| <b>5 pix</b>                  | 99,92 %             | 99,81 %            |

*Table 34 Reprojection error of TPs extracted to the enhanced self-calibration approach*

Again, the camera front is performing better than the camera back and this is a confirmation that probably the network of images was not perfectly projected or executed during the acquisition phase for this camera. This issue is identifiable also in the images reported in Figure 124. The overall process produced good results, and for both the cameras the major part of TPs presents a reprojection errors below 1 pixel.

A further analysis on TPs reprojection errors was achieved through the CloudCompare software, in order to verify if the spatial distribution of the different values was related with some other issues (occlusions, texture of the surveyed scene, etc.). Thus, the data previously extracted and filtered were imported and classified in the software.

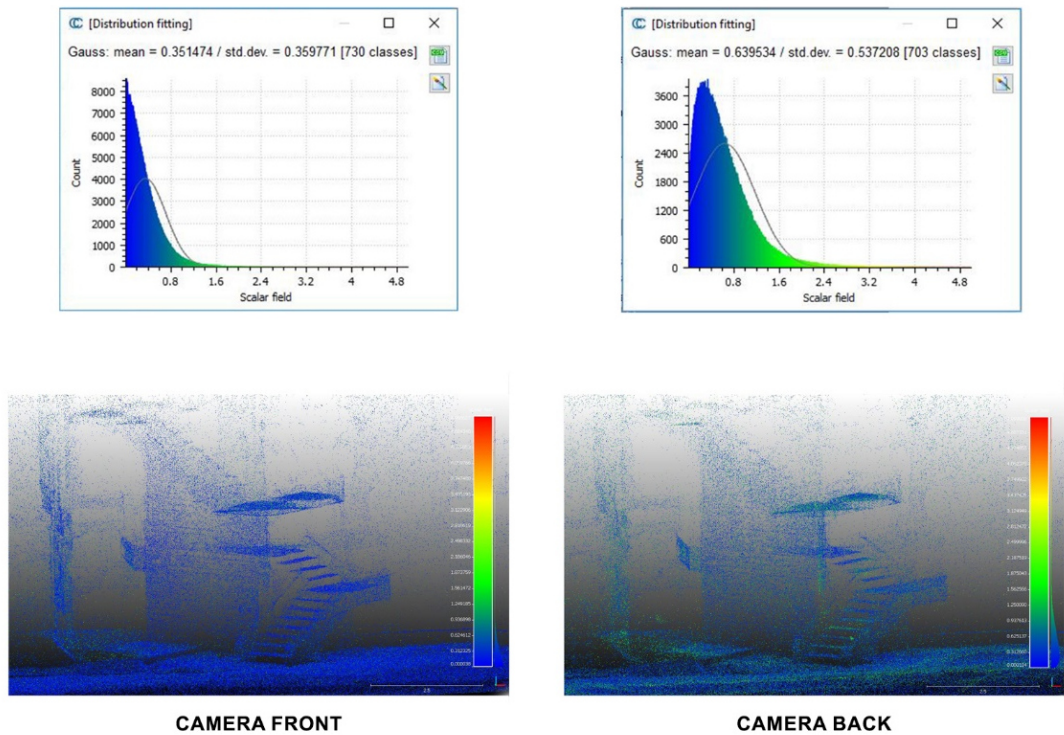


*Figure 124 Classification of the reprojection errors on TPs of the two cameras separately considered. Threshold set at 5 pixels*

This analysis confirmed, once again, the slightly lower performances of the camera back. In general terms, however, the distribution of reprojection errors doesn't seem to follow a scheme and TPs with higher errors are distributed all over the scene. Finally, to evaluate also the overall performances of the two cameras in reconstructing the objects geometrical features a further analysis was completed, using a TLS dataset of the calibration field as ground truth element. The acquisition and processing of the laser dataset were completed following consolidated approaches as described in (Chiabrandò, Spanò, et al., 2017; Teppati Losè et al., 2018). The models derived from the two cameras were then analysed both with C2C approaches and with the automatic generation of punctual cross-sections, in Figure 125 the two sample areas that were more deeply analysed are indicated.



*Figure 125 The two sample areas analysed: a corner between two walls and a portion of the fire stairs*

The point cloud derived from the laser data and the two photogrammetric projects were filtered and imported in the CloudCompare software; the filtering of the models was applied for two main reasons: to reduce the noise (especially in case of the photogrammetric cloud) and to perform the analyses on point cloud with a similar density (the laser data embedded indeed a larger number of points). The first sample analysed is the corner between two walls. The C2C tool was compute setting the laser data as reference and comparing the other two photogrammetric clouds.

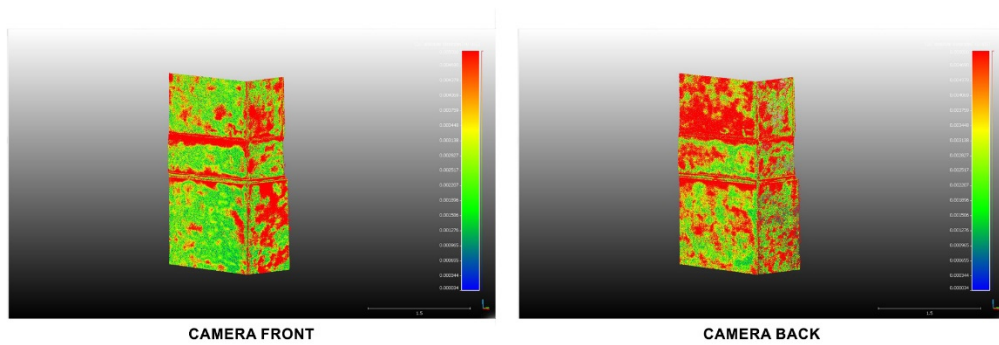


*Figure 126 C2C analysis on the corner wall. TLS set as reference and point cloud from front (left) and back (right) cameras as compared elements*

| Corner wall  | -0.01m<npts<0.01m | -0.005m<npts<0.005m | -0.002m<npts<0.002 m | -0.001m<npts<0.001m |
|--------------|-------------------|---------------------|----------------------|---------------------|
| Front Camera | 98%               | 80%                 | 48%                  | 29%                 |
| Back Camera  | 94%               | 72%                 | 28%                  | 13%                 |

*Table 35 Corner wall. C2C analyses of the sample area; number of points included in the preselected range of values*

As is possible to notice from Figure 126 and Table 35 it is confirmed that front camera is performing better than the back camera. Furthermore, the C2C analyses provides good values in terms of deviation of the geometric reconstruction derived from the photogrammetric approach with the one of the TLS set as ground truth. The same

considerations can be extended for the other sample area: as showed in Figure 127 and in Table 36.

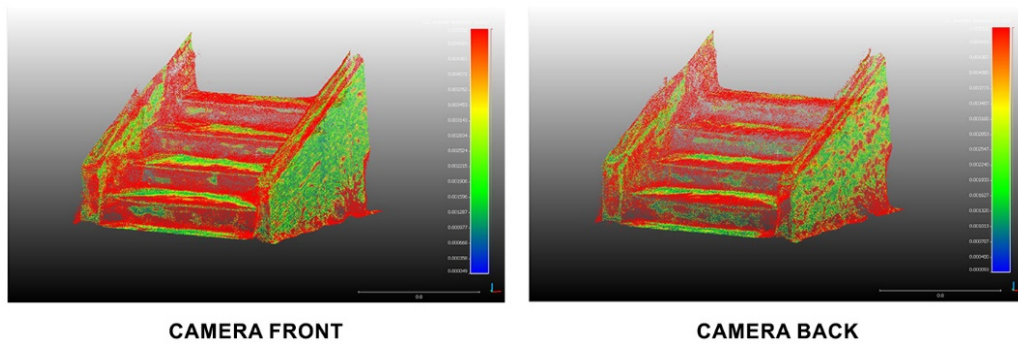


*Figure 127 C2C analysis on the stairs. TLS set as reference and point cloud from front (left) and back (right) cameras as compared elements*

| Stairs       | -0.01m<npts<0.01m | -0.005m<npts<0.005m | -0.002m<npts<0.002 m | -0.001m<npts<0.001m |
|--------------|-------------------|---------------------|----------------------|---------------------|
| Front Camera | 75%               | 53%                 | 27%                  | 15%                 |
| Back Camera  | 76%               | 52%                 | 23%                  | 12%                 |

*Table 36 Stairs. C2C analyses of the sample area; number of points included in the preselected range of values*

Moreover, another analysis was carried out on the sample related with the portion of fire stairs. As is shown in the following Figure 128, semi-automatic sections were extracted in the same point in each of the three datasets. It is clearly visible that both the cameras are not able to compete with the geometric reconstruction of the TLS, as expected, and that the resulting products extrapolated from the photogrammetric data are noisier and with a lower definition of the geometrical features of the object. However, it is interesting to notice that, again, the front camera is performing better than the back, confirming what reported before. The sections extracted are also interesting because they confirm the expected scale of the survey and the overall performances of these cameras, at least in the context of this sensor-object distances. Comparing the different sections extracted from the models and considering the TLS dataset as ground truth it is possible to make some considerations: both the datasets derived from the spherical images are producing a less detailed reconstruction of the considered object; moreover, the mean deviation of the sections extracted from the fisheye datasets from the TLS one is around 2 cm, allowing a representation scale of 1:100.

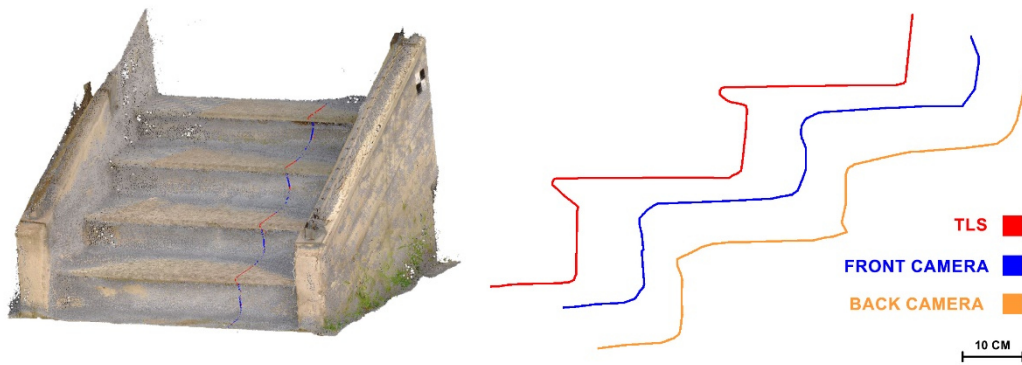


*Figure 128 Semi-automatic sections extracted from the different dataset of the stairs sample*

The I.O. parameters of the two cameras that composed the system were then employed to adopt an approach similar to the one presented in section 4.2.6, however the results were quite different. The GoPro system is provided with the GoPro Fusion Studio software, to perform the stitching of images. The software is dedicated to the stitching of images that are derived only from the homonymous system and is projected to be as user friendly as possible. The drawback resides in the limited possibilities for the user to interact in the different phases of the process of stitching. As for the Freedom 360 system, the idea was to test different stitching solution in order to validate which one was the best approach to adopt. Autopano Giga was the first alternative software tested, the stitching of the two circular fisheye is not always performed without issues. Often, the user's intervention is required starting from the preliminary estimation of image connection (through the manual selection of TPs) till the blending phase. The situation will not change even with the introduction of I.O. parameters of the two cameras and the stitching phase using this software is sometimes stressing and time consuming. Other tests performed with different stitching software solutions resulted in similar results. This issue can be explained considering the low overlap between the two cameras, as shown in Figure 129, resulting in a more difficult estimation of the correspondences between features on the two images.

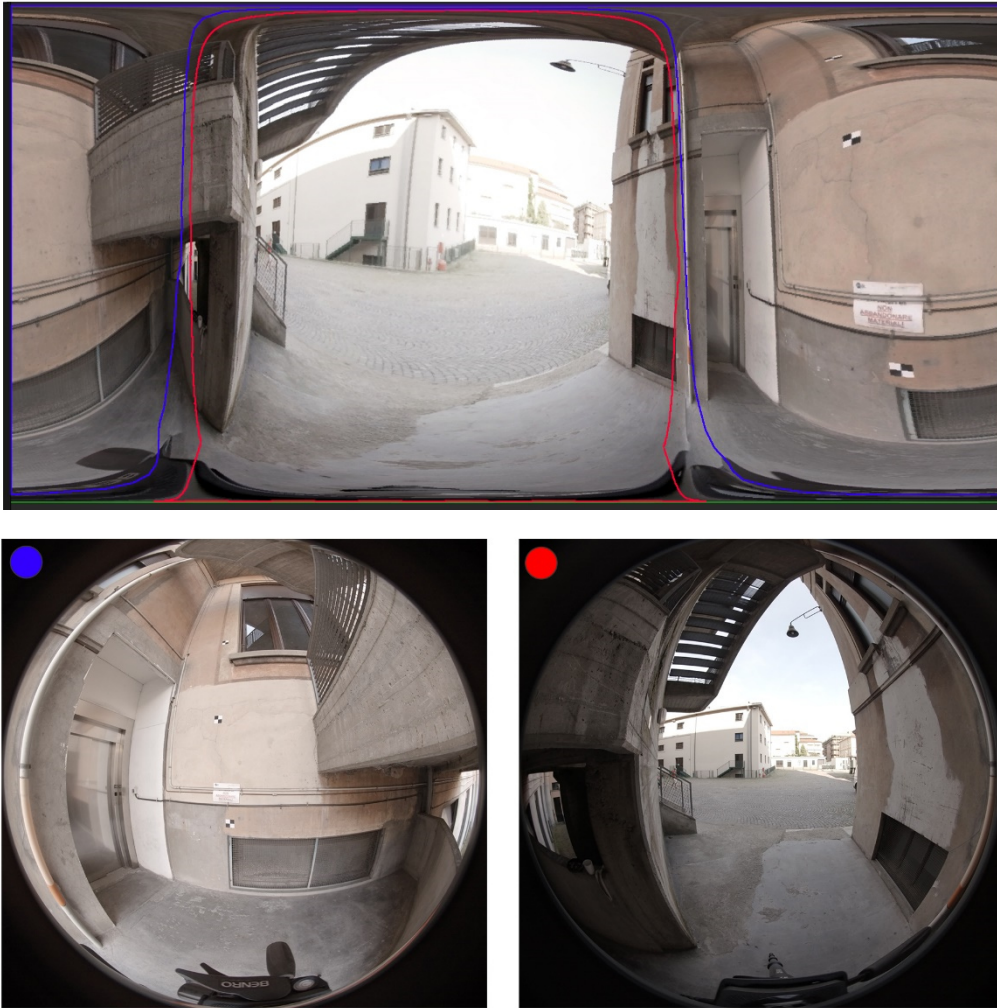


*Figure 129 GoPro Fusion. Stitching of the two cameras and overlapping areas between images*

Moreover, due to the recent launch of this camera on the market, it is also possible that the camera database of the major part of stitching software is not yet updated with the data of the GoPro Fusion. For this camera, at the present level of performances of the different software, the use of GoPro Fusion Studio seems to be the better option, sacrificing some control over the different phases of the stitching it is thus possible to rely on good stitching results thanks to the information of the two cameras characteristics and their relation, that are embedded in this proprietary solution. In the different tests performed the results of the stitching process were always good, and, thanks to the fact that GoPro Fusion Studio allows to access both to the raw data and to the rendered images, it is possible to maintain a control on the overall process. After this considerations and analyses on the best stitching approach to follow, more tests were performed on the calibration field but this time working with the spherical images derived from the stitching of the two cameras together (Figure 130).



*Figure 130 Example of spherical image of the calibration field derived from the stitching of front and back camera of GoPro Fusion*

The images were thus stitched together using the commercial solution that come with the GoPro Fusion, the Fusion Studio. As already reported this software allows few controls over the stitching process: for the user it is possible only to act on some parameters for the straighten of the horizon on the equirectangular projection and applying some correction to the colours and radiometric information of the image, however the stitched image is almost every time satisfying in term of overall quality. In this case, the tests performed on the calibration field were not devoted to the calibration of the system, but to the assessment of the geometric quality of the 3D model achievable with this approach. Agisoft Photoscan was again chosen for these tests, mainly because is one of the few software that, till today, allows to perform an SfM approach with spherical images.

A total of 55 spherical camera stations (Figure 131) were thus imported in Photoscan, the alignment of the images resulted in a sparse cloud of TPs of  $\approx 92.000$  (alignment parameters *high* and tie points e key points limit set at 0 in order to extract all the possible TPs).



*Figure 131 View of the acquisition scheme achieved with the GoPro Fusion*

The coordinates of the targets set on the calibration field were then imported and the targets were collimated on all the images where they were visible; again 7 targets were used as GCPs and 7 as CPs (RMSe value of GCPs and CPs is reported in the following Table 37).

| <b>RMSe on GCPs and CPs in the spherical project</b> |               |               |               |                 |
|--|---------------|---------------|---------------|-----------------|
| <b>360 IMAGES</b>                                    |               |               |               |                 |
|  | <b>X (cm)</b> | <b>Y (cm)</b> | <b>Z (cm)</b> | <b>TOT (cm)</b> |
| <b>GCPs</b>  | 0,432         | 0,997         | 0,359         | 1,144           |
| <b>CPs</b>   | 0,761         | 1,334         | 0,698         | 1,687           |

*Table 37 RMSe on GCPs and CPs for the processing of spherical images acquired in the calibration field*

It is important to notice that spherical images are considered free of distortion (as reported in section 3.6), thus the calibration of the spherical camera only consist in the estimation of the focal length of the virtual spherical camera. The python script for the extraction of the reprojection errors was applied also to the TPs computed in the alignment phase of the spherical images, the results are shown in Table 38.

| <b>TPs reprojection error</b> |                       |
|-------------------------------|-----------------------|
| <b>Reprojection error</b>     | <b>360 Images TPs</b> |
|                               | <b>% below</b>        |
| <b>0.5 pix</b>                | 41,17 %               |
| <b>1 pix</b>                  | 66,80 %               |
| <b>2 pix</b>                  | 88,14 %               |
| <b>5 pix</b>                  | 98,61 %               |

*Table 38 Reprojection error of TPs extracted from the processing of spherical images*

From the values contained in the table is possible to underline an overall good degree of success from the phase of TPs extraction during the first processing steps of the spherical

images. The densification step of the photogrammetric processing allows to obtain a dense cloud suitable to perform some analyses with the same strategies adopted for the two fisheye cameras. The same sample areas individuated in Figure 125 were segmented in this photogrammetric model and some analyses were achieved. The first analysis was again a C2C distance using the laser cloud of the calibration field as ground truth. The results of these analyses for the two sample areas are reported in the following Table 39 and showed in Figure 132.

| 360/TLS C2C | -0.01m<npts<0.01m | -0.005m<npts<0.005m | -0.002m<npts<0.002 m | -0.001m<npts<0.001 m |
|-------------|-------------------|---------------------|----------------------|----------------------|
| Corner wall | 62,9%             | 36,5                | 15,5%                | 8%                   |
| Stairs      | 50,5%             | 27,9%               | 12,2%                | 6,14%                |

*Table 39 Photogrammetric 360 model. C2C analyses of the sample areas; number of points included in the preselected range of values*

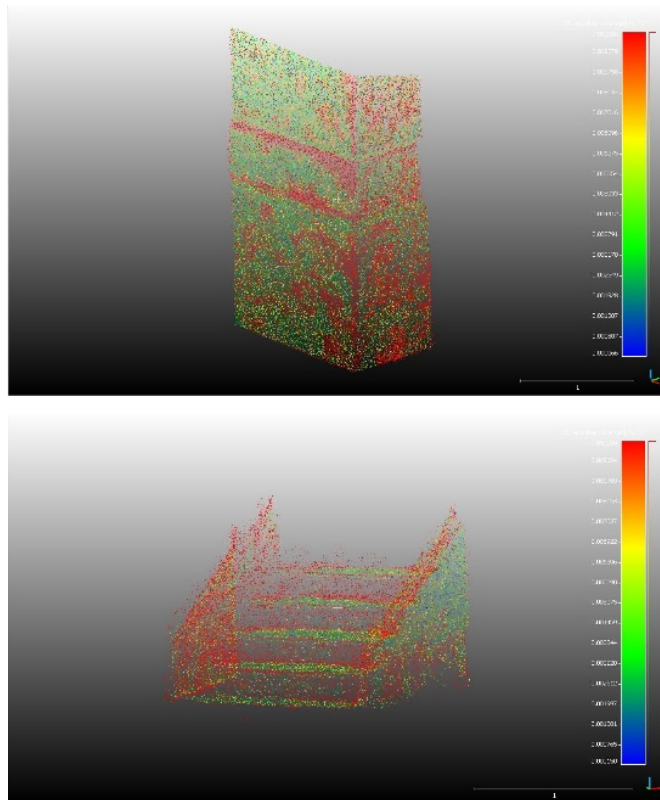


*Figure 132 C2C analysis on the two sample areas. TLS set as reference and point cloud from 360 images as compared elements. Corner wall on the left and stairs on the right*

Comparing the data of the spherical project with the ones of the back and front cameras is possible to notice a general lowering of the performances of the system, as expected. The overall resolution of the single spherical image is higher than the two fisheyes individually considered, however, the stitching process introduce some degradations of the image quality. Moreover, the mathematical modelling of spherical cameras in the SfM approach is a recent topic of research and thus less refined if compared to the model embedded in the software for fisheye lenses.

The results achieved in this first phase of tests were considered satisfying, it was possible to establish which performances can be expected for this system and the reachable overall accuracy. All these elements considered, it was decided to further examine the system in a real-world application scenario and further test were exploited, as it will be reported in section 4.2.

In a preliminary phase of this research the calibration of the Fusion system was not considered due to several reason, first of all the instability over the time of the system itself due to its COTS nature and secondly because few solution exists to absolve this task in a rapid and straight way without losing the benefit of working with systems for the rapid mapping, that is one of the main aims of this research. However, at the end of the drafting of this work a new release of Photoscan was announced by Agisoft. It was not possible to deeply test the new software, actually Photoscan changed its name in Metashape, and the list of features that were introduced. Thus, a first look at the release allows to notice some interesting features dedicated to the implementation of camera station (through a master-slave camera approach) and spherical images processing. It will be interesting in the future to evaluate if a relative orientation between the two fisheyes cameras can enhance the photogrammetric approach with these kinds of sensors.

## **4.3 Tests performed in the framework of CH documentation with 360 cameras**

### **4.3.1 Best practices and acquisition strategies**

The use on the field of 360 systems may seems easy since these sensors are conceived to record all the environment surrounding them, however things are a little bit more complicated. Similarly to the acquisitions performed with normal frame cameras different factors need to be taken into account when performing an acquisition and the dataset need to be acquired respecting some basic principles. The first factor that need to be considered is related with the acquisition distance between object and sensor that is a key element also for spherical photogrammetry. The operator can be tricked by the specifications of the employed 360 camera that usually report the resolution of the final spherical images, but it is fundamental to consider that this virtual image is derived from the alignment and fusion of data derived from different sensors that in general terms, especially for COTS and low-cost cameras, present low technical features. It is thus important to always bear in mind that the derived 360 images need to be considered, to simplify, as a fusion of the data

derived from the multiple sensors composing the system and that the specifications to consider as reference are the one of the single sensors. These systems allow for sure to reduce the number of camera station, being able to record wide portion of the environment, however the sensor to object distance selected can impact both on the accuracy of the photogrammetric process, both on the geometrical reconstruction of the scene. Some preliminary tests were performed in the Castello del Valentino court, venue of the Architecture department of the Politecnico of Turin, to evaluate the impact of this factors. Two acquisitions of the same portion of the south façade of the court were thus achieved with the GoPro Fusion camera applying different object-sensor distances: it was of 10 m in Set 1 and 5 m in Set 2. An overview of the two acquisitions schemes and two examples of the acquired images are reported in the following Figure 133.

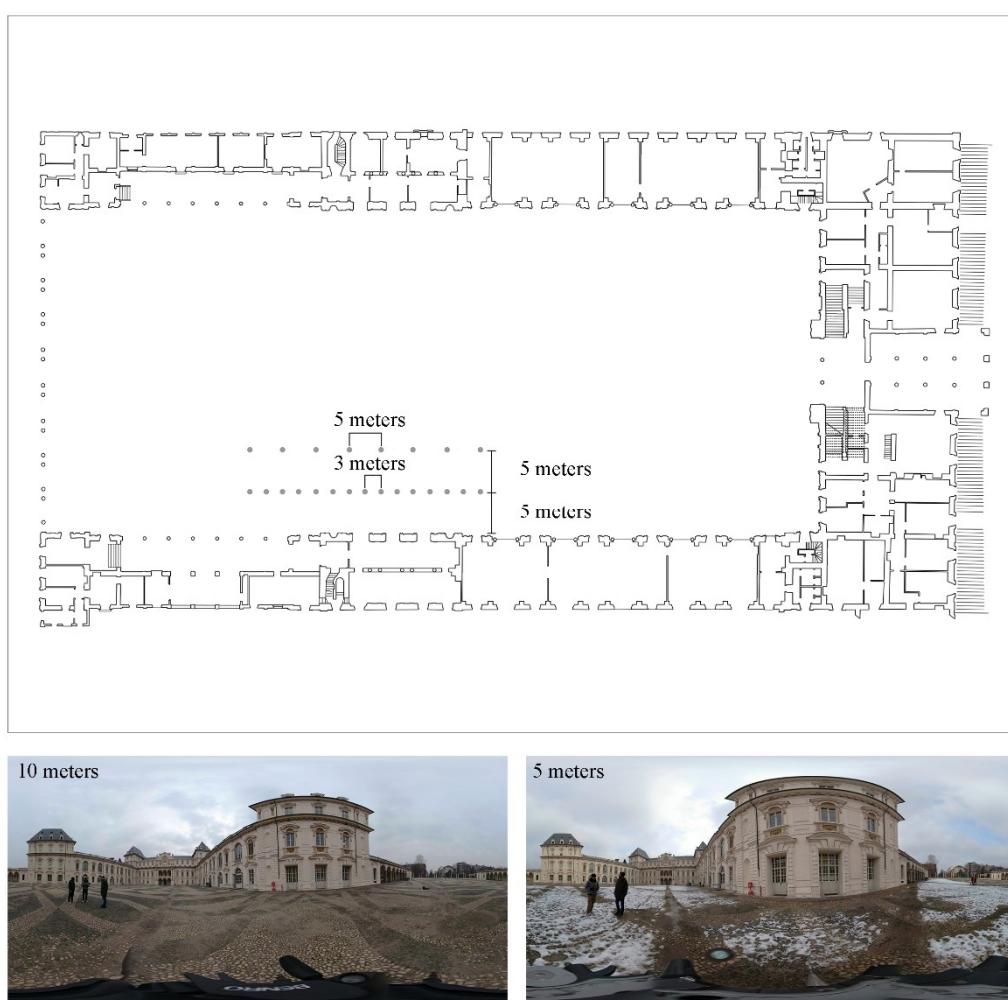


*Figure 133 Valentino, Castle. Example of images acquired with different sensor to object distance*

The two sets of images were then processed following the same approach: image orientation and TPs extraction, E.O. solved using GCPs (measured with TS), point cloud densification, triangulation of the model and generation of a mesh, texturization phase,

DSM generation and finally orthophoto production. Firstly, the overall accuracy of the process was assessed through GCPs and CPs, as reported in the following Table 40.

|                     | RMSe on GCPs | Reprojection error on GCPs | RMSe on CPs | Reprojection error on CPs |
|---------------------|--------------|----------------------------|-------------|---------------------------|
| <b>Set 1 (10 m)</b> | 0,029 m      | 0,545 pix                  | 0,031 m     | 0,466 m                   |
| <b>Set 2 (5 m)</b>  | 0,011 m      | 0,367 pix                  | 0,010 m     | 0,339 pix                 |

*Table 40 Valentino Castle, test on the impact of the sensor to object distance on GCPs and CPs RMSe value on the datasets acquired with the GoPro Fusion*

It is interesting to notice that both the RMSe values and the reprojection errors on the control points present clear improvements thank to the reduction of the sensor to object distance. The impact of the distance reduction is clearly visible also on the quality of the geometrical reconstruction of the scene. This issue is clear in the images collected in Figure 134, despite the noise present in both the models it is evident how the reduction of acquisition distance is impacting the overall geometrical reconstruction of the scene.

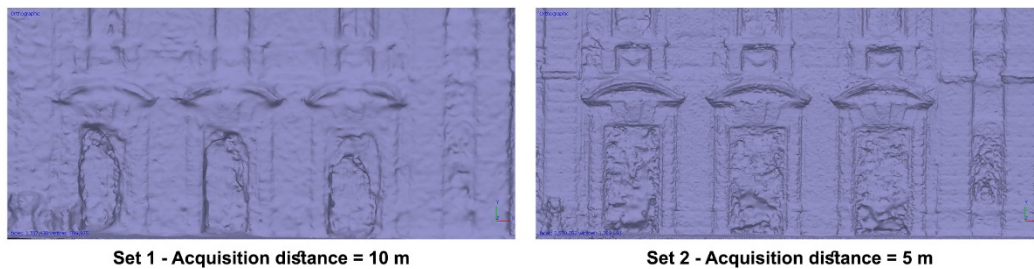


*Figure 134 Valentino Castle, 3D models derived from the two 360 datasets acquired at different distances from the object*

The model derived from Set 2 can provide a good reconstruction of the architectural features of the façade, while the model derived from Set 1 is producing a poor geometrical reconstruction and only the main features of the structure are underlined.

The noise present on these models is ascribable also to other two main factors: the presence of windows and the colour of the façade. In this case the overall photogrammetric process was stressed also from these other two factors. Another aspect that can be quite influencing during the acquisition with these sensors is related with the environmental conditions of the scene. In general terms, the sensors embedded in 360 systems are quite small and with a short focal length, this is dependent from the fact that usually they are derived from the market sector of action cameras, in which these specifications are common. This is a limit derived from the intrinsic characteristics of the cameras, performances in low-light conditions will be thus reduced also for the derived 360 images. This issue has to be considered especially if the camera is used for indoor acquisitions or also for outdoor acquisitions with bad lighting conditions.

Another factor that may seem prosaic, but needs to be reported, is related with the omnidirectional view of this system; during an acquisition it is crucial to remind that the camera is recording everything surrounding it. The deployment of these systems on the field needs to be accompanied with a change of perspective compared to standard frame cameras. The operator needs to monitor all the scene surrounding the camera for a certain distance in order to be aware of all the possible movements that can happen (people entering in the scene, objects moving, etc.) and also needs to be aware that he will also be present in the scene. This issue can be partially solved adopting some strategies during the acquisition phase, however this is not always possible, and this problem needs to be solved during the processing phases.

### **The three different acquisition strategies followed**

The images used for the test in the Valentino Castle were acquired using a photographic tripod on which the 360 camera was mounted and shooting the images remotely controlling the system, this is one of the three possible acquisition strategies that can be adopted: the other two are the “time lapse” mode and the video mode.

The first modality of acquisition, hereafter defined as **still images** acquisition mode, requires two main features: the use of a tripod and the possibility to remotely control the camera. Remote control features are embedded in the major part of 360 consumer grade cameras and generally a mobile device application is provided within the purchased system. These applications allow to set up all the parameters for the acquisition and to shoot from a certain distance from the camera, the limit of the range of connectivity between camera and mobile device is related with the communication technology used (Bluetooth, Wi-Fi, etc.) and the specification of the components devoted to this connection. Despite being the more efficient techniques in terms of quality of the images (the camera is stabilised on the tripod, the operator can often be able to hide himself from the range of acquisition of the system and can control the overall scene before shooting) it is for sure the less efficient on the field. This set up requires a lot of actions from the operator that, for each shoot, need to move the tripod and then hide himself before the acquisition of the image and is resulting in a high waste of time in the field. The main advantage of this approach is related, as already reported, with the quality of the image, and secondly with the possibility to carefully project the network of camera stations for the photogrammetric project. This solution is recommended only if the aim of the survey is to stress the system to its maximum performances or if the scene to record presents small dimensions. Selecting this approach can nullify one of the main advantages of 360 system, namely the ability to capture big areas in a limited amount of time with an overall good resolution.

The second possible acquisition modality, hereafter defined as **time lapse** acquisition mode, is related with the possibility of acquiring images at preselected interval for a defined period of time. As reported from the name, this modality is conceived for the creation of time lapse contents that contemplate the recording of a scene with images acquired from the same point of view within a selected range of time. This modality is generally devoted to the creation of videos derived from the union of the different frames acquired. For the photogrammetric approach developed in this thesis this acquisition mode was adopted in a slightly different way. After selecting the time lapse mode and deciding the shooting interval, the camera was not held still in the same position but was moved across the scene that need to be acquired. Considering the fact that this acquisition mode is not conceived for the camera to move around, several factors need to be taken under the control of the operator. First of all, the acquisition interval between images is quite important, it will influence also the speed of movement that the operator will adopt during the acquisition. A wrong setting of this interval can lead both to the collection of insufficient data, both to redundant data. As already stated, the speed that the operator can sustain during the acquisition across the scene is related with this parameter. There are no general rules for the setting of this parameters and a lot is left to the knowledge of the operator of the system he/she is using and of his experience with this approach on the field. In general terms, particular attention need to be devoted again to the light conditions of the scene: if the general illumination is low the operator will need to proceed slower in order to avoid blurry images and on the other hand if direct sunlight is present the operator will need to bear in mind that one or more cameras will be influenced by this element. A good shrewdness is to slow, or even stop, during the acquisition in areas that are more complex or need particular attention, in order to be sure to capture enough data to cover the whole scene. This approach is definitely able to speed up the operative phase on the field, on the other hand it is quite common to collect redundant data that need to be inspected and selected in a second time.

The third approach is the **video** recording approach. This approach is probably the easiest to adopt on the field, and the factors that can influence it are fewer. In general term, the operator just needs to select the video quality and the frame rate desired and then move freely across the scene. A good option is to maintain a high frame rate, comprehend between 25 and 60 fps. This factor can be useful in a second phase of the process, that will be described in the following sections, when frames are extracted and selected to be used in the photogrammetric approach. Having a higher number of frames per second can clearly grant a higher choice in this subsequent phase. Equally to the still images and time lapse mode, also in the video approach the same issues connected to the lighting of the scene, presence of people or moving objects, etc. need to be considered. Concerning this issue,

the high frame rate of the video can again be a good solution: the possibility of record blurry images is reduced (also because in general terms algorithms for video stabilisation are embedded in COTS 360 cameras) and moving objects can be eliminated thanks to the higher number of frames available.

All this factor considered, it is clear that the acquisition of data on the field need to be carefully projected also when using 360 systems. This is particularly important when working with the time lapse and video modalities that requires the operator to move across the scene and that are performed in a limited amount of time. During the acquisition several factors need to be considered when projecting the path to follow when moving across the scene. First of all, the object to sensors distance must be maintained as constant as possible, in order to achieve a coherent GSD across all the area to survey. In the case of time lapse and video mode the operator has less control over the distance between camera stations during the acquisition phase, but this issue can be solved in the pre-processing phase when, thanks to the redundant data generally acquired from these systems, it is possible to set up the desired distance between one camera and the following one. Secondly, the intrinsic characteristics of the sensors composing the 360 system need to be considered: these systems are generally composed from wide angle/fisheye lenses that produce different degrees of distortion across the sensor's area. Generally, the radial distortion is the predominant element and is increasing in the exterior edges of the sensor. Due to the fact that, as reported in section 3.5.4, spherical images are derived from the stitching of these sensors' images it is important to consider this element during the acquisition. The fact that the portions of the scene that will be recorder only from the exterior part of the sensors may present some error related with the sensors intrinsic characteristics need to be taken into account during the acquisition phase on the field.

Finally, the configuration of the network of camera stations is another important element that need to be considered while projecting the path to follow during the acquisitions. The test performed in this work have underlined that a good network of camera stations, with an overall good rigidity in terms of connection between different cameras, can enhance the photogrammetric process. Performing circular acquisition, with the aim of having the starting and ending point of the path in the same position is a good strategy to reduce some effects that can affect the orientation phase of the cameras and improve the connections between the different camera stations. Some examples of this scheme of acquisition are reported in the following Figure 135.

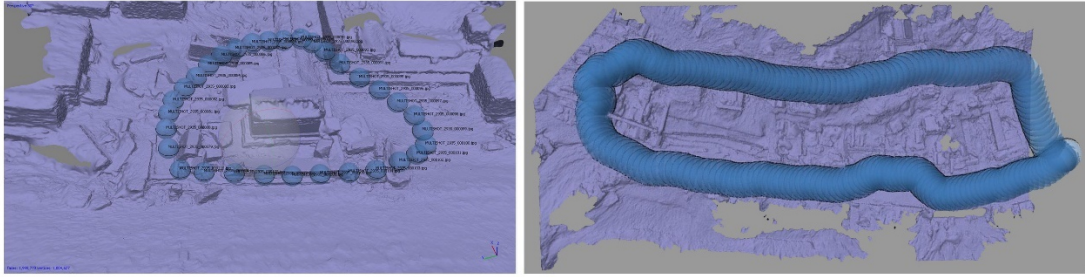


*Figure 135 Examples of “circular” acquisition performed with 360 systems*

### **4.3.2 Processing of data derived from 360 systems. To stitch or not to stitch? That’s the question.**

The first question related with the processing of data derived with 360 systems is whether it is better to work with the single images/videos or with the stitched 360 images. The choice of the modality that will be adopted will eventually influence all the processing pipeline that will be followed. Answering to this question it is not always easy and the choice is related with different factors. It is possible to say that it mainly depends on the specifications of the system employed. The two systems employed in this thesis have different characteristics and are thus a good example for the two different possible approaches to follow. After some tests and analyses it was decided to treat the data derived from the Freedom 360 individually for each camera and the data derived from the GoPro Fusion as stitched panorama.

The main issue with the Freedom 360 is connected with the stitching of the data recorded from the six action cameras into single spherical products, despite the attempt of improving the stitching process with the strategy exploited in section 4.2.6 it is quite difficult and time consuming to obtain good spherical products. This issue is related both with software and hardware aspects. From the software side the database of cameras implemented in the adopted solutions for the stitching is not complete enough to work with these data, while from the hardware side the adopted rig presents some manufacturing problems that complicate the generation of the spherical product. The strategy set up and tested allowed to improve the overall quality of the stitched products, however with a high cost in terms of time and manual intervention of the operator in the correction of these issues.

On the other hand, the GoPro Fusion represent the opposite situation: the images acquired from the two cameras separately considered need to be treated from the operator if used individually, due to the fact that they are automatically post processed in the dedicated stitching solution of GoPro during the generation of the spherical products, especially from the radiometric point of view. Moreover, the overall quality of the spherical products derived following the almost automatic process implemented in the GoPro Fusion Studio

software is generally providing good results. The processing of the data derived from the two cameras is thus highly time consuming and the adoption of software solution different from the one provided by GoPro is often delivering products under the expected quality. All these factors considered it was decided to process the data derived from the two systems following the two separated approaches described below.

The data of the Freedom 360 were processed separately for each camera and particular attention was dedicated to the estimation of the I.O. parameters of each sensor. The approach already described in section 4.2.6 was adopted in all the tests that were finalised with this system: the strategy of modifying the information embedded in the exif file to achieve a good degree of accuracy in the estimation of I.O. parameters for each cameras was adopted. This solution allows to achieve good results in the photogrammetric process and will be further described in the tests that will be presented.

Instead, the data derived from the GoPro Fusion were processed through the spherical photogrammetry approach. As reported above, this choice was sustained in particular from the overall good quality of the spherical products derived from the stitching pipeline embedded in the GoPro software solution. The processing of this type of data using an SfM approach presents some challenges as partially reported in section 3.6 and as will be further detailed in the tests that will be presented hereafter.

A general problem when working with 360 products is related with the presence in the acquired data of undesired elements, in respect to traditional photogrammetry with frame cameras. The first element of this kind is the operator that is carrying the system across the scene and is thus captured in every recorded frame. The second element that is more impacting if compared with traditional acquisitions is the background of the scene, the sky or other natural elements are frequently recorded from these systems due to the large field of view of the single cameras. These elements can often create some perturbation in the photogrammetric process, e.g. in the phase of TPs extraction they can create some outliers that can sometimes have a bad impact also on the overall estimation of cameras position and orientation. The most common solution to solve this kind of problem is through the creation of masks on the images used in the photogrammetric software, allowing to exclude the areas that can create issues. This is quite a time-consuming operation that is generally achieved manually by the operator and is probably the weakest point in the use of these systems in a photogrammetric pipeline.

### 4.3.3 Analyses and comparisons between acquisitions performed in time lapse and video mode. Validation of these approaches on four different datasets.

Among the three acquisitions strategies that were previously described, tests on the two archaeological sites selected were performed only on the time lapse and video modalities. The acquisition of still images was not adopted in the tests performed in this research due to the fact that this approach can nullify one of the main points of strength of these kind of systems for the documentation of CH, their rapidity of deployment on the field: i.e. the rapid mapping approach adopted in this research. Both the Freedom 360 and the GoPro Fusion were thus tested adopting these approaches. The Freedom 360 was tested in the site of Rocca San Silvestro while the GoPro Fusion were used to perform some acquisitions in the Northern Necropolis of Hierapolis.

#### Dataset 1. Time lapse strategy with Freedom 360. Rocca San Silvestro

The time lapse strategy with the Freedom 360 was adopted in the 2017 campaign at Rocca San Silvestro. The system was used to record part of the small medieval church of the village, Figure 136.

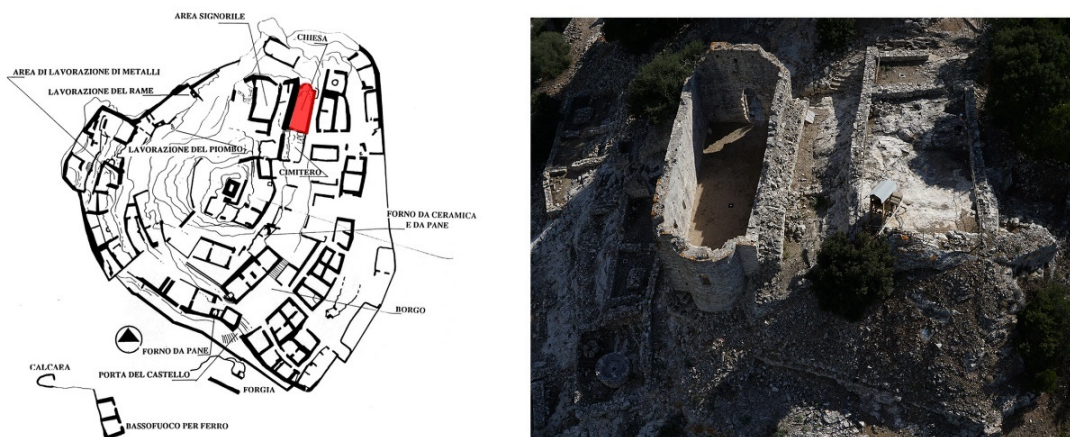


*Figure 136 Rocca San Silvestro, the medieval church. Position of the church on a general plan of the site (left – source: Francovich & Dallai, 2010) and an aerial image of the church in 2016*

The six GoPro Hero 4 were configured with the same set of parameters: resolution was set to 12MP, FoV to wide and shooting interval at 1 second between one image and the following. The rig was mounted on a carbon fibre monopod and cameras were then manually started, so they are not synchronised. The system mounted on the monopod was then carried across the area from the operator, an example of the positions of camera stations computed with the photogrammetric approach is reported in the following Figure 137.

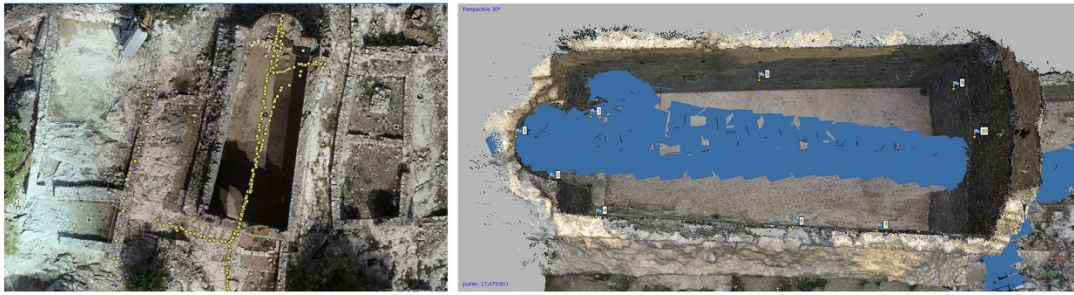


**Figure 137** Rocca San Silvestro, dataset 1. Acquisition scheme of the data collected in time lapse mode with the Freedom 360. Camera stations showed on an extract of the UAV's orthophoto (left) and on the 3D model in the photogrammetric software (right)

In a first time the collected data were processed with the metadata embedded in the original exif file of the cameras. This solution let the photogrammetric software, in this case Agisoft Photoscan, to compute the I.O. parameters of the six cameras as they were exactly the same. Adopting this approach led to a poor estimation of I.O. parameters and thus to a bad resolution of the TPs extraction and camera orientation phase.

The different characteristics of the six cameras have been already analysed before and a strategy to solve this problem have been proposed, this strategy have been adopted also in the processing of this dataset. The exif information embedded in the images were thus modified for all the six cameras, changing the information related to the camera model field, the process was then repeated. The main parameters of the processing of this dataset, after the exif modification are reported in the following Table 41. To validate the metric accuracy of the photogrammetric process a set of control points was used; the acquisitions with the Freedom 360 were performed in the 2017, thus during this field campaign control points were not measured in this area. To overcome this issue a TLS dataset acquired in 2016 was used: the coordinates of natural features were extracted from the dataset and used to solve the E.O. of the photogrammetric block, a total of 10 points were used (5 GCPs and 5CPs).

| Dataset 1. Freedom 360 – Time lapse approach |                            |              |         |           |          |
|--|----------------------------|--------------|---------|-----------|----------|
| Aligned images                               | Re-projection error (mean) | GSD (cm/pix) | TPs N°  | GCPs RMSe | CPs RMSe |
| Modified exif                                |                            |              |         |           |          |
| 355/356                                      | 2,11 pix                   | 1,6          | 163.106 | 0,010 m   | 0,024 m  |

**Table 41** Rocca San Silvestro, dataset 1. Processing parameters after the exif modification

As is possible to notice from the data reported in Table 41 the strategy of exif modification was able to guarantee the overall accuracy of the photogrammetric process, leading to the expected RMSe value on the control points for these kinds of sensors (Balletti et al., 2014). Considering the fact that the use of these sensors for the documentation of CH has been a topic of interest in recent years (Balletti et al., 2014; Kossieris et al., 2017; Teo, 2015), it

was decided to perform a comparison of this dataset with another one acquired with a DSLR camera. In the 2016 campaign at Rocca San Silvestro a set of acquisitions was carried out with a Canon EOS 5D Mark II equipped with a 24 mm lens. One of the datasets, composed by 396 images, was focused on the church and was processed with the same set of control points used for the Freedom 360 set; the main parameters of the processing of this dataset are reported in the following Table 42. The two datasets were processed adopting the same parameters.

| <b>Rocca San Silvestro, CRP 2017 datasets</b> |                                  |                     |                      |                     |                              |
|---|----------------------------------|---------------------|----------------------|---------------------|------------------------------|
| <b>N° images</b>                              | <b>Reprojection error (mean)</b> | <b>GSD (cm/pix)</b> | <b>RMSe GCPs (m)</b> | <b>RMSe CPs (m)</b> | <b>Sparse cloud (TPs) N°</b> |
| 396   | 0,66 pix                         | 0,7                 | 0,008                | 0,014               | 916.939                      |

*Table 42 Rocca San Silvestro, processing parameters of the CRP set acquired with the Canon EOS 5D Mark II*

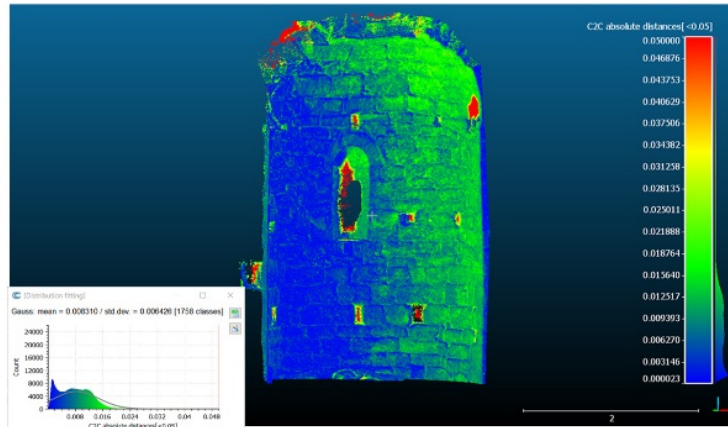
This dataset was acquired with a frame camera and adopting a traditional photogrammetric approach and is of particular interest due to fact that the acquisition was performed maintaining an object to sensor distance comparable with the one used in the case of the Freedom 360 allowing to evaluate the two datasets together. The CRP dataset was able to guarantee a lower GSD, half the one granted by the Freedom 360, thanks to the bigger sensor size of the DSLR. It is interesting to notice that, with this camera-lens configuration, the traditional CRP required almost the same number of images of the time-lapse acquisition. The accuracy of the two datasets is similar, with a slightly better performance of the DSLR. However, the Freedom 360 is definitely gaining the upper hand in term of time needed for the acquisition: the traditional acquisition with the DSLR required 30 minutes, while the acquisition of the area of the church with the Freedom 360 was achieved in less than 5 minutes.

After these considerations, an overall evaluation of the geometrical reconstruction provided by the two approaches was completed. Thus, the TLS dataset previously cited was also used to perform some C2C analyses on the two photogrammetric cloud, to assess the overall quality of the reconstruction. Among the different acquisitions performed on the field seven scans interested the area of the church and were thus selected and processed using the approach already described in section 4.1.2. The parameters of the processing of the TLS dataset are reported in the following Table 43.

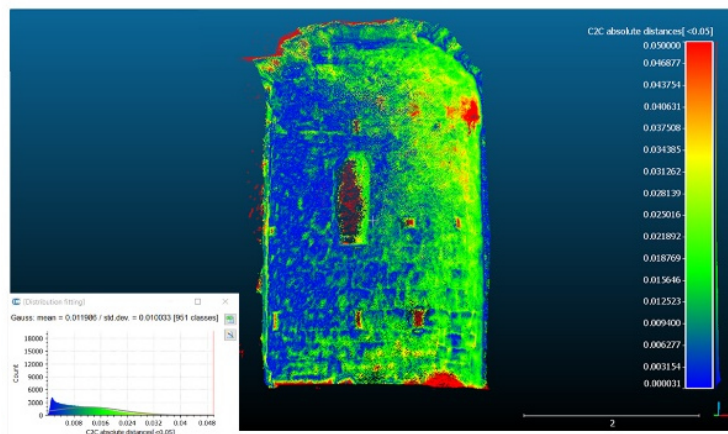
| <b>N° of scans</b> | <b>Cloud to cloud</b>                      |  | <b>Target based</b>                    |                                |
|--------------------|--|--|--|--------------------------------|
|                    | <b>Average tension on scan points (mm)</b> | <b>Average tension on scan points (&lt;4 mm)</b> | <b>Average tension on targets (mm)</b> | <b>Standard deviation (mm)</b> |
| 7                  | 2,8  | 64,7 %   | 6,6                                    | 3,91                           |

*Table 43 Rocca San Silvestro – church, accuracy of the TLS processing*

The portion of the model encompassing the apse of the church was then segmented in the two photogrammetric cloud and in the laser cloud. The TLS dataset was used as ground truth and both the photogrammetric cloud were the element analysed. This analysis was achieved in the CloudCompare software using the C2C distance tool and the maximum research distance was set to 0,05 m. A graphical representation of this analyses is showed in Figure 138.



**C2C analysis - TLS/CRP**



**C2C analysis - TLS/360**

*Figure 138 Rocca San Silvestro, graphical representation of the C2C distance analysis on the two photogrammetric datasets of the church compared with the TLS dataset*

A first qualitative analysis on these two representations is already able to provide some considerations on the overall performances of the two sensors: it is clear how the traditional CRP dataset is able to derive a 3D model closer to the one resulting from the TLS dataset. On the other hand, the 360 dataset present more deviation from the laser model and the overall noise is higher. It is also worth noticing that both the model underlines an area where the major deviations are concentrated (the left part of the apse), this is probably related with the characteristics of the laser dataset, but that the deviation on the 360 model are located also on other portions of the apse. A statistical analysis on the distribution of

the computed values for this analysis is reported in the following Table 44; three different thresholds were considered.

| Model   | Points<0,03 m | Points<0,01 m | Points<0,005m |
|---------|---------------|---------------|---------------|
| TLS/CRP | 98%           | 66,2%         | 34,4%         |
| TLS/360 | 96%           | 52%           | 29,2%         |

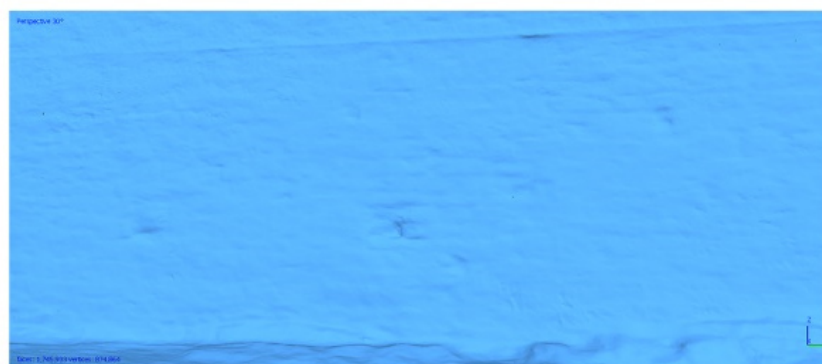
*Table 44 Rocca San Silvestro, mean values of the C2C distance analysis on the two photogrammetric datasets of the church compared with the TLS dataset*

These data confirm the considerations derived from the first qualitative analysis, underlining, as expected, a slightly better performance of the CRP dataset. However, the results achievable with the 360 dataset are definitely comparable, outlining the overall good performances of this system. It is also worth mentioning again that, while in the laser dataset codified target were used as control points, in the two photogrammetric dataset the control points were constitute from natural features; this factor is obviously affecting the overall metric accuracy of the photogrammetric processing.

Moreover, a qualitative analysis was also achieved on other two products derived from the photogrammetric datasets: the 3D continuous model and the orthophoto of one of the façades of the church. In the case of the 3D continuous model the difference between the CRP and 360 dataset is evident, as showed in Figure 139.



**3D polygonal model - CRP dataset**



**3D polygonal model - 360 dataset**

*Figure 139 Rocca San Silvestro, view of a portion of the 3D polygonal model derived from the two photogrammetric datasets*

Being the polygonal model derived from the dense clouds of the two datasets and considering that the densification process was able to generate more than the double number of points in the CRP photogrammetry the quality of the derivable mesh is easily explained. The mesh of the CRP dataset is more detailed and is able to represent all the features of the masonry composing the wall while the one the 360 dataset is significantly more smoothed, representing only the main geometrical features of the wall.

In the case of the orthoimages generated from the two dataset the differences between the two datasets is less marked. The resolution of the two images is similar, except for the radiometric contents, and both the dataset are able to provide a high detail of the masonry and its radiometric contents. However, it is clear in this case that the DSLR dataset is providing a better description of the radiometric contents of the recorded scene, gaining the upper hand in comparison with the 360 dataset. This issue is derived from the environmental conditions in which the acquisition was performed but is also ascribable to the sensors specifications; that are higher in case of DSLR. An extract of the two generated orthoimages of the west wall of the church is reported in the following Figure 140.



**Extract of orthoimage - CRP dataset**



**Extract of orthoimage - 360 dataset**

*Figure 140 Rocca San Silvestro, view of a portion of the orthophoto derived from the two photogrammetric datasets*

A more detailed analysis of the complete orthophoto of the west wall of the church and its use for archaeological researches will be reported in section 4.3.5.

## **Dataset 2. Video strategy with Freedom 360. Rocca San Silvestro**

In the site of Rocca San Silvestro, the Freedom 360 was used also testing the video strategy, as previously reported for the time lapse approach the start of the acquisition also in this case is manually launched by the operator that need to activate each of the six cameras independently. Even these acquisitions were achieved using a carbon fibre monopod that was handled by the operator while moving on the principal touristic paths present on the site. This modality of acquisition was tested on the southern part of Rocca San Silvestro, just after the main entrance of the castle, as reported in Figure 141.

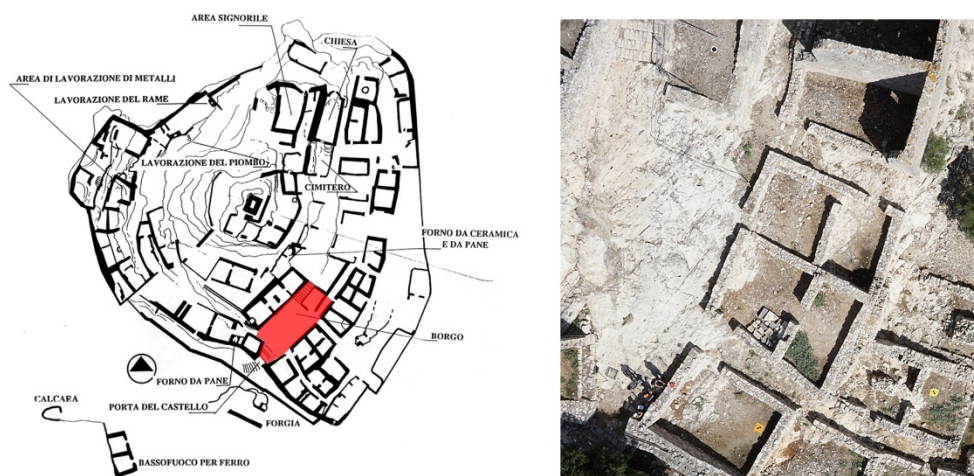


*Figure 141 Rocca San Silvestro, entrance of the site. Position on a general plan of the site (left – source: Francovich & Dallai, 2010) and an image of the area in 2016*

The videos were acquired with a resolution of 1920x1440 and 60 fps for a total length of around 15 minutes for each video.

A preliminary operation is thus necessary to synchronise all cameras together. This operation was completed using Autopano Video Pro (version 2.5.2) software by Kolor that allows to synchronise the videos following two main approaches: the first based on sound recognition and the second on motion recognition. A third approach allows to synchronize the dataset using a flash, but it was not functional in this case due to the fact that the acquisitions were performed during daytime and the sunlight is highly affecting the performances of this approach. All these approaches work in a similar way, attempting to recognize the same feature (produced by the operator during the recording phase) in all the six videos. In this case both the motion and sound approaches were completed and the sound-based one was the one producing the best results and was thus adopted. After this phase it was necessary to extract a set of frames from each video in order to use them in

the photogrammetric pipeline (Teo, 2015). Frames were thus automatically extracted for each camera selecting one frame each 60 frames, corresponding to 1 frame per second. The following phase is thus connected with the selection of the frames to use in the photogrammetric approach. This part of the work was performed manually and required a certain amount of time. The frames that have recorded this area were then selected from each camera and imported in Agisoft Photoscan: out of all the images derived from the six cameras only 210 were selected to be used in the photogrammetric approach. The processing parameters of this dataset are reported in Table 45. In this area codified control points were placed and measured in the 2017 campaign and were thus available for the photogrammetric processing. The orientation phase of this dataset is also influenced by the geometry of the acquisition and by the conformation of the area. Compared to dataset 1, the acquisition geometry was in this case weaker, due to the fact that a linear one-way acquisition was performed (Figure 142).



*Figure 142 Rocca San Silvestro, dataset 2. Acquisition scheme of the data collected in video mode with the Freedom 360. Camera stations showed on an extract of the UAVs orthophoto (left) and on the 3D model in the photogrammetric software (right)*

Moreover, the area recorded is composed by archaeological remains with a lower height compared to the church, providing features that are more difficult to approach, recognize and extract in the photogrammetric workflow.

| Dataset 2. Freedom 360 – Video Approach |         |              |           |                                    |          |                                   |
|---|---------|--------------|-----------|------------------------------------|----------|-----------------------------------|
| Aligned images                          | TPs N°  | GSD (cm/pix) | GCPs RMSe | Re-projection error on GCPs (mean) | CPs RMSe | Re-projection error on CPs (mean) |
| Modified exif                           |         |              |           |                                    |          |                                   |
| 210/210                                 | 170.719 | 0,4          | 0,006 mm  | 0,3 pix                            | 0,015 mm | 0,3 pix                           |

*Table 45 Rocca San Silvestro, dataset 2. Processing parameters on the modified exif dataset*

It is clear how also in this case the exif modification is influencing the overall quality of the photogrammetric process. With the native exif it was almost impossible to perform the

first step of the photogrammetric processing, while the exif modification is leading to a good metric accuracy of the overall process. In the 2017 campaign this area was acquired also with a TLS acquisition using a Faro Focus X 120 and codified markers were placed and measured across the area. The parameters for the processing of the TLS set in this area are reported in Table 46.

| N° of scans | Cloud to cloud                      |  | Target based                    |                         |
|-------------|-------------------------------------|--|---------------------------------|-------------------------|
|             | Average tension on scan points (mm) | Average tension on scan points (<4 mm) | Average tension on targets (mm) | Standard deviation (mm) |
| 3           | 4,3                                 | 50 %                                   | 12 mm                           | 7,44                    |

*Table 46 Rocca San Silvestro – south area, accuracy of the TLS processing*

The point cloud derived from the photogrammetric approach was thus validated using the TLS dataset as ground truth. A portion of the area acquired in dataset 2 was segmented both in the photogrammetric and laser dataset and further analyses were achieved. A C2C analysis was performed in CloudCompare software and the results are graphically represented in Figure 143.

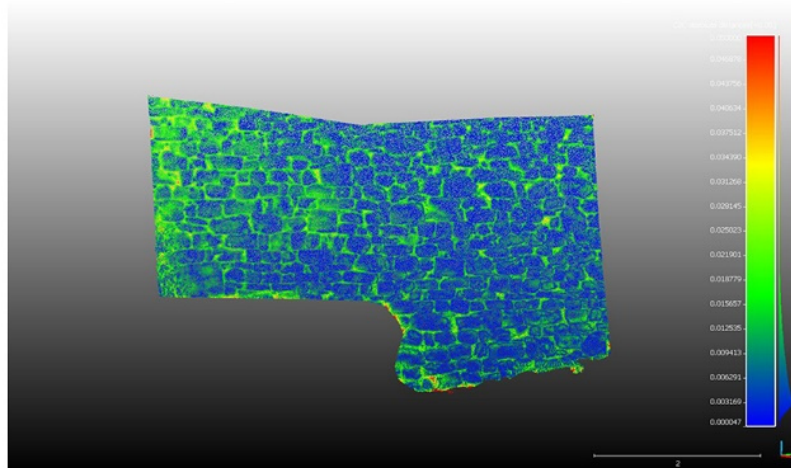


*Figure 143 C2C analysis between the TLS and photogrammetric dataset*

The performances of the photogrammetric cloud are quite good if compared with the TLS dataset: the 50% of points present a deviation of 0,005 m from the laser dataset, if we set the threshold to 0,01 m the percentage is of 74 %. These values confirm the overall good results achieved with this approach that is valid both from a metric and geometric point of view.

### **Dataset 3. Time lapse strategy with GoPro Fusion. Northern Necropolis Hierapolis**

The time lapse strategy was experimented also with the GoPro Fusion in the 2018 campaign in the archaeological site of Hierapolis. With this camera it is possible to set an interval

between one spherical acquisition and the following, as it was possible to do for the six cameras of the Freedom 360. However, this solution is more refined because the two cameras are controlled from the electronic components embedded in the system that is able to guarantee that the capture time of the two images is synchronized. The images resolution was set to the maximum value allowed by the system (18 MP, 9 MP for each of the two cameras composing the system) and the Fusion was used to record a portion of the Northern Necropolis of the Turkish site, that was under investigation from the Italian archaeological Mission. The camera was mounted on a small multipurpose tripod that can be handled by the operator, the shooting interval was set at 1 seconds and the path followed during the acquisition, reported in Figure 144, was completed across the area.



*Figure 144 Hierapolis, Northern Necropolis dataset 3. Acquisition scheme of the data collected in time lapse mode with the GoPro Fusion. Camera stations showed on an extract of the UAV's orthophoto (left) and on the 3D model in the photogrammetric software (right)*

The acquisition with this strategy was achieved in 5 minutes and a total of 317 images were acquired, covering an area of  $\approx 8.000 \text{ m}^2$ . A mean acquisition distance from the archaeological structures between 3 and 5 meters was maintained. After the stitching phase, completed in GoPro Fusion Studio, it was decided to apply a downsampling of the dataset, after having evaluated that the overlap between images was enough to sustain this operation. After this operation, 158 images were imported and processed in Agisoft Photoscan, 12 control points were used to evaluate the metric accuracy of the process (6 as GCPs and 6 as CPs); the main parameters of the processing are reported in the following Table 47.

| Dataset 3. GoPro Fusion – Time lapse Approach |              |         |           |                                    |          |                                   |
|---|--------------|---------|-----------|------------------------------------|----------|-----------------------------------|
| Aligned images                                | GSD (cm/pix) | TPs N°  | GCPs RMSe | Re-projection error on GCPs (mean) | CPs RMSe | Re-projection error on CPs (mean) |
| 158/158                                       | 0,47         | 109.930 | 0,021 m   | 0,82 pix                           | 0,024 m  | 0,98 pix                          |

*Table 47 Northern Necropolis, Hierapolis. Dataset 3. Processing parameters of the time lapse dataset*

The data reported confirm the overall good performances of the system: the data collected and processed in the photogrammetric solution outline a good value for the RMSe on both GCPs and CPs, allowing to grant a representation scale of the surveyed scene up to 1:100. The TLS dataset was acquired during the 2018 campaign with a Faro Focus 3D X330 and a wide area of the necropolis was acquired, main parameters of the processing of the laser dataset are reported in the following Table 48.

| N° of scans | Cloud to cloud                      |  | Target based                    |                         |
|-------------|-------------------------------------|--|---------------------------------|-------------------------|
|             | Average tension on scan points (mm) | Average tension on scan points (<4 mm) | Average tension on targets (mm) | Standard deviation (mm) |
| 15          | 2,6                                 | 62,1%                                  | 5,5                             | 4,8                     |

*Table 48 Hierapolis, Northern Necropolis. Accuracy of the TLS processing*

The laser 3D model and the model derived from the processing of dataset 3 were then segmented to encompass a portion of the area including some of the funeral structures. A C2C analysis was then performed in the CloudCompare software (maximum research distance set to 0,1 m), as showed in Figure 145 and reported in Table 49.

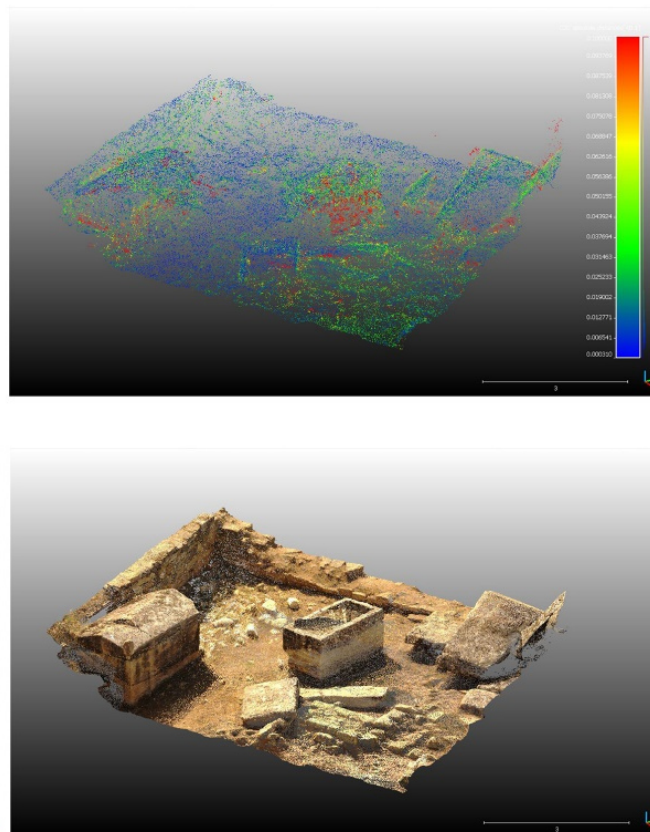


*Figure 145 Hierapolis, Northern Necropolis. C2C analysis (left) between dataset 3 and TLS dataset (right)*

| Model         | Points<0,03 m | Points<0,02m | Points<0,01 m | Points<0,005m |
|---------------|---------------|--------------|---------------|---------------|
| TLS/Dataset 3 | 78,3%         | 64,8%        | 40,5%         | 22,2%         |

*Table 49 Hierapolis, Northern Necropolis. Mean values of the C2C distance analysis on the dataset 3 and the TLS dataset*

Considering the number and resolution of the images processed in the photogrammetric solution adopted the overall deviation of the dataset 3 from the TLS dataset can be considered satisfying: around the 64% of points has a deviation lower than 0,02 m from the TLS reference dataset. The classification of the 360 cloud based on the deviation computed with the C2C distance tool is clearly showing two main aspects connected with the use of these sensors: the low density of the photogrammetric cloud and the presence of a diffused noise. This is connected with the resolution of the images used in the photogrammetric approach and the distortion present in the stitched 360 image that influence the overall process.

Another C2C analysis was achieved on this dataset using as reference cloud the one derived from the UAVs acquisition performed in 2018. The results of this analysis are reported in Figure 146 and Table 50. The aim of this analysis wasn't to validate the 360 dataset using the UAVs one (this operation was already achieved using the TLS dataset), but to underline the main differences between the models derived using two different techniques.

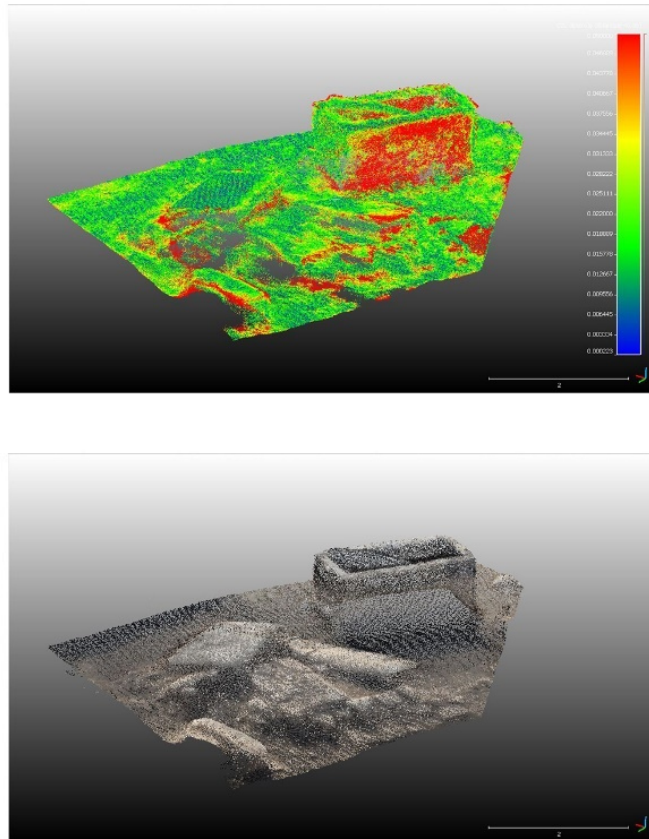


*Figure 146 Hierapolis, Northern Necropolis. C2C analysis (left) between dataset 3 and UAVs 2018 dataset (right)*

| Model          | Points<0,03 m | Points<0,02m | Points<0,01 m | Points<0,005m |
|----------------|---------------|--------------|---------------|---------------|
| UAVs/Dataset 3 | 91,2%         | 80,9%        | 57,3%         | 33,9%         |

*Table 50 Hierapolis, Northern Necropolis. Mean values of the C2C distance analysis on the dataset 3 and the UAVs 2018 dataset*

Some consideration can be reported for this analysis: first, the overall density of the UAVs dataset is more coherent with the 360 dataset compared to the one of the TLS, allowing to avoid a pre-processing of the cloud to complete the analysis. Secondly, it is interesting to underline the good performances of the 360 acquisition in reconstructing both the horizontal and vertical developments of the structures contained on the scene. Moreover, despite the use of oblique images and of a short acquisition distance the UAVs dataset is providing a lower quality on the geometrical reconstruction of the vertical developments of the structures, while the 360 system, thanks to the type of acquisition performed, is achieving good performances.

#### Dataset 4. Video strategy with GoPro Fusion. Northern Necropolis Hierapolis

In the area of the Northern Necropolis the GoPro Fusion was tested also adopting the video approach. The camera was set with the maximum video resolution available (5.2 K, 30 fps) and again mounted on the multipurpose tripod allowing the operator to freely move across the area. The path achieved through the area is similar to the one completed for the time lapse mode as shown in Figure 147. Compared to the time lapse mode this acquisition was slightly more peripheral, encompassing the area of interest without entering on it.



*Figure 147 Hierapolis, Northern Necropolis dataset 4. Acquisition scheme of the data collected in time lapse mode with the GoPro Fusion. Camera stations showed on an extract of the UAV's orthophoto (left) and on the 3D model in the photogrammetric software (right)*

Also in this case a mean acquisition distance from the archaeological structures between 3 and 5 meters was maintained. The time to complete the acquisition was of 3,5 minutes and an area of  $\approx 9.000 \text{ m}^2$  was covered. After the stitching phase a spherical video of around 15 Gb was obtained, confirming that the weight of data in terms of physical space on the hard drive is an issue that need not to be underestimated when working with these systems. Single frames were then extracted from the video selecting one frames each 30 (around 1 frame per second) and a total of 202 frames were extracted to be processed with a photogrammetric approach. The data were processed in Agisoft Photoscan and the main parameters of the processing are reported in the following Table 51.

| Dataset 4. GoPro Fusion – Video Approach |              |         |           |                                    |          |                                   |
|--|--------------|---------|-----------|------------------------------------|----------|-----------------------------------|
| Aligned images                           | GSD (cm/pix) | TPs N°  | GCPs RMSe | Re-projection error on GCPs (mean) | CPs RMSe | Re-projection error on CPs (mean) |
| 202/202                                  | 0,56         | 132.601 | 0,011 m   | 0,11 pix                           | 0,037 m  | 0,09 pix                          |

*Table 51 Northern Necropolis, Hierapolis. Dataset 4. Processing parameters of the video dataset*

Compared to dataset 3 this dataset presents a lower RMSe value on GCPs and a higher on CPs, however the two values are similar. Despite the similarity between the two acquisitions, dataset 4 presents a higher GSD, due to the lower resolution of the frames extracted from the video in respect with the images acquired in time lapse mode.

Similar analyses to the one achieved for dataset 3 were carried out also for dataset 4 using the TLS dataset (Table 48) as ground truth. The images in Figure 148 and the values reported in Table 52 underline a situation similar to the one of dataset 3, with some differences. The issues connected to the density of the point cloud derived from the photogrammetric approach and to the noise present on the model are evident as well, but another problem can be reported: some portions of the scene were not reconstructed in this dataset. This is related with two main factors: the lower resolution of the images and the slightly different acquisition scheme adopted for this dataset.

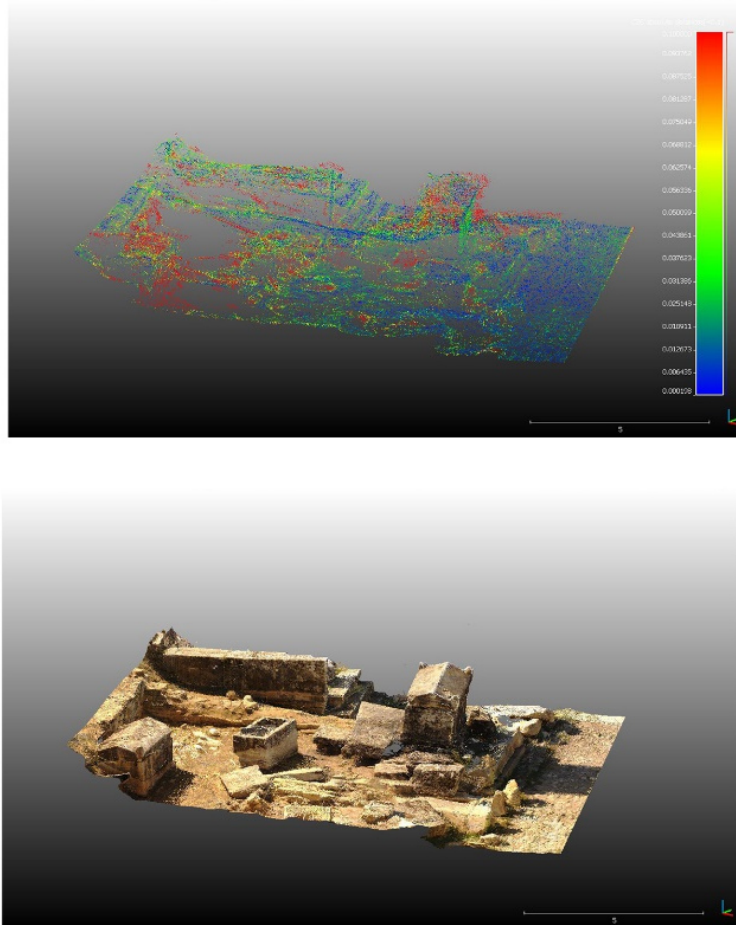


*Figure 148 Hierapolis, Northern Necropolis. C2C analysis (left) between dataset 4 and TLS dataset (right)*

Moreover, it needs to be reported that in general terms dataset 4 is performing a little worst than dataset 3. The overall percentage of points under a preselected threshold is lower in all the four intervals considered if compared with the data computed for dataset 3 (Table 49 and Table 52).

| Model         | Points<0,03 m | Points<0,02m | Points<0,01 m | Points<0,005m |
|---------------|---------------|--------------|---------------|---------------|
| TLS/Dataset 4 | 68,6%         | 54,3%        | 30,8%         | 16%           |

*Table 52 Hierapolis, Northern Necropolis. Mean values of the C2C distance analysis on the dataset 4 and the TLS dataset*

This systematic reduction of the overall quality of the generated 3D model is again related with the resolution of the frames extracted from the video, that were able to generate a less detailed 3D reconstruction.

Some final considerations can be made comparing the acquisition strategies performed in the site of Hierapolis for dataset 3 and 4: the time needed for completing the two acquisitions is similar while the result achievable through the photogrammetric processing of the data are in favour of the time lapse mode. It is possible to say that the time saved adopting the video mode is not worth the reduction of resolution required by this approach. Moreover, the reduction of acquisition distance performed near some archaeological structure in time lapse mode allow to generate a dense cloud able to reconstruct the whole geometry of the object recorded in detail. An example is reported in the following Figure 149 where a set of 30 images of dataset 3, collected around a single tomb of the Northern Necropolis, where able to achieve a complete geometrical reconstruction of the structure.

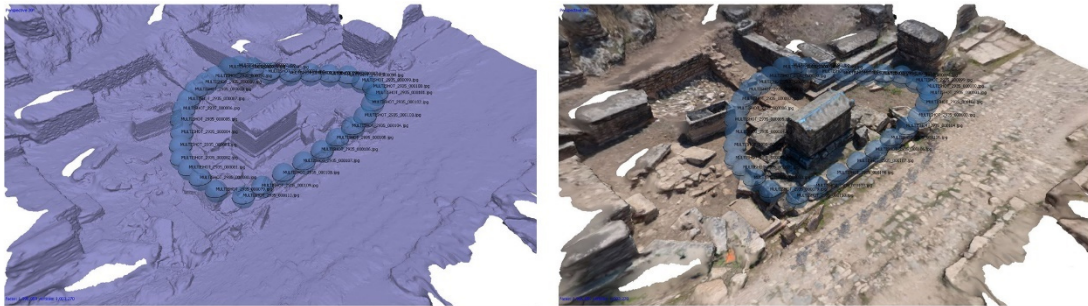


***Figure 149 Hierapolis, Northern Necropolis. Scheme of the acquisition performed around a single tomb with the GoPro Fusion***

These issues considered, the dataset that was further analysed in this work is the number 3, the one acquired with the time lapse approach. The video approach can be a good solution in cases where is not possible for the operator to move at a moderate speed or when the camera is mounted on a vehicle; the stabilisation of the video mode can make the difference in these operative scenarios.

Finally, an issue already reported in section 4.3, need some discussion: the presence of the operator on all the images acquired with the 360 system. If no strategies are adopted to cope with this issue, some major errors can occur in the photogrammetric process. One of the major examples is represented by the aberration that can be present in the orthophoto generated from the data collected with these kinds of systems, as showed in Figure 150.



*Figure 150 Hierapolis, Northern Necropolis. Examples of aberration that can be present on the orthoimage generated from the 360 dataset*

From this figure it is clear how not only the operator, but also its shadow, will be present in the generated orthophoto if no corrections are applied during the processing phase. This issue can be solved adopting two different approaches: creating and applying masks to all the images to exclude the portion of the image that include the operator from the processing or enhancing the generated orthophoto selecting which images use in the blending phase of the portion that present some aberrations.

The first approach is the most time consuming and its fully manual, the operator need to select the area that will be masked in each image. This procedure is however the most efficient, allowing to reduce also the presence of outliers in all the photogrammetric processing phase and not only on the phase of products generation.

On the other hand, the second approach is applied only on the phase of orthophoto generation and allows to remove the major aberrations. In Agisoft Photoscan this type of approach is possible thanks to a tool that is implemented in the software and allow to draw a polygon on the area of the orthoimage that need to be modify and grant the possibility to select which images will be used for that portion. Through this operation it is possible to

select only the part of the images where the operator, its shadows or other undesired elements are not present and remove them from the orthophoto.

#### 4.3.4 Georeferencing Strategies

Similar to the approaches described for the treatment of the UAVs data in section 4.1.2 three main strategies can be identified to solve the E.O. of the photogrammetric block of spherical images: direct georeferencing, use of GCPs and co-registration of datasets.

The **direct georeferencing** of the data collected with more performing systems, such as MMS, is a consolidated approach, and at the same time a strategy still researched, that involves different sensors such as GPS/GNSS or IMU to solve the E.O. phase of the photogrammetric processing. In recent time GPS/GNSS receiver started to be integrated also on COTS and low-cost systems, allowing to start experimenting similar approaches also on these systems, e.g. (Cavegn, Blaser, Nebiker, & Haala, 2018; Gabrlík, Cour-Harbo, Kalvodova, Zalud, & Janata, 2018). Among the two systems tested in this research the GoPro Fusion was the only one where a GPS/GNSS receiver was embedded. However, this approach was not tested in this research.

The use of **GCPs** is probably the most diffused solution adopted also for this type of data. The same recommendations already provided for the use of this approach with UAVs are valid also for spherical data, with a change in the scale of the problem due to the closest acquisition distance used with these systems. The dimension of the target is thus reduced, and their positioning is related with the structure of the scene, e.g. in case of narrow spaces or complex areas the distribution must be denser. Also in this case the positioning and measuring of control points, natural features or target, is probably the most time spending operation on the field.

Finally, the **co-registration** approach was tested also for this kind of datasets. In this case the aim was not to co-register two dataset acquired in different times, but to use an oriented dataset of UAVs images as anchor for a spherical dataset acquired the same day. This approach allows to reduce the time to dedicate to the topographic measurement on the field concentrating the resources only on the measurement of the control points for one dataset and solving the E.O. of the second one through a co-registration.

In the test performed with these 4 datasets the use of control points followed consolidated approaches, similar to the one already described for UAVs data. However, it is important to report some considerations. In dataset 1 the use of natural features as control points allows to reach a good accuracy of the generated model, moreover, the coordinates of the points were extracted from a laser dataset acquired and processed on another field campaign. The good results achievable with this procedure allow to perform acquisitions

with these systems on areas that were previously surveyed with other techniques without the need to measure again some control points. The use of coded target is always the recommended solution, thus if this strategy cannot be pursued it is possible to work with these systems with natural features extracted from other datasets. In the tests performed in this research, the results in terms of accuracy between dataset 1 (where natural features were used) and dataset 2 (where coded target were used) are comparable, as reported in Table 41 and Table 45. In dataset 3 a 4 coded target were used, they were distributed across all the scene surveyed and were measured with TS. This approach requires however some conditions and is not always achievable: first of all, the overall metric quality of the reference dataset must be known and guarantee, secondly well recognizable features between the two datasets must be present and well identifiable. The use of coded target measured with traditional topographic techniques is however the preferable solution, if the time and the resources available on the field are enough to complete these phases.

Another approach consists also in the use of known distances to scale the model generated in the photogrammetric approach, without georeferencing it. This is not a rigorous approach from the methodological point of view, however, it can be used in cases when it is not possible to achieve a complete survey of the area, but a low accuracy model can be useful for preliminary analyses. This approach was not considered in this research.

A **co-registration** approach was tested also on the dataset 3, the aim of this test was to solve the E.O. of the set of images acquired in time lapse mode using an UAVs dataset already processed. The UAVs dataset was acquired few hours before the spherical one and was processed following the standard photogrammetric pipeline; the main characteristics of this dataset have been already described in section 4.1.1 and Table 14. The parameters derived from the processing of this dataset are reported in Table 15.

The spherical images were thus imported in the UAVs processed dataset in Agisoft Photoscan and the aerial images were used as a rigid block to orient the terrestrial acquisition. Two quality checks on the overall accuracy of this approach were then performed: first the coordinates of the camera stations estimated with this approach were compared with the ones estimated following the standard processing of this dataset (Table 47); secondly, similar analysis were achieved using a set of control points. A view of the camera stations of the two datasets is reported in the following Figure 151.

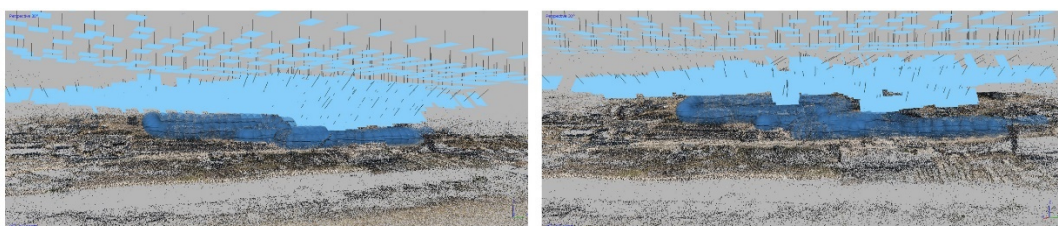


*Figure 151 Hierapolis, Northern Necropolis. Co-registration of dataset 3 with the UAVs acquisition*

For the first analysis the coordinates estimated for all the camera stations were extracted both from the traditional processing performed for dataset 3, both for the processing performed with the co-registration approach. The deviations between these two set of coordinates were evaluated for x,y and z components. The values derived from this analysis are reported in the following Table 53 with in addition the mean value of these deviations and the standard deviation for all the reported parameters analysed.

| Camera stations       |                         |                         |                         |                            |
|-----------------------|-------------------------|-------------------------|-------------------------|----------------------------|
| N° of camera stations | $\Delta X$ (m)          | $\Delta Y$ (m)          | $\Delta Z$ (m)          | Mean $\Delta$ (m)          |
| 158                   | 0,028                   | 0,023                   | 0,017                   | 0,022                      |
|                       | Std.Dev. $\Delta X$ (m) | Std.Dev. $\Delta Y$ (m) | Std.Dev. $\Delta Z$ (m) | Mean Std.Dev. $\Delta$ (m) |
|                       | 0,031                   | 0,015                   | 0,009                   | 0,018                      |

*Table 53 Hierapolis, Northern Necropolis. Co-registration approach, comparison on the coordinates of camera stations estimated with the co-registration approach and with the traditional approach*

As is possible to see from the values reported in the table, the overall estimation of the coordinates of camera stations with the co-registration approach is achieving good results in terms of accuracy. The mean value of the deviation is lower than 0,03 m for all the three components and there are no particular trends to underline. The data derived from this analysis were also represented in a gaussian distribution as reported in Figure 152.

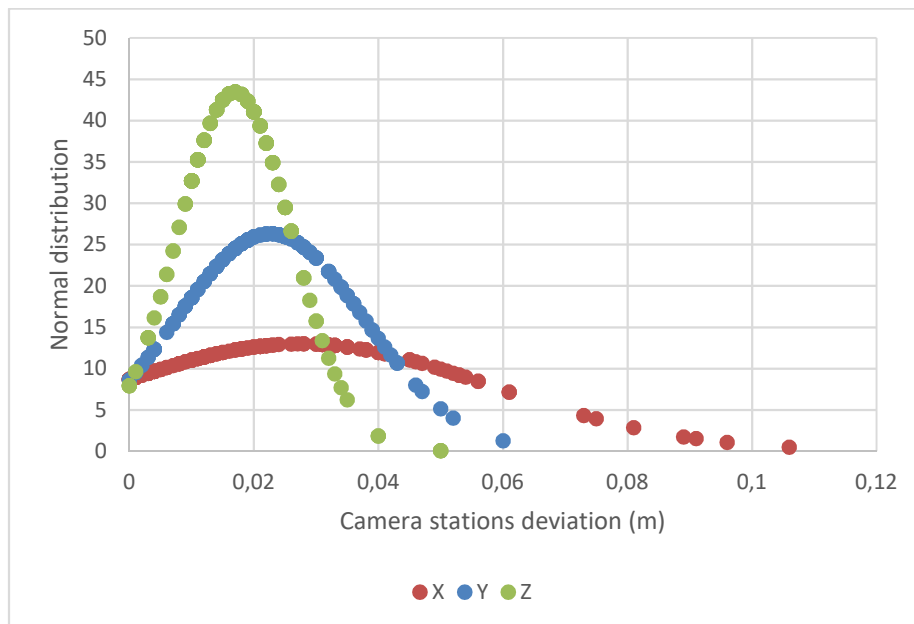


*Figure 152 Graphical representation of the normal distribution of the deviation in the three coordinates components between the camera positions estimated with the co-registration and the traditional approach*

The second analysis was achieved on a set of control points: the reference set of points was the one measured on the field with a TS and used for the processing of the UAVs dataset

while the compared set of points was estimated in the photogrammetric software after the implementation of the co-registration approach (the points were located on the set of oriented images and were computed as manual TPs). The results of this analysis are reported in the following Table 54.

| Control points       |                         |                         |                         |                            |
|----------------------|-------------------------|-------------------------|-------------------------|----------------------------|
| N° of control points | $\Delta X$ (m)          | $\Delta Y$ (m)          | $\Delta Z$ (m)          | Mean $\Delta$ (m)          |
| 8                    | 0,018                   | 0,027                   | 0,064                   | 0,036                      |
|                      | Std.Dev. $\Delta X$ (m) | Std.Dev. $\Delta Y$ (m) | Std.Dev. $\Delta Z$ (m) | Mean Std.Dev. $\Delta$ (m) |
|                      | 0,011                   | 0,028                   | 0,019                   | 0,019                      |

*Table 54 Hierapolis, Northern Necropolis. Co-registration approach, comparison on the coordinates of control points estimated with the co-registration approach and measured on the field*

The analysis of the data reported in this table allow to confirm again the overall accuracy achievable with this approach, it is however possible to add another consideration. Through this analysis is possible to underline a higher error on the deviation verifiable for the z component. This is probably related with the geometry of the acquisitions and the estimation of the I.O. parameters of the cameras, probably the values estimated for the focal length are in this case creating these major deviations on the z components. However, this is an issue that need to be further investigated to identify which elements are causing it. The objective of this tests was to validate the possibility to integrate two multi-sensors acquisitions, one terrestrial and one aerial, in order to enhance the overall operation to perform both in the field, both during the processing phases. Adopting a co-registration approach like the one validated in this section allows the operator to perform on the field the positioning a measuring of a single set of control points. Moreover, the two deployed sensors were used with different acquisition distances, thus is possible to perform also a multiscale approach with these datasets. Needless to say, the phase devoted to the position and measurement of control points is still a crucial and mandatory task that need to be completed on the field, however, it is possible to reduce the time that it requires and limit its impact on the time to spend for the fieldwork.

After the solution of the E.O. task through this approach it is possible to complete the photogrammetric workflow, disabling the UAVs dataset and following the standard pipeline.

### 4.3.5 Use of some of the photogrammetric products derived from the acquisitions performed with spherical systems.

#### Point cloud

The church of Rocca San Silvestro was recorded in two different years, 2016 with the CRP dataset and 2017 with the 360 dataset (number 3). In the time that intercurred between these two acquisitions major archaeological and restoration works were completed on the site (Arrighetti, 2017). The church was also involved in these works, the floor was excavated to investigate the archaeological features beneath it and then a new floor was created to substitute the original one. This operation was mainly achieved for two main reasons: to complete some structural interventions and improve the outflow of rainwaters. The data collected with the two different approaches allows to represent this operation. The point cloud derived from the 2016 CRP dataset was used as reference elements and the 2017 derived from the 360 dataset was the element compared. This analysis was achieved in the CloudCompare software where the C2C distance tool was used to compare the two datasets (max distance of research was set to 0,2 m). In Figure 153 is possible to see an extract of the two orthophotos generated with the photogrammetric approach, while in Figure 154 the analysis performed in CloudCompare is reported.



*Figure 153 Rocca San Silvestro, a portion of the church's floor in 2016 (left) and 2017 (right)*

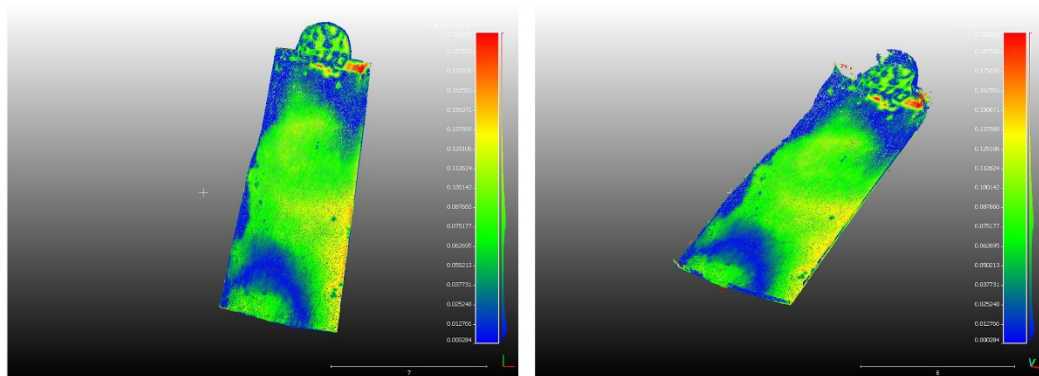
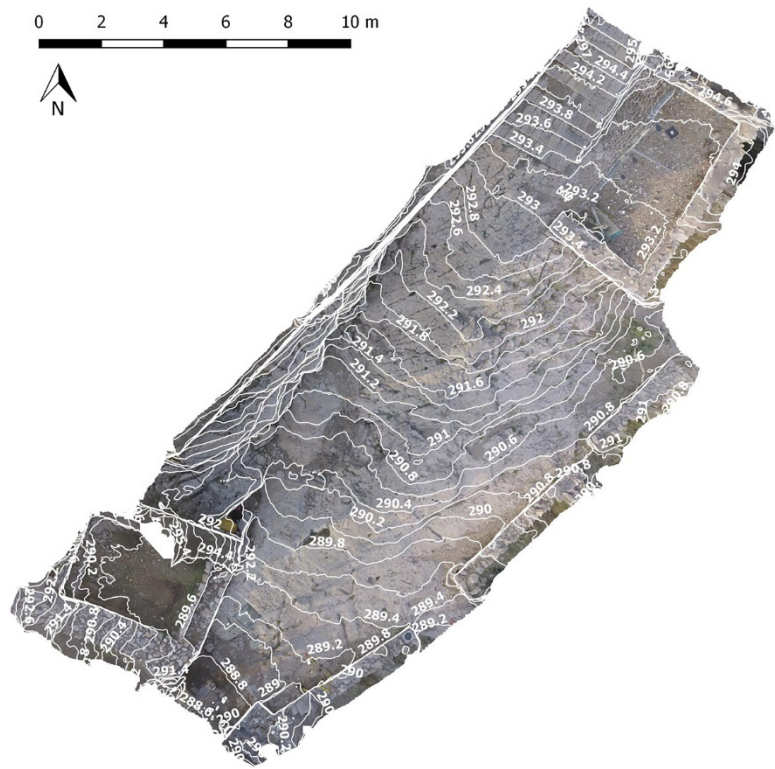


*Figure 154 Rocca San Silvestro. C2C analysis between CRP (2016) and 360 dataset (2017)*

This analysis allows to underline were the major changes between the original level of the floor and the level of the new floor created after the archaeological excavation.

### **DSM**

The DSM derived from the photogrammetric process were used to perform some analyses in a GIS environment. In the case of dataset 1 some analyses were performed to evaluate if the estimation of the flow of rainwater achievable from the data derived from these systems can be an instrument useful for the experts that are in charge of evaluating how it can affect the conservation of the archaeological remains. The analysis was performed both with some standard tool for the raster analysis, both testing some more advanced tools dedicated to hydrogeological analyses. For the latter both Qgis and ArcGis software were used, due to the fact that they can produce different outputs, while for the other analyses the Qgis software was used. The first step of this processing was dedicated to the automatic extraction of contour line from the DSM. The threshold for contour line extraction was set to 0,20 m and the results of the processing are reported in the following Figure 155, as is possible to notice the contour lines are represented both on the orthophoto and both on a shaded representation of the DSM.



The second analysis performed was focused on the slope analysis, performed on the DSM, the results of this analysis are reported in the following Figure 156.

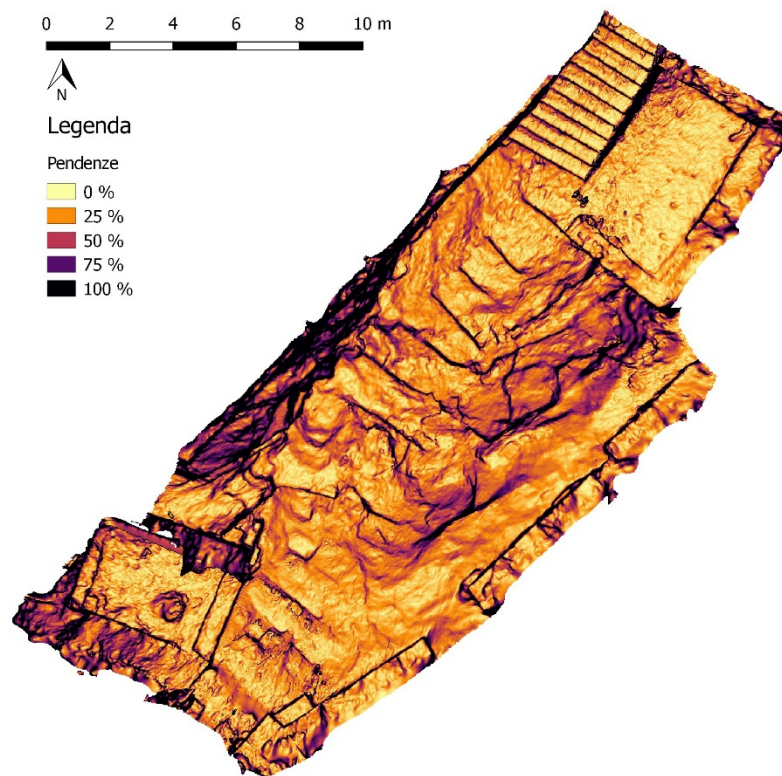


*Figure 156 Rocca San Silvestro, dataset 2. Slope analysis performed on the DSM.*

In the previous image the slope of the area is represented in scalar colours and the inclination is expressed in percentages. From this analysis it is clear how the slopes are developing from the southern part of the area to the northern, with also a growth of the slope inclination on the east part. After this analysis, it was decided to experiment some of the tools and algorithms implemented in the two GIS software for hydrogeological analyses to evaluate the impact of the rainfall on the area and eventually to analyse the surface runoff and its impact on the archaeological structures.

These tools and algorithms are projected to be used on a territorial scale, however it is possible to use them also on a more detailed scale like the one of dataset 2.

The first step, necessary to complete the following hydrological analysis, is the flow direction computation (Garbrecht & Martz, 1997; Spanò & Guardini, 2012; Tarboton, 1997). The output of this tool is a raster representing the flow direction of each cell to its downslope neighbour or neighbours. The eight-node method (D8) was used in this case (Siqueira, et al., 2016), it models the flow direction from each cell to its steepest downslope neighbour, as showed in Figure 157.

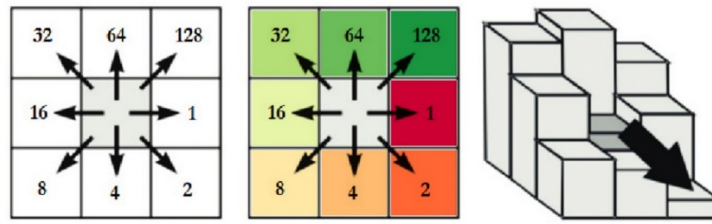


*Figure 157 D8 method coding to identify flow direction (left), codification used in this research (centre), schematic representation of the method process of flow direction assignment (right). Source: (elaborated from: Siqueira, et al., 2016)*

This algorithm was used to calculate the flow direction in dataset 2, the output of this computation is reported in the following Figure 158.

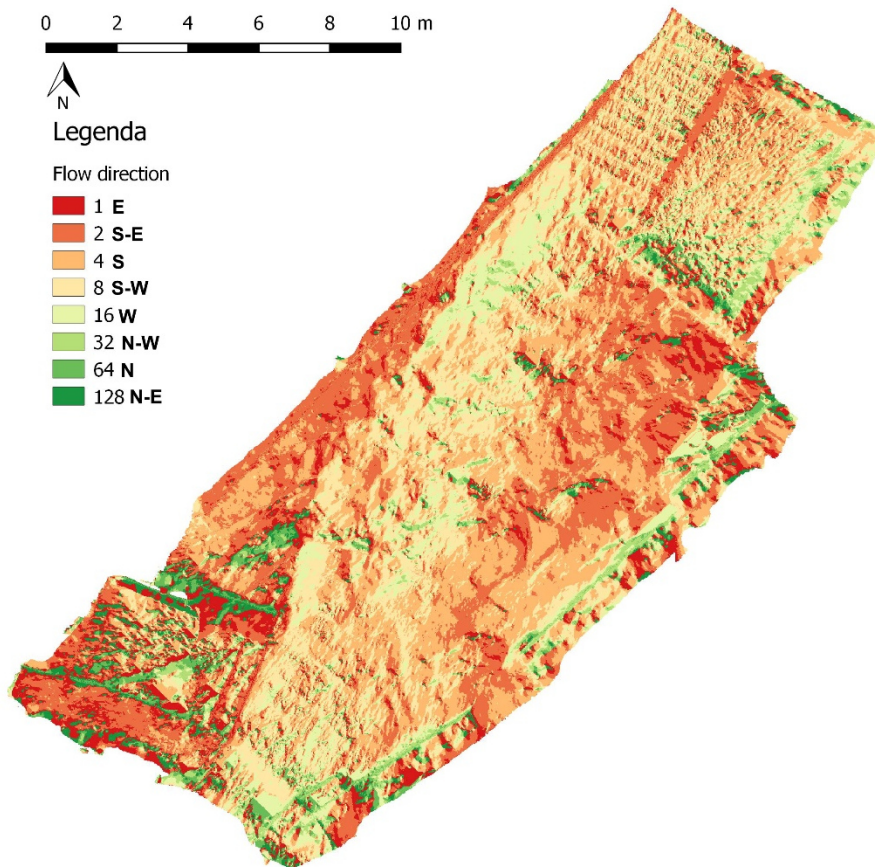


*Figure 158 Rocca San Silvestro, dataset 2. Flow direction analysis computed with the D8 method.*

This analysis provides a first indication on the major flow direction connected to the morphology of the area analysed, however it is possible to further process the dataset starting from these first results.

Applying the flow accumulation tool it is possible to calculate the value of accumulated flow for each cell (Jenson & Domingue, 1988); a schematic representation of how this algorithms works is reported in the following Figure 159.

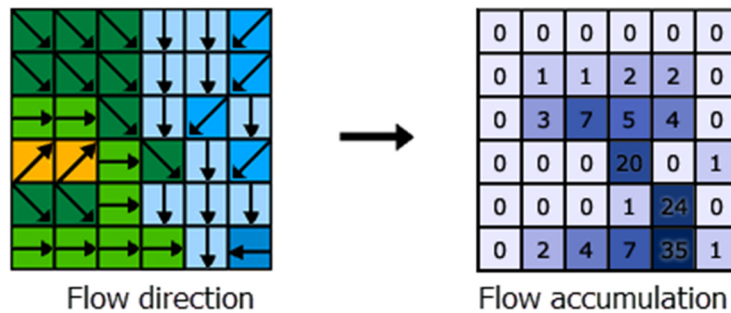


Figure 159 Flow accumulation computation method. Source: (<http://pro.arcgis.com>)

These analyses can be detailed and expanded in several different directions, in this case the watershed, upslope area that contribute to the water flow, were also computed starting from the DSM and the computed flow directions; results of this analysis are reported in the following Figure 160. This analysis is underlining the different watershed present in this area and how they contribute to the waterflow in the different streams.

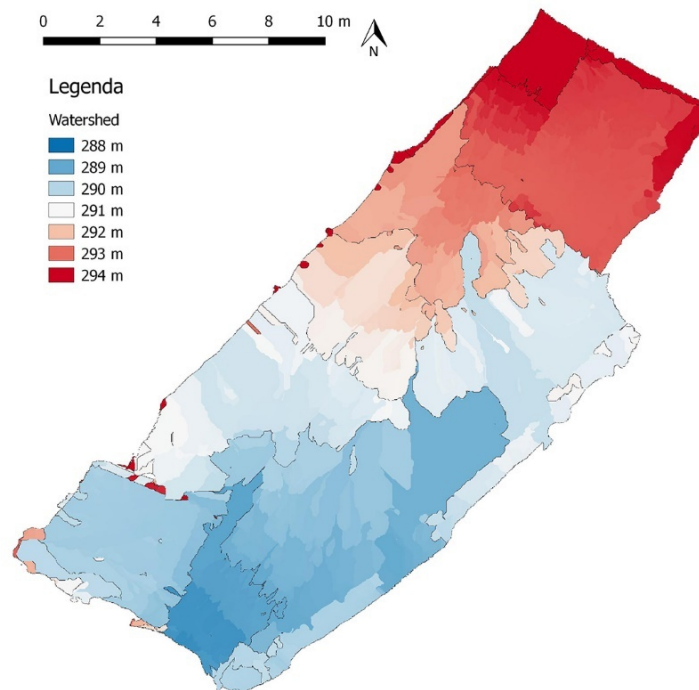
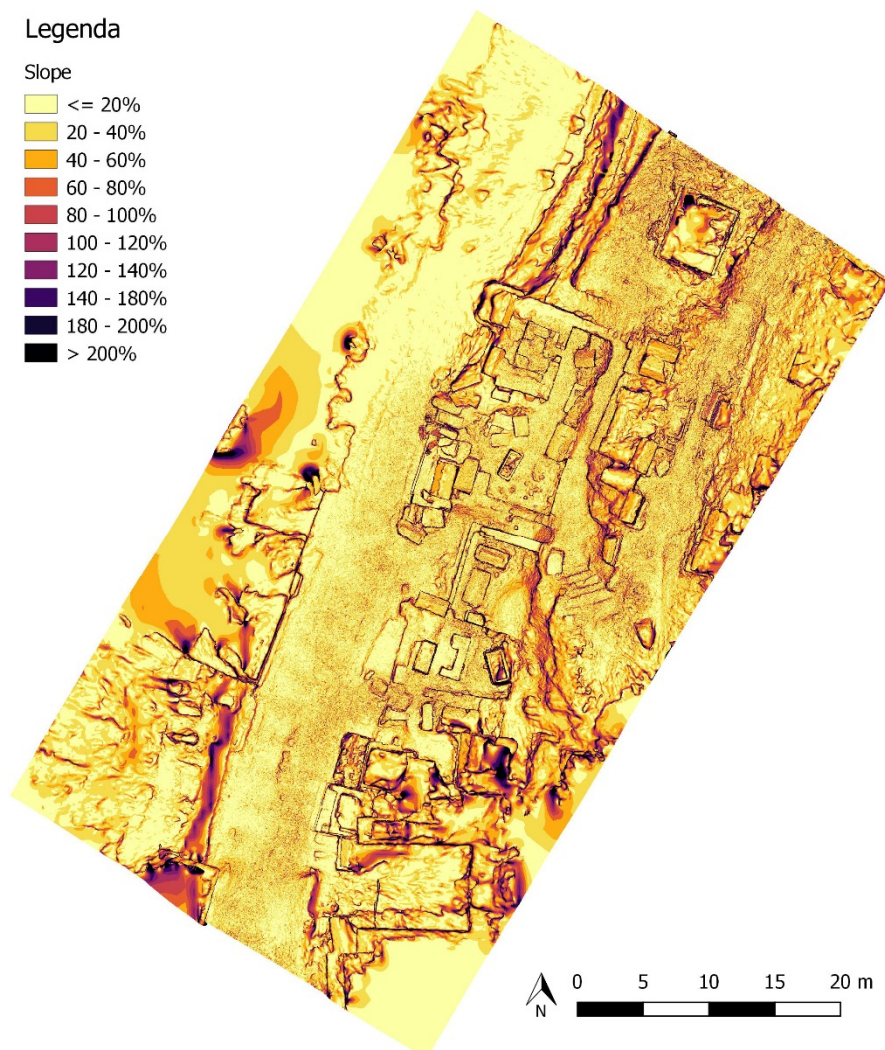


Figure 160 Rocca San Silvestro, dataset 2. Watersheds (top) and the related stream network (down)

All the analyses presented can represent an useful tool for the management of an archaeological site, especially for restoration and conservation purposes. Knowing the

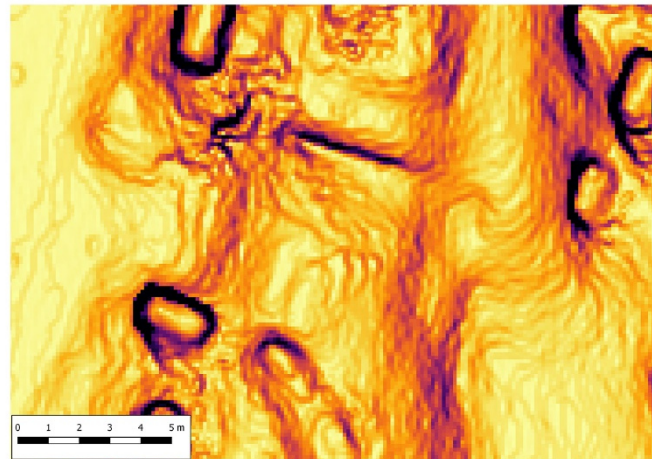
main streams direction of an area, the watershed basins, etc. it is possible to programme interventions to enhance water catchment and prevent stagnation near the archaeological structures. Moreover, it is possible to project new channellings for water runoff starting from these analyses. These analyses can also be useful to better understand how the site was projected in the past, contributing to the archaeological research. In this case it is interesting for example to notice how the waterflow was carefully projected and all the water of this area during the rainfall was collected and directed outside of the site, through the main entrance.

Similar analysis were also performed on the products derived from the processing of the spherical dataset acquired with the GoPro Fusion; for the reasons reported in section 4.3.2 the dataset used for the analyses that will be presented is the number 3, acquired in time lapse mode. First, a slope analysis was achieved on the DSM and the results of this computation are reported in the following Figure 161.

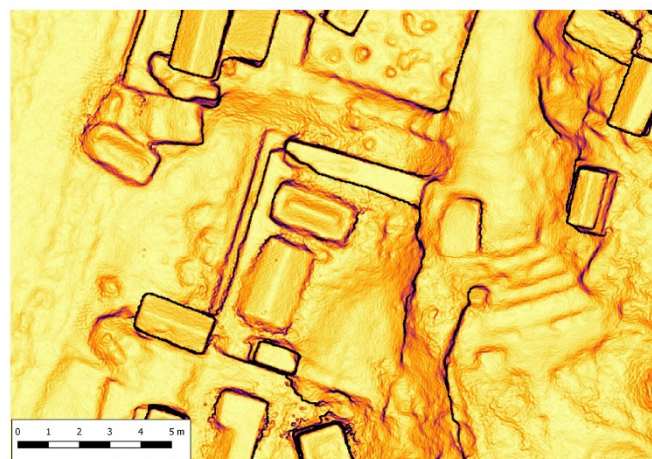


*Figure 161 Hierapolis, Northern Necropolis. Slope analysis on the DSM derived from the processing of the spherical dataset 3*

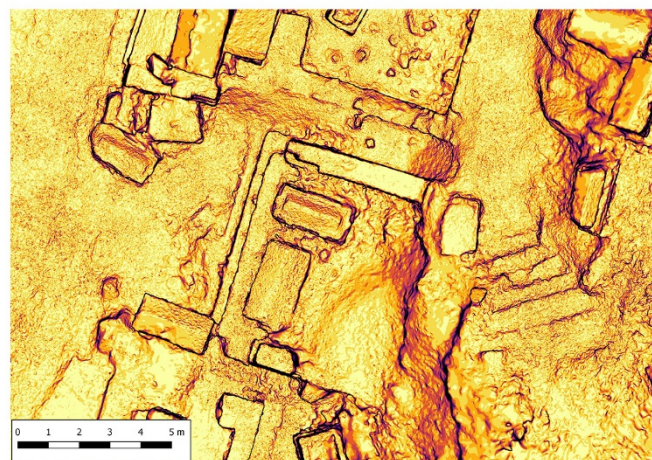
The same analysis has been performed also on the UAVs datasets already presented, in order to evaluate the different results that can be achieved with datasets acquired using different sensors and acquisitions approaches. An overview of the results achieved on the different datasets is reported in the following Figure 162, on a small sample area of the Necropolis.



**2017. UAV. 40/50 m**



**2018. UAV. 15/25 m**



**2018. 360/CRP**

*Figure 162 Hierapolis, Northern Necropolis. Slope analysis performed on different datasets with different resolutions*

As is possible to see from the image, the first big change in the resolution of the analysis performed is related with the change of the scale of the DSM. The different approaches adopted in 2017 and 2018 for the UAVs flights produced a different resolution of the products derivable from the photogrammetric process, this issue has been already stressed in section 4.1. The second aspect that need to be underlined is the comparison between the 2018 aerial dataset and the terrestrial one. It is interesting to notice how the 360 system was able to produce a model detailed and complete enough to cope with the aerial one. As already described, the products derived from this 360 sensor are characterize from the presence of a diffuse noise and this issue is recognizable also on the DSM. However, the slope analysis derived from this terrestrial dataset, despite this noise, is delivering results that are as complete as the one performed on the UAVs dataset and also on a more detailed scale.

Finally, an analysis that was already performed for the UAVs 2018 dataset, the extraction of topographic profile using the qProf plugin (section 4.1.3), was achieved also for the 360 dataset. An example of the results of this analysis on the 360 dataset is reported in the following Figure 163, where the resolution of the products derived from this dataset allows to extract profiles also for smaller portion of the area if compared with the analyses achieved for the UAVs dataset. In this case for example it was possible to define the profile of a series of stone steps connecting two different levels of the necropolis (profile B-B') or to define the connection between the level of the main road that crosses the necropolis and a series of structures overlooking it (profile A-A').

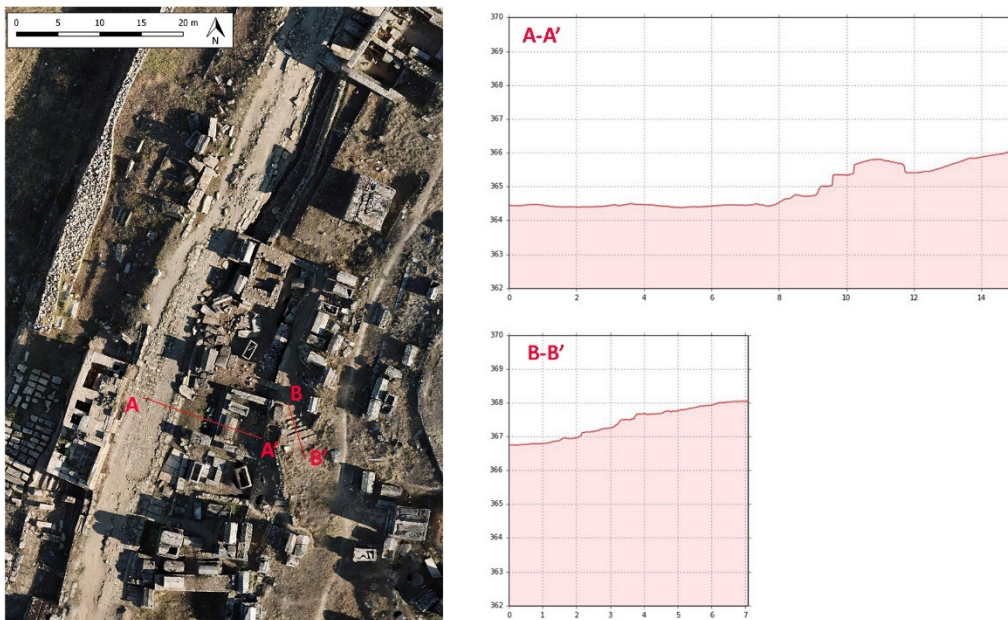


**Figure 163** Hierapolis, Northern Necropolis. Terrain profiles extracted in Qgis with the qProf plugin on the 360 acquisition (dataset 3)

## Ortophoto

The use of orthophotos for the study and analysis of archaeological structures is a consolidated practice and data derived from traditional imaging sensors are often used to report stratigraphic analysis, decay classification, etc. A qualitative comparison of the orthophoto derivable from the Freedom 360 system have been already reported in section 4.3.3. To further deepen this analysis, an orthophoto derived from the Freedom 360 system in the dataset 1 was used to report some stratigraphic analyses described in (Arrighetti, 2017).

The orthophoto of the west wall of the church of Rocca San Silvestro was thus extracted from the 360 dataset and the result of this operation is reported in the following Figure 164.



*Figure 164 Rocca San Silvestro, dataset 1. Stratigraphic analyses of the west wall of the church (source: Arrighetti, 2017) reported on the orthophoto generated from the Freedom 360 system*

As is possible to see from the image, the 360 system was able to satisfy the requirements of this procedure. With a GSD of 0,7 cm and an accuracy on control points comprehend between 1 and 2 centimeters, it is possible to work on a scale that range from 1:100 to 1:50. The orthophoto derived from these kinds of systems, with an appropriate processing, is thus suitable to sustain traditional archaeological investigation, such as the representation of the different building phases of a structure through the study of stratigraphic units.

Moreover, also the 360 dataset collected in the Northern Necropolis of Hierapolis was used to generate an orthophoto of the area surveyed. This orthophoto was used to evaluate a potential update of survey data that were previously acquired in the same area (further archaeological excavations were completed in the time between the two acquisitions). The data published in (D'Andria et al., 2008) were thus overlaid on the orthophoto derived from

the processing of the 360 dataset acquired in time lapse mode (dataset 3), the results of this operation are reported in the following Figure 165. It is interesting to notice how this operation allows to identify the structures that were unearthed in the time between the two acquisitions and to outline object that were eventually moved to proceed further in the excavations. It is possible to state that spherical images are in this case definitely competitive with the products derivable from an UAVs survey and that spherical photogrammetry can be considered a good technique to update archaeological maps in a scale between 1:200 and 1:500 (the produced orthophoto has a GSD of 0,5 cm/pix and a RMSe value on GCPs and CPs comprehend between 2 and 4 centimetre).



*Figure 165 Hierapolis, Northern Necropolis. Overlay of the data derived from "Atlante di Heirapolis di Frigia, Vol. II" and the orthophoto generated from the spherical dataset (dataset 3)*

# Chapter 5

## Discussion

The research conducted during the development of this thesis work allows to underline and report some final considerations.

Concerning UAVs platforms, the first topic that was discussed is related with the acquisition phase and is focused on the issues connected with the phases of flight planning and camera orientation. It has been reported that the introduction of oblique images allowed to test new solutions for UAVs photogrammetry and started several researches on an overall enhancement of both the acquisition and processing of aerial datasets of images, becoming a consolidated approach. The phase of images acquisition is always a crucial phase of the overall photogrammetric process and especially in the case of UAVs, where it is possible to complete this phase automatically thanks to the creation and fulfilment of automatic flight plans, it needs to be carefully projected and achieved. The planning of different flight plans that can be integrated between each other's and that can exploit the best features of different configurations allows to reach highly detailed 3D models enhancing also the time to be dedicated to the fieldwork. Following this direction, two main topics have been investigated and analysed: the characteristics related with the flight and the ones related with the camera set up.

The tests performed during the development of the presented research allowed to underline the best set up to adopt in relation with the conformation of the surveyed scene/object (e.g. height of the structures and their main development, shape of the object, etc.), the type of platform and sensors deployed on the field (e.g. FoV, resolution, etc.) and the desired output of the survey (e.g. the metric accuracy, the quality of the geometric reconstruction, the desired scale of representation, etc.). In general terms, if the object to survey presents low developments on the elevation component a nadiral acquisition performed following standard flight plans can be sufficient to complete the survey. This solution allows also to acquire bigger area, thus working on a territorial scale, partially sacrificing a complete and accurate reconstruction of the vertical developments features present on the surveyed area. These types of applications are for example suitable for the studies conducted in the field of landscape archaeology and are competitive with the data derived from remote sensing applications, allowing to reach a more detailed scale, lowering also the cost connected with the achievement of the survey.

When the vertical developments are present and marked on the scene/object to survey and it is important to achieve a complete documentation also of these features, the use of oblique images is mandatory. The integration of this kind of images with the nadiral acquisitions allows to complete the reconstruction also of these vertical features. The flight plan will also be modified to maximize the contribute of oblique images and the direction of the flight lines will be harmonized with the main development of the surveyed scene/object. In cases where this vertical development is concentrated in a well identifiable conformation, e.g. settlements or structures that were projected and built in a conical/cylindrical shape like Rocca San Silvestro, towers, etc., the combination of oblique images with a circular flight planning is a decisive element. The above described scenarios can be perfectly integrated in the researches connected with the building archaeology field, allowing to reach a good reconstruction of both the vertical developments of the surveyed structures and their connections with the terrain.

In the field archaeology both the previously described approaches can be adopted, depending on the conformation of the excavated area to survey. In case of a deep excavation, or in cases where structures remains were unearthed during the excavation, the use of oblique images is recommended; while in other scenarios the sole nadiral images can be sufficient to reach the desired detail of the survey.

In general terms a strategy that allows to achieve good results in terms of metric accuracy of the process is related with the planning of crossed grids of flight lines that follows the main directions of the development of the scene/object that need to be surveyed, integrating nadiral and oblique acquisitions and introducing the circular flight when the conformation of the scene/object is favourable.

Furthermore, the altitude on which the flight can be performed, and thus the achievable GSD, is different in these three scenarios: in the first scenario described (landscape) medium-high altitude flights can be performed in order to widen the surveyed area, in the second scenario (building) the altitude need to be reduced to increment the details of the surveyed scene/object, finally, in the third scenario (field) the flight altitude can be further reduced up to really low flights, to grant the high detailed that is needed for these kinds of applications.

As reported in the development of the dissertation, the first tests that were performed with a commercial platform allowed to set up and validate the methodological framework that was then extended to COTS and low-cost systems. The growth of the availability of these systems on the market was a striking element in the diffusion of UAVs photogrammetry and its applications, however, each platform needs to be carefully analysed and tested in order to stress its limits and define the best application scenarios.

The analyses on the impact of the factors mentioned above were also extended to the geometrical reconstruction provided by the 3D models derived from the processing of the different configurations of dataset. These analyses were achieved both evaluating the different point clouds individually, both comparing them with a reference dataset provided by a TLS acquisition, used as ground truth element. The analyses on the single point clouds allowed to confirm the crucial contribute of oblique images also in the geometrical reconstruction of the scene/object: this contribute is particularly evident on the vertical development of the surveyed structures, especially if they are in a good state of conservation.

The geometrical reconstruction provided by the different configurations of data was evaluated also thanks to the semiautomatic extraction of sections from the 3D models. It need to be reported that thanks to the combination of the operative practices described above for the flight planning and camera orientation phases, UAVs photogrammetric approach can reach accuracy levels of geometrical reconstruction that are competitive with the ones provided by a TLS survey, with a better cost-effectiveness relation, both in terms of time needed for the acquisitions and both in terms of the overall cost of the survey and processing operations. Moreover, the different tests performed underlined also the better performances of the UAVs datasets in reconstructing the upper part of the archaeological structures, especially in areas that are difficult to cover with a TLS survey.

The same issues analysed for the automatic flight planning can be transposed in cases where it is necessary to achieve manual flights. Similar flights configurations were then achieved performing different manual flights and the dataset collected were processed and analysed. Another topic that was deepened is related with the georeferencing strategies for the processing of UAVs dataset. The positioning and measuring of control points is one of the most time spending operation to complete on the field and thus several strategies have been proposed in this research to enhance the operations connected with this phase. The first approach is connected again with the possibility to combine the different acquired dataset in order to reduce the number of GCPs to be positioned and measured on the field. The aim of this approach is thus to enhance the number and also the distribution of GCPs on the field, trying to reduce it but without losing the control over the overall accuracy of the photogrammetric processing. Several tests were achieved in this sense on the selected CH test sites and it is interesting to report that also in this case the contribute of oblique images is the strength factor of the strategy. These tests allowed to validate the proposed strategy, however the position of control points must be projected in order to have them well distributed on the scene to survey and their distribution must also be planned in combination with the different flight plans that will be completed. Moreover, the role of

control points is still fundamental to assess and guarantee the metric accuracy of the photogrammetric processing and of the derived products.

It was however underlined that the proposed strategy for the enhancement of the number of control points can be performed thanks to the optimisation of the flight planning phase, up to sets of control points composed from 4 to 6 points. This strategy was tested and validated on two different scenarios: the survey of single buildings or structures and the survey of small-medium area, allowing to maintain the RMSE values on GCPs and CPS in an order of few centimeters.

The second approach that was proposed in connection with the georeferencing issue of UAVs data is related with a co-registration strategy: this approach was initially developed in fields of application different from the one of CH, thus it was tested in this research for the documentation of the archaeological heritage. This approach was tested on two datasets acquired in two different years following the same modalities of flight plan and camera orientation previously proposed, tested and validated. The metric accuracy of the approach proposed in this research was validated using a set of control points and allowed to assess a mean deviation of the values from the two sets of points in the range of few centimeters; the points of strength and the weaknesses of this approach were reported and some best practices for its application in real case scenarios were described.

The products derived from the co-registration approach were deeply analysed and their use for the study and monitoring of archaeological excavations and structures over time was tested and assessed. These products allowed to identify the areas where major changes happened between the two acquisitions and can represent a useful instrument for an almost real time monitoring and studying of the archaeological investigations, as well as to perform several multi-temporal analyses. The proposed approach and the use of the derived products represent new solutions that were tested and validated; the achieved results allowed to stress new uses of these multitemporal datasets opening new interesting scenarios that can be further developed to enhance the overall process of the archaeological documentation.

The analyses performed on the different products were able to underline the same features in two main areas of excavation and were thus validating each other. Moreover, a qualitative evaluation was also achieved inspecting the field documentation that was acquired during the two campaigns performed in the Turkish site.

On the other hand, the second part of Chapter 4 is dedicated to terrestrial sensors and techniques and in particular to spherical images and systems. The first section of the chapter is devoted to the definition of camera calibration approaches used in this research and how they were adopted in connection with the two different spherical sensors that were tested. This stage of the research allowed to deeply analyse the main characteristics of the two

systems and to better understand how they can be used in the field and with which degree of confidence.

One of the main issues when working with modern 360 cameras, i.e. systems that create a spherical image thanks to the use of different single cameras embedded on the same device and not stitching several images acquired from the same camera, is related with the different characteristics of the sensors that compose the system itself. This peculiar feature of these 360 systems needs to be considered both when working separately with the images acquired, both when using the spherical images after having completed the stitching phase. This issue was analysed in this research for two categories of 360 systems: the so-called DIY and the COTS systems. In case of the DIY solutions the test performed allowed to set up an appropriate strategy to estimate the I.O. parameters of the six cameras composing the tested system, enhancing both the stitching phase and the accuracy of the overall photogrammetric processing. Thanks to a modification of the information embedded in the Exif file it was possible to achieve a correct calibration of the different cameras, that were previously treated from the different photogrammetric software tested as they were identical. The original Exif generated from the six cameras was thus creating several issues in the photogrammetric processing and in the stitching phases. These issues were related with the fact that all the six cameras were marked in the Exif files with a unique camera model and a single set of I.O. parameters was computed for all the cameras. A strategy to solve these issues was proposed and validated introducing a modification in the different Exif files of the six cameras, creating a new camera model for each one of them, in order to estimate a correct set of I.O. parameters for all the cameras. The test performed allowed to demonstrate the differences between the computed sets of parameters for the six cameras and it was also possible to enhance both the photogrammetric processing and the stitching phase. As was described in the dissertation, this approach was validated in a dedicated 3D calibration test field that was set up for this purpose and that allowed to evaluate the effectiveness of the proposed strategy both from the point of view of the metric accuracy achievable and from the quality of the geometrical reconstruction of the acquired object. The estimated I.O. parameters were carefully considered for all the six cameras and the different issues that affected this phase of the processing before the Exif modification were identified and analysed.

Similar analyses were replicated also for the tested 360 COTS system but with a different outcome: for this 360 system, composed from only two sensors, the estimated I.O. parameters are returning comparable results between the two cameras. This factor is leading to a more precise stitching between the two cameras.

For this reason, it was decided to treat the data acquired from these two categories of sensors following different strategies and with the aim of providing some indications that

can be used to define a set of guidelines for the use of these type of systems for photogrammetric approaches.

The first issue to deal with was connected with the acquisition of data on the field with these systems: several factors are indeed affecting the acquisition phase, such as the acquisition distance, the omnidirectional view of the system, the conformation of the scene, etc., Moreover, the traditional acquisition schemes of photogrammetry needed to be revised and modified to better exploit the specific features of these systems.

Three main acquisition strategies have been thus proposed for the collection of data with these kinds of systems: still images, time lapse and video mode; the main features of each one of them have been identified and underlined.

As already reported, another tricky phase of the use of the data derived from these systems is connected with the processing phase: the main issue is connected with deciding whether to process the single images acquired or the stitched 360 panoramas. This issue is also related with the type of platform employed for the acquisition; in this work two of the three proposed acquisition strategies were tested for both the processing approaches. The two different 360 camera systems were deployed in the field for the documentation of two archaeological sites: Rocca San Silvestro and Hierapolis. In Rocca San Silvestro the processing approach with separated images was followed, while in Hierapolis the data collected were processed as stitched spherical images. In all the tests performed both strength and weak points of the proposed strategy were analysed, and the main issues connected with the processing of these type of data have been reported.

In general terms, the choice of working with single images or stitched panoramas is mainly related with the characteristics of the employed 360 system and the time and resources needed to complete the stitching phase. When the stitching phase is difficult and long to perform or when the achieved panoramas are not satisfying in terms of quality, i.e. when stitching errors are present, it is better to work with the single images separated. On the other hand, when the overall quality of the stitched panoramas is ensured and the stitching phase can be solved in a rapid way thank to custom and automatic solutions, it is possible to work with the spherical panoramas. Moreover, this choice is also related with the employed software solution and how it can deal with these types of data. Up to date, few software solutions were able to correctly deal with the photogrammetric processing of spherical images, while the solution of issues related with the treatment of fisheyes cameras (that are generally employed in 360 systems), is a more consolidated practice. To summarize, in case of more recent COTS solution, that are ensuring the restitution of good quality spherical panoramas, the processing of spherical images is a good strategy to follow, while in case of DIY systems, the potentialities of the immersive acquisition of the environment can be exploited also working with the single images separately.

In the site of Rocca San Silvestro, the DIY system was tested on two different areas: the time lapse mode was deployed on the remains of the small church of the medieval village, while the video mode was adopted to acquire a portion of the area near the main entrance of the ancient settlement.

After the processing phase, the products derived from the time lapse dataset (dataset 1) were evaluated performing some analyses both with a reference TLS dataset, both with a traditional CRP acquisition performed with a DSLR. The main differences between this last dataset and the 360 one were evaluated and a cost-effectiveness analysis was achieved as well. While the traditional dataset is still maintaining the upper hand in terms of quality of the survey products (both in terms of accuracy, geometrical and radiometric contents) nevertheless, the 360 dataset is achieving comparable results, especially if the time components is considered (the time factor is definitely more favourable for the 360 system). Furthermore, also the dataset acquired in video mode (dataset 2) was processed and analysed. In this case, one of the main issues was related with the reduction of resolution of the acquisition that is automatically performed by the tested system when acquiring data in video mode. To test how much this reduction can affect the photogrammetric processing the derived 3D models was analysed using a TLS dataset as ground truth.

On the other hand, in the site of Hierapolis the COTS 360 system was deployed on the field to acquire the same area adopting the two different acquisition strategies. Both the time lapse mode (dataset 3) and video mode (dataset 4) datasets were processed and analysed, in this case it was also necessary to insert in the overall workflow the stitching phase of the data collected on the field that were transformed into spherical contents. Both the datasets were analysed from the metric accuracy point of view, using a set of TS measured control points, and from the geometric accuracy point of view with a reference TLS dataset.

All the analyses and considerations achieved for the four datasets allowed to define some final remarks that need to be considered during the acquisitions performed with this kind of systems, especially connected with the acquisition mode to adopt depending on the scene/object that need to be surveyed, the time available on the field and the expected outputs of the survey.

After all the tests performed on the different acquisition strategies, it was underlined that the best approach to adopt is the one defined as time-lapse mode. This approach is able to maintain the maximum resolution of the camera, granting at the same time the possibility to freely and rapidly move around the scene to survey preserving an overall good quality of the acquired images. The video mode is not providing a time reduction of the acquisition phase valuable enough to justify the reduction of the resolution of the acquired data. This approach is thus to adopt only in cases where the stabilisation provided by the video mode is mandatory to compensate possible vibrations and acquire good quality data.

Moreover, the issues connected with the omnidirectional FoV of these systems have been reported as well, e.g. the presence of the operator on the acquired images, how he/she can affect both the photogrammetric process and the generated products and how to deal with this issue.

As in the section dedicated to UAVs systems, also in the case of 360 cameras the issues connected with the different solutions that can be adopted for the georeferencing of the models have been identified and underlined. In the case of 360 systems the focus was set more specifically on the co-registration approach: the aim was to co-register data derived from different sensors but acquired in the same moment, more specifically a terrestrial and an aerial dataset.

The terrestrial dataset acquired with the 360 system was thus co-register with an UAVs acquisition of the same area; the UAVs dataset was processed following the traditional photogrammetric pipeline and was used as rigid block to orient the 360 dataset, that was co-registered in the phase of TPs extraction and image matching, in a following phase the UAVs images were discarded and the 360 oriented dataset was processed with the standard photogrammetric approach. The accuracy of this approach was evaluated with two quality checks: the coordinates of the camera stations estimated with co-registration approach were compared with the coordinates of the same camera stations estimated in the traditional approach, and secondly similar analyses were performed on a set of control points. Both these analyses provided a mean deviation of the analysed data in the order of few centimeters, confirming the metric validity of the proposed approach.

The validation of the proposed approach opens interesting scenarios for the use of the 360 data: on the one hand it allows to potentially reduce the time that need to be dedicated on the field for the positioning and measurement of control points, and from the other hand it allows to prefigure the use of 360 data in a multi-sensors and multi-scale scenario.

This approach represents a new solution and is still not investigated in the scientific literature, however the first tests performed are returning interesting results that are definitely worth to be further extended and investigated. The integration of 360 data with the ones derived from other sensors is a new scenario that can be developed in several different directions and will be probably be an important topic of interest in the years to come.

The final part of this section is dedicated to the analysis on the products derivable from these 360 systems: the focus of this part of the research was to assess if the products derivable from the processing of these data with a photogrammetric approach were suitable to perform different analyses that are usually achieved for other kinds of systems and with which level of confidence. Analyses were thus achieved on the point clouds, DSM and orthophotos. The use of these products was stressed to perform different kinds of analyses

and to evaluate their use in the researches connected with the study and documentation of archaeological features. Depending on how the dataset is acquired and processed, its use can be integrated in the traditional process of archaeological documentation. The tests performed with the DIY system, allowed for example to produce a high detail orthophoto of a façade of the San Silvestro church, in a scale between 1:100 and 1:50, that was used as a support to report the previously achieved stratigraphic analyses. Similarly, the dataset acquired in the site of Hierapolis with the COTS 360 system was further analysed in this sense. In this case the derived orthophoto can be considered suitable for a representation scale between 1:200 and 1:500. The bigger scale achievable with this dataset is related with the type of acquisition performed that, on the other hand, was able to cover a bigger area if compared with the DIY system. In this second case, spherical systems can also be considered competitive with the acquisitions performed with UAVs systems and they can be useful to update the archaeological documentation of certain areas. Aside for the metric and geometric contents of these datasets, it is important to underline also the quality of the embedded radiometric information. Despite being still not comparable with other image-based systems, these 360 platforms are able to provide a good quality of data in this sense, a factor that is important for the archaeological investigation.

# Chapter 6

## Conclusion

The research presented in this dissertation has been focused on the use of two main categories of image-based sensors (UAVs and 360 cameras) for the rapid documentation of CH artefacts, and in particular these two categories of sensors have been tested for the documentation of some archaeological structures of two main sites. The time component has become in the last decades a central issue also in the field of documentation connected with CH. For this reason, the first part of the presented work is dedicated to the definition of what is intended as rapid mapping in the geomatics community and how this sector of research can be connected with the documentation of CH. Range-based and image-based techniques have both contributed in the transformation and evolution of this sector of research, and their joint use in applications connected to MMSs is still a topic of research that create a great interest in the geomatics community. The research presented in this thesis was focused only on image-based techniques, that were analysed from different points of view.

First of all, a selection was performed on the literature connected with the definition of standards and guidelines allowing from one side to define the framework in which this thesis work was inserted, and consequently also the tests and analyses to perform on the selected instruments and techniques, and from the other side to underline an issue that is in general common for standards and specifications but that is more remarkable in this field of research: their aging. In the research connected with the documentation of CH and in particular in the fields derived from geomatics it is possible to observe the lack of an updated work of summary concerning the definition of general standards and specifications for the last years. This fact is probably related with the rapid evolution that the sector of geomatics undergone in the last decade, thanks to the developments that interested both sensors and instruments, both the methodological approaches to the research. The rate of growth didn't allow yet the researchers to gain the right perspective on the major changes that happened in these last years and more time is necessary to reach the maturity of the reflection on this evolution. These facts considered, it is probably time for the community of researchers in this field to perform a step backwards, gain the right perspective once again on all the last years' phenomena and summarize the evolution that the discipline has undergone with new recognized and common standards and guidelines. This is not an easy

process and it requires a great effort from all the members of this community, but it is probably the right time to complete it.

The effort that researchers in the field of geomatics are doing in order to complete this updating is noteworthy but is limited to specific sectors of the research and on specific instruments or methodologies. The community of researchers need to join forces and work together to elaborate a common reflection on this theme, the research has probably reached its maturity and before the next technological evolution it is necessary to complete this phase. This is an issue that must be resolved in the following years, in order to further proceed with the development and evolution of the discipline. It is now clear the need of these guidelines, especially in the field of CH documentation: the contributes that can come from the different instruments and techniques need to be evaluated and connected with the needs of the documentation of this kind of artefacts, in order to create a virtuous circle between the users and the providers of the survey data and products.

A future development of the research presented could be thus connected to the provision of a complete analysis of the investigated sensors and all the issues connected with their deployment in the field of CH documentation in order to provide a base of reflection to set up new standards and guidelines in this field.

Especially for the 360 systems it will be necessary to further extend the tests presented in this work in order to achieve a complete overview of their use and their potentialities for the documentation of CH. After having completed this step, it will be possible to set up a series of guidelines and best practices, also for their integration with other instruments and techniques, in order to achieve multi-sensors and multi-scale survey and models. A preliminary analysis on this topic have been performed with the integration achieved between 360 terrestrial acquisition and UAVs acquired data but needs to be further validated on other datasets and the proposed approach must be enhanced.

In the last years, time has assumed a central role and thus all the phases of the work needed to be enhanced: from the acquisition of the data in the field, through their processing and till the generation of the different products. Even though it is true that the time component has a more central role if compared with the past, the accuracy and the resolution of the data collected and processed need not to suffer too much from the valorisation of this component. The methodologies and instruments developed in the last years consented, in a first instance, to speed up the acquisition phase, allowing to collect large dataset in few time (both aerial and terrestrial) and reducing the time to spend on the field. Part of the tests performed in this research were thus addressed in this direction. Secondly, the evolution of the approaches and software allows to speed up also the processing phase and thus the generation of the final products of the survey. Compared with other more consolidated survey techniques, the use of 360 systems is particularly efficient in the acquisition phase,

especially if compared with CRP acquisitions performed with frame cameras or with TLS acquisitions, that requires more time on the field to complete the acquisition phase. On the other hand, the 360 dataset requires in general terms more time to be dedicated to the pre-processing phases (e.g. for the stitching of the images, the down sampling of the acquired dataset, the phase of masks creation, etc.). Moreover, due to the fact that photogrammetric approaches connected with 360 systems are quite new and the methodology connected with their deployment is still developing, their use still need to be enhanced.

Aside from the integration in the traditional archaeological documentation pipeline, the most promising approaches in this sense are connected with the multitemporal monitoring of archaeological structures and excavations. These multitemporal approaches can really become one of the revolutionary elements in the archaeological documentation, allowing to innovate the traditional approaches and focusing on the time-component that has always been one of the crucial points also in the archaeological research. New challenges will come from this point in the next years: the connection between geomatics and archaeologists need to be strengthened and the needs of both the communities must converge in the creation of optimized approaches. The documentation of the archaeological heritage is evolving, the new generations of archaeologists are approaching these issues with a curious eye on the contributes that can derive from the geomatic community and from their side, geomatics researchers need to guarantee their support in this process and work together with archaeologists to complete it.

As for UAVs the lowering of the cost of sensors and platforms, thanks to their development as COTS systems, interested also other categories of instruments and techniques in the field of geomatic. Spherical cameras are a good example of this process: the development of this systems for commercial entertainment purposes transformed old research fields of geomatic and opened new ones. At this stage of the research spherical systems and thus spherical photogrammetry are interesting and promising tools and the research on their application in the field of CH documentation is starting again with new strength. Several issues and research topics are emerging in connection with these approaches and there is still a lot to be studied and solved to bring this sector to its maturity. In the research presented in this contribute different types of these systems have been analysed and their use with SfM approaches for the documentation of archaeological heritage have been stressed. New issues are emerging from the adoption of these methods if compared with photogrammetric approaches completed with frame cameras, e.g. the geometrical modelling of spherical cameras, acquisition strategies, etc., and a lot is still to research and understand about these systems. This thesis work was focused on the one hand on the analysis of the systems and the performances of the different cameras that compose them and on the other hand on all the issues connected with the deployment of these systems in

the field for the survey of the archaeological heritage, with the resolution of the products derivable and how and with which scale they can contribute to the documentation of this type of heritage. Different acquisition strategies were tested and validated as well as different processing strategies; finally, the use of various products derived from the photogrammetric processing of spherical data was stressed in order to evaluate how they can respond to the archaeological needs.

The deployment of UAVs in the field of CH documentation is nowadays a consolidated practice, the research presented in this thesis was thus focused on the test and validation of different acquisition strategies that are not fully explored yet and with the possibility of proposing a new strategy for the co-registration of UAVs and 360 data.

Concerning this last approach, as for other sensors and techniques the integration between different datasets will probably be one of the most researched topics in the following years. This integration can be intended as the possibility of use spherical dataset to enhance different phases of the photogrammetric processing, as tested in this research, or as well as the fusion of data derived from different sensors in the direction of achieving multi-sensors and multi-scale models.

One of the issues that is occupying and will probably occupy the researchers in the following years is connected with the georeferencing of the data collected on the field with this rapid mapping approaches. This sector of the research is for sure more developed in the field of UAVs, where solutions as RTK and PPK are already established and where the researchers are stressing these technologies in order to define their limits and potentialities in connection with different scales of applications. Similar approaches have already been developed as well for more refined MMS that combine IMU and GPS/GNSS to retrieve the position of the systems and georeference the collected data and the derived products. All these solutions are deployed and adopted mainly in case of expensive commercial solutions while for low cost and COTS system this approach is still not achievable due to the lower quality of the positioning systems embedded in such systems. In the following years this will probably represent an issue to deal with and hopefully the development of such systems will allow to adopt similar procedures also working with less expensive systems. Another limit that will probably be overcome is the one of the low resolution of spherical commercial systems. These systems are directly derived from the commercial sector of action cameras and for this reason the embedded sensors are generally small, and the resolution of the collected data limited. Together with the development of the algorithms related with the spherical photogrammetry these systems have all the credential to become a standard technique for the rapid documentation of archaeological heritage and CH in general. Moreover, the flexibility of these type of data is opening new scenarios also for the valorisation of CH sites, the data collected for photogrammetric approaches can

easily be used for other purposes, such as the creation of virtual tours or immersive contents in general. The interest of the geomatics community on these kinds of systems and techniques can be traced also through a rapid overview, obviously non complete, of the research products of the last years dedicated to spherical photogrammetry in general, as reported in the following Figure 166.

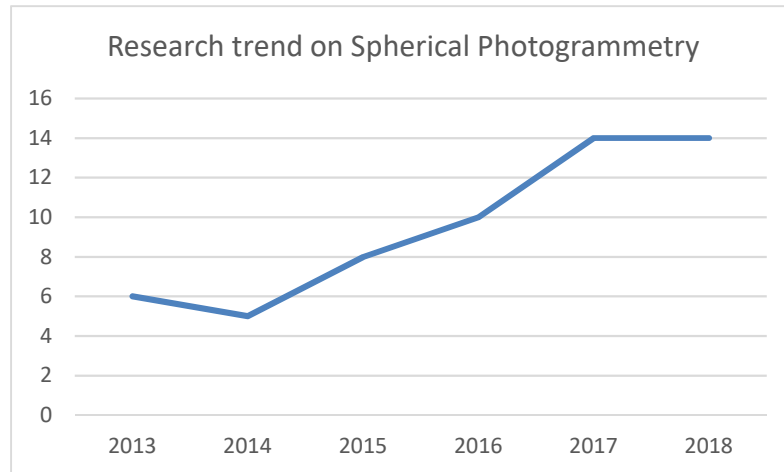


***Figure 166 Research trend (not complete) of the works related with spherical photogrammetry***

As is possible to notice from the preliminary analysis reported in Figure 166 after a first phase in which the research on spherical photogrammetry was developed mainly by Fangi and his group, it is possible to underline a constant growth in the numbers of researches dedicated to this topic, until a consolidation in the past year. This trend underlines the growth of interest of the researchers on this topic and will probably continue to growth in the next years. As well as happened for UAVs, spherical photogrammetry will probably gain its maturity establishing its own research addresses and methodology.

## References

- Abate, D., Toschi, I., Sturdy-Colls, C., & Remondino, F. (2017). A low-cost panoramic camera for the 3d documentation of contaminated crime scenes. *International Archives of the Photogrammetry, Remote Sensing and Spatial Information Sciences - ISPRS Archives*, 42(2W8), 1–8. <https://doi.org/10.5194/isprs-archives-XLII-2-W8-1-2017>
- Abbey, S. G., Theatre, R., Pisa, C., Zeppa, F., & Fangi, G. (2010). Spherical Photogrammetry for Cultural Heritage - Categories and Subject Descriptors. *October*, 3–6.
- Abdel-Aziz, Y. ., Karara, H. M., & Hauck, M. (2015). Direct Linear Transformation from Comparator Coordinates into Object Space Coordinates in Close-Range Photogrammetry. *Photogrammetric Engineering & Remote Sensing*, 81(2), 103–107. <https://doi.org/10.14358/PERS.81.2.103>
- Abraham, S., & Hau, T. (1997). Towards autonomous highprecision calibration of digital cameras. In *Videometrics V, Proceedings of SPIE Annual Meeting* (Vol. 3174, pp. 82–93). <https://doi.org/10.1117/12.279802>
- Adami, A., Fassi, F., Fregonese, L., & Piana, M. (2018). Image-based techniques for the survey of mosaics in the St Mark's Basilica in Venice. *Virtual Archaeology Review*, 9(19), 1. <https://doi.org/10.4995/var.2018.9087>
- Aguilera, D. G., Gómez Lahoz, J., & Finat Codes, J. (2012). *A new method for vanishing points detection in 3D reconstruction from a single view*.
- Aicardi, I. (2017). *UAVs for spatial data acquisition. Sensors evaluation, flight design and planning, multi-temporal solutions (PhD Thesis)*. Italy.
- Aicardi, I., Chiabrando, F., Grasso, N., Lingua, A., Noardo, F., & Spanò, A. T. (2016). UAV photogrammetry with oblique images: First analysis on data acquisition and processing. *International Archives of the Photogrammetry, Remote Sensing and Spatial Information Sciences - ISPRS Archives*, 2016-Janua(July), 835–842. <https://doi.org/10.5194/isprsarchives-XLI-B1-835-2016>
- Aicardi, I., Nex, F., Gerke, M., & Lingua, A. (2016). An Image-Based Approach for the Co-Registration of Multi-Temporal UAV Image Datasets. *Remote Sensing*, 8(9), 779. <https://doi.org/10.3390/rs8090779>
- Ajmar, A., Boccardo, P., Disabato, F., & Giulio Tonolo, F. (2015). Rapid Mapping: geomatics role and research opportunities. *Rendiconti Lincei*, 26(S1), 63–73. <https://doi.org/10.1007/s12210-015-0410-9>
- Akkaynak, D., Treibitz, T., Xiao, B., Gürkan, U. A., Allen, J. J., Demirci, U., & Hanlon, R. T. (2014). Use of commercial off-the-shelf digital cameras for scientific data acquisition and scene-specific color calibration. *Journal of the Optical Society of America A*, 31(2), 312. <https://doi.org/10.1364/JOSAA.31.000312>
- Alidoost, F., & Arefi, H. (2017). Comparison of UAS-based photogrammetry software for 3D point cloud generation: a survey over a historical site. In *ISPRS Annals of the Photogrammetry, Remote Sensing and Spatial Information Sciences* (Vol. 4, pp. 55–61). <https://doi.org/10.5194/isprs-annals-IV-4-W4-55-2017>
- Ambrosia, V. G., Wegener, S., Zajkowski, T., Sullivan, D. V., Buechel, S., Enomoto, F., ... Hinkley, E. (2011). The Ikhana unmanned airborne system (UAS) western states fire imaging missions: From concept to reality (2006-2010). *Geocarto International*, 26(2), 85–101. <https://doi.org/10.1080/10106049.2010.539302>

- Anderson, R. C. (1982). Photogrammetry: The pros and cons for archaeology. *World Archaeology*, 14(2), 200–205. <https://doi.org/10.1080/00438243.1982.9979860>
- Andrews, D., Bedford, J., & Bryan, P. (2009). *Metric Survey Specifications for Cultural Heritage*. Retrieved from [www.HistoricEngland.org.uk](http://www.HistoricEngland.org.uk)
- Arrighetti, A. (2017). Rocca San Silvestro. Archeologia per il restauro. Firenze: Dip. Architettura. Firenze. Retrieved from [https://www.academia.edu/35343309/ARRIGHETTI\\_A.\\_2017\\_Rocca\\_San\\_Silvestro.\\_Archeologia\\_per\\_il\\_restauero\\_Firenze](https://www.academia.edu/35343309/ARRIGHETTI_A._2017_Rocca_San_Silvestro._Archeologia_per_il_restauero_Firenze)
- ASPR. (2014). ASPRS Positional Accuracy Standards for Digital Geospatial Data. *Photogrammetric Engineering & Remote Sensing*, 81(3). <https://doi.org/10.14358/PERS.81.3.A1-A26>
- Balletti, C., Guerra, F., Scocca, V., & Gottardi, C. (2015). 3D integrated methodologies for the documentation and the virtual reconstruction of an archaeological site. *International Archives of the Photogrammetry, Remote Sensing and Spatial Information Sciences - ISPRS Archives*, 40(5W4), 215–222. <https://doi.org/10.5194/isprsarchives-XL-5-W4-215-2015>
- Balletti, C., Guerra, F., Tsioukas, V., & Vernier, P. (2014). Calibration of action cameras for photogrammetric purposes. *Sensors (Switzerland)*, 14(9), 17471–17490. <https://doi.org/10.3390/s140917471>
- Balzani, M., Santopuoli, N., Grieco, A., & Zaltron, N. (2004). Laser Scanner 3D Survey in Archaeological Field: The Forum Of Pompeii. In *International Conference on Remote Sensing Archaeology* (pp. 169–175).
- Barazzetti, L., Fangi, G., Remondino, F., & Scaioni, M. (2010). Automation in Multi-Image Spherical Photogrammetry for 3D Architectural Reconstructions. *Vast 2010*, 2312. <https://doi.org/10.2312/PE/VAST/VAST10S/075-081>
- Barazzetti, L., Previtali, M., & Roncoroni, F. (2017a). 3D modelling with the samsung gear 360. In *International Archives of the Photogrammetry, Remote Sensing and Spatial Information Sciences - ISPRS Archives* (Vol. 42, pp. 85–90). <https://doi.org/10.5194/isprs-archives-XLII-2-W3-85-2017>
- Barazzetti, L., Previtali, M., & Roncoroni, F. (2017b). Fisheye lenses for 3D modeling: Evaluations and considerations. *International Archives of the Photogrammetry, Remote Sensing and Spatial Information Sciences - ISPRS Archives*, 42(2W3), 79–84. <https://doi.org/10.5194/isprs-archives-XLII-2-W3-79-2017>
- Barazzetti, L., Previtali, M., & Roncoroni, F. (2018). Can we use low-cost 360 degree cameras to create accurate 3D models? In *International Archives of the Photogrammetry, Remote Sensing and Spatial Information Sciences - ISPRS Archives* (Vol. 42, pp. 69–75). <https://doi.org/10.5194/isprs-archives-XLII-2-69-2018>
- Barber, D., & Mills, J. (2007). *3D Laser Scanning for Heritage. Advice and guidance to users on laser scanning in archaeology and architecture*.
- Barceló, J. A., & Pallarés, M. (1996). A critique of G.I.S. in archaeology. From visual seduction to spatial analysis. *Archeologia e Calcolatori n. VII - 1996*.
- Bay, H., Ess, A., Tuytelaars, T., & Van Gool, L. (2008). Speeded-Up Robust Features (SURF). *Computer Vision and Image Understanding*, 110(3), 346–359. <https://doi.org/10.1016/j.cviu.2007.09.014>
- Benassi, F., Dall'Asta, E., Diotri, F., Forlani, G., Morra di Cella, U., Roncella, R., ... Santise, M. (2017). Testing Accuracy and Repeatability of UAV Blocks Oriented with GNSS-Supported Aerial Triangulation. *Remote Sensing*, 9(2), 172. <https://doi.org/10.3390/rs9020172>
- Berger, M., Levine, J., Gustavo Nonato, L., Taubin, G., & Silva, C. T. (2011). *An End-to-End Framework for Evaluating Surface Reconstruction*.
- Bewley, R. H. (2003). Aerial survey for archaeology. *The Photogrammetric Record*, 18(104), 273–292. <https://doi.org/10.1046/j.0031-868X.2003.00023.x>
- Bianchi, G., Bruno, N., Dall'Asta, E., Forlani, G., Re, C., Roncella, R., ... Zerbi, A. (2016). Integrated survey for architectural restoration: A methodological comparison of two case studies. In *International Archives of the Photogrammetry, Remote Sensing and Spatial Information Sciences - ISPRS Archives* (Vol. 41, pp. 175–182).

- <https://doi.org/10.5194/isprsarchives-XLI-B5-175-2016>
- Biasion, A., Dequal, S., & Lingua, A. (2004). A new procedure for the automatic production of true orthophotos. *International Archives of Photogrammetry, Remote Sensing and Spatial Information Sciences*, 35, 1682–1777. <https://doi.org/10.1016/j.tox.2014.03.010>
- Bipm. (2006). International Vocabulary of Metrology – Basic and General Concepts and Associated Terms ( VIM ) 3 rd edition Final draft 2006-08-01 Vocabulaire international de métrologie – Concepts fondamentaux et généraux et termes associés ( VIM ) 3 e édition Projet f, (Vim), 1–127.
- Bitelli, G., Camassi, R., Gusella, L., & Mognol, A. (2004). Image change detection on urban area: the earthquake case. *International Archives of Photogrammetry and Remote Sensing*, 35, 692–697.
- Blake, W. H. (2010). What is the future of metric heritage documentation and its skills? *International Archives of the Photogrammetry, Remote Sensing and Spatial Information Sciences - ISPRS Archives*, 38(PART 5), 98–102.
- Blázquez, M., Colomina, I., & Castelldefels, S. (2012). On INS/GNSS-based Time Synchronization in Photogrammetric and Remote Sensing Multi-Sensor Systems. <https://doi.org/10.1127/1432-8364/2012/01041>
- Boccardo, P., Chiabrando, F., Dutto, F., Tonolo, F., & Lingua, A. (2015). UAV Deployment Exercise for Mapping Purposes: Evaluation of Emergency Response Applications. *Sensors*, 15(7), 15717–15737. <https://doi.org/10.3390/s150715717>
- Boehler, W., Heinz, G., & Marbs, A. (2002). The potential of non-contact close range laser scanners for cultural heritage recording. In *In XVIII. International Symposium of CIPA (September 2001)* (pp. 430–436).
- Böhler, W. (2005). Comparison of 3D laser scanning and other 3D measurement techniques. In M. Baltsavias, A. Gruen, L. van Gool, & M. Pateraki (Eds.), *Recording, Modelling and Visualisation of Cultural Heritage*. CRC Press.
- Bolognesi, M., Furini, A., Russo, V., Pellegrinelli, A., & Russo, P. (2015). Testing the low-cost rpas potential in 3D cultural heritage reconstruction. In *International Archives of the Photogrammetry, Remote Sensing and Spatial Information Sciences - ISPRS Archives* (Vol. 40, pp. 229–235). <https://doi.org/10.5194/isprsarchives-XL-5-W4-229-2015>
- Brito, J. H., Angst, R., Köser, K., & Pollefeys, M. (2013). Radial Distortion Self-Calibration. *Proc. IEEE Conf. Computer Vision and Pattern Recognition*, 1368–1375. <https://doi.org/10.1109/CVPR.2013.180>
- Brogio, G. Pietro. (2002). L'Archeologia dell'architettura in Italia nell'ultimo quinquennio (1997-2001). *Arqueologia de La Arquitectura*, 1, 19–26.
- Brogio, G. Pietro, & Cagnana, A. (2012). *Archeologia dell'architettura*.
- Brown, D. (1966). Decentering Distortion of Lenses. *Photometric Engineering*, 32(3), 444–462.
- Brown, D. (1971). Close-range camera calibration. *PHOTOGRAMMETRIC ENGINEERING*, 37(8), 855–866.
- Brown, M., & Lowe, D. (2007). Automatic Panoramic Stitching Using Invariant Features. *International Journal on Computer Vision (IJCV)*, 74(1), 59–73. <https://doi.org/10.1007/s11263-006-0002-3>
- Bujakiewicz, A., Kowalczyk, M., Podlasiak, P., & Zawieska, D. (2006). 3D Reconstruction and Modelling of the Contact Surfaces for the Archaeological Small Museum Pieces. *International Archives of Photogrammetry and Remote Sensing*, 36(Part 5), 56–61.
- Calantropio, A., Chiabrando, F., Sammartano, G., Spanò, A. T., & Teppati Losè, L. (2018). UAV strategies validation and remote sensing data for damage assessment in post-disaster scenarios. *International Archives of the Photogrammetry, Remote Sensing and Spatial Information Sciences - ISPRS Archives*, 42(3W4). <https://doi.org/10.5194/isprs-archives-XLII-3-W4-121-2018>
- Calantropio, A., Chiabrando, F., Rinaudo, F., & Teppati Losè, L. (2018). Use and evaluation of a short range small quadcopter and a portable imaging laser for built heritage 3D documentation. In *International Archives of the Photogrammetry*,

- Remote Sensing and Spatial Information Sciences - ISPRS Archives* (Vol. 42, pp. 71–78). <https://doi.org/10.5194/isprs-archives-XLII-1-71-2018>
- Calantropio, A., Colucci, E., & Teppati Losè, L. (2017). Rapid Mapping for Built Heritage At Risk Using Low-Cost and Cots Sensors. a Test in the Duomo Vecchio of San Severino Marche. *ISPRS - International Archives of the Photogrammetry, Remote Sensing and Spatial Information Sciences*, XLII-2/W8(November), 59–66. <https://doi.org/10.5194/isprs-archives-XLII-2-W8-59-2017>
- Calantropio, A., Deseilligny, M. P., Rinaudo, F., & Rupnik, E. (2018). Evaluation of photogrammetric block orientation, *XLIII*(June), 4–7.
- Calantropio, A., Patrucco, G., Sammartano, G., & Teppati Losè, L. (2018). Low-cost sensors for rapid mapping of cultural heritage: first tests using a COTS Steadicamera. *Applied Geomatics*, 10(1), 31–45. <https://doi.org/10.1007/s12518-017-0199-6>
- Campana, S. (2017). Drones in Archaeology. State-of-the-art and Future Perspectives. *Archaeological Prospection*, 24(4), 275–296. <https://doi.org/10.1002/arp.1569>
- Campana, S., & Remondino, F. (2008). Fast and detailed digital documentation of archaeological excavations and heritage artifacts. *Layers of Perception: Proceedings of the 35th International Conference on Computer Applications and Quantitative Methods in Archaeology (CAA), Berlin, Germany, April 2-6, 2007*, 36–42. Retrieved from [https://publikationen.uni-tuebingen.de/xmlui/bitstream/handle/10900/61506/18\\_Campana\\_Remondino\\_CAA\\_2007.pdf?sequence=2](https://publikationen.uni-tuebingen.de/xmlui/bitstream/handle/10900/61506/18_Campana_Remondino_CAA_2007.pdf?sequence=2)
- Carbonnell, M. (1989). *Photogrammétrie appliquée aux relevés des monuments et des centres historiques*.
- Cardenal Escarcena, J., Mata de Castro, E., Pérez García, J. L., Mozas Calvache, A., Fernández del Castillo, T., Delgado García, J., ... Castillo, J. C. (2011). Integration of photogrammetric and terrestrial laser scanning techniques for heritage documentation. *Virtual Archaeology Review*, 2(3), 53–57.
- Cavegn, S., Blaser, S., Nebiker, S., & Haala, N. (2018). Robust and accurate image-based georeferencing exploiting relative orientation constraints. In *ISPRS Annals of the Photogrammetry, Remote Sensing and Spatial Information Sciences* (Vol. 4, pp. 57–64). <https://doi.org/10.5194/isprs-annals-IV-2-57-2018>
- Ceraudo, G. (2013). Aerial Photography in Archaeology (pp. 11–30). Springer, Cham. [https://doi.org/10.1007/978-3-319-01784-6\\_2](https://doi.org/10.1007/978-3-319-01784-6_2)
- Chandler, J. H., Fryer, J. G., & Jack, A. (2005). Metric capabilities of low-cost digital cameras for close range surface measurement. *The Photogrammetric Record*, 20(109), 12–26. <https://doi.org/10.1111/j.1477-9730.2005.00302.x>
- Chase, A. F., Chase, D. Z., Fisher, C. T., Leisz, S. J., & Weishampel, J. F. (2012). Geospatial revolution and remote sensing LiDAR in Mesoamerican archaeology. *Proceedings of the National Academy of Sciences of the United States of America*, 109(32), 12916–21. <https://doi.org/10.1073/pnas.1205198109>
- Cheok, G. S., Lytle, A. M., & Saidi, K. S. (2008). ASTM E57 3D imaging systems committee: An update - art. no. 69500J. In *Laser Radar Technology and Applications Xiii* (Vol. 6950, pp. J9500–J9500). <https://doi.org/10.1117/12.791929>
- Chia-Kai Liang, Li-Wen Chang, & Chen, H. H. (2008). Analysis and Compensation of Rolling Shutter Effect. *IEEE Transactions on Image Processing*, 17(8), 1323–1330. <https://doi.org/10.1109/TIP.2008.925384>
- Chiabrandò, F., D’Andria, F., Sammartano, G., & Spanò, A. (2017). UAV photogrammetry for archaeological site survey. 3D models at the Hierapolis in Phrygia (Turkey). *Virtual Archaeology Review*, 9(18), 28. <https://doi.org/10.4995/var.2018.5958>
- Chiabrandò, F., Di Lolli, A., Patrucco, G., Spanò, A. T., Sammartano, G., & Teppati Losè, L. (2017). Multitemporal 3D modelling for cultural heritage emergency during seismic events: Damage assesment of S. Agostino church in Amatrice (RI). In *International Archives of the Photogrammetry, Remote Sensing and Spatial Information Sciences - ISPRS Archives* (Vol. 42). <https://doi.org/10.5194/isprs-archives-XLII-5-W1-69-2017>
- Chiabrandò, F., Lingua, A., Maschio, P., & Teppati Losè, L. (2017). The influence of flight

- planning and camera orientation in UAVs photogrammetry. A test in the area of rocca San Silvestro (LI), Tuscany. In *International Archives of the Photogrammetry, Remote Sensing and Spatial Information Sciences - ISPRS Archives* (Vol. 42). <https://doi.org/10.5194/isprs-archives-XLII-2-W3-163-2017>
- Chiabrando, F., Nex, F., Piatti, D., & Rinaudo, F. (2011). UAV and RPV systems for photogrammetric surveys in archaeological areas: two tests in the Piedmont region (Italy). *Journal of Archaeological Science*, 38(3), 697–710. <https://doi.org/10.1016/J.JAS.2010.10.022>
- Chiabrando, F., Sammartano, G., & Spanò, A. T. (2017). A comparison among different optimization levels in 3D multi-sensor models. A test case in emergency context: 2016 Italian earthquake. *ISPRS - International Archives of the Photogrammetry, Remote Sensing and Spatial Information Sciences*, XLII-2/W3, 155–162. <https://doi.org/10.5194/isprs-archives-XLII-2-W3-155-2017>
- Chiabrando, F., & Spanò, A. (2013). Points clouds generation using tls and dense-matching techniques. A test on approachable accuracies of different tools. In *ISPRS Annals of the Photogrammetry, Remote Sensing and Spatial Information Sciences* (Vol. 2, pp. 73–78). <https://doi.org/10.5194/isprsannals-II-5-W1-67-2013>
- Chiabrando, F., Spanò, A. T., Sammartano, G., & Teppati Losè, L. (2017). UAV oblique photogrammetry and LiDAR data acquisition for 3D documentation of the Hercules Fountain. *Virtual Archaeology Review*, 8(16), 83. <https://doi.org/10.4995/var.2017.5961>
- Chiabrando, F., & Teppati Losè, L. (2017). Performance evaluation of COTS UAV for architectural heritage documentation. A test on s.giuliano Chapel in Savigliano (CN) - Italy. In *International Archives of the Photogrammetry, Remote Sensing and Spatial Information Sciences - ISPRS Archives* (Vol. 42, pp. 77–84). <https://doi.org/10.5194/isprs-archives-XLII-2-W6-77-2017>
- Christian Heipke, Karsten Jacobsen, H. W. (2002). Analysis of the results of the OEEPE test “integrated sensor orientation.” *Integrated Sensor Orientation – Test Report and Workshop Proceedings, OEEPE Official Publications*, 43, 31–49.
- Chunhua, H., Yong, F., Zhihong, J., Jihong, Z., & Zengqi, S. (2006). Mission Planning for Unmanned Aerial Vehicles. In *The Proceedings of the Multiconference on “Computational Engineering in Systems Applications”* (pp. 597–601). IEEE. <https://doi.org/10.1109/CESA.2006.4281723>
- Cingolani, E., & Fangi, G. (2011). Spherical Panoramas, and non Metric Images for Long Range Survey, the San Barnaba Spire, Sagrada Familia, Barcelona, Spain. *Geoinformatics FCE CTU*, 6(0), 109–117. <https://doi.org/10.14311/gi.6.15>
- Clarke, T. A., & Fryer, J. F. (1998). The development of camera calibration methods and models Photogrammetric Record. *Photogrammetric Record*, 16(91), 51–66.
- Colomina, I., & Molina, P. (2014). Unmanned aerial systems for photogrammetry and remote sensing: A review. *ISPRS Journal of Photogrammetry and Remote Sensing*, 92, 79–97. <https://doi.org/10.1016/j.isprsjprs.2014.02.013>
- Conolly, J., & Lake, M. (Mark W. . (2006). Geographical information systems in archaeology, 338.
- Cramer, M. (1996). *Exterior Orientation by Direct Measurement of Camera Position and Attitude*.
- Cramer, M., Haala, N., & Stallmann, D. (2000). *Direct Georeferencing Using GPS/Inertial Exterior Orientations for Photogrammetric Applications*. IAPRS (Vol. XXXIII).
- Cresswell, J. (Ed. . (2010). *Oxford dictionary of word origins*. Oxford University Press.
- D’Andria, F., Caggia, M. P., & Ismaelli, T. (2016). *Hierapolis di Frigia VIII*.
- D’Andria, F., Scardozi, G., & Spanò, A. (2008). *Atlante di Hierapolis di Frigia*. (E. Yayinlari, Ed.). Istanbul.
- D’Annibale, E. (2011). Image Based Modeling from Spherical Photogrammetry and Structure for Motion. The Case of the Treasury, Nabatean Architecture in Petra. *Geoinformatics FCE CTU*, 6(0), 62–73. <https://doi.org/10.14311/gi.6.9>
- D’Annibale, E., & Fangi, G. (2009). Interactive Modelling by Projection of Oriented Spherical Panorama -- Ad Deir, Petra, Jordan. In *3D-ARCH 2009: 3D Virtual*

- Reconstruction and Visualization of Complex Architectures* (Vol. XXXVIII).  
<https://doi.org/10.1007/s00421-007-0565-x>
- D'Annibale, E., Piermattei, L., & Fangi, G. (2011). Spherical Photogrammetry As Emergency Photogrammetry. *XXIII CIPA Symposium*.
- D'Annibale, E., Tassetti, A. N., & Malinverni, E. S. (2013). From Panoramic Photos to a Low-Cost Photogrammetric Workflow for Cultural Heritage 3D Documentation. *International Archives of Photogrammetry, Remote Sensing and Spatial Information Sciences, XL-5/W2*, 2–6. <https://doi.org/10.5194/isprsarchives-XL-5-W2-213-2013>
- D'Ayala, D. ., & Smars, P. (2003). *Minimum requirements for metric use of non-metric photographic documentation*.
- Dabove, P., Di Pietra, V., & Lingua, A. (2018). Close range photogrammetry with tablet technology in post-earthquake scenario: Sant'Agostino church in Amatrice, 22, 463–477. <https://doi.org/10.1007/s10707-018-0316-7>
- Dalamagkidis, K., Valavanis, K. P., & Piegler, L. A. (2012). Aviation History and Unmanned Flight. In *On Integrating Unmanned Aircraft Systems into the National Airspace System* (pp. 11–42). Dordrecht: Springer Netherlands. [https://doi.org/10.1007/978-94-007-2479-2\\_2](https://doi.org/10.1007/978-94-007-2479-2_2)
- Dalamagkidis, K., Valavanis, K. P., Piegler, L. A., Dalamagkidis, Konstantinos; Valavanis, Kimon P.; Piegler, L. A., & Valavanis, Kimon P.; Oh, Paul; Piegler, L. A. (2009). *On Integrating Unmanned Aircraft Systems into the National Airspace System*.
- Dall'Asta, E., Thoeni, K., Santise, M., Forlani, G., Giacomini, A., Roncella, R., ... Roncella, R. (2015). Network Design and Quality Checks in Automatic Orientation of Close-Range Photogrammetric Blocks. *Sensors*, 15(4), 7985–8008. <https://doi.org/10.3390/s150407985>
- Dell'Unto, N., Landeschi, G., Apel, J., & Poggi, G. (2017). 4D recording at the trowel's edge: Using three-dimensional simulation platforms to support field interpretation. *Journal of Archaeological Science: Reports*, 12, 632–645. <https://doi.org/10.1016/j.jasrep.2017.03.011>
- Dell'Unto, N., Landeschi, G., Leander Touati, A. M., Dellepiane, M., Callieri, M., & Ferdani, D. (2016). Experiencing Ancient Buildings from a 3D GIS Perspective: a Case Drawn from the Swedish Pompeii Project. *Journal of Archaeological Method and Theory*, 23(1), 73–94. <https://doi.org/10.1007/s10816-014-9226-7>
- Dequal, S., & Lingua, A. (2003). True orthophoto of the whole town of Turin. *Proceedings of the XIXth International Symposium, CIPA 2003: New Perspectives to Save Cultural Heritage: Antalya (Turkey), 30 September-04 October, 2003*, (June), 263–268. Retrieved from <http://cipa.icomos.org/wp-content/uploads/2018/11/Dequal-Lingua-True-orthophoto-of-the-whole-town-of-Turin.pdf>
- Devereux, B. J., Amable, G. S., Crow, P., & Cliff, A. D. (2005). The potential of airborne lidar for detection of archaeological features under woodland canopies. *Antiquity*, 79(305), 648–660. <https://doi.org/10.1017/S0003598X00114589>
- Djindjian, F. (1998). GIS usage in worldwide archaeology. *Archeologia e Calcolatori n. IX - 1998*.
- Donadio, E., & Spanò, A. T. (2015). Data Collection and Management for Stratigraphic Analysis of Upstanding Structures (pp. 34–39). <https://doi.org/10.5220/0005470200340039>
- Doneus, M., Briese, C., Fera, M., & Janner, M. (2008). Archaeological prospection of forested areas using full-waveform airborne laser scanning. *Journal of Archaeological Science*, 35(4), 882–893. <https://doi.org/10.1016/j.jas.2007.06.013>
- Doneus Neubauer, W., M. (2005). 3D laser scanners on archaeological excavations. *CIPA The International Archives of Photogrammetry, Remote Sensing and Spatial Information Sciences, XX Interna*, 226–231.
- Dong, P., & Guo, H. (2012). A framework for automated assessment of post-earthquake building damage using geospatial data. *International Journal of Remote Sensing*, 33(1), 81–100. <https://doi.org/10.1080/01431161.2011.582188>
- Drewett, P. L. (1999). *Field Archaeology: An Introduction*.
- Duarte, D., Nex, F., Kerle, N., & Vosselman, G. (2017). Towards a more efficient detection

- of earthquake induced façade damages using oblique UAV imagery. In *International Archives of the Photogrammetry, Remote Sensing and Spatial Information Sciences - ISPRS Archives* (Vol. 42, pp. 93–100). <https://doi.org/10.5194/isprs-archives-XLII-2-W6-93-2017>
- Eisenbeiß, H. (2009). *UAV Photogrammetry*. Institut für Geodäsie und Photogrammetrie Eidgenössische Technische Hochschule Zürich.
- El-Hakim, S. F., Beraldin, J.-A., Picard, M., & Godin, G. (2004). Detailed 3D reconstruction of large-scale heritage sites with integrated techniques. *IEEE Computer Graphics and Applications*, 24(3), 21–29. <https://doi.org/10.1109/MCG.2004.1318815>
- Ellum, C., & El-Sheimy, N. (2002). Land-based mobile mapping systems. *Photogrammetric Engineering and Remote Sensing*, 68(1), 13–17.
- Everaerts, J. (2008). The Use of Unmanned Aerial Vehicles (UAVs) for Remote Sensing and Mapping. *The International Archives of the Photogrammetry, Remote Sensing and Spatial Information Sciences*, XXXVII(Part B1), 1187–1192.
- Everaerts, J. (2009). *NEWPLATFORMS – Unconventional Platforms (Unmanned Aircraft Systems) for Remote Sensing. Technical Report 56. European Spatial Data Research (EuroSDR)*.
- Ezequiel, C. A. F., Cua, M., Libatique, N. C., Tangonan, G. L., Alampay, R., Labuguen, R. T., ... Palma, B. (2014). UAV aerial imaging applications for post-disaster assessment, environmental management and infrastructure development. *2014 International Conference on Unmanned Aircraft Systems (ICUAS)*, (August), 274–283. <https://doi.org/10.1109/ICUAS.2014.6842266>
- Fangi, G. (2007). The Multi-image spherical Panoramas as a tool for Architectural Survey. *XXI International CIPA Symposium*, (October), 0256--1840.
- Fangi, G. (2015a). Documentation of some Cultural Heritage Emergencies in Syria In August 2010 by Spherical Photogrammetry. *ISPRS Annals of Photogrammetry, Remote Sensing and Spatial Information Sciences*, II-5/W3(September), 401–408. <https://doi.org/10.5194/isprsannals-II-5-W3-401-2015>
- Fangi, G. (2015b). Towards an easier orientation for spherical photogrammetry. *International Archives of the Photogrammetry, Remote Sensing and Spatial Information Sciences - ISPRS Archives*, 40(5W4), 279–283. <https://doi.org/10.5194/isprsarchives-XL-5-W4-279-2015>
- Fangi, G., & Nardinocchi, C. (2013). Photogrammetric processing of spherical panoramas. *Photogrammetric Record*, 28(143), 293–311. <https://doi.org/10.1111/phor.12031>
- Fangi, G., Pierdicca, R., Sturari, M., & Malinverni, E. S. (2018). Improving spherical photogrammetry using 360°OMNI-Cameras: Use cases and new applications. In *International Archives of the Photogrammetry, Remote Sensing and Spatial Information Sciences - ISPRS Archives* (Vol. 42, pp. 331–337). <https://doi.org/10.5194/isprs-archives-XLII-2-331-2018>
- Fazeli, H., Samadzadegan, F., & Dadrasjavan, F. (2016). Evaluating the potential of RTK-UAV for automatic point cloud generation in 3D rapid mapping. In *International Archives of the Photogrammetry, Remote Sensing and Spatial Information Sciences - ISPRS Archives* (Vol. 41, pp. 221–226). <https://doi.org/10.5194/isprsarchives-XLI-B6-221-2016>
- Fernandez-Diaz, J. C., Carter, W. E., Shrestha, R. L., Leisz, S. J., Fisher, C. T., Gonzalez, A. M., ... Elkins, S. (2014). Archaeological prospection of north Eastern Honduras with airborne mapping LiDAR. In *2014 IEEE Geoscience and Remote Sensing Symposium* (pp. 902–905). IEEE. <https://doi.org/10.1109/IGARSS.2014.6946571>
- Fernández-Hernández, J., González-Aguilera, D., Rodríguez-Gonzálvez, P., & Mancera-Taboada, J. (2015). Image-Based Modelling from Unmanned Aerial Vehicle (UAV) Photogrammetry: An Effective, Low-Cost Tool for Archaeological Applications. *Archaeometry*, 57(1), 128–145. <https://doi.org/10.1111/arcm.12078>
- Fernandez Galarreta, J., Kerle, N., & Gerke, M. (2015). UAV-based urban structural damage assessment using object-based image analysis and semantic reasoning. *Nat. Hazards Earth Syst. Sci*, 15, 1087–1101. <https://doi.org/10.5194/nhess-15-1087-2015>

- Flack, D., & Hannaford, J. (2005). Fundamental Good Practice in Dimensional Metrology - No. 80, (80), 227.
- Foley, J. D., Fischler, M. A., & Bolles, R. C. (1981). *Graphics and Image Processing Random Sample Consensus: A Paradigm for Model Fitting with Applications to Image Analysis and Automated Cartography*.
- Förstner, W. (2009). Computer Vision and Remote Sensing – Lessons Learned. *Photogrammetric Week*, 241–249.
- Förstner, W., & Wrobel, B. P. (2016). *Photogrammetric Computer Vision. Statistics, Geometry, Orientation and Reconstruction* (Vol. 11). Springer. <https://doi.org/10.1007/978-3-319-11550-4>
- Forte, M., Dell’Unto, N., Issavi, J., Onsurez, L., & Lercari, N. (2012). 3D Archaeology at Çatalhöyük. *International Journal of Heritage in the Digital Era*, 1(3), 351–378. <https://doi.org/10.1260/2047-4970.1.3.351>
- Francovich, R., & Dallai, L. (2010). Colline Metallifere (Tuscany, Italy). *ArchéoSciences*, (34), 277–287. <https://doi.org/10.4000/archeosciences.2843>
- Fraser, C. (1997). Digital camera self-calibration. *ISPRS Journal of Photogrammetry and Remote Sensing*, 52(4), 149–159. [https://doi.org/10.1016/S0924-2716\(97\)00005-1](https://doi.org/10.1016/S0924-2716(97)00005-1)
- Fraser, C. (2001). Photogrammetric Camera Component Calibration: A Review of Analytical Techniques (pp. 95–121). Springer, Berlin, Heidelberg. [https://doi.org/10.1007/978-3-662-04567-1\\_4](https://doi.org/10.1007/978-3-662-04567-1_4)
- Fraser, C. (2013). Automatic Camera Calibration in Close Range Photogrammetry. *Photogrammetric Engineering & Remote Sensing*, 79(4), 381–388. <https://doi.org/10.14358/PERS.79.4.381>
- Fraser, C., & Remondino, F. (2006). Digital camera calibration methods: considerations and comparisons. *International Archives of Photogrammetry Remote Sensing and Spatial Information Sciences*, 36(5), 266–272.
- Fregonese, L., Fassi, F., Achille, C., Adami, A., Ackermann, S., Nobile, A., ... Santoriello, A. (2016). 3D survey technologies: investigations on accuracy and usability in archaeology. The case study of the new “Municipio” underground station in Naples. *Acta IMEKO*, 5(2), 55–63.
- Fregonese, L., Taffurelli, L., Adami, A., Chiarini, S., Cremonesi, S., Helder, J., & Spezzoni, A. (2017). Survey and modelling for the bim of Basilica of San Marco in Venice. In *International Archives of the Photogrammetry, Remote Sensing and Spatial Information Sciences - ISPRS Archives* (Vol. 42, pp. 303–310). <https://doi.org/10.5194/isprs-archives-XLII-2-W3-303-2017>
- Fritsch, D., & Syll, M. (2015). Photogrammetric 3D reconstruction using mobile imaging. In R. Creutzburg & D. Akopian (Eds.), *Mobile Devices and Multimedia: Enabling Technologies, Algorithms, and Applications 2015*. International Society for Optics and Photonics. <https://doi.org/10.1117/12.2083332>
- Fryer, J. G., & Brown, D. (1986). Lens Distortion for Close-Range Photogrammetry. *Photogrammetric Engineering and Remote Sensing*, 52(1), 51–58.
- Fryer, J., Mitchell, H., & Chandler, J. H. (2007). *Applications of 3D measurement from images*. [https://doi.org/10.1111/j.1477-9730.2009.00545\\_1.x](https://doi.org/10.1111/j.1477-9730.2009.00545_1.x)
- Fusiello, A. (2018). *Visione computazionale : tecniche di ricostruzione tridimensionale*. Franco Angeli.
- Fussell, A. (1982). Terrestrial photogrammetry in archaeology. *World Archaeology*, 14(2), 157–172. <https://doi.org/10.1080/00438243.1982.9979857>
- Gabrlík, P., Cour-Harbo, A. la, Kalvodova, P., Zalud, L., & Janata, P. (2018). Calibration and accuracy assessment in a direct georeferencing system for UAS photogrammetry. *International Journal of Remote Sensing*, 39(15–16), 4931–4959. <https://doi.org/10.1080/01431161.2018.1434331>
- Galantucci, L. M., Pesce, M., & Lavecchia, F. (2016). A powerful scanning methodology for 3D measurements of small parts with complex surfaces and sub millimeter-sized features, based on close range photogrammetry. *Precision Engineering*, 43, 211–219. <https://doi.org/10.1016/J.PRECISIONENG.2015.07.010>
- Gallo, A., Muzzupappa, M., & Bruno, F. (2014). 3D reconstruction of small sized objects

- from a sequence of multi-focused images. *Journal of Cultural Heritage*, 15(2), 173–182. <https://doi.org/10.1016/J.CULHER.2013.04.009>
- Garagnani, S. (2017). Archaeological Building Information Modeling: beyond scalable representation of architecture and archaeology. *Archeologia e Calcolatori*, 28(2), 141–149. Retrieved from [http://www.archcalc.cnr.it/indice/PDF28.2/09\\_Garagnani.pdf](http://www.archcalc.cnr.it/indice/PDF28.2/09_Garagnani.pdf)
- Garbrecht, J., & Martz, L. W. (1997). The assignment of drainage direction over flat surfaces in raster digital elevation models. *Journal of Hydrology*, 193(1–4), 204–213. [https://doi.org/10.1016/S0022-1694\(96\)03138-1](https://doi.org/10.1016/S0022-1694(96)03138-1)
- Georgiadis, C., & Tsioukas, V. (2000). Fast and accurate documentation of archaeological sites using in the field photogrammetric techniques. *International Archives of Photogrammetry and Remote Sensing*, XXXIII, 28–32. Retrieved from [http://www.isprs.org/proceedings/XXXIII/congress/part5/28\\_XXXIII-part5s.pdf](http://www.isprs.org/proceedings/XXXIII/congress/part5/28_XXXIII-part5s.pdf)
- Georgopoulos, A., Ioannidis, C., & Valanis, A. (2010). Assessing the Performance of a Structured Light Scanner. *ISPRS Archives of Photogrammetry, Remote Sensing and Spatial Information Sciences*, XXXVIII(5), 250–255.
- Georgopoulos, A., Oikonomou, C., Adamopoulos, E., & Stathopoulou, E. K. (2016). Evaluating unmanned aerial platforms for cultural heritage large scale mapping. *ISPRS - International Archives of the Photogrammetry, Remote Sensing and Spatial Information Sciences*, XLI-B5, 355–362. <https://doi.org/10.5194/isprsarchives-XLI-B5-355-2016>
- Gerke, M., & Przybilla, H.-J. (2016). Accuracy Analysis of Photogrammetric UAV Image Blocks: Influence of Onboard RTK-GNSS and Cross Flight Patterns. *Photogrammetrie - Fernerkundung - Geoinformation*, 2016(1), 17–30. <https://doi.org/10.1127/pfg/2016/0284>
- Gini, R., Pagliari, D., Passoni, D., Pinto, L., Sona, G., & Dosso, P. (2013). UAV PHOTOGRAMMETRY: BLOCK TRIANGULATION COMPARISONS. *ISPRS - International Archives of the Photogrammetry, Remote Sensing and Spatial Information Sciences*, XL-1/W2(September), 157–162. <https://doi.org/10.5194/isprsarchives-XL-1-W2-157-2013>
- Giones, F., & Brem, A. (2017). From toys to tools: The co-evolution of technological and entrepreneurial developments in the drone industry. *Business Horizons*, 60(6), 875–884. <https://doi.org/10.1016/j.bushor.2017.08.001>
- Glassner, A. S. (1989). *An Introduction to Ray tracing*. Elsevier Science.
- Gómez-Candón, D., De Castro, A. I., & López-Granados, F. (2014). Assessing the accuracy of mosaics from unmanned aerial vehicle (UAV) imagery for precision agriculture purposes in wheat. *Precision Agriculture*, 15(1), 44–56. <https://doi.org/10.1007/s11119-013-9335-4>
- Gonçalves, G. R., Pérez, J. A., & Duarte, J. (2018). Accuracy and effectiveness of low cost UASs and open source photogrammetric software for foredunes mapping. *International Journal of Remote Sensing*, 1–19. <https://doi.org/10.1080/01431161.2018.1446568>
- Gonzalez-Aguilera, D., López-Fernández, L., Rodriguez-Gonzalvez, P., Hernandez-Lopez, D., Guerrero, D., Remondino, F., ... Gaiani, M. (2018). GRAPHOS - open-source software for photogrammetric applications. *The Photogrammetric Record*, 33(161), 11–29. <https://doi.org/10.1111/phor.12231>
- Gottardi, C., & Guerra, F. (2018). Spherical images for cultural heritage: Survey and documentation with the NIKON KM360. In *International Archives of the Photogrammetry, Remote Sensing and Spatial Information Sciences - ISPRS Archives* (Vol. 42, pp. 385–390). <https://doi.org/10.5194/isprs-archives-XLII-2-385-2018>
- Granshaw, S. I. (2016). Photogrammetric Terminology: Third Edition. *Photogrammetric Record*, 31(154), 210–252. <https://doi.org/10.1111/phor.12146>
- Gruen, A., & Beyer, H. A. (2001). System Calibration Through Self-Calibration. In *Calibration and Orientation of Cameras in Computer Vision*. (pp. 163–193). Springer, Berlin, Heidelberg. [https://doi.org/10.1007/978-3-662-04567-1\\_7](https://doi.org/10.1007/978-3-662-04567-1_7)
- Grun, A. (1982). The Accuracy Potential of the Modern Bundle Block Adjustment I in Aerial

- Photogrammetry. *Photogrammetric Engineering and Remote Sensing*, 48(1), 45–54.
- Grussenmeyer, P., & Al Khalil, O. (2002). *The photogrammetric record, an international journal of photogrammetry* (Vol. 17).
- Grussenmeyer, P., & Khalil, O. AL. (2008). A comparison of photogrammetry software packages for the documentation of buildings. *The Mediterranean Surveyor in the New Millennium*. Retrieved from <https://halshs.archives-ouvertes.fr/halshs-00281254/document>
- Grussenmeyer, P., Landes, T., Voegtle, T., & Ringle, K. (2008). Comparison methods of terrestrial laser scanning, photogrammetry and tacheometry data for recording of cultural heritage buildings. In *ISPRS Congress Proceedings, Beijing* (pp. 213–218).
- Gruszczynski, W., Matwij, W., & Cwiakala, P. (2017). Comparison of low-altitude UAV photogrammetry with terrestrial laser scanning as data-source methods for terrain covered in low vegetation. *ISPRS Journal of Photogrammetry and Remote Sensing*, 126, 168–179. <https://doi.org/10.1016/j.isprsjprs.2017.02.015>
- Guerra-Hernández, J., Cosenza, D. N., Rodriguez, L. C. E., Silva, M., Tomé, M., Díaz-Varela, R. A., & González-Ferreiro, E. (2018). Comparison of ALS- and UAV(SfM)-derived high-density point clouds for individual tree detection in Eucalyptus plantations. *International Journal of Remote Sensing*, 39(15–16), 5211–5235. <https://doi.org/10.1080/01431161.2018.1486519>
- Guidi, G., & Remondino, F. (2012). 3D Modelling from Real Data. In *Modeling and Simulation in Engineering*. InTech. <https://doi.org/10.5772/30323>
- Guo-Qing Wei, & Song De Ma. (1994). Implicit and explicit camera calibration: theory and experiments. *IEEE Transactions on Pattern Analysis and Machine Intelligence*, 16(5), 469–480. <https://doi.org/10.1109/34.291450>
- Haarbrink, R. B. (2012). UAS for geo-information: current status and perspectives. *ISPRS - International Archives of the Photogrammetry, Remote Sensing and Spatial Information Sciences*, XXXVIII-1/, 207–212. <https://doi.org/10.5194/isprarchives-xxxviii-1-c22-207-2011>
- Habib, A., & Morgan, M. (2013). Stability Analysis and Geometric Calibration of Off-the-Shelf Digital Cameras. *Photogrammetric Engineering & Remote Sensing*, 71(6), 733–741. <https://doi.org/10.14358/pers.71.6.733>
- Habib, A., & Morgan, M. F. (2003). Automatic calibration of low-cost digital cameras. *Optical Engineering*, 42(4), 948. <https://doi.org/10.1117/1.1555732>
- Ham, Y., Han, K. K., Lin, J. J., & Golparvar-Fard, M. (2016). Visual monitoring of civil infrastructure systems via camera-equipped Unmanned Aerial Vehicles (UAVs): a review of related works. *Visualization in Engineering*. <https://doi.org/10.1186/s40327-015-0029-z>
- Häming, K., & Peters, G. (2010). The structure-from-motion reconstruction pipeline-a survey with focus on short image sequences, 46(5), 926–937.
- Harris, E. C. (1989). *Principles of archaeological stratigraphy*. Elsevier.
- Hartley, R. (2017). Unmanned aerial vehicles in forestry-reaching for a new perspective. *NZ Journal of Forestry*, 62(1).
- Hayakawa, Y. S., Oguchi, T., Komatsubara, J., Ito, K., Hori, K., & Nishiaki, Y. (2007). Rapid on-site topographic mapping with a handheld laser range finder for a geoarchaeological survey in Syria. *Geographical Research*, 45(1), 95–104. <https://doi.org/10.1111/j.1745-5871.2007.00431.x>
- He, J., Li, Y., & Zhang, K. (2012). Research of UAV Flight Planning Parameters, 3, 43–45. <https://doi.org/10.4236/pos.2012.34006>
- He, M., Zhu, Q., Du, Z., Hu, H., Ding, Y., & Chen, M. (2016). A 3D Shape Descriptor Based on Contour Clusters for Damaged Roof Detection Using Airborne LiDAR Point Clouds. *Remote Sensing*, 8(3), 189. <https://doi.org/10.3390/rs8030189>
- Heikkila, J., & Silven, O. (1997). A four-step camera calibration procedure with implicit image correction. In *Proceedings of IEEE Computer Society Conference on Computer Vision and Pattern Recognition* (pp. 1106–1112). IEEE Comput. Soc. <https://doi.org/10.1109/CVPR.1997.609468>
- Hernandez-Lopez, D., Felipe-Garcia, B., Gonzalez-Aguilera, D., & Arias-Perez, B. (2013).

- An Automatic Approach to UAV Flight Planning and Control for Photogrammetric Applications. *Photogrammetric Engineering & Remote Sensing*, 79(1), 87–98. <https://doi.org/10.14358/PERS.79.1.87>
- Herrmann, C., Wang, C., Strong Bowen, R., Keyder, E., Krainin, M., Liu, C., & Zabih, R. (2018). Robust image stitching with multiple registrations. In *The European Conference on Computer Vision (ECCV)*. [https://doi.org/10.1007/978-3-030-01216-8\\_4](https://doi.org/10.1007/978-3-030-01216-8_4)
- Høhle, J. (2008). *Photogrammetric Measurements in Oblique Aerial Images. Photogrammetrie, Fernerkundung, Geoinformation*.
- Holdener, D., Nebiker, S., & Blaser, S. (2017). Design and Implementation of a Novel Portable 360 ° Stereo Camera System With Low-Cost Action Cameras, *XLII*(November), 28–29.
- Honkavaara, E., Saari, H., Kaivosoja, J., Pölönen, I., Hakala, T., Litkey, P., ... Pesonen, L. (2013). Processing and Assessment of Spectrometric, Stereoscopic Imagery Collected Using a Lightweight UAV Spectral Camera for Precision Agriculture. *Remote Sensing*, 5(10), 5006–5039. <https://doi.org/10.3390/rs5105006>
- Howland, M. D., Kuester, F., & Levy, T. E. (2014). *PHOTOGRAMMETRY IN THE FIELD: DOCUMENTING, RECORDING, AND PRESENTING ARCHAEOLOGY. Mediterranean Archaeology and Archaeometry* (Vol. 14).
- Ikeuchi, K., & Sato, Y. (2001). *Modeling from Reality* (Kluwer Aca). Norwell.
- Ioannides, M., Georgopoulos, A., & Scherer, M. (2005). Standards in Cultural Heritage: the missing grammar for the digital documentation of the past. In *XX CIPA Symposium, ...*
- Jaakkola, A., Kukko, A., Yu, X., Kaartinen, H., Lehtomäki, M., & Lin, Y. (2010). A low-cost multi-sensoral mobile mapping system and its feasibility for tree measurements. *ISPRS Journal of Photogrammetry and Remote Sensing*, 65(6), 514–522. <https://doi.org/10.1016/j.isprsjprs.2010.08.002>
- Jacobsen, K. (2000). *Direct / integrated sensor orientation-pros and cons*.
- JCGM. (2012). International Vocabulary of Metrology – Basic and General Concepts and Associated Terms ( VIM ) 3 rd edition. Vocabulaire international de métrologie – Concepts fondamentaux et généraux et termes associés ( VIM ) 3e édition. *ORGANISATION INTERNATIONALE DE MÉTROLOGIE LÉGALE*, (Vim), 1–127.
- Jenson, S. K., & Domingue, J. O. (1988). *Extracting Topographic Structure from Digital Elevation Data for Geographic Information System Analysis* (Vol. 54).
- Kadobayashi, R., Kochi, N., & Furukawa, R. (2004). Comparison and Evaluation of Laser Scanning and Photogrammetry and Their Combined Use for Digital Recording of Cultural Heritage. In *The International Archives of the Photogrammetry, Remote Sensing and Spatial Information Sciences 35 (Part B5)* (pp. 401–406).
- Katsianis, M., Tshipidis, S., Kotsakis, K., & Kousoulakou, A. (2008). A 3D digital workflow for archaeological intra-site research using GIS. *Journal of Archaeological Science*, 35(3), 655–667. <https://doi.org/10.1016/j.jas.2007.06.002>
- Katsianis, M., Tshipidis, S., Kotsakis, K., Koussoulakou, A., & Manolopoulos, Y. (2006). Integrating excavation recording, data management and object representation through GIS | Markos Katsianis - Academia.edu. *Proceedings of the International Congress “Cultural Heritage And New Technologies” Workshop 10*.
- Katz, M. (2002). *Introduction to Geometrical Optics*. WORLD SCIENTIFIC. <https://doi.org/10.1142/5135>
- Ke, R., Li, Z., Tang, J., Pan, Z., & Wang, Y. (2018). Real-Time Traffic Flow Parameter Estimation From UAV Video Based on Ensemble Classifier and Optical Flow. *IEEE Transactions on Intelligent Transportation Systems*, 1–11. <https://doi.org/10.1109/TITS.2018.2797697>
- Keane, J. F., & Carr, S. S. (2013). A brief history of early unmanned aircraft. *Johns Hopkins APL Technical Digest*, 32(3).
- Keay, S. J., Parcak, S. H., & Strutt, K. D. (2014). High resolution space and ground-based remote sensing and implications for landscape archaeology: the case from Portus, Italy. *Journal of Archaeological Science*, 52, 277–292.

- <https://doi.org/10.1016/J.JAS.2014.08.010>
- Kenefick, J. F., Gyer, M. S., & Harp, B. F. (1972). *Analytical Self-Calibration*.
- Koistinen, K. (2000). 3D Documentation for archaeology during Finnish Jabal Haroun project. *International Archives of Photogrammetry and Remote Sensing*, 33(B5/1; PART 5), 440–445.
- Kondratiev, N. D. (1925). *The major economic cycles*.
- Kossieris, S., Kourouniotti, O., Agrafiotis, P., & Georgopoulos, A. (2017). Developing a Low-Cost System for 3D Data Acquisition. *ISPRS - International Archives of the Photogrammetry, Remote Sensing and Spatial Information Sciences*, XLII-2/W8(November), 119–126. <https://doi.org/10.5194/isprs-archives-XLII-2-W8-119-2017>
- Koutsoudis, A., Vidmar, B., Ioannakis, G., Arnaoutoglou, F., Pavlidis, G., & Chamzas, C. (2014). Multi-image 3D reconstruction data evaluation. *Journal of Cultural Heritage*, 15(1), 73–79. <https://doi.org/10.1016/J.CULHER.2012.12.003>
- Kraus, K. (2007). *Photogrammetry : geometry from images and laser scans*. Walter De Gruyter.
- Kwan, M. P., & Ransberger, D. M. (2010). LiDAR assisted emergency response: Detection of transport network obstructions caused by major disasters. *Computers, Environment and Urban Systems*, 34(3), 179–188. <https://doi.org/10.1016/j.compenvurbsys.2010.02.001>
- Kwiatek, K. (2012). 360° FILM BRINGS BOMBED CHURCH TO LIFE. *ISPRS - International Archives of the Photogrammetry, Remote Sensing and Spatial Information Sciences*, XXXVIII-5(March), 69–76. <https://doi.org/10.5194/isprsarchives-XXXVIII-5-W16-69-2011>
- Kwiatek, K., & Tokarczyk, R. (2014). Photogrammetric applications of immersive video cameras. In *ISPRS Annals of the Photogrammetry, Remote Sensing and Spatial Information Sciences* (Vol. 2, pp. 211–218). <https://doi.org/10.5194/isprsannals-II-5-211-2014>
- Kwiatek, K., & Tokarczyk, R. (2015). Immersive photogrammetry in 3D modelling. *Geomatics and Environmental Engineering*, 9(2), 51. <https://doi.org/10.7494/geom.2015.9.2.51>
- Läbe, T., & Förstner, W. (2004). Geometric stability of low-cost digital consumer cameras. *Proceedings of the 20th ISPRS Congress, Istanbul, Turkey*, 528–535.
- Lague, D., Brodu, N., & Leroux, J. (2013). Accurate 3D comparison of complex topography with terrestrial laser scanner: Application to the Rangitikei canyon (N-Z). *ISPRS Journal of Photogrammetry and Remote Sensing*, 82, 10–26. <https://doi.org/10.1016/j.isprsjprs.2013.04.009>
- Lasaponara, R., & Masini, N. (2012). *Satellite remote sensing : a new tool for archaeology*. Springer.
- Letellier, R. (2007). *RECORDIM: Guiding Principles & Illustrated Examples*. Los Angeles Recording,: The Getty Conservation Institute.
- Letellier, R., Schmid, W., LeBlanc, F., Eppich, R., Cabbi, A., & Getty Conservation Institute. (2011). *Recording, documentation, and information management for the conservation of heritage places Guiding principles*. Donhead Pub.
- Levin, A., Zomet, A., Peleg, S., & Weiss, Y. (2004). Seamless Image Stitching in the Gradient Domain. In *LNCS 3024 - Computer Vision - ECCV 2004*. 3.
- Li, M., Cheng, L., Gong, J., Liu, Y., Chen, Z., Li, F., ... Song, X. (2008). Post-earthquake assessment of building damage degree using LiDAR data and imagery. *Science in China, Series E: Technological Sciences*, 51(SUPPL. 2), 133–143. <https://doi.org/10.1007/s11431-008-6014-1>
- Linder, W. (2009). *Digital photogrammetry a practical course*. Control. <https://doi.org/10.4324/9780203305959>
- Lingua, A., Noardo, F., Spanò, A., Sanna, S., & Matrone, F. (2017). 3D model generation using oblique images acquired by UAV. In *International Archives of the Photogrammetry, Remote Sensing and Spatial Information Sciences - ISPRS Archives* (Vol. 42, pp. 107–115). <https://doi.org/10.5194/isprs-archives-XLII-4-W2-107-2017>

- Lo Brutto, M., Garraffa, A., & Meli, P. (2014). UAV platforms for cultural heritage survey: First results. In *ISPRS Annals of the Photogrammetry, Remote Sensing and Spatial Information Sciences* (Vol. 2, pp. 227–234). <https://doi.org/10.5194/isprsannals-II-5-227-2014>
- Lock, G., & Pouncett, J. (2017). Spatial thinking in archaeology: Is GIS the answer? *Journal of Archaeological Science*, 84, 129–135. <https://doi.org/10.1016/J.JAS.2017.06.002>
- Logothetis, S., & Stylianidis, E. (2016). BIM open source software (OSS) for the documentation of Cultural Heritage. *Virtual Archaeology Review*, 7(15), 28–35. <https://doi.org/10.4995/var.2016.5864>
- López, J. A. B., Jiménez, G. A., Romero, M. S., García, E. A., Martín, S. F., Medina, A. L., & Guerrero, J. A. E. (2016). 3D modelling in archaeology: The application of Structure from Motion methods to the study of the megalithic necropolis of Panoria (Granada, Spain). *Journal of Archaeological Science: Reports*, 10, 495–506. <https://doi.org/10.1016/j.jasrep.2016.11.022>
- Lowe, D. (2004). Distinctive Image Features from Scale-Invariant Keypoints. *International Journal of Computer Vision*.
- Luhmann, T. (2004). A historical review on panorama photogrammetry. *International Archives of the Photogrammetry, Remote Sensing and Spatial Information Sciences*, 35(5), 8. <https://doi.org/10.1.1.101.2588>
- Luhmann, T., Fraser, C., & Maas, H. G. (2016). Sensor modelling and camera calibration for close-range photogrammetry. *ISPRS Journal of Photogrammetry and Remote Sensing*, 115, 37–46. <https://doi.org/10.1016/j.isprsjprs.2015.10.006>
- Luhmann, T., Robson, S., Kyle, S. A., & Harley, I. A. (2006). *Close range photogrammetry: principles, techniques and applications*. Whittles Publishing. <https://doi.org/10.1111/phor.12114>
- Luhmann, T., Robson, S., Kyle, S., & Boehm, J. (2013). *Close-Range Photogrammetry and 3D Imaging*. (W. de Gruyter, Ed.).
- Luhmann, T., & Tecklenburg, W. (2004). 3-D Object Reconstruction From Multiple-Station Panorama Imagery. *Institute for Applied Photogrammetry and Geoinformatics*, 1–8. Retrieved from [www.oldenburg.de](http://www.oldenburg.de)
- Manfreda, S., McCabe, M., Miller, P., Lucas, R., Pajuelo Madrigal, V., Mallinis, G., ... Toth, B. (2018). On the Use of Unmanned Aerial Systems for Environmental Monitoring. *Remote Sensing*, 10(4), 641. <https://doi.org/10.3390/rs10040641>
- Mangiameli, M., Muscato, G., Mussumeci, G., & Milazzo, C. (2013). A GIS application for UAV flight planning. *IFAC Proceedings Volumes*, 46, 147–151. <https://doi.org/10.3182/20131120-3-FR-4045.00025>
- Mara, H., Breuckmann, B., & Lang-Auinger, C. (2009). Multi-spectral high-resolution 3D-acquisition for rapid archaeological documentation and analysis. In *European Signal Processing Conference* (pp. 1205–1209). Retrieved from <https://ieeexplore.ieee.org/abstract/document/7077507>
- Markiewicz, J. S., Lapiński, S., Bienkowski, R., & Kaliszewska, A. (2017). The example of using the Xiaomi cameras in inventory of monumental objects-first results. In *International Archives of the Photogrammetry, Remote Sensing and Spatial Information Sciences - ISPRS Archives* (Vol. 42, pp. 133–140). <https://doi.org/10.5194/isprs-archives-XLII-2-W8-133-2017>
- Massart, D. L., Kaufman, L., Rousseeuw, P. J., & Leroy, A. (1986). Least median of squares: a robust method for outlier and model error detection in regression and calibration. *Analytica Chimica Acta*, 187, 171–179. [https://doi.org/10.1016/S0003-2670\(00\)82910-4](https://doi.org/10.1016/S0003-2670(00)82910-4)
- McCoy, M. D., & Ladefoged, T. N. (2009). New developments in the use of spatial technology in archaeology. *Journal of Archaeological Research*. <https://doi.org/10.1007/s10814-009-9030-1>
- Moons, T., Vergauwen, M., & Gool, L. Van. (2015). 3D reconstruction from multiple images.
- Morgenthal, G., & Hallermann, N. (2016). Quality Assessment of Unmanned Aerial

- Vehicle (UAV) Based Visual Inspection of Structures. *Advances in Structural Engineering*, 17(3), 289–302. <https://doi.org/10.1260/1369-4332.17.3.289>
- Morrison, K. (2013). Mapping Subsurface Archaeology with SAR. *Archaeological Prospection*, 20(2), 149–160. <https://doi.org/10.1002/arp.1445>
- Mundy, J. L. (1993). The Relationship between photogrammetry and computer vision. *Optical Engineering and Photonics in Aerospace Sensing*, 92–105. <https://doi.org/10.1117/12.155818>
- Murtiyoso, A., Grussenmeyer, P., & Freville, T. (2017). Close range uav accurate recording and modeling of St-Pierre-Le-Jeune Neo-Romanesque church in Strasbourg (France). *International Archives of the Photogrammetry, Remote Sensing and Spatial Information Sciences - ISPRS Archives*, 42(2W3), 519–526. <https://doi.org/10.5194/isprs-archives-XLII-2-W3-519-2017>
- Nex, F. (2009). *Multi-image matching and LiDAR data new integration approach*. Politecnico di Torino.
- Nex, F., & Remondino, F. (2014). UAV for 3D mapping applications: A review. *Applied Geomatics*, 6(1), 1–15. <https://doi.org/10.1007/s12518-013-0120-x>
- Nicolae, C., Nocerino, E., Menna, F., & Remondino, F. (2014). Photogrammetry applied to problematic artefacts. In *International Archives of the Photogrammetry, Remote Sensing and Spatial Information Sciences - ISPRS Archives* (Vol. 40, pp. 451–456). <https://doi.org/10.5194/isprsarchives-XL-5-451-2014>
- Niederheiser, R. ; Mokros, M. ; Lange, J. ; Petschko, H. ; Prasicek, G. ; & Elberink, S. O. (2018). DERIVING 3D POINT CLOUDS FROM TERRESTRIAL PHOTOGRAPHS - COMPARISON OF DIFFERENT SENSORS AND SOFTWARE. *Citation*, 41, 685–692. <https://doi.org/10.5194/isprsarchives-XLI-B5-685-2016>
- Nikolakopoulos, K. G., Soura, K., Koukouvelas, I. K., & Argyropoulos, N. G. (2017). UAV vs classical aerial photogrammetry for archaeological studies. *Journal of Archaeological Science: Reports*, 14, 758–773. <https://doi.org/10.1016/j.jasrep.2016.09.004>
- Niven, L., Steele, T. E., Finck, H., Gernat, T., & Hublin, J.-J. (2009). Virtual skeletons: using a structured light scanner to create a 3D faunal comparative collection. *Journal of Archaeological Science*, 36(9), 2018–2023. <https://doi.org/10.1016/J.JAS.2009.05.021>
- Nocerino, E., Menna, F., & Remondino, F. (2014). Accuracy of typical photogrammetric networks in cultural heritage 3D modeling projects. *International Archives of the Photogrammetry, Remote Sensing and Spatial Information Sciences - ISPRS Archives*, 40(5), 465–472. <https://doi.org/10.5194/isprsarchives-XL-5-465-2014>
- Nowakowski, A. (2018). Calibration of radial lens distortion using a Gaussian model, 56(October 2017), 1–10. <https://doi.org/10.1117/1.OE.56.10.103103>
- Oth, L., Furgale, P., Kneip, L., & Siegwart, R. (2013). Rolling Shutter Camera Calibration. <https://doi.org/10.1109/CVPR.2013.179>
- Özyeşil, O., Voroninski, V., Basri, R., & Singer, A. (2017). A survey of structure from motion. *Acta Numerica*, 26, 305–364. <https://doi.org/10.1017/S096249291700006X>
- Pagani, A., & Stricke, D. (2011). Structure from motion using full spherical panoramic cameras. *Int. Conf. on Computer Vision Workshops (ICCV Workshops)*. IEEE, 2011, 375–382.
- Parenti, R. (2002). Dalla stratigrafia all'archeologia dell'architettura. Alcune recenti esperienze del laboratorio senese. *Arqueología de La Arquitectura*, 1, 73–82. Retrieved from <http://arqarqt.revistas.csic.es/index.php/arqarqt/article/viewArticle/7>
- Patias, P. (2006). Cultural heritage documentation. *International Summer School "Digital Recording and 3D Modeling"*, (April), 24–29.
- Patias, P. (2007). Cultural heritage documentation. In J. Fryer, H. Mitchell, & J. Chandler (Eds.), *Applications of 3D Measurement from Images*. Whittles Publishing.
- Peinado Checa, Z., Fernández Morales, A., & Agustín Hernández, L. (2014). Combinación de fotogrametría terrestre y aérea de bajo coste: el levantamiento tridimensional de la iglesia de San Miguel de Ágreda (Soria). *Virtual Archaeology Review*, 5(10), 51–58.

- Pellenz, J., Lang, D., Neuhaus, F., & Paulus, D. (2010). Real-time 3D mapping of rough terrain: A field report from Disaster City. In *2010 IEEE Safety Security and Rescue Robotics* (pp. 1–6). IEEE. <https://doi.org/10.1109/SSRR.2010.5981567>
- Perfetti, L., Polari, C., & Fassi, F. (2017). Fisheye photogrammetry: Tests and methodologies for the survey of narrow spaces. *International Archives of the Photogrammetry, Remote Sensing and Spatial Information Sciences - ISPRS Archives*, *42(2W3)*, 573–580. <https://doi.org/10.5194/isprs-archives-XLII-2-W3-573-2017>
- Perfetti, L., Polari, C., & Fassi, F. (2018). Fisheye multi-camera system calibration for surveying narrow and complex architectures. In *International Archives of the Photogrammetry, Remote Sensing and Spatial Information Sciences - ISPRS Archives* (Vol. 42, pp. 877–883). <https://doi.org/10.5194/isprs-archives-XLII-2-877-2018>
- Petrie, G. (2010). An Introduction to the Technology Mobile Mapping Systems. *GeoInformatics*, *13(1)*. <https://doi.org/10.1201/9781420025842.ch2>
- Pierrot-Deseilligny, M., & Clery, I. (2012). Apero, an open source bundle adjustment software for automatic calibration and orientation of set of images. *ISPRS - International Archives of the Photogrammetry, Remote Sensing and Spatial Information Sciences*, *XXXVIII-5/*, 269–276. <https://doi.org/10.5194/isprsarchives-XXXVIII-5-W16-269-2011>
- Pollefeys, M. (2003). 3D Capture of Archaeology and Architecture With a Hand-Held Camera. *International Journal*, *XXXIV(5)*, 262–267.
- Pomaska, G. (2001). Image Acquisition for Digital Photogrammetry Using “Off the Shelf” and Metric Cameras. *Proceedings of the XVIII. International Symposium, CIPA 2001*, 490–495. <https://doi.org/10.1007/s12518-010-0025-x>]
- Powlesland, D., Lyall, J., Hopkinson, G., Donoghue, D., Beck, M., Harte, A., & Stott, D. (2006). Beneath the sand—remote sensing, archaeology, aggregates and sustainability: a case study from Heslerton, the Vale of Pickering, North Yorkshire, UK. *Archaeological Prospection*, *13(4)*, 291–299. <https://doi.org/10.1002/arp.297>
- Ramos, A. P., & Prieto, G. R. (2016). Only image based for the 3D metric survey of gothic structures by using frame cameras and panoramic cameras. *International Archives of the Photogrammetry, Remote Sensing and Spatial Information Sciences - ISPRS Archives*, *41(July)*, 363–370. <https://doi.org/10.5194/isprsarchives-XLI-B5-363-2016>
- Remondino, F., Barazzetti, L., Nex, F., Scaioni, M., & Sarazzi, D. (2012). Uav Photogrammetry for Mapping and 3D Modeling – Current Status and Future Perspectives. *ISPRS - International Archives of the Photogrammetry, Remote Sensing and Spatial Information Sciences*, *XXXVIII-1/(September)*, 25–31. <https://doi.org/10.5194/isprsarchives-XXXVIII-1-C22-25-2011>
- Remondino, F., & Campana, S. (2014). *3D recording and modelling in archaeology and cultural heritage: theory and best practices*. *BAR international series 2598*. <https://doi.org/10.1177/0959683614545031>
- Remondino, F., & El-Hakim, S. (2006). Image-based 3D Modelling: A Review. *The Photogrammetric Record*, *21(September)*, 269–291. <https://doi.org/10.1111/j.1477-9730.2006.00383.x>
- Remondino, F., El-Hakim, S., Gruen, A., & Zhang, L. (2008). Turning images into 3-D models: Developments and performance analysis of image matching for detailed surface reconstruction of heritage objects. *IEEE Signal Processing Magazine*, *25(4)*, 55–64. <https://doi.org/10.1109/MSP.2008.923093>
- Remondino, F., Girardi, S., Rizzi, A., Benedetti, S., & Gonzo, L. (2009). 3D Virtual Reconstruction and Visualization of Complex Architectures – the “ 3D-Arch ” Project. *International Archives of the Photogrammetry, Remote Sensing and Spatial Information Sciences*, *XL-5/W4*, 25–27.
- Remondino, F., Guarnieri, A., & Vettore, A. (2005). 3D modeling of close-range objects: photogrammetry or laser scanning? In J.-A. Beraldin, S. F. El-Hakim, A. Gruen, & J. S. Walton (Eds.) (Vol. 5665, p. 216). International Society for Optics and Photonics. <https://doi.org/10.1117/12.586294>

- Remondino, F., Nocerino, E., Toschi, I., & Menna, F. (2017). A critical review of automated photogrammetric processing of large datasets. In *International Archives of the Photogrammetry, Remote Sensing and Spatial Information Sciences - ISPRS Archives* (Vol. 42, pp. 591–599). <https://doi.org/10.5194/isprs-archives-XLII-2-W5-591-2017>
- Remondino, F., Spera, M. G., Nocerino, E., Menna, F., & Nex, F. (2014). State of the art in high density image matching. *Photogrammetric Record*, 29(146), 144–166. <https://doi.org/10.1111/phor.12063>
- Remondino, F., & Stylianidis, E. (Eds.). (2016). *3D recording, documentation and management of cultural heritage*. Whittles Publishing.
- Remondino, F., Toschi, I., Gerke, M., Nex, F., Holland, D., McGill, A., ... Magarinos, A. (2017). Oblique aerial imagery for nma – some best practices. *Official Publication - EuroSDR, 2017*(66), 62–76. <https://doi.org/10.5194/isprsarchives-XLI-B4-639-2016>
- Rester, M., Spruyt, P., De Groeve, T., Damme, O. Van, & Ali, A. (2013). *Unmanned Aerial Systems for Rapid Mapping UASRapidMap. Joint Research Centre, TR, Rept. LB-NA-26451-EN-N*. Joint Research Centre, TR, Rept. LB-NA-26451-EN-N. <https://doi.org/10.2788/58375>
- Richter, A. M., Kuester, F., Levy, T. E., & Najjar, M. (2012). Terrestrial laser scanning (LiDAR) as a means of digital documentation in rescue archaeology: Two examples from the Faynan of Jordan. In *2012 18th International Conference on Virtual Systems and Multimedia* (pp. 521–524). IEEE. <https://doi.org/10.1109/VSMM.2012.6365967>
- Rieke, M., Foerster, T., Geipel, J., & Prinz, T. (2012). HIGH-PRECISION POSITIONING AND REAL-TIME DATA PROCESSING OF UAV-SYSTEMS. *ISPRS - International Archives of the Photogrammetry, Remote Sensing and Spatial Information Sciences, XXXVIII-1/*, 119–124. <https://doi.org/10.5194/isprsarchives-XXXVIII-1-C22-119-2011>
- Riisgaard, S., & Blas, M. R. (2004). SLAM for Dummies. *Massachusetts Institute Of Technology Projects*, 1–127.
- Roosevelt, C. H., Cobb, P., Moss, E., Olson, B. R., & Ünlüsoy, S. (2015). Excavation is Destruction Digitization: Advances in Archaeological Practice. *Journal of Field Archaeology*, 40(3), 325–346. <https://doi.org/10.1179/2042458215Y.0000000004>
- Rupnik, E., Daakir, M., & Pierrot Deseilligny, M. (2017). MicMac – a free, open-source solution for photogrammetry. *Open Geospatial Data, Software and Standards*, 2(1), 14. <https://doi.org/10.1186/s40965-017-0027-2>
- Rupnik, E., Nex, F., & Remondino, F. (2014). Oblique multi-camera systems-orientation and dense matching issues. *International Archives of the Photogrammetry, Remote Sensing and Spatial Information Sciences - ISPRS Archives*, 40(3W1), 107–114. <https://doi.org/10.5194/isprsarchives-XL-3-W1-107-2014>
- Salvi, J., Armanguè, X., & Batlle, J. (2002). A comparative review of camera calibration methods with accuracy evaluation. *Pattern Recognition*, 35, 1617–1635.
- Samaan, M., Héno, R., & Pierrot-Deseilligny, M. (2013). Close-range photogrammetric tools for small 3D archaeological objects. *ISPRS - International Archives of the Photogrammetry, Remote Sensing and Spatial Information Sciences, XL-5/W2*, 549–553. <https://doi.org/10.5194/isprsarchives-xl-5-w2-549-2013>
- Sammartano, G. (2018). *Suitability Of 3D Dense Models For Rapid Mapping Strategies On Cultural Heritage Documentation And Conservation. Validation of metric and non-metric information extraction from integrated solutions. (Doctoral dissertation)*. Politecnico di Torino.
- Sapirstein, P., & Murray, S. (2017). Establishing Best Practices for Photogrammetric Recording During Archaeological Fieldwork. *Journal of Field Archaeology*, 42(4), 337–350. <https://doi.org/10.1080/00934690.2017.1338513>
- Sauerbier, M., & Eisenbeiss, H. (2010). Uavs for the Documentation of Archaeological Excavations. *Proceedings of the Isprs Commission V Mid-Term Symposium Close Range Image Measurement Techniques*, 38(5), 526–531.
- Schneider, D., Schwalbe, E., & Maas, H. G. (2009). Validation of geometric models for fisheye lenses. *ISPRS Journal of Photogrammetry and Remote Sensing*, 64(3), 259–

266. <https://doi.org/10.1016/j.isprsjprs.2009.01.001>
- Schöning, J., & Heidemann, G. (2015). Evaluation of Multi-view 3D Reconstruction Software (pp. 450–461). Springer, Cham. [https://doi.org/10.1007/978-3-319-23117-4\\_39](https://doi.org/10.1007/978-3-319-23117-4_39)
- Scianna, A., Gristina, S., & Paliaga, S. (2014). Experimental BIM Applications in Archaeology: A Work-Flow (pp. 490–498). Springer, Cham. [https://doi.org/10.1007/978-3-319-13695-0\\_48](https://doi.org/10.1007/978-3-319-13695-0_48)
- Siqueira, V., Fleischmann, A., Jardim, P., Fan, F., Collischonn, W., Siqueira, V. A., ... Collischonn, W. (2016). IPH-Hydro Tools: a GIS coupled tool for watershed topology acquisition in an open-source environment. *Revista Brasileira de Recursos Hídricos*, 21(1), 274–287. <https://doi.org/10.21168/rbrh.v21n1.p274-287>
- Spanò, A. T., Chiabrando, F., Sammartano, G., & Teppati Losè, L. (2018). Integrated imaging approaches supporting the excavation activities. Multi-scale geospatial documentation in hierapolis (TK). In *International Archives of the Photogrammetry, Remote Sensing and Spatial Information Sciences - ISPRS Archives* (Vol. 42, pp. 1075–1082). <https://doi.org/10.5194/isprs-archives-XLII-2-1075-2018>
- Spanò, A. T., & Guardini, N. (2012). A sustainable approach in 3D documentation for historical buildings restoration. Valentino Castle buildingyard. In C. A. Ferrari (Ed.), “*Science and technology for the Safeguard of Cultural Heritage in the Mediterranean Basin*” (Vol. I, pp. 134–143). Istanbul: ITA.
- Stek, T. D. (2016). Drones over Mediterranean landscapes. The potential of small UAV’s (drones) for site detection and heritage management in archaeological survey projects: A case study from Le Pianelle in the Tappino Valley, Molise (Italy). *Journal of Cultural Heritage*, 22, 1066–1071. <https://doi.org/10.1016/J.CULHER.2016.06.006>
- Stöcker, C., Bennett, R., Nex, F., Gerke, M., & Zevenbergen, J. (2017). Review of the current state of UAV regulations. *Remote Sensing*, 9(5), 33–35. <https://doi.org/10.3390/rs9050459>
- Stöcker, C., Nex, F., Koeva, M., & Gerke, M. (2017). Quality assessment of combined IMU/GNSS data for direct georeferencing in the context of UAV-based mapping. In *International Archives of the Photogrammetry, Remote Sensing and Spatial Information Sciences - ISPRS Archives* (Vol. 42, pp. 355–361). <https://doi.org/10.5194/isprs-archives-XLII-2-W6-355-2017>
- Strecha, C. (2014). The rayCloud – A Vision Beyond the Point Cloud The rayCloud – A Vision Beyond the Point Cloud. *FIG Congress 2014*, (June 2014), 1–8.
- Strecha, C., & Glassey, L. (2015). Quality Assessment of 3d Reconstruction Using Fisheye and Perspective Sensors, (March). <https://doi.org/10.5194/isprsannals-II-3-W4-215-2015>
- Suman, S., Rastogi, U., & Tiwari, R. (2016). *Image Stitching Algorithms-A Review. Circulation in Computer Science* (Vol. 1). Retrieved from [www.ccsarchive.org](http://www.ccsarchive.org)
- Sutheerakul, C., Kronprasert, N., Kaewmoracharoen, M., & Pichayapan, P. (2017). Application of Unmanned Aerial Vehicles to Pedestrian Traffic Monitoring and Management for Shopping Streets. *Transportation Research Procedia*, 25, 1717–1734. <https://doi.org/10.1016/J.TRPRO.2017.05.131>
- Szeliski, R. (2006). Image Alignment and Stitching. *Handbook of Mathematical Models in Computer Vision*. Retrieved from [https://pdfs.semanticscholar.org/004e/cb7a7de33991c0a4d626ce7d79262e63f626.pdf?\\_ga=2.54135016.1961332555.1522736123-1526779410.1522736123](https://pdfs.semanticscholar.org/004e/cb7a7de33991c0a4d626ce7d79262e63f626.pdf?_ga=2.54135016.1961332555.1522736123-1526779410.1522736123)
- Szeliski, R., & Shum, H.-Y. (1997). Creating full view panoramic image mosaics and environment maps. In *Proceedings of the 24th annual conference on Computer graphics and interactive techniques - SIGGRAPH '97* (pp. 251–258). New York, New York, USA: ACM Press. <https://doi.org/10.1145/258734.258861>
- Tao, C. V., & Li, J. (2017). *Advances in Mobile Mapping Technology. Advances in Mobile Mapping Technology*. <https://doi.org/10.4324/9780203961872>
- Tarboton, D. G. (1997). A new method for the determination of flow directions and upslope areas in grid digital elevation models. *Water Resources Research*, 33(2), 309–319.

- <https://doi.org/10.1029/96WR03137>
- Teo, T. (2015). Video-based point cloud generation using multiple action cameras. In *International Archives of the Photogrammetry, Remote Sensing and Spatial Information Sciences - ISPRS Archives* (Vol. 40, pp. 55–60). <https://doi.org/10.5194/isprsarchives-XL-4-W5-55-2015>
- Teo, T., Shih, P. T. Y., Yu, S. C., & Tsai, F. (2016). The use of UAS for rapid 3D mapping in geomatics education. In *International Archives of the Photogrammetry, Remote Sensing and Spatial Information Sciences - ISPRS Archives* (Vol. 41, pp. 95–100). <https://doi.org/10.5194/isprsarchives-XLI-B6-95-2016>
- Teppati Losè, L., Chiabrando, F., & Spanò, A. (2018). Preliminary evaluation of a commercial 360 multi-camera RIG for photogrammetric purposes. In *International Archives of the Photogrammetry, Remote Sensing and Spatial Information Sciences - ISPRS Archives* (Vol. 42, pp. 1113–1120). <https://doi.org/10.5194/isprs-archives-XLII-2-1113-2018>
- Thiel, C., & Schmullius, C. (2017). Comparison of UAV photograph-based and airborne lidar-based point clouds over forest from a forestry application perspective. *International Journal of Remote Sensing*, 38(8–10), 2411–2426. <https://doi.org/10.1080/01431161.2016.1225181>
- Thoeni, K., Guccione, D. E., Santise, M., Giacomini, A., Roncella, R., & Forlani, G. (2016). The potential of low-cost rpas for multi-view reconstruction of sub-vertical rock faces. In *International Archives of the Photogrammetry, Remote Sensing and Spatial Information Sciences - ISPRS Archives* (Vol. 41, pp. 909–916). <https://doi.org/10.5194/isprsarchives-XLI-B5-909-2016>
- Torii, A., & Imiya, A. (2007). Computation of Epipolar Geometry and Trifocal Tensor from Spherical Images. *Computer Vision Winter Workshop*.
- Torii, A., Imiya, A., & Ohnishi, N. (2005). Two-and three-view geometry for spherical cameras. *Proc. of the Sixth Workshop on Omnidirectional Vision, Camera Networks and Non- Classical Cameras*, 105, 29–34.
- Toro, F. G., & Tsourdos, A. (2018). *UAV Sensors for environmental monitoring*. MDPI AG - Multidisciplinary Digital Publishing Institute.
- Torr, P. H. S. (2002). Bayesian Model Estimation and Selection for Epipolar Geometry and Generic Manifold Fitting. *International Journal of Computer Vision*, 50(1), 35–61. <https://doi.org/10.1023/A:1020224303087>
- Toschi, I. (2014). *Validation tests and best practices supporting automated procedures in image-based 3D modelling*.
- Tournadre, V., Pierrot-Deseilligny, M., & Faure, P. H. (2015). UAV linear photogrammetry. In *International Archives of the Photogrammetry, Remote Sensing and Spatial Information Sciences - ISPRS Archives* (Vol. 40, pp. 327–333). <https://doi.org/10.5194/isprsarchives-XL-3-W3-327-2015>
- Tralli, D. M., Blom, R. G., Zlotnicki, V., Donnellan, A., & Evans, D. L. (2005). Satellite remote sensing of earthquake, volcano, flood, landslide and coastal inundation hazards. In *ISPRS Journal of Photogrammetry and Remote Sensing* (Vol. 59, pp. 185–198). <https://doi.org/10.1016/j.isprsjprs.2005.02.002>
- Tripolitsiotis, A., Prokas, N., Kyritsis, S., Dollas, A., Papaefstathiou, I., & Partsinevelos, P. (2017). Dronesourcing: a modular, expandable multi-sensor UAV platform for combined, real-time environmental monitoring. *International Journal of Remote Sensing*, 38(8–10), 2757–2770. <https://doi.org/10.1080/01431161.2017.1287975>
- Tsai, R. Y. (1987). A Versatile Camera Calibration Technique for High-Accuracy 3D Machine Vision Metrology Using Off-the-Shelf TV Cameras and Lenses. *IEEE Journal on Robotics and Automation*, 3(4), 323–344. <https://doi.org/10.1109/JRA.1987.1087109>
- Tucci, G., & Bonora, V. (2014). New technologies for Cultural Heritage Documentation and Conservation: the role of geomatics. *Newton's Bulletin*, (November).
- Vallet, J., Panissod, F., Strecha, C., & Tracol, M. (2012). Photogrammetric performance of an ultra light weight swinglet “UAV.” *ISPRS - International Archives of the Photogrammetry, Remote Sensing and Spatial Information Sciences*, XXXVIII-1/,

- 253–258. <https://doi.org/10.5194/isprsarchives-xxxviii-1-c22-253-2011>
- Verhoeven, G. J. (2009). Providing an Archaeological Bird's-eye View - an Overall Picture of Ground-based Means to Execute Low-altitude Aerial Photography (LAAP) in Archaeology. *Archaeological Prospection*, (16).
- Verhoeven, G. J. (2011). Taking computer vision aloft - archaeological three-dimensional reconstructions from aerial photographs with photoscan. *Archaeological Prospection*, 18(1), 67–73. <https://doi.org/10.1002/arp.399>
- Verhoeven, G. J. (2012). Near-Infrared Aerial Crop Mark Archaeology: From its Historical Use to Current Digital Implementations. *Journal of Archaeological Method and Theory*, 19(1), 132–160. <https://doi.org/10.1007/s10816-011-9104-5>
- Verhoeven, G. J. (2016). Basics of photography for cultural heritage imaging. In E. Stylianidis & F. Remondino (Eds.), *3D recording, documentation and management of cultural heritage* (pp. 127–251). Whittles Publishing.
- Vetrivel, A., Gerke, M., Kerle, N., & Vosselman, G. (2015). Identification of damage in buildings based on gaps in 3D point clouds from very high resolution oblique airborne images. *ISPRS Journal of Photogrammetry and Remote Sensing*, 105, 61–78. <https://doi.org/10.1016/j.isprsjprs.2015.03.016>
- Voigt, S., Kemper, T., Riedlinger, T., Kiefl, R., Scholte, K., & Mehl, H. (2007). Satellite Image Analysis for Disaster and Crisis-Management Support. *IEEE Transactions on Geoscience and Remote Sensing*, 45(6), 1520–1528. <https://doi.org/10.1109/TGRS.2007.895830>
- Voigt, S., Schneiderhan, T., Twele, A., Gähler, M., Stein, E., & Mehl, H. (2011). Rapid Damage Assessment and Situation Mapping: Learning from the 2010 Haiti Earthquake. *American Society for Photogrammetry and Remote Sensing*, 77(9), 923–931.
- Wahbeh, W., & Nardinocchi, C. (2015). Toward the Interactive 3D Modelling Applied to Ponte Rotto in Rome. *Nexus Network Journal*, 17(1), 55–71. <https://doi.org/10.1007/s00004-015-0238-8>
- Wahbeh, W., Nebiker, S., & Fangi, G. (2016). Combining Public Domain and Professional Panoramic Imagery for the Accurate and Dense 3D Reconstruction of the Destroyed Bel Temple in Palmyra. *ISPRS Annals of Photogrammetry, Remote Sensing and Spatial Information Sciences*, III-5(June), 81–88. <https://doi.org/10.5194/isprs-annals-III-5-81-2016>
- Waldhäusl, P., Ogleby, C. L. (1994). 3 x 3 rules for simple photogrammetric documentation of architecture. *INTERNATIONAL SOCIETY FOR ...*, 1.
- Waldhäusl, P., Ogleby, C. L., Lerma, J. L., & Georgopoulos, A. (2013). 3 x 3 rules for simple photogrammetric documentation of architecture.
- Wang, G., Tsui, H. T., Hu, Z., & Wu, F. (2005). Camera calibration and 3D reconstruction from a single view based on scene constraints. *Image and Vision Computing*, 23(3), 311–323. <https://doi.org/10.1016/j.imavis.2004.07.008>
- Wenzel, K., Rothermel, M., Fritsch, D., & Haala, N. (2013). Image Acquisition and Model Selection for Multi-View Stereo. In *International Archives of the Photogrammetry, Remote Sensing and Spatial Information Sciences* (Vol. XL-5/W1, pp. 251–258). <https://doi.org/10.5194/isprsarchives-XL-5-W1-251-2013>
- Wester-Ebbinghaus, W. (1980). AERIAL PHOTOGRAPHY BY RADIO CONTROLLED MODEL HELICOPTER. *The Photogrammetric Record*, 10(55), 85–92. <https://doi.org/10.1111/j.1477-9730.1980.tb00006.x>
- Winkelbach, S., & Wahl, F. M. (2001). Shape from 2D Edge Gradients. In Radig B. & Florczyk S. (Eds.), *Pattern Recognition. DAGM 2001* (pp. 377–384). Springer, Berlin, Heidelberg. [https://doi.org/10.1007/3-540-45404-7\\_50](https://doi.org/10.1007/3-540-45404-7_50)
- Xu, Z., Wu, L., Shen, Y., Li, F., Wang, Q., Wang, R., ... Wang, R. (2014). Tridimensional Reconstruction Applied to Cultural Heritage with the Use of Camera-Equipped UAV and Terrestrial Laser Scanner. *Remote Sensing*, 6(11), 10413–10434. <https://doi.org/10.3390/rs6110413>
- Yanagi, H., & Chikatsu, H. (2010). 3D modeling of small objects using macro lens in digital very close range photogrammetry. *Remote Sensing and Spatial Information*

*Sciences, XXXVIII.*

- Zhang. (2000). A Flexible New Technique for Camera Calibration. *IEEE Transactions on Pattern Analysis and Machine Intelligence*, 22.
- Zhang, R., Tsai, P. S., Cryer, J. E., & Shah, M. (1999). Shape from shading: A survey. *IEEE Transactions on Pattern Analysis and Machine Intelligence*, 21(8), 690–706. <https://doi.org/10.1109/34.784284>
- Zheng, H., Cheng, T., Zhou, M., Li, D., Yao, X., Tian, Y., ... Zhu, Y. (2018). Improved estimation of rice aboveground biomass combining textural and spectral analysis of UAV imagery. *Precision Agriculture*, 1–19. <https://doi.org/10.1007/s11119-018-9600-7>